Geographical Location Optimisation of Wind and Solar Photovoltaic Power Capacity in South Africa using Mean-variance Portfolio Theory and Time Series Clustering

By

Christiaan Johannes Joubert

Thesis presented in partial fulfilment of the requirements for the degree Master of Engineering in Electrical Engineering at Stellenbosch University

Supervisor: Prof. H.J. Vermeulen
Department of Electrical and Electronic Engineering

March 2017

Declaration

By submitting this thesis/dissertation electronically, I declare that the entirety of the work contained therein is my own, original work, that I am the sole author thereof (save to the extent explicitly otherwise stated), that reproduction and publication thereof by Stellenbosch University will not infringe any third party rights and that I have not previously in its entirety or in part submitted it for obtaining any qualification.

C.J. Joubert

March 2017

Acknowledgements

I would like to thank the following people for their contribution during this project:

- My study leader, Prof H.J. Vermeulen, for his valuable guidance and inputs throughout my two years at Stellenbosch University. Thanks are also due to Prof H.J. Vermeulen's family who opened up their home to the crowd of master's students and their circle of friends on many occasions.
- My mother, Marina Joubert, father, Stefan Joubert, brother, Peter Joubert, aunt, Juanita Du Toit, grandmother, Irene Du Toit, as well as my late grandparents Pieter du Toit, Chris Joubert and Rita Joubert. To the extent that I have achieved anything in my life it would undoubtedly not have been possible without their unwavering love, sacrifice and support.
- Yoko Yuan, who showed enormous patience and strength while waiting for two years for me to complete my master's.
- All my fellow masters students in room E222, Almero de Villiers, George Blignault, Edwin Mangwende, Vicki Vermeulen and Tielman Nieuwoudt who made my time in Stellenbosch unforgettable.
- The director of the Centre for Renewable and Sustainable Energy Studies at Stellenbosch University, Prof J.L. Van Niekerk, who awarded me a bursary which enabled me to pursue a master's degree and switch to a career in renewable energy.
- Karin Kritzinger, a researcher at the Centre for Renewable and Sustainable Energy Studies at Stellenbosch University, for being a friend and an enthusiastic supporter of my work and future career plans.
- Dylan Jacklin, an old friend from the residence in Pretoria who joined me in Stellenbosch in 2016 and who made sure that a printed copy of this thesis reached my study leader while I was attending a conference in Malaysia.
- My industrial mentor, Riaan Smit from Eskom, who patiently listened to my project updates and helped me whenever I needed any data from Eskom.

Abstract

Throughout the world, there is a lot of pressure on governments and electricity utilities to try to mitigate the possible effects of climate change by reducing emissions of greenhouse gases and investing in renewable energy sources. Wind power and solar photovoltaic power represent the bulk of the installed renewable energy capacity. However, these energy sources are stochastic and highly dependent on weather conditions and exhibit marked diurnal and seasonal cyclic behaviour. It follows that power systems with a high penetration of wind and solar power present challenges to grid operators in the sense that renewable power cannot be dispatched on demand as is the case with conventional power generation plants.

There are several studies in the literature which investigate the possibility of optimising the location of wind farms so as to reduce the variability of the cumulative wind power output. The majority of these studies employ mean-variance optimisation, which is a quadratic programming method that is used in finance theory to construct efficient share portfolios. Several studies suggest the inclusion of solar photovoltaic power and load profiles in the mean-variance optimisation procedure, but little work has been done to investigate the effects. A problem with the mean-variance optimisation is that it often assigns low capacities to certain sites, with no clear alternatives, which makes part of its solution unfeasible in the face of practical and economic considerations. Time series clustering has been suggested as a possible solution to this problem, but the literature is sparse when it comes to time series clustering implementations combined with mean-variance optimisation.

In this investigation, wind power and solar photovoltaic power time series were simulated for a South African case study. An optimal clustering methodology was identified for the simulated renewable power time series and the results of the clustering procedure was used as an input in a mean-variance optimisation procedure that was adapted to include wind power, solar photovoltaic power and load profiles.

The complete optimisation methodology has been studied in four case studies using clearly defined key performance indicators. The results of the case studies are a clear indication of the potential of methodology to optimally distribute wind power and solar photovoltaic power capacity that could reduce the adverse impacts on the conventional generation capacity that are typically associated with large penetrations of renewable power capacity.

Opsomming

Regoor die wêreld is daar 'n baie druk op regerings en elektrisiteitmaatskappye om te probeer om die moontlike gevolge van klimaatsverandering te versag deur die vrystelling van kweekhuisgasse te verminder en te belê in hernubare energiebronne. Windkrag en fotovoltaïese sonkrag verteenwoordig die grootste deel van die geïnstalleerde kapasiteit van hernubare energie. Maar hierdie energiebronne is stogastiese en baie afhanklik van weerstoestande en toon duidelike daaglikse en seisoenale sikliese gedrag. Dit volg dus dat kragstelsels met 'n hoë penetrasie van wind- en sonkrag ’n uitdaging verteenwoordig aan kragstelseloperateurs in die sin dat hernubare krag nie kan gewek word op aanvraag soos in die geval van konvensionele kragopwekkingstasies nie.

Daar is verskeie studies in die literatuur wat die moontlikheid ondersoek van die optimering van die ligging van windplase ten einde die wisselvalligheid van die kumulatiewe windkraglewering te verminder. Die meerderheid van hierdie studies gebruik sogenaamde gemiddelde-variansie optimering, wat ’n kwadratiese programmeringmetode is wat gebruik word in die finansiële teorie om doeltreffende aandeleportefeuljes te bou. Verskeie studies dui na die insluiting van fotovoltaïese sonkrag en vragprofiele in die gemiddelde-variansie optimering proses, maar min werk gedoen is om die gevolge te ondersoek. ’n Probleem met die gemiddelde-variansie optimering is dat dit dikwels lae kapasiteite toeken aan sekere plekke, met geen duidelike alternatiewe nie, wat deel van die oplossing ondoenlik maak in die aangesig van praktiese en ekonomiese oorwegings. Tydreeks-groepering is voorgestel as ’n moontlike oplossing vir hierdie probleem, maar die literatuur is yl wanneer dit kom by die implementerings van tydreeksgroeperings, gekombineer met gemiddelde-variansie optimering.

In hierdie ondersoek is windkrag- en fotovoltaïese sonkrag-tydreekse gesimuleer vir ’n Suid-Afrikaanse gevallestudie. ’n Optimale groeperingsmetode is geïdentifiseer vir die gesimuleerde hernubare krag-tydreekse en die resultate van die groeperingsprosedure is gebruik as ’n inset in ’n gemiddelde-variansie optimeringsproses wat aangepas is om windkrag, fotovoltaïese sonkrag en vragprofiele in te sluit.

Die volledige optimeringsmetode is ondersoek in vier gevallestudies met behulp van duidelik gedefinieerde sleutel prestasie-aanwysers. Die resultate van die gevallestudies is ’n duidelike aanduiding van die potensiaal van die metode om windkrag- en fotovoltaïese sonkragkapasiteit te versprei, wat die negatiewe impak op die konvensionele opwekkingskapasiteit, wat tipies geassosieer word met ’n groot hoeveelhede hernubare krag kapasiteit, kan verminder.

Table of Contents

List of Figures

List of Tables

1 Project motivation and project description

1.1 Introduction

Throughout the world, there is a lot of pressure on governments and electricity utilities to try to mitigate the possible effects of climate change by reducing the emissions of greenhouse gases and investing in renewable energy sources [1]. In South Africa there is also currently a critical shortage of generating capacity and reserve, resulting in sustained periods of load shedding to maintain the national grid stability whenever there are unforeseen losses of generating capacity or unavoidable maintenance work to complete [2]. In light of the fact that traditional power plants, such as coal or nuclear, take a long time from initial planning to grid connection, typically five years or more [3], renewable energy sources, such as wind or solar, are an excellent alternative as they can be constructed and connected to the grid within two to three years.

In South Africa, the Department of Energy and Eskom (the national electricity utility) is currently in the process of introducing renewable energy sources financed by private entities to the national grid [4]. This program is called the Renewable Energy Independent Power Producer Procurement Program (REIPPPP). Wind power generation, solar energy from photovoltaic (PV) installations and concentrated solar power form the bulk of the renewable generating capacity currently under consideration [4]. The REIPPPP awards long term power purchasing agreements to preferred bidders on an annual basis. So far, four rounds have been successfully completed with a total generating capacity of 5243 MW from 79 projects, with a total of 2660 MW going to 26 onshore wind power generating projects and 2296 MW to 45 solar photovoltaic power generating projects [5].

The Department of Energy promulgated the Integrated Resource Plan (IRP) 2010-30 in March 2011, which provides a guideline for investment in different technology choices in the South African power sector [6]. The report was to be updated every two years to account for new developments in the energy sector and a changing electricity demand outlook. The latest update to the report was released in November 2013 [7]. The latest update gives short-term guidelines, one of which advocates for the continuation of the REIPPPP, but with additional annual rounds (of 1000 MW PV capacity; 1000 MW wind capacity and 200 MW CSP capacity). The aim is to continue with the program until at least 2030, although falling levels of demand due to energy efficiency programs and depressed economic activity has created some uncertainty around the REIPPPP. However, many of the conventional base-load generating plants in the fleet of Eskom are aging, and the potential to replace these plants with renewable energy sources has to be investigated.

The power output profiles of most renewable energy sources, and more specifically power from wind farms, are highly dependent on weather conditions, resulting in a power source of a stochastic rather than deterministic nature [8]. This not only introduces operational challenges, but also complicates the calculation of financial indicators such Return on Investment (ROI), etc. In order to analyse the potential for wind power generation in South Africa, site specific historical wind speed data is required. In the case of solar photovoltaic power, the historical ambient temperature and solar irradiance data is required.

The data needed to do solar photovoltaic power simulations have historically been available from different sources, whereas wind speed data with adequate time and spatial resolution was lacking. In 2009, the Department of Energy, along with several partners and technical agencies, established the Wind Atlas of South Africa (WASA) project [9]. The project aimed to produce mesoscale wind data for the Western Cape, as well as large regions of the Northern Cape and Eastern Cape, as these regions represent the areas with the most potential for wind power generation. As of March 2014, two numerical wind atlases have been produced using different modelling methods.

1.2 Project motivation

It is clear that wind power and solar photovoltaic power generation will play a decisive role in the future energy mix in South Africa [10]. There are however, several issues that need to be addressed before large scale integration of wind power and solar photovoltaic power can commence.

The stochastic nature of wind and solar photovoltaic power provides several challenges with regard to operational aspects such as state estimation, system stability, voltage distributions, economic dispatch, maintenance scheduling, etc. There is an abundance of research regarding the optimisation of the microsite level layout of individual wind farms, as well as very short-term (milliseconds up to a few minutes) and short-term (48–72 hours) forecasting methods to predict site specific wind power [11] and solar photovoltaic power generation [12]. However, there is a need for a longer-term study with the view to build the right size of wind farms and solar photovoltaic farms in the right geographic locations in order for their power generation profile to match national load profile. It is desirable to cluster these renewable farms in the right geographic locations so that they contribute the maximum amount annually and during peak load hours, but also to spread out the clusters enough to maximise the renewable power contribution that can statistically be relied upon in a short-term scenario, thereby limiting the variance of the residual load that the conventional generation fleet has to supply.

As briefly mentioned in section 1.1, the WASA project provides historical mesoscale wind data for the Western Cape, as well as large regions of the Northern Cape and Eastern Cape. The numerical mesoscale models assume a flat, uniform terrain, with no obstacles and with 3 cm roughness everywhere [9]. It ignores the microscale level typography's effect on the wind speed, such as the effects from elevation, surface roughness and large obstacles. Proprietary software packages, such as WAsP, are available to do microscale modelling of wind farms. As part of the WASA project, ten wind masts were erected in different parts of South Africa to measure wind data over three years and compile an observed wind atlas. The observed wind atlas data was used to validate the wind data from the numerical mesoscale models. The more recent of the two numerical wind atlases that have been produced so far is the Weather, Research and Forecasting (WRF) model. It correlated extremely well with the observed wind atlas. Its data was made available on 14 March 2014, and comprised the hourly wind speed and direction for the period 01-09-1990 to 31-12-2012 at 100 m above ground level with a spatial resolution of 27 km x 31 km blocks covering the specified region. Assuming that most wind farms will be built in conditions very similar to those assumed by the mesoscale model, it is fair to say that accurate wind data is now available in South Africa for the input to large scale wind power integration studies. This can be combined with temperature data and commercially available solar irradiance data to perform a wind farm and solar photovoltaic farm location and size optimisation study.

The financial and economic feasibility of renewable farms also play a major role in the optimisation problem. Traditionally, a major criticism of renewable energy sources has been the high price per megawatt hour of energy produced. However, as economies of scale have grown and the use of wind energy and solar photovoltaic energy has become more widespread than was the case previously, the capital costs associated with constructing these renewable farms has decreased to the point where it can compete directly with conventional generating plants without the need for a subsidy. There is a need however to investigate the impact that increased renewable energy generation will have on the conventional generating fleet and how that impacts on the overall cost of electricity generation.

Another challenge facing large scale integration of renewable power is the capacity of the South African electricity grid to absorb its intermittent power generation. Ideally wind farms and solar photovoltaic farms should be placed close to the existing grid infrastructure, and not exceed the technical transmission limits in order to avoid instability. This is an important factor considering that

the growth and expansion of the electricity grid in South Africa was traditionally centred around the majority of large coal power stations in the north eastern region of the country, which in turn were built with proximity to large coal mines in mind. As a result, the transmission infrastructure is relatively weak in the Western Cape, Northern Cape and Eastern Cape, which are the areas with the highest wind power generating potential. Although there are plans in place to expand the grid, the probability of large-scale grid expansion is extremely low due to the high costs and budget constraints at Eskom. The existing grid capacity therefore does serve as a constraint.

The REIPPPP consists of successive rounds of competitive bidding, where long-term power purchasing agreements are awarded to preferred bids which are evaluated on a 70/30 basis, with the former allocated to price per kWh of power produced, and the latter to non-price "economic development" criteria, including job creation, local content benefits and local community development [4]. With the exception of the concentrated solar power projects, the power purchase agreements associated with the REIPPPP implement a flat feed-in tariff. The offerings from Independent Power Producers (IPPs) therefore focus on maximising the return on investment by locating plants for maximum cumulative energy production, irrespective of time of use (TOU) grid requirements. The penetration of renewable energy is still relatively small and concerns around the impact of intermittent renewable power on the grid have not yet translated into any changes to the procurement program. A strong argument can be made that geographic location of wind farms and solar photovoltaic farms and the inherent potential for power generation that match the national load profile should play a greater role in the decision-making. It generates an optimisation problem that requires a formal methodology that can be used to incorporate all the necessary input parameters and constraints with the view to find optimum future geographic locations and sizes of wind farms and solar photovoltaic farms.

1.3 Project description

1.3.1 Research objectives

The project background and discussions presented in section 1.2 give rise to the following research objectives:

- Formulation of a simple model topology for simulation of power output profiles of wind energy and solar photovoltaic energy sources with the view to do long-term prediction/forecasting and optimisation.
- Development of an optimisation procedure that incorporates the predicted wind power and solar photovoltaic power generating profiles as well as grid connection capacity constraints in order to produce practicable solutions in terms of the optimal size and geographic distribution of renewable power generating sources from the perspective of the national load profile.
- Analysis of the results of the optimisation procedure in terms of clearly defined key performance indicators, with the view to study the benefits of the optimisation procedure and the impact of stochastic renewable energy sources on utility load-balancing.

1.3.2 Research methodology

The main objective of the research therefore focuses on determining optimal size and geographic distribution of wind farms and solar photovoltaic farms in South Africa in order for their power generating profile to match the national load profile. The project objectives translate into the following research methods and activities:

- *Conduct a literature review:*

  The focus of this literature study is as follows:

  - The current state of renewable energy in South Africa and its future prospects.
  - Wind and solar photovoltaic power simulation methodologies, as well as the availability of weather data required for wind and solar photovoltaic power simulation.
  - Academic papers related to optimisation of size and location of wind farms and solar photovoltaic farms, as well as the impact of different ratios of wind and solar photovoltaic power generation capacity.
  - Time series clustering, particularly as it pertains to enabling the optimisation procedure.
  - Key performance indicators pertaining to the increased penetration of renewable energy, especially regarding the effect of renewable energy integration on the conventional generation fleet and load balancing.

- *Mathematical formulation of the renewable power simulation and optimisation procedure*

  A formal mathematical formulation is required to serve as a reference and to remove any ambiguity regarding the eventual software implementation of the renewable power simulation models and the complete optimisation procedure.

- *Data acquisition*

  The data that is required to perform this study has to be identified and acquired from the relevant sources. This includes data pertaining to the wind and solar photovoltaic power simulation, national load data, grid constraints as well as GIS data on the South African landscape and its high voltage electricity grid.

- *Software implementation*

  The proposed models of wind power and solar photovoltaic power simulation, as well as the complete optimisation procedure have to be implemented in suitable software packages. The choice of software package will depend on the availability of built-in functions and capabilities, as well as the speed of software implementations, as a considerable amount of data is used are the study.

- *Performing a range of relevant case studies.*

  A range of relevant case studies will be performed to investigate the potential impact of using the optimisation procedure as well as the impact of future large penetrations of renewable energy sources.

- *Analysis of results and presentation of conclusions and recommendations*

  The results of the case studies will be analysed in order to draw conclusions regarding the impact of the optimisation procedure. Recommendations will also be presented that highlight the usefulness of the optimisation procedure and the future work that will improve the accuracy and enhance the impact of a similar study.

1.4 Thesis structure

The remainder of this document is structured as follows:

- *Chapter 2: Literature review:*

  The relevant literature is reviewed.

- *Chapter 3:Renewable Energy Simulation*

  The details of the wind power and solar photovoltaic power simulation methods are provided.

- *Chapter 4:Time Series Clustering*

  The details of the complete time series clustering methodology are provided.

- *Chapter 5:Mean-variance Optimisation*

  The mathematical formulation of the classical mean-variance formulation is provided, as well as the formulation as applied to wind power variance minimisation. Next, the mean-variance formulations that incorporate solar photovoltaic power and load data are presented.

- *Chapter 6: Key Performance Indicators*

  The selected key performance indicators are presented.

- *Chapter 7: Data Acquisition and Processing*

  The details are provided of all the data that was collected for this investigation, as well as any processing that was performed.

- *Chapter 8: Software Implementation*

  The details of the software implementation are provided, including the software packages that were used and the workflow employed throughout the investigation.

- *Chapter 9:Case Studies and Results*

  The results of the renewable power simulation procedures for South Africa and the time series clustering procedures are presented. Next, four cases studies are performed to analyse different aspects of clustered mean-variance optimisation.

- *Chapter 10: Conclusions and recommendations:*

  Final conclusions and recommendations for further work are presented.

Chapters 3-6 effectively constitute the methodology section and chapters 7-8 effectively constitute the implementation section. The chapters have been separated due to the depth of the topics that are covered.

2 Literature Review

2.1 Overview

This chapter presents the relevant literature that was consulted during the initial stages of the investigation. A brief overview is provided of the state of renewable energy in South Africa, after which the following topics are explored:

- *Renewable power simulation methods:* This section explores the methods that are employed in the literature to simulate wind power and solar photovoltaic power time series.
- *Weather datasets used for renewable power simulation:* This section explores the available weather datasets (including wind speed, solar irradiance and temperature data) that are employed in the literature to simulate wind power and solar photovoltaic power time series.
- *Renewable energy integration studies:* This section explores the key performance indicators related to renewable power integration (including power system security, power system adequacy and capacity credit) and the studies which investigate the effect of different ratios of wind power and solar photovoltaic power.
- *Wind farm location optimisation studies:* This section explores the studies that have been performed that deal with wind farm location optimisation. Most of these studies employ mean-variance portfolio optimisation but several other methods found in the literature are also reviewed.
- *Time series clustering:* This section gives a brief introduction to time series clustering as well as giving an overview of studies which have employed time series clustering in renewable energy research, as well as mean-variance optimisation studies.

2.2 Renewable Energy in South Africa

2.2.1 Integrated Resource Plan 2011

The integrated resource plan (IRP) represents the South African government's proposed new electricity generating fleet to be built for South Africa for the period 2010 to 2030, considering the future electricity demands of the country. The goal of the IRP was to determine how this future electricity demand would be met in terms of generating capacity, type, timing and cost. It was promulgated on 25 March 2011 after two rounds of public participation during June 2010 and November and December 2010.

In the IRP several scenarios were investigated which each produced a least-cost solution in terms of new generating builds. The different scenarios considered impacts and constraints related to factors such as current generating build delays, carbon dioxide emission limits, carbon taxes, possible regional development of different electricity import options and enhanced demand side management. In the scenarios, the electricity system was modelled using the power market and system simulator tool, PLEXOS. The scenarios were assessed using a multi-criteria decision-making framework (MCDF) that considered carbon dioxide emissions, cost of electricity, water consumption, uncertainty factors, localisation potential and regional development of electricity import options. A balanced scenario was developed from workshops with government departments considering the results of all scenarios and the MCDF analysis. The balanced scenarios were said to represent the best trade-off between least-investment cost and other key constraints, and risks such as climate change mitigation, security of supply, localisation potential and regional development.

The IRP proposed that the existing and committed power plants (that includes 10 GW of new coal power plants), should be supplemented by 9.6 GW of nuclear; 6.3 GW of coal; 17.8 GW of renewables and 8.9 GW of other sources for generating electricity.

The financial and technical data that was used to formulate the IRP was provided by the Electric Power Research Institute (EPRI). It was specified that the IRP should function as a "living plan" that was to be updated every two years.

2.2.2 Renewable Energy Independent Power Producer Procurement Program

The Renewable Energy Independent Power Producer Procurement Program (REIPPPP) is the s competitive tenders program of the South African government, managed by the Department of Energy (DoE), where the private sector submits bids to build renewable power plants in order to secure 20 year power purchase agreements.

The first round of competitive bidding started in August 2011. Out of a possible 53 bids, 28 preferred bidders were selected, with the agreements finalised on 5 November 2012. The first projects came online in November 2013.

The bids are evaluated on a 70/30 basis, with the former allocated to price per kWh of power produced, and the latter to non-price "economic development" criteria, including job creation, local content benefits and local community development [4].

By October 2015, four rounds of bidding had been successfully concluded with 92 projects having been selected, which in total represented 6 385 MW of capacity. According to the South African Treasury this attracted a total of R193bn in private sector investment, of which 28% (R53.2bn) came from foreign investment [13]. The total capacity allocated to each kind of technology is given in Table 2.1.

Table 2.1 Breakdown of the REIPPPP Capacity Allocation by Bid Window and Technology

Technology	Capacity allocated in First Bid Window (MW)	Capacity allocated in Second Bid Window (MW)	Capacity allocated in Third Bid Window (MW)	Capacity allocated in Fourth Bid Window (MW)
Solar Photovoltaic	710.2	348.9	442.5	813
Onshore Wind	641.4	559	788	1367
Concentrated Solar Power	150	50	400	-
Small Hydro (≤ 40 MW)	-	14.3	-	4.5
Landfill Gas	-	-	18	-
Biomass	-	-	16	62
Biogas	-	-	-	-
Total	**1 501.6**	**972.2**	**1 664.5**	**2246.5**

With the exception of the concentrated solar power projects from bid window 3 onwards, the power purchase agreements associated with the REIPPPP implement a flat feed-in tariff. The offering from Independent Power Producers (IPPs) therefore focus on maximising the return on investment by locating plants for maximum cumulative energy production.

One of the major successes of the REIPPPP has been the continually decreasing prices in the successive rounds of bidding, specifically for wind power projects and solar photovoltaic power projects. In bid window 1, the average price of wind energy per MWh was R1 363 (in inflation adjusted 2014 Rand), which decreased to R619 in bid window 4. In the case of solar photovoltaic energy, the price decreased from R 3 288 to R786 respectively. As of September 2016, 43 of the REIPPPP projects are fully online, representing 2 062 MW of capacity, including 13 wind farms (953 MW), 27 solar photovoltaic farms (995 MW), one concentrated solar power plant (100 MW) and two hydroelectric power plants (14.3 MW).

2.2.3 Integrated Resource Plan Update 2013

An updated version of the IRP was released for public comment on 21 November 2013. This version accounted for new developments in the energy sector in South Africa, such as updated technology costs as well as a revised electricity demand outlook. The IRP update projected that the annual electricity demand in 2030 would be in the range of 345-416 TWh as opposed to 454 TWh expected in the original IRP, in addition to a lower peak electricity demand of 61 200 MW as opposed to 67 800 MW.

Although the IRP update assumed an optimistic Gross Domestic Product (GDP) growth rate of 5.4% as stated in the National Development plan (NDP) of South Africa, it did emphasise the risk of overbuilding generating capacity to meet that target. Due to the increased uncertainty related to the potential for shale gas exploration in South Africa, increased climate mitigation requirements and uncertainty in the cost of nuclear capacity and future fuel costs, the IRP update also proposed a more flexible approach to generating capacity planning to take into account the different outcomes based on changing assumptions which differed from the more fixed approach used in the original IRP.

In the long term the IRP update provides recommendations on which investment to pursue under different conditions, should they arise. In the short term (specified as two to three years) the IRP update provided several guidelines which include the proposition that the decision to build more

nuclear power capacity in South Africa could be delayed owing to the reduced demand forecast, options for regional and domestic gas exploration are pursued and shale exploration stepped up, and that the Renewable Energy Independent Power Producer Program be continued with additional annual rounds (of 1 000 MW PV capacity; 1 000 MW wind capacity and 200 MW CSP capacity).

The base case scenario in the IRP update, which represents an update of the original IRP assumptions, proposed the following generating capacities for 2030:

Table 2.2 Technology options arising from IRP 2010 and the IRP Update Base Case in 2030 [6].

Technology option	**IRP 2010 (MW)**	**IRP Update Base Case (MW)**
Existing Coal	34746	36230
New Coal	6250	2450
Combined Cycle Gas Turbines	2370	3550
Open Cycle Gas Turbines/Gas	7330	7680
Hydro Imports	4109	3000
Hydro Domestic	700	690
Power Sharing (including Imports)	2912	2900
Nuclear	11400	6660
Solar Photovoltaic	8400	9770
Concentrated Solar Power	1200	3300
Wind	9200	4360
Other	915	640
TOTAL	**89532**	**81350**

The notable changes include the reduced need for new coal and nuclear generation capacity, as well as a different composition of renewable energy generating capacity (increased solar photovoltaic and concentrated solar power capacities and reduced wind power capacities). The financial and technical data that was used to formulate the IRP update was again provided by EPRI.

The IRP update of 2013 has not been officially adopted, and as such the IRP 2010 is still the official plan of the South African government. However, many stakeholders across different industries regard the IRP 2011 to be out of date.

2.3 Renewable Energy Simulation

2.3.1 Overview

In order to do renewable energy integration studies, renewable power simulations need to be performed. Some studies focus on simplified annual energy production (AEP) simulations using wind speed and solar irradiance probability distributions, but the focus here is on spatio-temporal simulation that yield simulated power time series associated with a specific location. This section introduces the approaches that have been observed in the literature to do spatio-temporal wind and solar photovoltaic power simulation.

2.3.2 Wind Power Simulation

The power output of the wind farms depends primarily on the wind speed at each wind turbine in the wind farm. An idealised wind turbine power curve is shown in Fig. 2.1. As the wind speed increases, the wind turbine generates increased power up until a rated wind speed, after which the power production remains constant at the nameplate capacity (rated power). When the wind speed passes

the cut-out wind speed, the wind turbine shuts down for safety reasons and ceases to produce any power.

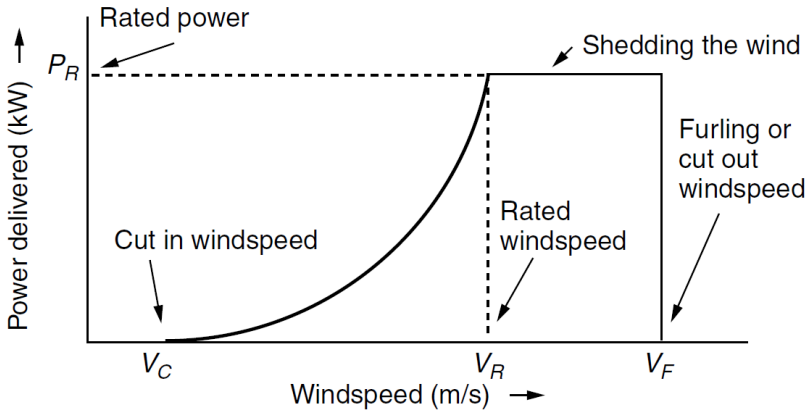

Fig. 2.1 ***Idealised wind turbine power curve*** [14]**.**

The wind speed at each turbine is dependent on wake effects resulting from large objects such as buildings or trees as well as wind turbines that are located upwind. The wake effects changes depending on local typography, the speed of the wind coming into the wind farm and the direction that the wind is coming from. The layout of wind farms are highly dependent on the local landscape and local wind resource, and are typically designed using microsite level design software packages such as WAsP (Wind Atlas Analysis and Application Program).

The majority of academic papers that focus on future wind power integration studies ignore the specific layout of potential wind farms and therefore ignore the wind direction and wake effects, instead choosing to consider the wind speed data only. In 2013 both Carrillo *et al.* [15] and Lydia *et al.* [16] published review articles on the approaches used to model wind turbines.

A common approach is to simulate wind power time series using either a generic wind turbine power curve or a wind turbine power curve that has been obtained from a manufacturer. It is usually not specified exactly how the wind turbine power curves are used to convert the historical wind speed data into wind power data, and it is assumed that discrete points on the wind turbine power curves are used to produce a function in the software using interpolation. As the studies usually focus on onshore wind farms, the size of the wind turbines typically varies from 1 GW to 3 GW. Degeilh and Singh performed a wind farm location optimisation study in Texas (USA) using 3 MW Vestas V90 power curves [17]. Santos-Alamillos *et al.* investigated the spatial variability of wind energy resources in Spain using a cubic spline interpolation method to model 2 MW Vestas V90 turbines for onshore locations and 3 MW Vestas V90 turbines for offshore locations [18].

Some academic papers instead make use of piecewise-defined functions that imitate typical wind turbine power curves. In this approach, the wind turbine power curve is generally divided into four parts, with each part described by a particular mathematical function. The functions are typically two horizontal functions that go through the origin for wind speeds lower than the cut-in wind speed and higher than the cut-out wind speed, a horizontal function that goes through the rated power for wind speeds above the rated wind speed and a polynomial or cubic function for wind speeds between the cut-in and rated wind speeds. An example of this can be seen in wind farm location optimisation studies performed by McWilliam *et al.* in Alberta (Canada) [19], Lowery and O'Malley in the United Kingdom [20] and Grothe and Schnieders in Germany [21].

Ignoring the local typography and layout of a wind farm will necessarily have an impact on the accuracy of the simulation. Another issue with wind power simulation is the spatial resolution of the historical wind speed data. A multi turbine power curve methodology was developed by Nørgaard and Holttinen to compensate for single historical wind speed time series that represent large geographical areas [22]. The method involves several steps but essentially involves a convolution of the Gaussian distribution with a chosen wind turbine power curve in order to approximate the smoothing effect of distributing many turbines in a relatively small geographic area. The methodology takes into account the size of the geographic area, the mean wind speed and the wind turbulence intensity, and is shown to simulate historic wind power outputs more accurately than just using a wind turbine power curve. A visual representation of the multi-turbine power curve is shown in Fig. 2.2. An approach similar to that of Nørgaard and Holttinen was used by Reichenberg *et al*. to investigate the variance dampening effect of optimising the geographic location of wind farm locations [23].

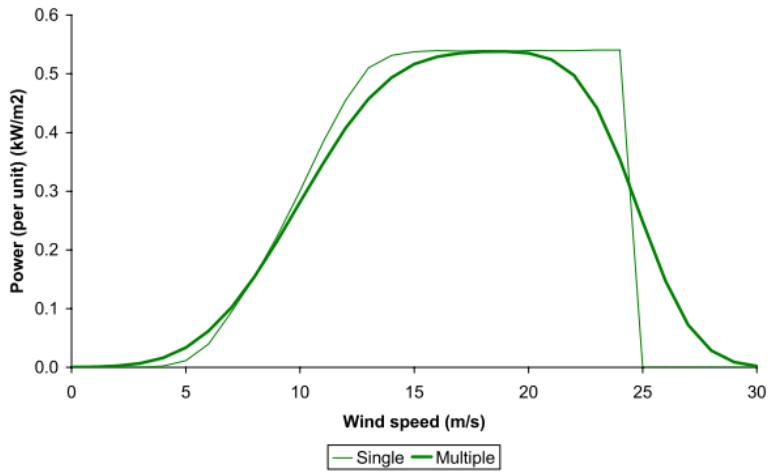

Fig. 2.2 Visual Representation of the multi-turbine power curve approach [22]**.**

A similar modelling method to that of Nørgaard and Holttinen was also used by Andresen *et al*. to produce a renewable energy atlas for energy system analysis for Denmark [24], where historical wind power production data was used to fine tune certain simulation parameters in order to improve accuracy. The authors compared the multi-turbine power curve approach with the normal (single) wind turbine power curve interpolation approach, and found that the multi-turbine power curve approach showed better agreement with the actual wind turbine output data as can be seen in Fig. 2.3.

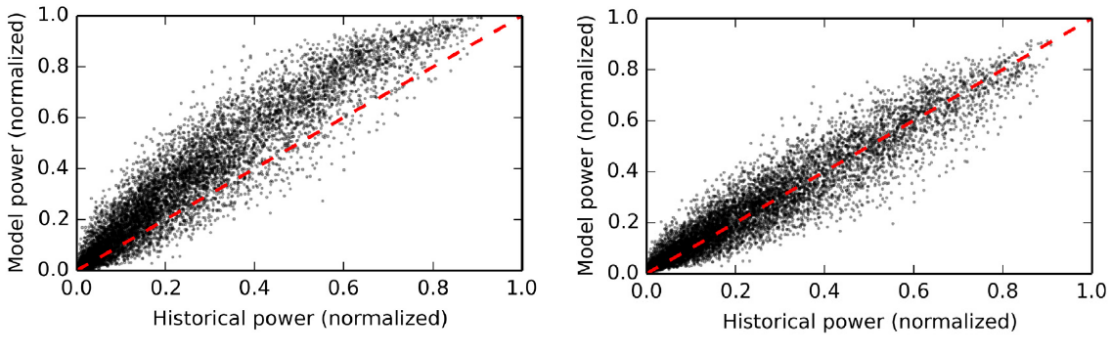

Fig. 2.3 Comparison of the single wind turbine power curve interpolation approach (left) and the multi-turbine power curve approach (right) in the study by Andresen et al. [24]***, both plotted against actual historical wind turbine outputs.***

Other novel approaches to wind power simulation have also been proposed. Wood *et al*. developed a stochastic model to produce synthetic time series of wind power at several locations based on a measured time series of wind speed from a reference site [25]. Using a case study in south-eastern Australia it was shown that, even though the local typography was ignored, the stochastic properties of the modelled time series compared well measured data.

2.3.3 Solar Photovoltaic Power Simulation

The power output of the solar photovoltaic farms depends primarily on the solar irradiance that is inclined on the solar photovoltaic panel, also referred to as the tilted irradiance, and the temperature of the photovoltaic cell, although many other factors can influence the power output. Fig. 2.4. shows the three irradiance components which make up the total inclined irradiance, namely the direct irradiance, the diffuse irradiance and reflected irradiance [26]. The direct irradiance is the irradiance that hits the panel on a direct path from the sun, the diffuse irradiance is the irradiance that has been scattered by molecules and particles in the atmosphere and the reflected irradiance is the irradiance that is reflected off other objects in the area surrounding the panel.

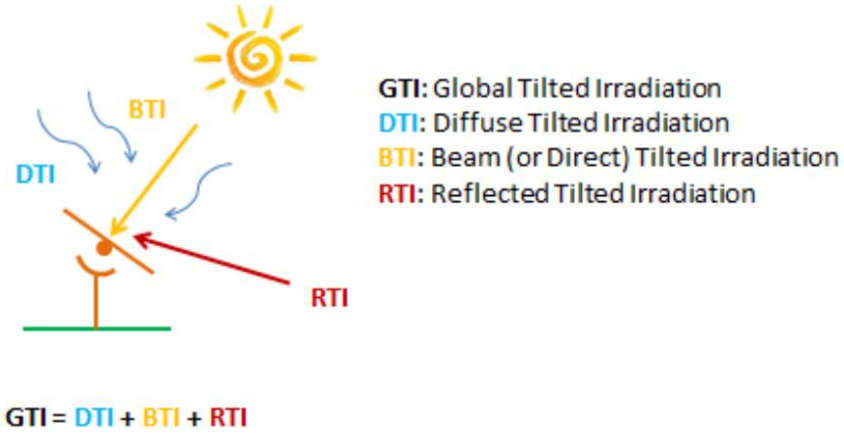

Fig. 2.4 The three components that make up to total inclined irradiance [26]**.**

Mahela and Shaik published a review on grid interfaced solar photovoltaic systems [27], including an overview of all the technical aspects involved in a solar photovoltaic system including the solar cell, the PV array, maximum power point tracking, filters, DC-DC converters, inverters and control techniques. These technical details will not be further investigated here as the interest is in a simple

model topology to simulate solar photovoltaic power. A simplified layout of a typical grid-connected solar photovoltaic system is shown in Fig. 2.5. The solar photovoltaic panels produce DC power which is converted to AC power by an inverter in order to facilitate connection to the grid [14]. The inverter efficiency depends on the percentage of full load. A typical inverter efficiency curve is shown in Fig. 2.6.

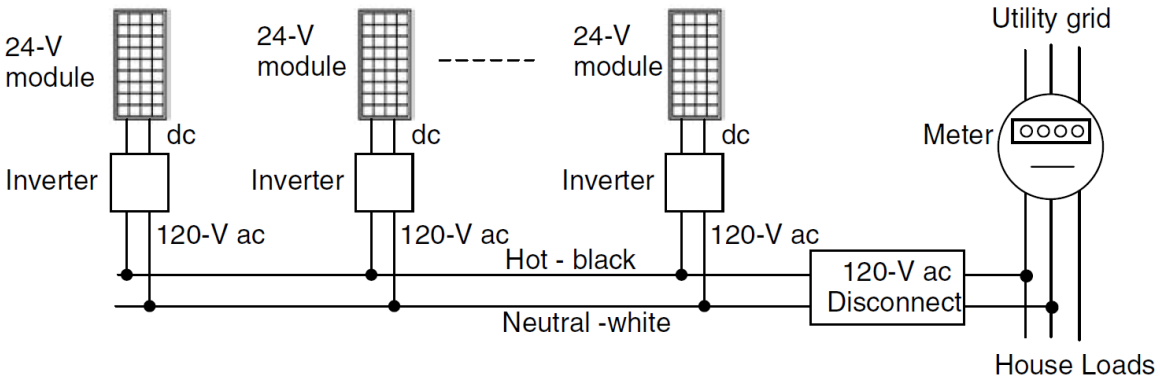

Fig. 2.5 Simplified layout of a typical grid connected solar photovoltaic system [14]**.**

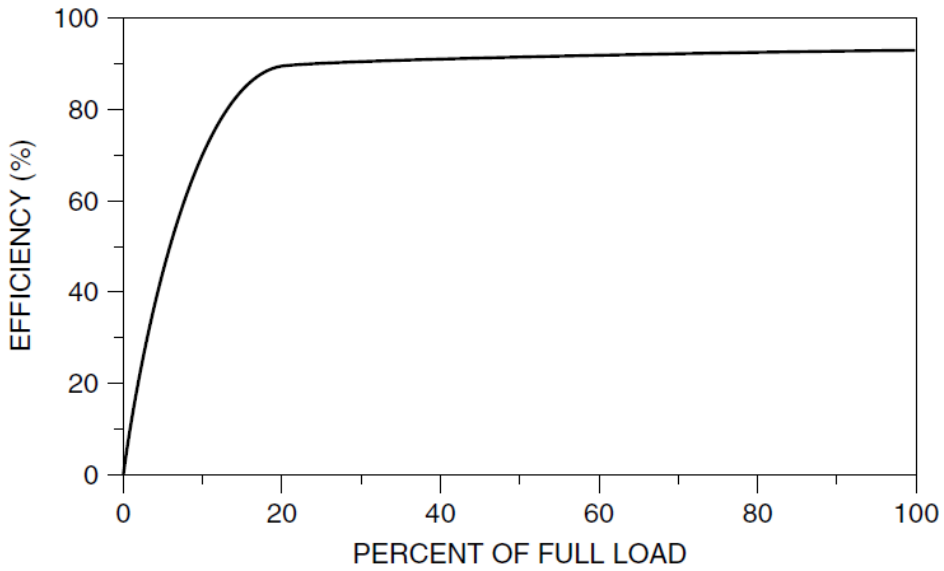

Fig. 2.6 A typical inverter efficiency curve [14]**.**

Solar photovoltaic power simulations are usually performed using one of several existing software packages. Some of the software packages that are used include:

- PV Watts [28]: A free tool developed by NREL that is used exclusively to estimate the energy production and cost of grid-connected photovoltaic systems.
- System Advisor Model (SAM) [29]: A free tool developed by NREL that is used to assess the performance and financial viability of large renewable energy projects, including photovoltaic systems, battery storage, concentrated solar power, geothermal power, biomass power and wind power.
- PVSyst [30]: A commercial software package that is used to perform detailed solar photovoltaic power simulations for prospective installations in order to assess the financial viability.

2.4 Weather Datasets

2.4.1 Overview

In order to perform the wind power and solar photovoltaic power simulations described in section 2.3, historical weather data with adequate time and spatial resolution are required. Depending on where the in world these renewable power simulations are to be performed, this data might or might not be available. This section introduces some major open source and proprietary databases that provide this kind data.

2.4.2 Wind Datasets

There is a variety of wind data available in the world today. Wind data can generally be divided into three categories based on the spatial resolution of the data, namely macroscale (50 km–200 km), mesoscale (1 km–50 km) and microscale (10 m–100 m). Macroscale wind data is found in global weather databases such as the Modern-Era Retrospective analysis for Research and Applications (MERRA), a database of Nasa. These datasets are modelled and compiled using a variety of sources including weather stations, aircraft and satellite instrumentation [20]. Mesoscale wind data, which is usually modelled using macroscale wind data and other inputs, is typically used for large-scale wind power integration studies. Microscale wind data is needed for wind turbine siting within a wind farm, and is modelled using either measured wind data at a certain location or mesoscale wind data as well as local typographical inputs.

Wind datasets, also called wind atlases, are datasets that provide statistical information on the wind resource of a particular area on either a mesocale or microscale. Wind atlases generally provide wind speed probability distributions, wind roses (diagrams showing the relative frequency of wind directions) and wind resource maps that are constructed from the data, and most wind atlases additionally provide wind speed and wind direction time series data at a certain time resolution, usually at either 10 minute or hourly intervals.

Wind atlases can generally be divided into two categories based on how they were produced, namely observational wind atlases and numerical wind atlases [31]. Observational wind atlases are created using microscale modelling methods by incorporating measured time series data of wind speed and direction, as well as characteristics of the local topography including elevation, roughness and obstacles, which is usually obtained from satellite data. In the absence of long-term, high quality measured wind data, a numerical wind atlas method is usually applied. Numerical wind atlas methods use macroscale global weather datasets, such as the NCEP/NCAR global reanalysis data-set (National Centers for Environmental Prediction and National Center for Atmospheric Research respectively), as well as local typographical characteristics to produce mesoscale wind data that cover a large area, usually an entire country. There are several numerical wind atlas methods, including the Karlsruhe Atmospheric Mesoscale model (KAMM), the Weather, Research and Forecasting (WRF) model, the High resolution Regional Model (HRM) and the High Resolution Limited Area Model (HIRLAM) [32]. Mesoscale wind data from numerical wind atlases are often compared to observational wind atlases for verification and validation purposes.

2.4.2.1 International Wind Atlases

There are many wind atlases available worldwide and the following review should by no means be considered exhaustive. One of the first comprehensive wind atlases was the European wind atlas [33], which was produced in 1989 by Risø National Laboratory. This wind atlas contained long-term wind speed probability distributions, monthly mean wind speeds, mean cubed wind speeds and the average

daily wind speed pattern for every month. In addition, the spectral power density of the deviations from the average monthly daily pattern was also presented. The statistics were constructed using measured data from 220 meteorological stations as an input to the WAsP computer program. The data from the European wind atlas was used by Beyer and Nottebaum [34] to synthesise hourly wind speed time series in 1995.

An observational wind atlas and numerical wind atlas was created for Egypt in 2006 [35] with a spatial resolution of 7.5 km. The numerical wind atlas, which utilised the KAMM mesocale model, covered the entire land area of Egypt, while the observational wind atlas covered the areas surrounding 30 meteorological stations.

A wind atlas for the Iberian peninsula was presented by Gastón *et al*. in 2008 [36] using the Skiron mesoscale model for the wind speed in 2006 on a 0.1° spatial resolution. The wind map that was produced was validated using measured wind data from 50 meteorological stations.

A wind atlas was created for Greece in 2006, and updated in 2008, using measured wind data from around 200 measurement stations. Kotroni *et al* [37] produced a complimentary wind atlas for Greece in 2013 using the MM5 numerical wind atlas method for a typical wind year at 10-minute time resolution and 2 km spatial resolution. The typical wind year was constructed using data from certain months over a 20 year period using the method proposed by Hall *et al* [38].

In 2008, a Finnish wind atlas was produced using the HIRLAM and AROME (Application of Research to Operations at MEsoscale) mesoscale models [39]. This wind atlas replaced the Finnish wind atlas of 1991. A spatial resolution of 2.5 km was employed, but in areas with the most favourable characteristics for wind power production, the output of the mesocale model was used as an input to a diagnostic downscaling method with WAsP to create wind data with a higher spatial resolution of 250 m. A 48-month reference period was constructed for the mesoscale simulation from data that represents 1989 until 2007.

In 2015 the National Renewable Energy Laboratory (NREL) and Vaisala collaborated to produce the Wind Integration National Dataset (WIND) Toolkit that is meant to support wind power integration studies in the United States [40], expanding upon the Western Wind and Solar Integration Study (WWSIS) data set that was created in 2008. The WIND Toolkit presents meteorological data (including wind speed) produced by the WRF method, with a 5-minute time resolution and 2 km spatial resolution for more than 126 000 sites that have been identified as potential future locations for wind farms. The data spans the period from 2007 until 2013, and also includes the wind power production time series produced using site-specific wind turbine classes and simulated power forecasts that have been produced to mimic the power forecast methods used in industry.

2.4.2.2 Wind Atlas of South Africa

The Wind Atlas of South Africa (WASA) project was started in 2009 by the South African government and several industry and academic partners including the South African National Energy Research Institute (SANERI), the Council for Scientific and Industrial Research (CSIR), the University of Cape Town (UCT), the South African Weather Service (SAWS), Risø National Laboratory and Technical University of Denmark (DTU). The project aimed to produce both an observational and numerical wind atlas for South Africa, with the former being used to validate the results of the latter. The project would cover a large region spanning across the Northern Cape, Western Cape and Eastern Cape, as this represented the area where most of the wind farms in South Africa were projected to be built.

For the observational wind atlas, 10 masts were erected at selected sites throughout South Africa to record wind speeds at different heights, as well as other meteorological data. The location of the masts can be seen in Fig. 2.7

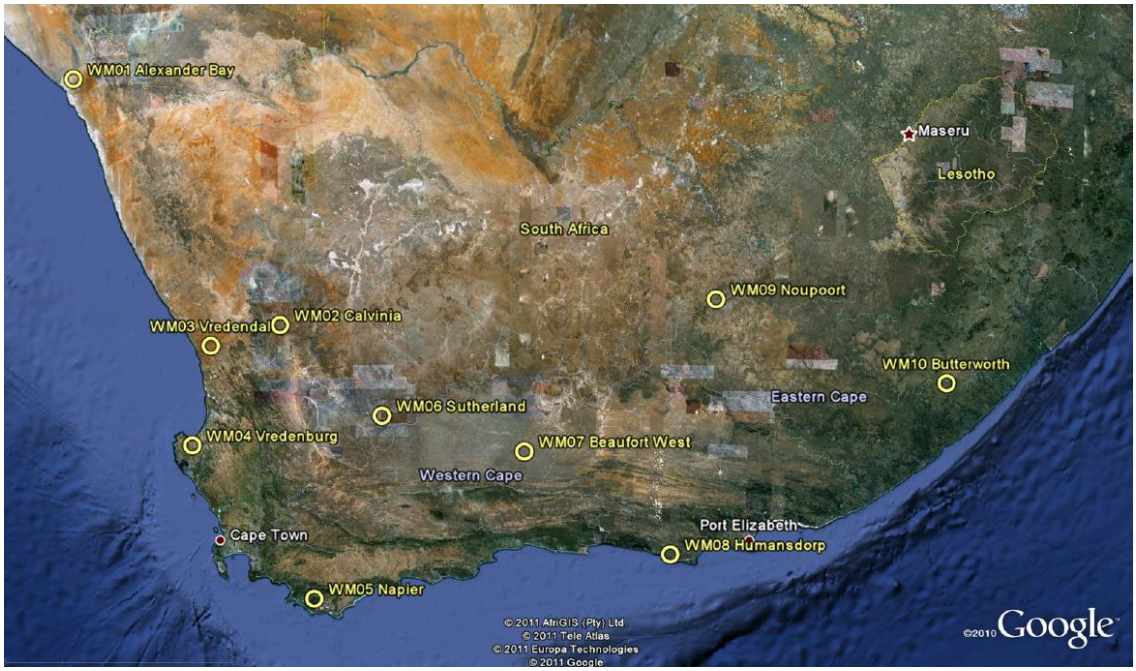

Fig. 2.7 Locations of the 10 meteorological masts in the WASA project [41]**.**

Two numerical wind atlases have been produced in the WASA project. The first numerical wind atlas was produced using the KAMM-WAsP method in 2012, resulting in 15 000 data points on a 5 km x 5 km spatial resolution. The second numerical wind atlas was produced in 2014 using the WRF method, resulting in 40000 data points on a 3 km x 3 km spatial resolution. Each of these data points are available for download by the public as .lib files, which can be used as an input in the WAsP program to do wind turbine micrositing within wind farms. It was found that the KAMM-WAsP method slightly underestimated the wind resource when compared to observational wind atlas, with a mean bias and mean absolute bias of −8.2% and 9.3% respectively. The WRF method performed better, showing an average under or overestimation of 4.7% across all sites [31]. Overall, the WRF method overestimated the wind resource by 2.5%. A map of the mean wind speeds across the project area can be seen in Fig. 2.8.

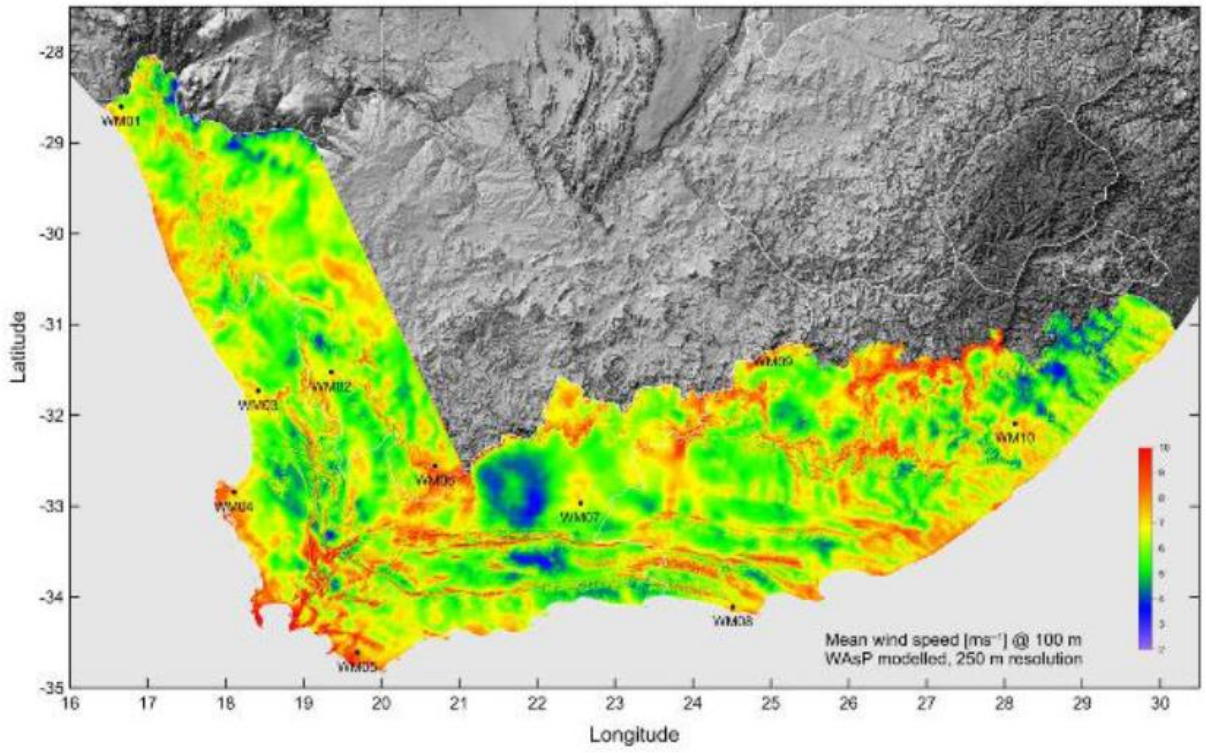

Fig. 2.8 Mean Wind Speed Map produced by the WRF method in the WASA project [9]**.**

The WASA project also availed itself of time series data, which was produced using the WRF method, with a spatial resolution of 27 km x 31 km resulting in 527 time series covering the project area. The time series data comprised hourly wind speed at 100 m and wind direction for the period 01-09-1990 to 31-12-2012.

2.4.3 Solar Datasets

In order to perform solar photovoltaic power simulations, a minimum requirement is historical solar irradiance data and temperature data. Temperature data is usually sourced from national weather services, while solar irradiance data can be obtained from weather stations or calculated from meteorological satellite data. There are many free sources of solar irradiance data, although high quality data normally comes in the form of proprietary data sources such as SolarGIS [42] or SODA [43].

In 2014, SolarGIS developed maps that showed the annual solar irradiance levels in South Africa. Fig. 2.9 shows annual sums of global horizontal irradiance for South Africa.

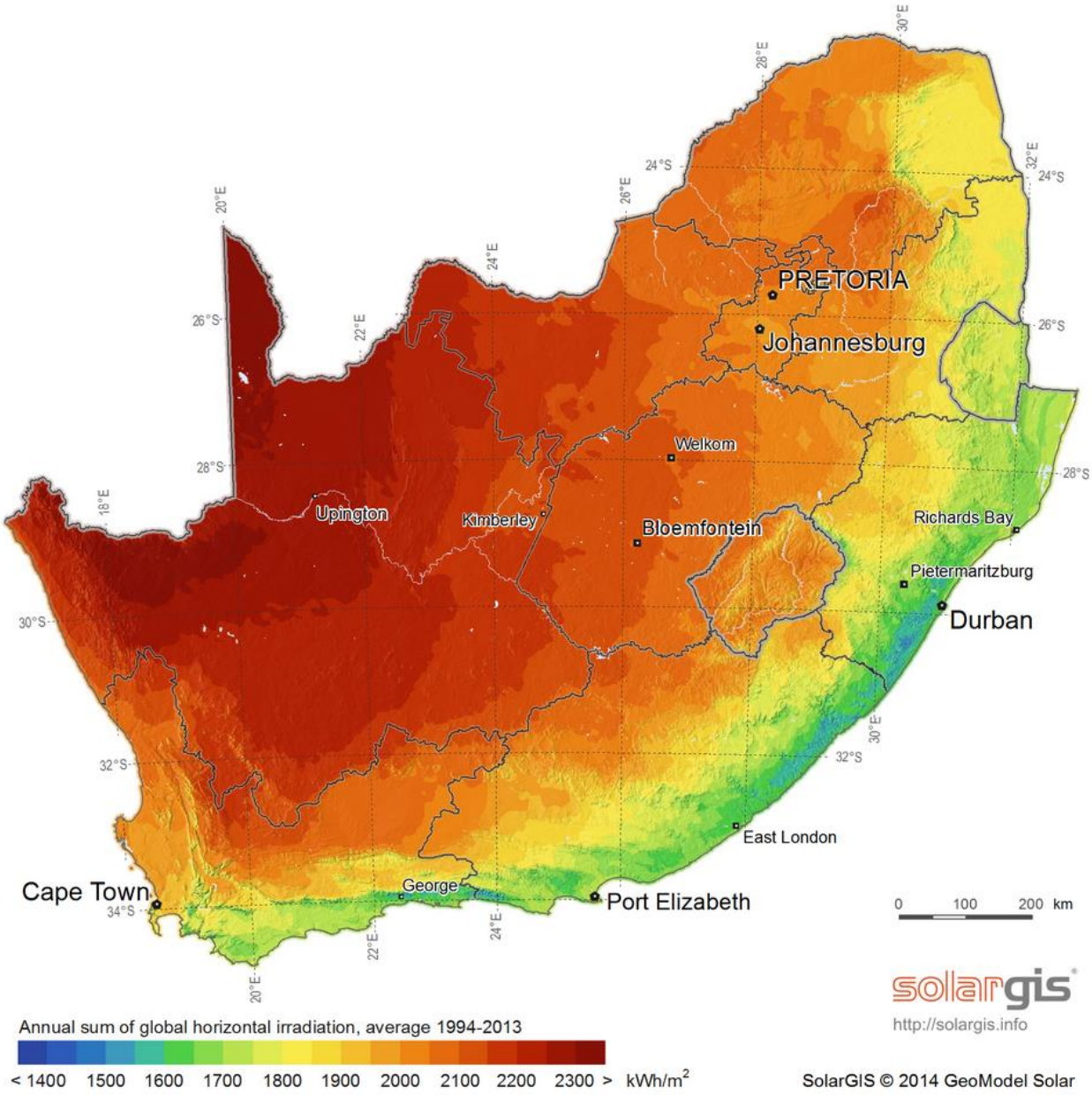

Fig. 2.9 Map of global horizontal irradiance in South Africa by SolarGIS [44]**.**

2.5 Renewable Energy Integration Studies

2.5.1 Overview

There exists a vast amount of literature on renewable energy integration studies. This section introduces two topics that are under consideration in this study. The first is the key performance indicators that are related to increased renewable energy penetration. This topic deals with the ways in which the impact of increasing renewable energy sources on the power system is quantified. The second topic deals with the ratio of wind farm capacity to solar photovoltaic capacity. These two sources represent the main technologies that are under consideration for large scale integration, yet they deliver very different power profiles, which complement the load profile of each country in a different way. Several studies exist that try to determine the optimal ratio of wind power to solar power by considering different optimisation targets. A critical aspect of wind and solar power

integration studies that is not considered in this overview, is the need for increased operating reserves, of which a comprehensive review was published by Holttinen *et al.* [45] in 2012.

2.5.2 Key Performance Indicators Related to Increased Renewable Energy Penetration

When a new power plant is added to a power system, its impact on the reliability of the power system is of interest. The reliability of a power system is divided into two parts, namely power system security and power system adequacy [46]. Power system security deals with the ability of a power system to maintain steady power delivery in the event of a critical failure of one of the power system components such as a large power station or a critical transmission line. Power system adequacy deals with the ability of a power system to meet the load demand at any given time, i.e. having enough installed capacity with sufficient reserve, considering all the factors that influence the ability of different technologies to deliver power when it is needed.

2.5.2.1 Power System Security

In terms of power system security, it is broadly understood that renewable energy sources such as wind power and solar power contributes positively to the ability of a power system to absorb critical failures at any given time [47]. The reason for this is twofold. First, both these renewable energy sources are distributed, reducing their dependence on any one transmission link or node. Secondly, the sizes of the generators are considerably smaller than that of conventional generators, meaning that the failure of a typical wind turbine or solar panel is much less significant than that of a coal, gas or nuclear generator. There is concern around the impact of cloud cover moving over solar photovoltaic plants, which could result in a very sudden interruption of power flow from that plant. Jewell and Ramakumar [48] used solar power simulations to quantify the time that it would take, in a worst case scenario, for a solar photovoltaic power system to go from full power production to zero power production when a squall line of cloud cover moves across an otherwise clear sky. They found that in the case where the solar photovoltaic power system is spread across 10 km^2, the time for complete power loss is 1.8 minutes. In the case where the solar photovoltaic power system is spread across 1 000 km^2 and 100 000 km^2, the time for complete power loss increases to 17.6 minutes and 175.7 minutes respectively. Rowlands *et al*. [49] performed a study on solar photovoltaic power dispersion in Ontario, Canada, which found that increasing reductions in solar photovoltaic power variability could be achieved by dispersing solar photovoltaic plants up to 800 km away from each other, after which the reductions in variability become insignificant. Shivashankar *et al*. [50] published a comprehensive review on the methods that are used to mitigate the power fluctuation of solar photovoltaic systems. The methods include geographical dispersion, different energy storage technologies and backup diesel generators. Although graphical dispersion is found to reduce the variability of wind power output, the paper concludes that the use of storage technologies will become indispensable at high penetrations of solar photovoltaic power. The review also mentioned the methods that are used to do solar photovoltaic power forecasts, with artificial neural networks currently outperforming other methods.

2.5.2.2 Power System Adequacy

There are several measures that are used when accessing power system adequacy. These include the loss of load expectation (LOLE) and the loss of load probability (LOLP). The LOLP is the probability that the full load demand will not be met at a given point in time:

$$LOLP_i = p(L_i^T > C_i) \tag{2.1}$$

where $p()$ indicates probability, L_i^T is the total load at time i and C_i is the available generation capacity at time i.

The loss of load expectation (LOLE) is the number of hours during a given timeframe, usually specified as a year, that the load will not be met:

$$LOLE = \sum_{i=1}^{T} LOLP_i \tag{2.2}$$

The LOLE is usually calculated by means of a capacity outage probability table (COPT), which represents the different capacity outage levels and their associated probabilities [51]. A COPT is constructed by convolving the capacities and forced outage rates (FOR) of the conventional generation plants. Convolution of the COPT and the load duration curve results in the LOLE. In the absence of detailed generation plant data, the targeted loss of load expectation (LOLE) is often chosen as 0.1 days/year.

It is difficult to model renewable energy sources in the traditional way using FORs, because their ability to deliver power relies heavily on the weather and not so much on mechanical availability. Conventional generation units can be modelled as 2-state distributions (available or unavailable), whereas renewable energy sources produce a range of different power output levels that depends on the weather. Therefore, in terms of power system adequacy, different penetrations of renewable energy sources result in broadly two different types of studies. At low to medium penetrations of renewable energy sources, a certain amount of conventional generating capacity can effectively be displaced (or in the case of increasing annual load demand, conventional generating capacity expansion can be avoided). In this case, the capacity value and capacity credit are examined, and is further discussed below in section 2.5.2.3. Studies that consider high penetrations, where the capacity credit of renewable energy sources become very low, focus rather on the backup generating or storage needs that will be necessary to maintain the power system adequacy. Studies of this nature are described in section 2.5.2.4.

2.5.2.3 Capacity Credit of Renewable Power Plants

There have been a lot of publications that deal with the capacity value and capacity credit of renewable energy plants, resulting in many different proposed methods to determine these values. To provide a complete overview of all the publications regarding the capacity value and capacity credit of renewable energy sources is beyond the scope of this thesis, and as such the discussion is limited to three publications that have often been cited in the literature. The three publications focus on the methods used to determine the capacity value of conventional units, wind farms and solar photovoltaic farms. We also include one study that performed an in-depth investigation of factors that influence the capacity value calculation of wind farms when using the preferred method from one of the above-mentioned publications.

The capacity value is broadly defined as the amount of additional load that can be served due to the addition of the generator, while maintaining the existing levels of reliability [46]. Capacity credit is simply the capacity value associated with a specific generator, divided by the total power capacity of that generator, as shown here:

$$\text{capacity credit} = \frac{\text{capacity value}}{\text{nameplate capacity}} \tag{2.3}$$

Amelin [52] published a study in 2009 where four methods of determining the capacity credit of conventional power plants were compared. The four methods are:

- the equivalent firm capacity method
- the effective-load carrying method
- the equivalent conventional power plant method
- the guaranteed capacity method.

Each method determines a capacity (usually in MW) associated with a new power plant added to a system that is analogous to the capacity value. In the first three methods, the load demand is taken into account and the methods are all concerned with how the new unit affects the LOLP of the system. In this study the LOLP is calculated using a duration curve that is used to represent the probability distribution of the equivalent load. The duration curve is determined by the Baleriaux-Booth [53] formula. The mathematical details of all the methods can be found in the study [52]. The equivalent firm capacity is defined as the size of a fictitious power plant with a 100% availability that brings about the same decrease in LOLP as the actual added power plant (which will necessarily have an availability of less than 100%). The effective-load carrying method, which was first proposed by Garver [54], determines the largest constant load that can be added to a system due to the addition of the new power plants, without increasing the LOLP. The equivalent conventional power plant method is similar to the firm capacity method, but instead specifies that the fictitious power plant, that will reduce the LOLP by the same amount as the actual added power plant, has a reference availability that is usually specified as 95%. The guaranteed capacity method determines the least capacity which can be expected to be available with a given probability. All four methods were applied to 1000 MW conventional power plant with a FOR of 10%, that is added to test systems with different levels of installed capacity, mean load levels, load variances and availabilities of the existing capacities. All in all there existed 135 different test systems. The existing capacity ranged from 15 GW to 30 GW, the mean load levels ranged from 60% to 73% of installed capacity (the loads were all normally distributed), the load variances ranged from 8% to 12% of mean load and the existing plants availabilities ranged from 90% to 94%. All four methods were also applied to 2800 MW of wind power capacity that has a probability distribution that is based on actual data from Sweden. The size of the wind power capacity was chosen so that it has roughly the same energy production over a given timeframe as the 1000 MW of the capacity of a conventional power plant. The results from the case study showed that the method used to calculate the capacity credit can have a significant impact. The equivalent firm capacity method and the effective-load carrying method displayed similar results, while the equivalent conventional power plant method depends on an arbitrarily chosen availability, but shows the same trends as the first two methods. Expectedly, the guaranteed capacity method, which was the only method that does not incorporate the load demand, did not correlate well with the other methods. Another clear trend was that in both the case of the conventional plant addition and the wind power capacity addition, the capacity credit tended to be higher when added to systems with high LOLP, i.e. the added capacity contributed more to lowering the LOLP. The capacity credit decreased with the penetration level of the added capacity. As expected, the capacity credit for the added wind power capacity was lower than what it was for the added conventional power capacity. The author concludes by suggesting that either the equivalent firm capacity or equivalent load carrying capacity methods be used.

In 2008, the Wind Power Coordination Committee and Power Systems Analysis, Computing and Economics committee of the IEEE Power and Energy Society (PES) set up a task force to provide clarity on the issue of capacity credit of wind power capacity. The taskforce's meeting resulted in the publication by Keane *et al*. [46] in 2011, which put forth a preferred method for the calculation of

wind farm capacity while also reviewing some of the popular approximation methods. The preferred LOLE method consists of three steps:

- In the first step, the LOLE is calculated for a system by considering the load time series and the COPT of the conventional generators as described in section 2.5.2.2.
- In the second step, the wind power output time series of the wind capacity in question is subtracted from the load time series, and the resulting residual load time series is used to calculate a new LOLE as in the first step. The new LOLE will necessarily be lower than the LOLE in the case with no wind power.
- In the last step, a constant load is added iteratively to the residual load time series until the LOLE equals the LOLE that was calculated in the first step.

To be clear, the residual load time series in step 2 above is formulised as

$$L_i^R = L_i^T - \sum_{x=1}^{N} W_i^x \tag{2.4}$$

where L_i^R is the residual load at time i, L_i^T is the total load at time i, N is the number of wind farms, W_i^x is the wind power output at wind farm x at time i.

The authors highlight that this method is based on the original definition of capacity value, i.e. the amount of additional load that can be served due to the addition of a certain wind power capacity (while maintaining the same reliability). The main strength of this method is that is captures the correlation between the wind power output and the load time series. The authors also emphasise that any capacity value calculation is only as reliable as its input data. Due to the significant inter-annual variation, it is stated that using data for one year is not adequate. The data that is required for this preferred method are the following [46]:

- multi-year load time series of at least an hourly time resolution
- wind power output time series that exactly overlaps with the load time series
- complete inventory of the capacity, forced outage rates and maintenance schedules of the conventional generation units.

As this data is not always available, there exist several capacity value approximation methods. The review of the capacity value approximation methods in this publication draw from the work done by Dent *et al.* [55], and the methods include the Garver approximation based method, multi-state unit representation, annual peak calculations and the Z-statistic method. Another approximation method is the peak-period capacity factors method, but the authors indicate that this method should be used as a quick screening method rather than a formal capacity value approximation method because it captures neither the variability of wind power nor the correlation between wind power and load.

The Garver approximation based method stems from a graphical method to calculate the effective load carrying capability (ELCC) of a generator that was introduced by Garver in 1966 [54]. The Garver approximation based method is convenient because it only requires the load time series and the wind power time series. The Garver capacity value approximation makes the assumption that $LOLP \propto e^{\left(\frac{L^T}{m}\right)}$, and calculates the capacity value, a, as follows [56]:

$$a = m \cdot \ln\left(\frac{\sum_{i=1}^{L} \frac{e^{L_i^T}}{m}}{\sum_{i=1}^{L} \frac{e^{L_i^R}}{m}}\right) \tag{2.5}$$

where m is the system characteristic and is explained below, L^T and L^R are the load time series and the residual load time series respectively, i represents the ith data point in the time series with L data points.

The variable m (Garver system characteristic) is defined as the megawatts of load increase necessary to give an annual risk (LOLE) that is e times larger than the designated risk, where e is the base of the system of natural logarithms, 2.718 [54]. Garver provided graphical and computational methods to determine m, as well as a method of approximating it as follows [54]:

$$\text{estimate of } m = \sum_{u=1}^{U} \left(C_u \cdot FOR_u\right) \tag{2.6}$$

where U is the total number of generating units in the system, C_u is the total capacity of the uth unit and FOR_u is the forced outage rate of the uth unit. In the absence of detailed generating unit data, the system characteristic m is sometimes assumed to be 4% of peak load [8].

The difference between the preferred LOLE method for capacity value calculation and the Garver approximation method can best be understood by looking at the load duration curve (LDC). The LDC is visualised by sorting the load time series in descending order, as presented by Ueckerdt *et al.* [8] in Fig. 2.10.

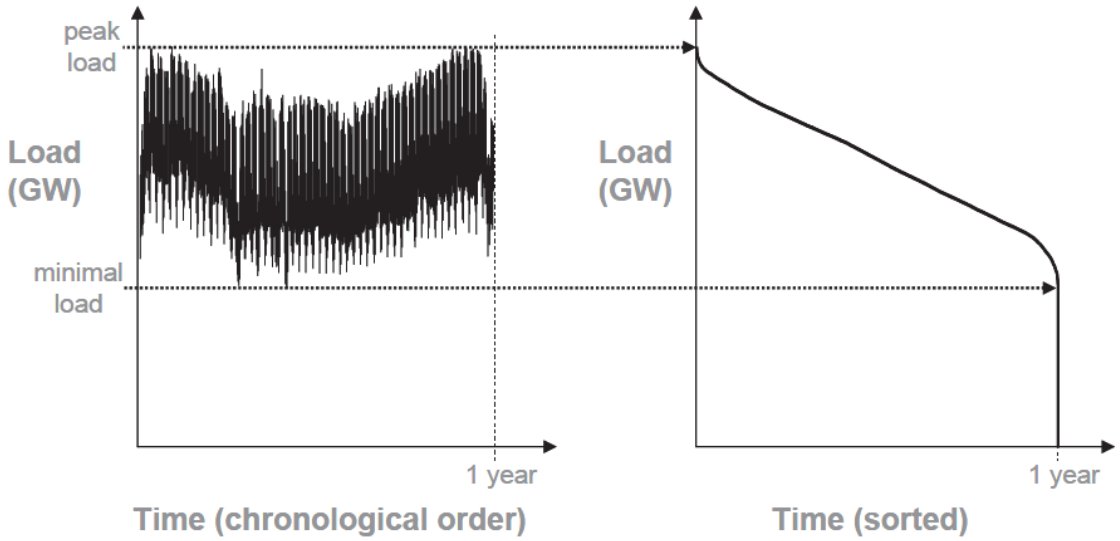

Fig. 2.10 Visualisation of the load duration curve as presented by Ueckerdt et al [8]**.**

The same procedure can be followed in the case of the residual load time series to create the residual load duration curve (RLDC) as seen in Fig. 2.11.

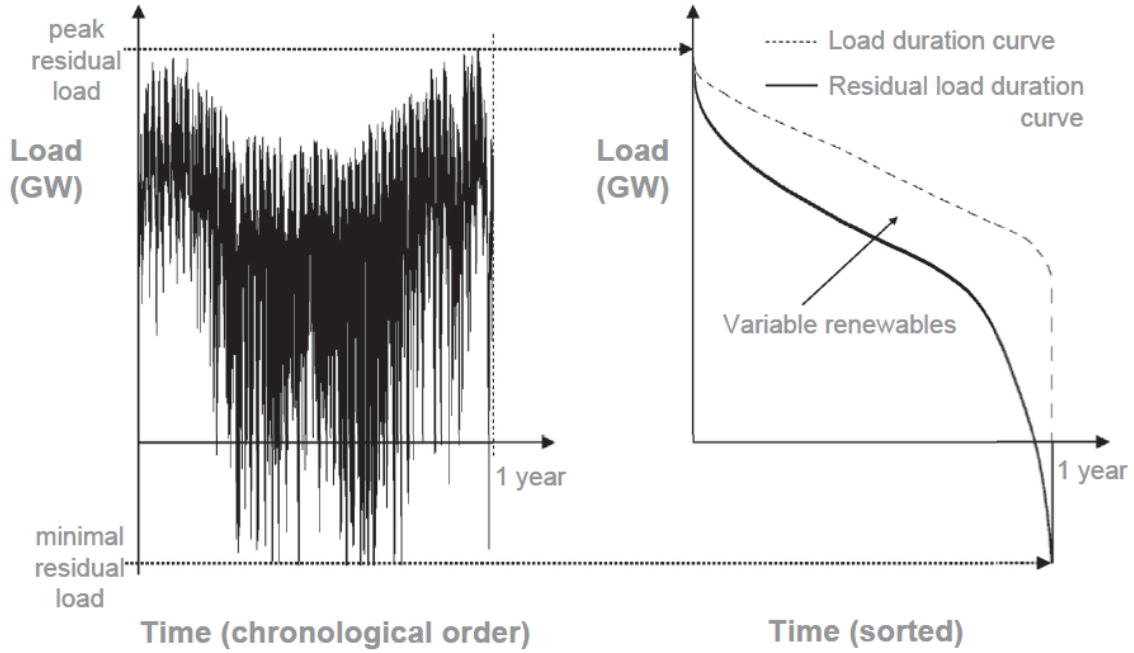

Fig. 2.11 Visualisation of the residual load duration curve as presented by Ueckerdt et al [8]**.**

The preferred LOLE method for capacity value calculation uses a LOLE that is calculated using the FORs of the conventional generating units. This LOLE, which is typically around 0.1 days per year, specifies the single points on the LDC and the RLDC that are considered, close the top left of the graphs in Fig. 2.10 and Fig. 2.11 where the x-axis is for example $2.4/8760$ of the length of the time series. In the Garver approximation based method, where the LOLE is not known, the entire load time series and residual load time series are taken into account, but because the ratio of exponentials is implicit in equation (2.5), the peak load and residual load values to the top left contribute much more than the rest of the respective time series.

If a complete wind power time series that is time synchronous with the load data, is unavailable, the Garver approximation based method can still be used by employing the multi-state unit representation method, where the wind power output is modelled as a power unit that has multiple levels of power output with associated probabilities (ranging between 0 and full rated power). In this case, the capacity value, a, reduces to [57]:

$$a = -\frac{1}{m}\ln\left(\sum_{x}^{X} p_x e^{-m w_x}\right) \tag{2.7}$$

where X is the number of different states that the wind power output can take, p_x is the probability that the wind power output is w_x.

The multi-state unit representation method can also be used on its own, without the Garver approximation. The LOLE is then calculated in the traditional way using the COPT as described in section 2.5.2.2, modelling the conventional generating units as dual state (either available or not) and the wind power units as multi-state. The main weakness of the multi-state representation method is that the correlation between load and wind power output is lost. This can be compensated for by using different probability distributions for different hours of the day, or by employing Markov models for different states of wind power output. However, the effect that certain weather conditions will have on the load is difficult to capture using this methodology.

Dent *et al.* [55] performed a case study in Great Britain, where the peak demand and LOLE are 60 GW and 0.061 hour/year respectively, and found that the Garver approximation based method with multi-state unit representation provided a good approximation, only overestimating the capacity credit at low penetrations when compared to the preferred LOLE method, as can be seen in Fig. 2.12. The three different lines of the Garver approximation based method with multi-state unit representation (90%, 95%, 97%) represents three different cases where the wind power output probability during 10%, 5% and 3% of peak load demand were considered.

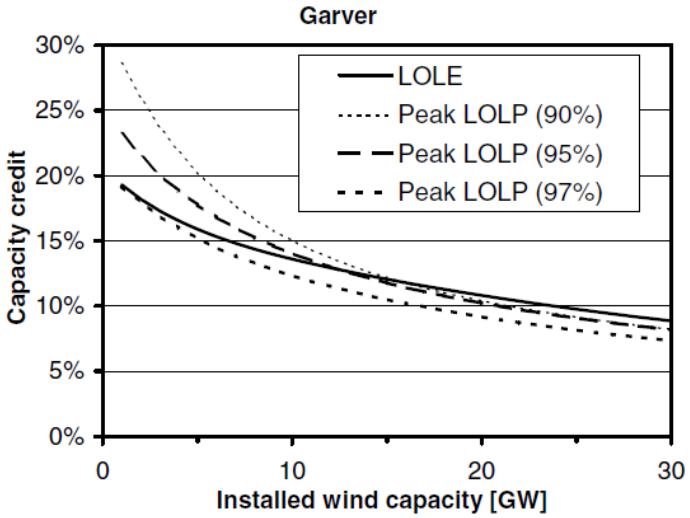

Fig. 2.12 Comparison of preferred LOLE capacity value calculation with the Garver approximation method with multi-state unit representation, for a case study in Great Britain [55].

Annual peak calculations can be performed using multi-state unit representation, by considering only the LOLP at the time of annual peak load. Thus, probability distributions are needed for the peak load and the wind power output during the specific time of year. This measure is used as a proxy for system risk in some countries [46]. Because the peak load only occurs once a year and not necessarily in the exact same time of year, obtaining accurate probability distributions for wind power output is seen as a major hurdle. Several approaches have been followed to mitigate this limitation, including the use of the entire peak season or using a subset of days that imitate the peak load day.

The Z-statistic method, the final capacity value approximation method considered by Keane *et al.* [46], was proposed by Dragoon and Dvortsov [58] in 2006. In this method, the difference between the available resources and the peak load demand, referred to as surplus of available generation, is assumed to have a normal distribution and its mean is given by [58]:

$$\overline{S} = \overline{R} - \overline{L} \tag{2.8}$$

where $\overline{S}$ is the mean surplus during peak hours, $\overline{R}$ is the mean resources available during peak load hours and $\overline{L}$ is the mean peak load. As per the central limit theorem, as the system becomes larger, i.e. as it consists of a larger amount of generating units, the probability distribution of the surplus available generation will approach the normal distribution. The probability distribution of S is shown in Fig. 2.13.

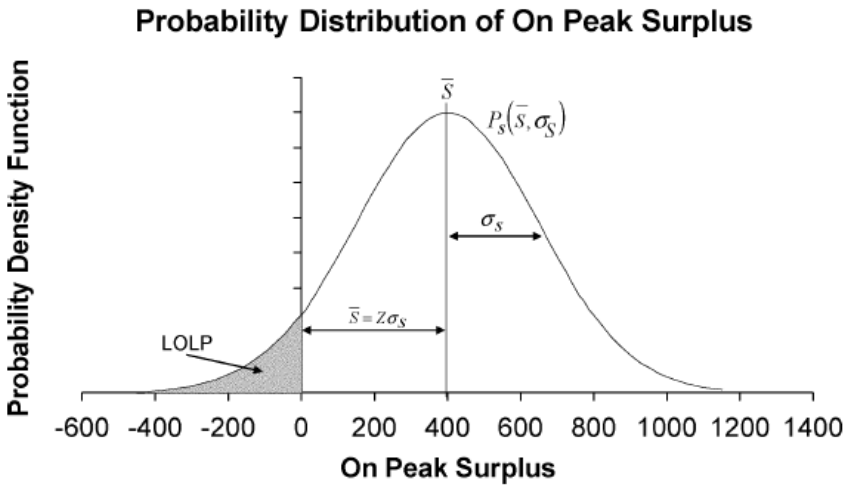

Fig. 2.13 Probability Distribution of Surplus Generation [58]**.**

The paper recognises that the surplus of available generation is a random variable and that the ratio of the expected (mean) surplus to the standard deviation of the surplus is an indication of resource adequacy, as given by the Z-statistic [58]:

$$Z = \frac{\bar{S}}{\sigma_s} \tag{2.9}$$

where σ_s is the standard deviation of the surplus available generation about the mean. As indicated on Fig. 2.13, the LOLP probability is calculated as the area of the probability distribution that falls to the left of zero, i.e. when the load exceeds the available generating capacity. It follows that systems with higher Z-statistics will have lower LOLPs. When additional generating capacity, such as wind power capacity, is added to the system, the Z-statistic will increase. In this case, the amount of load that can be added to the system, while keeping the Z-statistic constant (maintaining a constant LOLP), is defined as the effective load carrying capability and provides the approximation for the capacity value of wind power. More formally, the capacity value, a, is approximated as [58]

$$a = \bar{\mu} - \frac{Z_0 \sigma_w}{\sigma_s} \tag{2.10}$$

where $\bar{\mu}$ is the mean wind power output, Z_0 is the Z-statistic before the addition of wind power and σ_w is the standard deviation of the wind power output. There are two assumptions in this method.

- When adding wind power output, which typically does not have a normally distributed power output, the shape of the surplus available generation does not change significantly (although the mean and standard deviation might change).
- The standard deviation of the wind power output, σ_w, is smaller than the standard deviation of the surplus available generation, σ_s.

Both these assumptions only hold true for low penetrations of wind power. Indeed, in the case study by Dent *et al.* [55] of Great Britain that was mentioned above, the results of the Z-statistic method started deviating from the preferred LOLE method for higher penetrations of wind power, as can be seen in Fig. 2.14 (here the preferred LOLE method is indicated as “COPT”, while “Normal” indicates a method that is similar to the preferred method with the addition that the conventional generating

fleet availability is modelled as a normal distribution instead of using the FORs of individual unitsto compute a COPT).

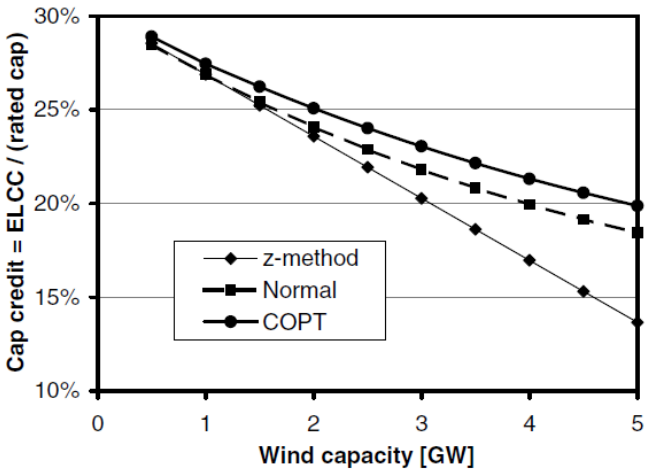

Fig. 2.14 Comparison of preferred LOLE capacity value calculation (marked as "COPT") with the Z-statistic method approximation for capacity value for a case study in Great Britain [55]**.**

In 2016, Nguyen *et al*. [59] published a study on the factors that influence the capacity value of wind power. The method used to calculate the capacity value in this study is the preferred LOLE calculation method from Keane *et al*. [46]. As discussed above, the traditional factors include FORs of conventional power stations, system reliability targets, and the correlation between wind power output and system load which is captured by the residual load. This in depth investigation, which used the Australian National Electricity Market power system as a case study, examined the effects of the number of wind farms and wind installed capacity, as well as the length of historic time series data on demand and wind resources. The study concluded that subjective factors regarding wind power simulation can affect the capacity value estimates and highlighted the importance of capturing extreme risk events in the data, such as periods of extremely high temperatures which could result in high levels of demand. In the case of the Australian National Electricity Market, it was found that extreme load events occurred for about nine days in the fifteen year dataset. Including these extreme load events reduced the capacity credit from about 12–15% to about 7–9%. The fact that capacity value calculations showed significant variance in this one study, even when using the preferred calculation method, caused the authors to suggest that capacity value estimates should not be regarded as definite contribution values, but rather as indicative figures that aid policy making and investment decisions for electrical power systems.

Madaeni *et al*. [56] published a study in 2013 on the capacity value estimation techniques for solar photovoltaic power. They compared traditional methods, including effective load carrying capability and equivalent conventional power, with several of the above-mentioned capacity value approximation methods including a weighted capacity factor-based approximation, the Garver approximation based method, the Garver approximation based method with multi-state generators and the Z-statistic method. A case study was performed for 14 sites in the Western Electricity Coordinating Council (WECC) region in the United States with hourly data from 1998 to 2005. The capacity value of 100 MW-DC (translating to 83.4 MW-AC under standard test conditions) of solar photovoltaic capacity was considered for each site in isolation, and as such the authors emphasise that this is a study on the marginal addition of solar photovoltaic power that does not take into account the decreasing capacity values that are associated with large penetrations of solar photovoltaic power. The solar photovoltaic power time series were modelled using the Solar Advisor Model (SAM) of the National Renewable Energy Laboratory. The results show that solar photovoltaic power has a

lower effective load carrying capability than an equivalent conventional power rating, due to the fact that computing the effective load carrying capability involves iterative addition of a constant load, essentially comparing the solar photovoltaic power with a fully reliable generator. It is therefore expected that this value will be lower than the equivalent conventional power rating, where a non-zero FOR is assumed. Using the root-mean-square error (RMSE) between the results of the approximation methods and the capacity value as calculated using the effective load-carrying capability method, it is shown that the weighted capacity factor based method provides the best estimate, although all methods showed a RMSE of less than 10%. The paper also emphasises the cases where capacity values of solar power might be high despite relatively low capacity factors, due to the correlation of solar power with the regional load.

2.5.2.4 Effect of Increasing Share of Renewable Energy on Conventional Generation Type

At larger penetrations of renewable energy, the total capacity credit of the total renewable energy portfolio becomes very low, and the focus in such instances shifts to the storage needs and the type of conventional (dispatchable) generating capacity that will be needed to supply the load. The bulk of today's load is supplied by base-load generating plants using coal, gas and nuclear technologies. The majority of these plants were not designed to ramp up and down on daily or hourly time scales. With a high penetration of variable renewable energy in the power system, the demand for base-load generating will be less, whereas demand for load-following plants and peaking plants will likely increase in addition to the integration of more energy storage capacity and demand side management (DSM) strategies. Relatively few broad studies exist on the type of generating plants that will be needed in the future as the exact generating fleet makeup needed to supplement the renewable energy sources of a region is very specific to the system and physical grid layout. Two such broad studies are presented here, each with their own methodologies to determine the sizes of conventional generation of different flexibility classes. These methodologies are not meant to prescribe the exact makeup, but rather to provide insight into the changing generating needs as the penetration of renewable energy sources increase.

Tarroja *et al*. [60] published a study on the different metrics that can be used to measure the impact of renewable energy on utility load-balancing, using primarily the characteristics of the residual load time series (referred to as the "net load signal"). The characteristics of the net load signal that were considered include parameters such as the maximum, minimum, range and capacity factor, as well as metrics such as the surplus renewable fraction, load duration curve, daily occurrences of maximum/minimum values, generator duration counts and power spectral density. The generator duration counts metric, also referred to as the generator capacity by type metric, is investigated further in this overview. The generator duration counts metric is a novel high-level statistical method that is proposed to estimate the size of balance generator types (peaker, load-following or base-load) that will be required to meet the load. This metric is calculated using only the net load signal and ignores other elements such as the spinning reserve requirements or demand side management.

Each of three types of generators, namely base-load, load-following and peaker plants are assigned a duration period length, which represents the typical average time that the specific type of generator will be online. The duration period lengths are given in Table 2.3. These duration period lengths are based on an examination of actual generator dispatch from Federal Energy Regulatory Commission in the year 2000 for the state of California.

Table 2.3 Generator Type Duration Period Lengths [60]**.**

Generator Type	Duration Period Length	Typical generator types
Peaker	≤5 h	Natural-gas brayton cycle Reciprocating engines
Load-following	6-168 h	Natural-gas combined cycle Natural-gas rankine cycle Natural-gas brayton cycle
Base-load	169+ h	Nuclear rankine cycle Coal-powered rankine cycle Gasified coal-powered combined cycle

Next, the base-load, load-following and peaker plant totals are initialised as 0 MW. Generator duration lengths are obtained by examining the net load signal at different power levels which are increased by equal increments, P_{inc}, from zero. P_{inc} is arbitrarily specified as 10 MW in this study. At each power level, the periods of generator operation at or above that power level are located and each of their durations recorded. A graphical representation of this process is presented in Fig. 2.15. The generator duration lengths (t1, t2, t3, …) are grouped according to duration period lengths of the different types of generators. P_{inc} is then divided into three parts in the same proportion as the generator duration length groupings and added to the base-load, load-following and peaker plant totals.

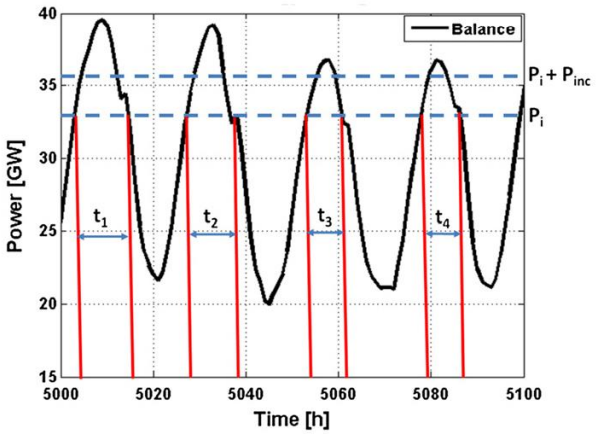

Fig. 2.15 Visualisation of the generator duration counts metric by Tarroja et al. [60]**.**

For example, if at 33 GW, zero of the generator duration lengths are longer than 168 hours, two thirds of the generator duration lengths are between 6 hours and 168 hours and the remaining third of the generator duration lengths are less than 6 hours, 0 MW will be added to the base-load total, 6.66 MW will be added to the load-following total and 3.33 MW will be added to the peaker total. In effect this means that the marginal demand at between 33 GW and 33.01 MW will be served by load-following plants 66.6% of the time and by peaker plants 33.3% of the time. After this process is repeated for successive power levels up until the maximum value of the net load signal, the totals for the different types of generators are obtained.

It is emphasised that this method ignores the actual dispatch scenarios that stem from market operations in regional balancing entities, and that it is intended to provide a rough estimation of typical generator dispatch by type [60]. This method also assumes that there is no uninterruptable base load, and that renewable energy curtailment will only occur in cases where the load is smaller

than the total renewable power, i.e. where the net load signal is negative. In some real world scenarios, it might be more economical to keep base-load stations online and curtail renewable energy sources during low residual demand periods. The authors also emphasise that this method estimates the capacity of different generator types to meet the load, and not the energy obtained from each type, i.e. the capacity factors of each type.

A case study is performed that considered increasing penetrations of wind and solar photovoltaic power, along with a small percentage of hydro, biomass, biogas, and geothermal power in California in the United States [60]. The assumed proportions of the different technologies, which vary by penetration level, are adapted from different sources and can be seen in Fig. 2.16.

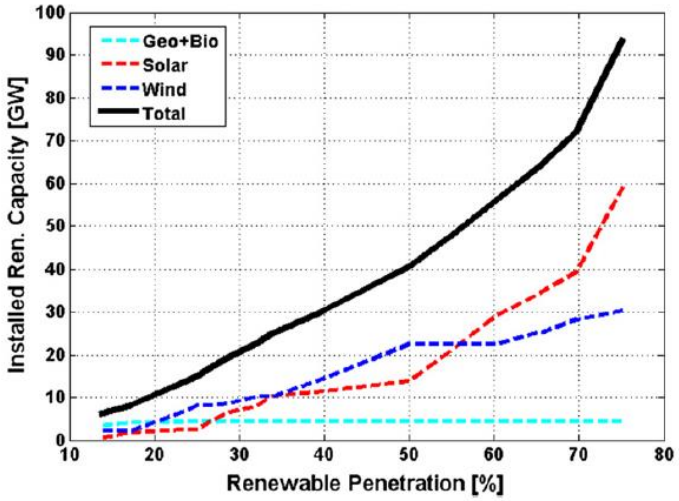

Fig. 2.16 Projected technology proportions in the increasing penetration of renewable energy in the California case study by Tarroja et al. [60]**.**

Using the assumed technology proportions and hourly weather data, the combined renewable energy time series of different penetrations of renewable energy were simulated, ranging from 13% to 75%. These simulated time series are then used in conjunction with load data for the entire state of California to calculate the generator capacity by type metric, which can be seen in Fig. 2.17. It is clear that as renewable energy penetrations increase, the base-load generation total decreases while the load following total remains fairly constant. The peaking generation total also remains fairly constant up until around 40% penetration of renewables, after which it gradually increases, mainly due to the increased reliance on variable wind and solar photovoltaic power. The authors note that increasing solar power capacity tends to displaces base-load capacity with peaking power capacity, while increasing wind power capacity tends to replace base-load capacity with load-following capacity. However, the interaction between the wind and solar photovoltaic power cause the increasing load-following capacity requirements from wind power also to be displaced by peaking power capacity.

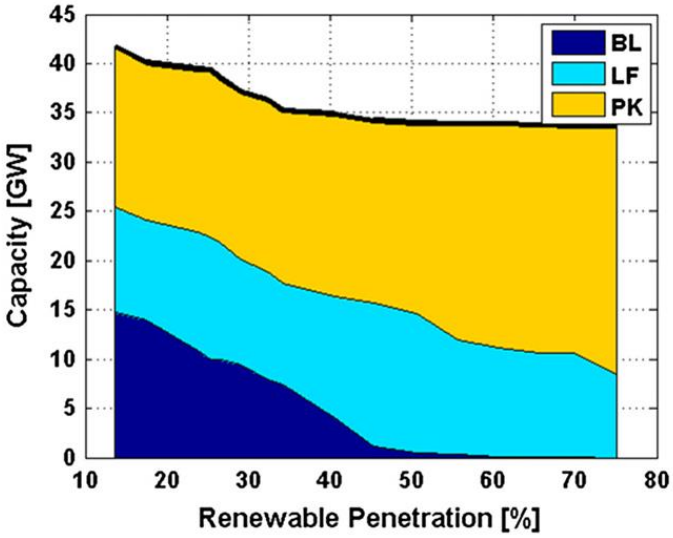

Fig. 2.17 Results of the generator capacity by type metric for the California case study by Tarroja et al. [60]**.**

Schlachtberger *et al*. [61] performed a study on the need for dispatchable generating capacity from different flexibility classes when power systems transform from low to high shares of variable renewable power generation. The flexibility classes try to capture the different timescales of renewable energy variability that are linked to the associated weather patterns, namely diurnal (intra-day), synoptic (intra-week), and seasonal timescales. The study assumes that all residual load will be covered by three sources that represent the aggregated contribution of all generating units in the respective flexibility class. The dispatch of each of the three sources is determined using an optimisation procedure that minimises the excess and deficit of backup energy with small installed capacities and high utilisation. The objective function incorporates terms and variables that dictate the order in which the three systems are dispatched. Two of the three flexibility classes are each assigned a maximum ramp rate by considering the current load time series, i.e. the load time series without significant shares of renewable energy in the system. In order to determine the maximum ramp rate in each of the two cases, the current load time series is smoothed using convolution with a Gaussian kernel. In the case of the slowest flexibility class, the Gaussian kernel has a standard deviation of one week, whereas in the case of the medium flexibility class it has a standard deviation of one day. After the smoothing procedure the signal is differentiated, and the maximum ramp rate of the each flexibility class is assigned as the maximum of the differentiated, smoothed signal. As the fastest flexibility class is assumed to be able to meet the load at all times, its ramp rate is left unconstrained. More details on the methodology can be found in the publication.

The study considers eight years of hourly weather and load data in Germany and Europe as a whole, and assumes that any added renewable energy capacity is made up of 70% wind power capacity and 30% solar photovoltaic power capacity. The result of the dispatch procedure for Germany can be seen in Fig. 2.18, where the dispatch of the three sources in the case of 0%, 50% and 100% renewable energy penetration are shown for a two-week period in October 2000. Note that penetration is defined as the ratio of the capacity factor of the renewable energy to the mean load.

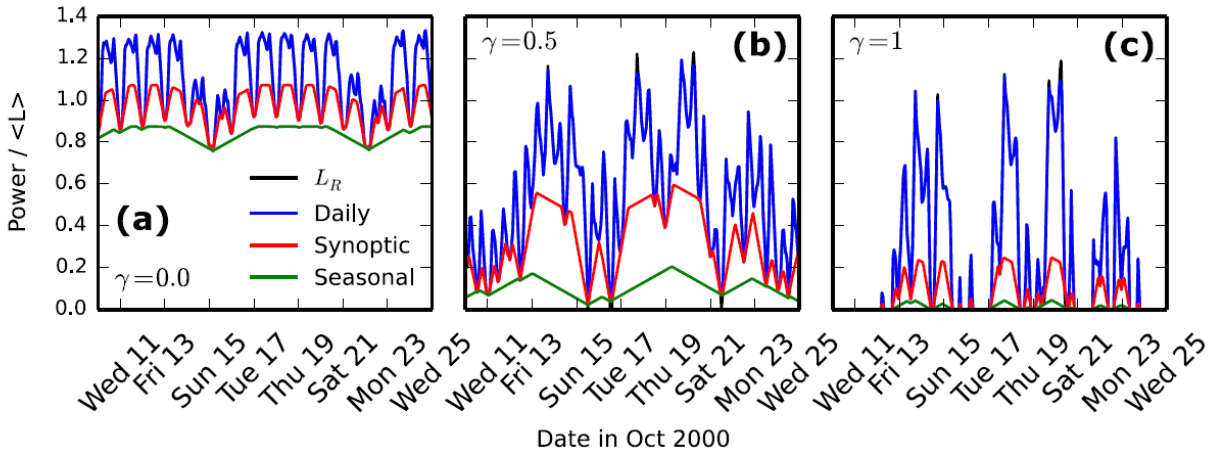

Fig. 2.18 Example of the dispatch result of the three flexibility classes (normalised to mean load) in the case of different renewable energy penetrations in the study by Schlachtberger et al. [61]**.**

The dispatch result is analysed and the maximum capacities for each of the three flexibility classes are captured. The total capacities needed in the three flexibility classes are shown in Fig. 2.19. It is clear that the need for the slowest flexibility class (seasonal) reduces while the share of renewables increases, while the medium flexibility class initially increases up to about a 40% or 50% share of renewables after which it decreases. It is also clear that there are major advantages to integrating the European power system, as the total backup generating capacity reduces from 120% of mean load in the case of Germany alone, to about 90% of mean load in the aggregated European case. This trend continues for higher shares of renewables.

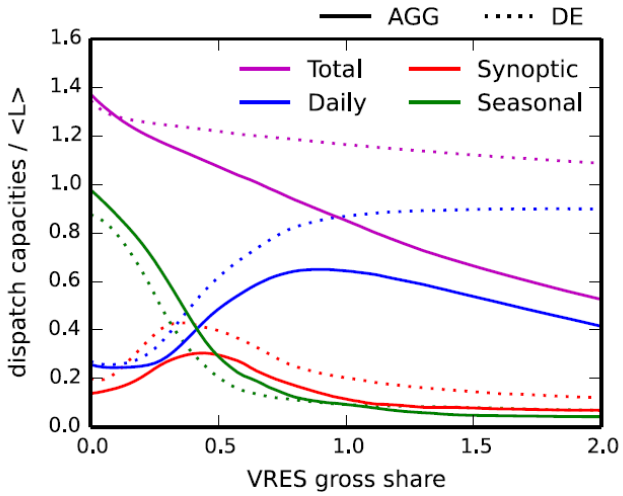

Fig. 2.19 Capacities of the different flexibility classes (normalised to mean load) needed to supplement different shares of renewable energy in Germany (DE) and Europe (AGG) in the study by Schlachtberger et al. [61]**.**

2.5.3 Ratios of Wind Farm Capacity to Solar Photovoltaic Farm Capacity

Many publications exist in the literature that study the optimal ratio of wind power capacity to solar photovoltaic power capacity by considering different simulation and optimisation strategies. The majority of these studies consider large penetrations of renewable energy, typically 20% penetration to 100% penetration and more. Unless stated otherwise, penetration level is defined as the mean power output of the respective renewable technology divided by the mean load.

2.5.3.1 Minimisation of Curtailed Wind and Solar Photovoltaic Energy in New York State

Nikolakakis and Fthenakis [62] performed a study in 2011 on the optimal ratio of wind power capacity to solar photovoltaic capacity in the state of New York in the United States. The authors define a grid flexibility variable, where the minimum level that the conventional generating fleet can ramp down to is stated as a percentage of annual peak load, and the grid flexibility is defined as 100% minus the minimum ramp-down level. For example, if the peak load is 30 000 MW and the minimum ramp-down level is 9 000 MW (30% of peak load), then the grid flexibility is specified as 70%. The authors then optimise the ratio of wind and solar photovoltaic capacity to minimise the spilled power, with any renewable power produced that exceeds the grid flexibility being spilled. The study involves different scenarios with solar photovoltaic only, wind only and a combination of the two technologies where the system is assumed to have grid flexibilities of 70%, 80%, 90% and 100% and the maximum amount of spilled energy is defined by the user. The optimisation consists of an iterative procedure where wind capacity is added to a given solar capacity in 100 MW increments until the spilled energy constraint is reached. Load data, as well as solar radiation and wind data on an hourly timescale was collected for 2005 and power simulations were performed. More details on the power simulations can be found in the study. In terms of the physical distribution of the solar photovoltaic and wind plants, it is assumed that the capacity is uniformly distributed throughout the eligible sites in the state. The impact of increasing wind only and solar photovoltaic only scenarios can clearly be seen by looking at the residual load duration curves (RLDC), as seen in Fig. 2.20. RLDCs were discussed in section 2.5.2.3. The assumed flexibility limits are also shown. The spilled energy is the area between the grid flexibility line and the RLDC on the bottom right of the graphs. At low penetrations of both wind and solar photovoltaic power, most of the produced power is absorbed. However, as the respective penetrations increase, the amount of spilled energy is higher in the case of wind power.

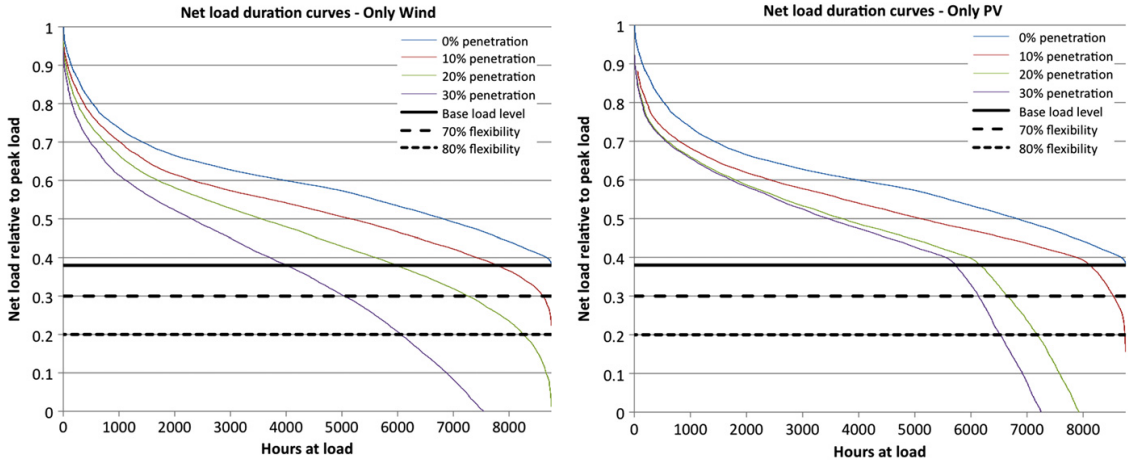

Fig. 2.20 The RLDCs of increasing wind only and solar photovoltaic only scenarios in the study for New York State by Nikolakakis and Fthenakis [62]**.**

By considering a mix of wind and solar photovoltaic capacity, the authors find that a higher penetration of renewable energy can be achieved that result in the same spilled energy in the wind only or solar photovoltaic only scenarios (for a given flexibility level). The results of the optimal mix of wind and solar capacity using the optimisation procedure, allowing for 3% of energy to be curtailed, for each assumed grid flexibility is shown in Fig. 2.21 (the solid lines represent wind capacity and the dotted lines represent solar photovoltaic capacity). As an example, to achieve 25% of energy penetration for the 70% flexibility scenario, 14.5 GW of solar photovoltaic capacity and 11.1 GW of wind capacity are needed. Using this methodology, the optimal ratio of wind to solar power thus depends on the assumed grid flexibility and the penetration level.

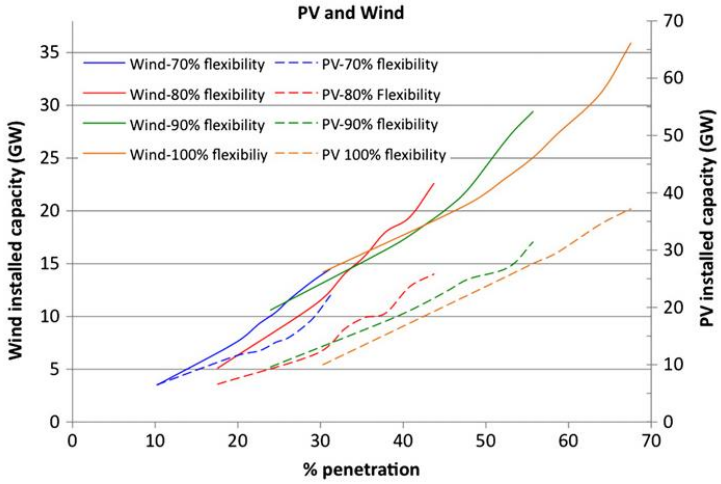

Fig. 2.21 Optimal wind and solar photovoltaic capacities, allowing 3% of renewable energy to be curtailed, for the assumed grid flexibilities in the study for New York State by Nikolakakis and Fthenakis [62]**.**

When the same penetration of optimal wind and solar photovoltaic capacity is compared with solar photovoltaic only and wind only scenarios, it is clear that the optimal combination results in less spilled energy as can be seen by looking at the RLDCs in Fig. 2.22.

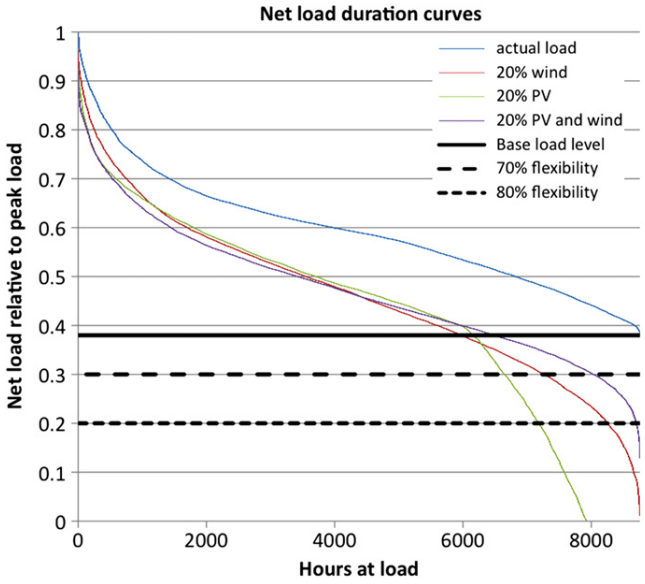

Fig. 2.22 The RLDCs of the 20% penetration of optimal wind and solar photovoltaic scenario compared with the solar photovoltaic only and wind only scenarios in the study for New York State by Nikolakakis and Fthenakis [62]**.**

2.5.3.2 Optimisation of Storage, Balancing Energy and Levelised Cost of Electricity in the United States

Becker *et al.* [63] presented a study on the optimised mixes of wind and solar photovoltaic capacities in the United States, as well as optimal transmission grid extensions between Regional Transmission Organisations (RTO). The study assumed a 100% penetration of wind and solar energy and considered three optimisation goals, namely minimising storage energy capacity (where stored renewable energy has to cover load), minimising system imbalance energy (where conventional

generation is used to balance the load), and minimising levelised costs of renewable electricity generation (where conventional generation is again used to balance the load). For each optimisation goal the study also considered two cases where there is no transmission capacity between any RTOs and where there is unconstrained transmission capacity between adjacent RTOs.

When minimising storage energy capacity, the authors assumed a perfect storage system, i.e. there occurs no losses when charging or discharging the system. Because a 100% penetration of renewable sources is also assumed (mean renewable power is equal to mean load), there will necessarily be enough energy produced to meet the load, with a certain size of storage capacity necessary to shift power production to when it is needed. A storage time is employed for different ratios of wind power capacity to solar power capacity, and the optimal wind power ratio is the one that results in the minimum storage capacity. The results for the unconstrained transmission scenario can be seen on the left of Fig. 2.23, whereas the result for each individual RTO with no transmission capacity can be seen on the right. The error bars represent wind ratios that would result in a 1% change in capacity size (% in terms of mean load) and the dotted line indicate the weighted mean wind ratio. In both cases the wind ratio is quite low, varying between 0% and 35%. The authors propose that there are two reasons for the high ratio of solar photovoltaic capacity, the first being that solar photovoltaic power shows much less seasonal variation than wind power at this latitude, and is therefore more suitable to charging any storage capacity. The second reason is that the daily solar power profile is typically correlated with the daily load profile, where peak loads typically occur during the middle of the day.

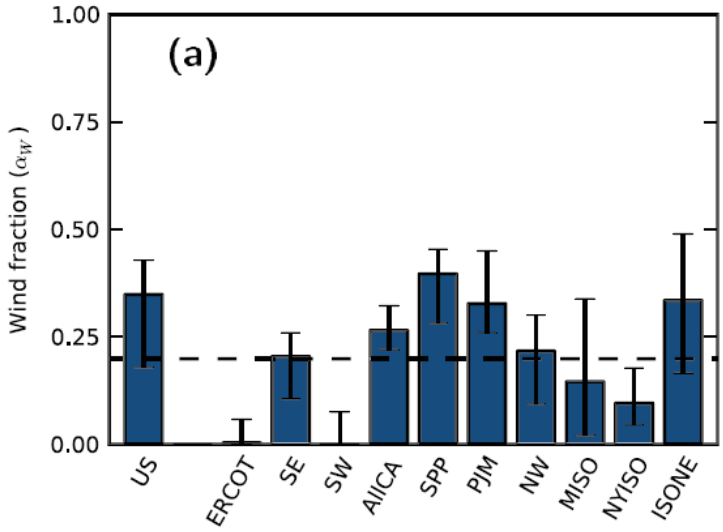

Fig. 2.23 Optimal wind power capacity for the entire US and each individual RTO in order to minimise storage capacity in the study by Becker et al. [63]**.**

In the second optimisation goal, where system imbalance energy was minimised, it is assumed that there is no energy storage and that any negative mismatch, where the load exceeds the renewable power generation, has to be covered by dispatchable power generation. The results of the optimal wind ratios can be seen in Fig. 2.24. This result looks very different from the case where storage energy has to be minimised. In the both the unconstrained transmission case and the zero transmission case, the wind ratios are extremely high, typically more than 75%. The main reason for this is that wind power exhibits a much better overall correlation with the load than solar photovoltaic power, which only generates power during the day.

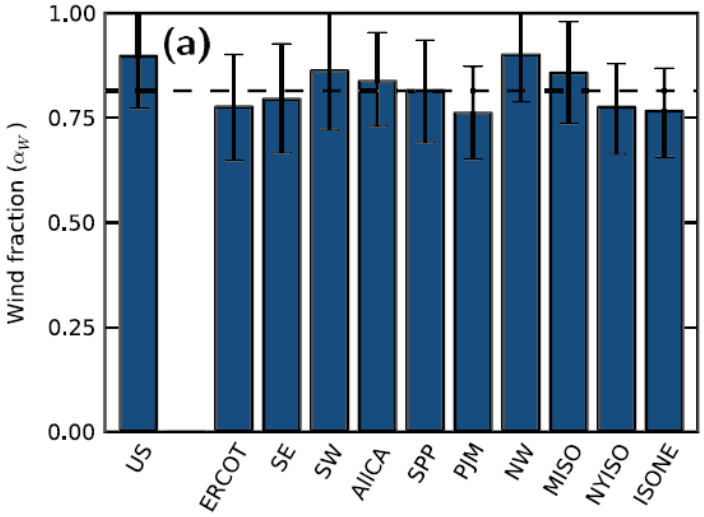

Fig. 2.24 Optimal wind power capacity for the entire US and each individual RTO in order to minimise balancing energy in the study by Becker et al. [63]**.**

In the final optimisation goal, the levelised cost of electricity (LCOE) is minimised. As in the second optimisation goal, it is assumed that there is no storage and any residual load has to be covered by conventional generation. A localised cost of energy for both wind and solar photovoltaic power were determined in each RTO by considering the capacity factors of each technology in the respective RTO, in conjunction with a cost multiplier variable that incorporates local labour, material and equipment costs. In the dispatch procedure, the LCOE is subject to the effects of renewable energy curtailment, reflecting the fact that costs can only be recovered for renewable energy that was not curtailed. The results of the optimal wind ratios can be seen in Fig. 2.25. There is more variance between the individual RTOs than in the previous optimisation strategies, reflecting the fact that capacity factors and other costs can vary in different regions.

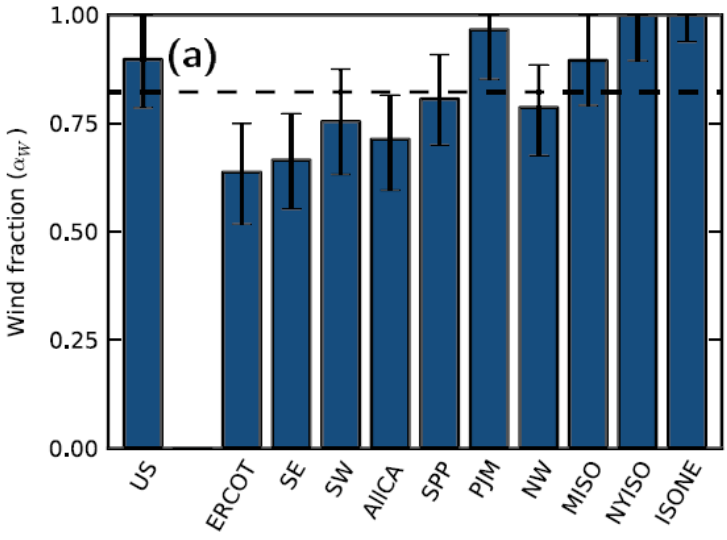

Fig. 2.25 Optimal wind power capacity for the entire US and each individual RTO in order to minimise LCOE in the study by Becker et al. [63]**.**

This study showed that the optimal ratio of wind and solar power capacity can vary by optimisation goal and by region. In this study the optimal expansion of the transmission grid was also investigated

using a DC-load flow approach with a simulated annealing optimisation strategy, but will not be exhibited here.

2.5.3.3 The Effect of Wind Power to Solar Photovoltaic Power Ratio on Capacity Credit and Overproduction in Indiana (US) and Germany

In 2015, Ueckerdt *et al.* [8] produced a study on the effects of different penetrations of wind and solar photovoltaic capacity in two regions, namely the US state of Indiana and Germany. The three impacts that the authors examined include the capacity credit, the reduced utilisation of dispatchable plants and overproduced renewable generation. As these two regions have very different load profiles, the authors set out to determine how the impacts of these technologies would differ in the regions. All three these impacts can be inspected by looking at the residual load duration (RLDC) of the system as can be seen in Fig. 2.26. RLDCs were discussed in section 2.5.2.3.

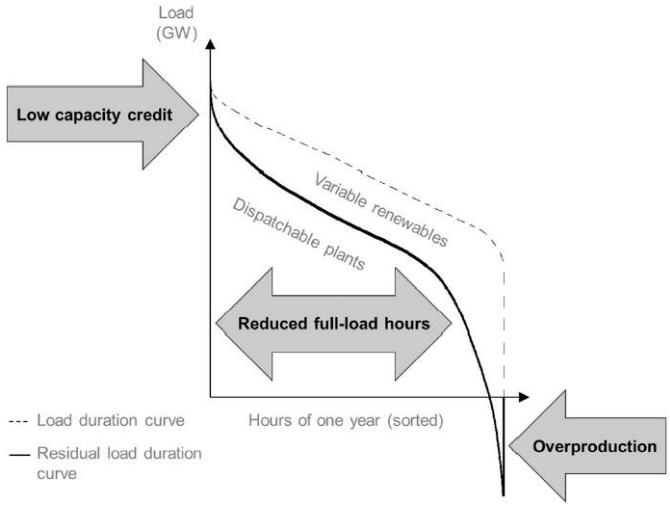

Fig. 2.26 Low capacity credit, reduced full load hours of conventional plants and overproduction of renewables as seen on the RLDC [8]**.**

More details on the reduced utilisation of base-load plants can be found in the study. Here we will take a closer look at the capacity credit and overproduction of wind and solar photovoltaic power in these regions. The authors obtained synchronous load and weather data on a quarter hourly timescale for Germany and the US state of Indiana, performed the relevant renewable energy simulations and used the Garver approximation-based method to determine the capacity credit, which is discussed in section 2.5.2.3. The authors mention that the load profiles of Germany and Indianas are representative of Europe and the United States respectively. The results for the capacity credit of different ratios of renewable energy in the two regions can be seen in Fig. 2.27. The bottom two graphs represent the scenarios where exclusively wind or solar photovoltaic capacity is considered.

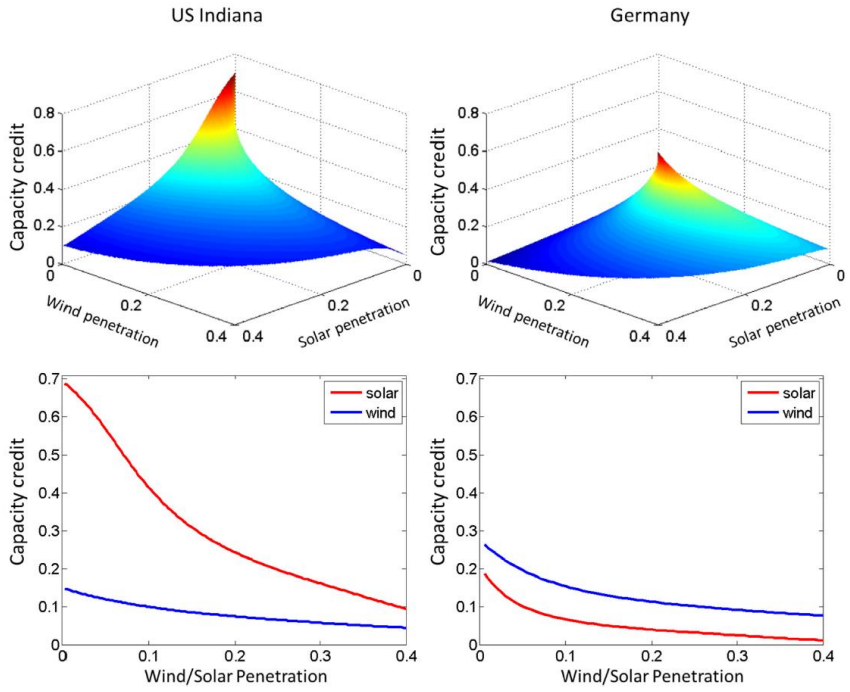

Fig. 2.27 Capacity credit (Garver Approximation Method) for different ratios of wind and solar photovoltaic penetrations in Indiana and Germany in the study by Ueckerdt et al. [8]**.**

It is clear that solar photovoltaic capacity has a much larger capacity value in Indiana than in Germany. This can best be understood by looking at Fig. 2.28, where the average daily load and solar photovoltaic generation are displayed for summer and winter. It is clear that the hour of peak solar photovoltaic generation shows good agreement with the peak load in Indiana which occurs in summer, while the peak load in Germany occurs in the winter and also later in the day where solar photovoltaic power generation is zero.

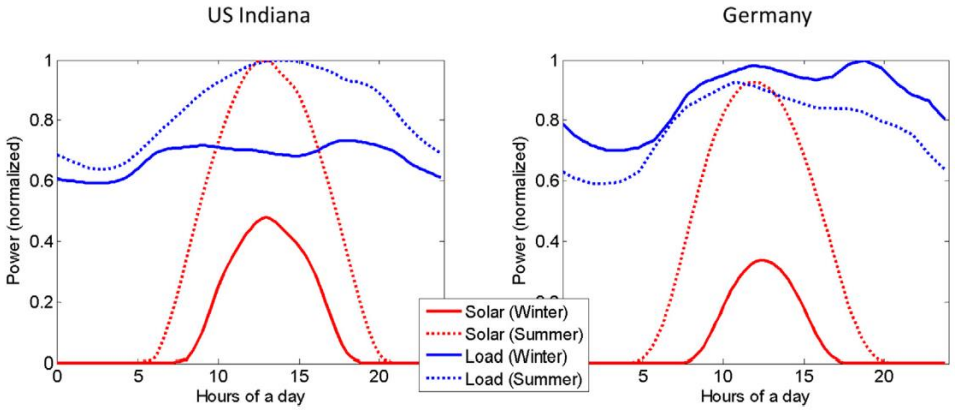

Fig. 2.28 Average daily load and solar photovoltaic generation profile in Indiana and Germany for winter and summer in the study by Ueckerdt et al. [8]**.**

The overproduction of wind and solar photovoltaic energy considering different ratios of the respective technologies can be seen in Fig. 2.29. It is clear that in Germany larger shares of wind power capacity do not pose much of a risk in terms of overproduction, whereas solar photovoltaic power above 20% penetration causes high levels of overproduction. In the case of 40% penetration, overproduction is minimised with a 100% wind farm capacity. The risk of overproduction is more

balanced in Indiana, where in the case of 40% penetration a ratio of 2:1 would minimise overproduction (66.6% wind power capacity to 33.3% solar photovoltaic capacity).

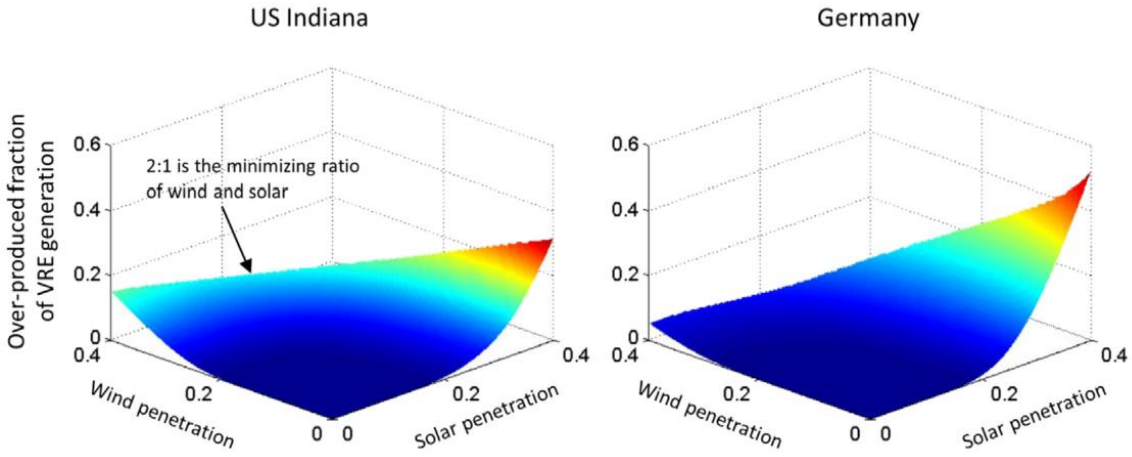

Fig. 2.29 Overproduction of renewable energy in Indiana and Germany in the study by Ueckerdt et al. [8]**.**

Ueckerdt *et al.* [8] present several conclusions, including the fact that solar penetrations below 20% are easier to integrate in Indiana than in Germany, but penetrations of above 20% present major challenges. Wind power integration presented similar challenges in Indiana and Germany.

2.5.3.4 Summary and Critique

Three studies have been presented that study the effect of wind power to solar photovoltaic power ratios in the United States and Europe. The studies consider different optimisation goals, including minimising storage capacity, minimising balancing energy, minimising LCOE and maximising capacity credit.

These studies however did not take into account the effect that variable renewables will have on the increased costs of conventional generation. Due to the hourly variability of wind and solar photovoltaic power, the conventional generating fleet is projected to encounter increased ramping requirements, as well as more stop and start procedures, which will necessarily have a cost implication. In order to study the effects that different ratios of wind and solar photovoltaic power could have on a particular conventional generating fleet, detailed grid-level optimal power dispatch simulations are necessary. Eser *et al.* [64] performed such a study for five countries in central Europe for three assumed penetration levels for wind and solar photovoltaic power capacity in 2020, based on the National Energy Action Plan of Germany.

In the absence of detailed grid-level optimal power dispatch simulations, mean-variance optimisation (discussed in section 2.6.2 below) could potentially be used to minimise the variance of the residual load in order to minimise the ramping that would be needed from the conventional generating fleet. This is explored in the work in this thesis.

2.6 Wind Farm Location Optimisation

2.6.1 Overview

There is a variety of wind farm location optimisation studies available in the literature. Although some novel approaches have been proposed, the majority of wind farm optimisation studies focus on

using mean-variance portfolio theory to optimise the location and size of wind farms. The mean-variance portfolio theory approach attempts to minimise the variance of combined power output from wind farms, while some other studies have different optimisation goals, such as minimising the probability of low power output or minimising losses on the high voltage electricity grid. This section investigates the wind farm location optimisation studies found in the literature. As this literature pertains directly to the work undertaken in this thesis, a summary and critique is provided in section 2.6.4.

2.6.2 Wind Farm Location Optimisation using Mean-variance Portfolio Theory

Mean-variance portfolio theory, also known as Markowitz portfolio theory, was first proposed by Markowitz in 1952 [65]. In mean-variance portfolio theory an investor seeks to minimise risk for a preferred yield when investing in shares on the stock market. This problem equates well with the problem of locating wind generation capacity with the view to maximise the cumulative power contribution whilst minimising variability. Simulated or measured historical wind data sets are used to simulate theoretical wind turbine power time series using a given wind turbine power curve for each of the potential locations using one of the methods described in 2.3.2. The covariance between proposed wind farm locations (equated to risk) is minimised for different capacity factors (equated to mean portfolio return). The problem translates to a quadratic programming problem that can be solved for given capacity factors to yield a set of solutions known as the efficient frontier. Solutions on the efficient frontier represent a mathematically optimal mix of wind farm capacities and locations with a minimum level of variance for a given mean capacity factor. More details on the mathematical formulation are provided in section 5.2.

In 2005 Hansen performed a small wind farm optimisation study in North Carolina using mean-variance portfolio theory [66]. The study was useful for introducing the method but at the time however, there was no large scale wind data available and the study relied upon measured wind speed data from three sites which was collected in different years, which somewhat limited the adequacy of the results. The measured wind speed data was used to simulate wind power time series using the Vestas 1.6 MW turbine. The study also proposed using mean-variance theory on a subset of the time series data, in hours that represented peak demand periods in winter and summer.

Mean-variance portfolio theory has been proposed to solve offshore wind farm location optimisation in the UK by Drake and Hubacek [67] in 2007, but the mathematical details of how the optimisation is performed were not provided. Wind speed data was obtained from four buoys located at least 40 km from the nearest coastline and the wind power time series were simulated using the Vestas V90 3.0 MW wind turbine power curve. The authors noted that using buoys located closer to the coastline (in the order of 1.5 km to 3 km) would have been ideal, as this represented the actual typical location of offshore wind farms, but this data was not available. The study considered the allocation of 2.7 GW of wind farm capacity in two scenarios. In the first scenario the 2.7 GW would be located in a single location and in the second scenario the capacity would be distributed across four locations using mean-variance portfolio theory. The results indicated that the wind power variability could be reduced in the order of 36% as a result of the optimal distribution. With many possible solutions of minimised variance for a given mean power output on the efficient frontier, this study also proposed picking a solution on the efficient frontier with the maximum power generation per unit of risk. In mean-variance portfolio theory this is sometimes referred to as the coefficient of variation, and is simply calculated as the standard deviation divided by the mean.

Hansen and Levine performed a wind farm mean-variance study in 2008 using measured wind speed data from 95 locations in the United States [68]. The study considered optimal distributions of wind farm capacity within states, namely Texas, Kansas, Minnesota, and North Dakota as well as an

optimal distribution considering all locations within the Midwest Reliability Organization region (comprising Minnesota and North Dakota). The authors noted that using more than three years of data would be ideal in order to capture the effect of inter-annual variation, but the available data only overlapped to cover the whole of 2004. The measured wind speed datasets were scaled to the correct heights using the wind profile power law and converted to wind power time series using the 2 MW Vestas V80 wind turbine power curve. The optimisation results confirmed that distributing wind farms optimally across different sites caused a drastic reduction in the time duration in which there is zero power production. Traube at al. [69] expanded upon the work of Hansen and Levine by expanding the geographic area of the study, expanding the timeframe of the study to three years (2002–2004) at the cost of losing some data sets which did not completely cover this period and including solar photovoltaic power systems. The wind power time series were simulated as before while the solar photovoltaic time series were simulated for an idealized 1-axis polar mount tracking photovoltaic system with a maximum power point (MPP) tracker. The study considered the optimal allocation of 100 MW of renewable energy capacity, although the authors noted that the choice of 100 MW was essentially arbitrary and the results could easily be scaled up. The results indicated that expanding the timeframe of the study from one year to three years did not have a significant impact on the results, while expanding the geographic area significantly decreased the variability of the combined wind power output. It was also observed that including solar photovoltaic power systems resulted in a portfolio with 18% lower variability than the optimised wind portfolio alone.

Cassola *et al*. [70] presented a wind farm mean-variance study of wind farm locations in Corsica, the fourth largest island in the Mediterranean off the coast of France, using three years (1 October 1996 to 30 September 1999) of measured wind speed data from ten measurement stations on the coastal regions around the island, averaged over three hours. Even though the physical area of the study is relatively small, the authors cite their previous research [71] that confirms that Corsica contains at least two so-called distinct wind climate regimes, i.e. different winds with different intensities, durations and, most importantly, different areas where they typically occur. The previous research also separated the wind measuring stations into three distinct anemological regions (clusters) based on the wind speed time series, the result of which is carried over to the mean-variance study. The authors also detail how the wind speed measurements, which were measured at a height of 10 m, are scaled to the correct turbine height. This method is validated using measured wind speeds from an actual wind farm located close to one of the measurement stations. The wind speed time series is converted to wind power time series using the Enercon E40/600 wind turbine power curve, which has a rated power of 600 kW and hub height of 50 m, and again validated by comparing it with power time series obtained from a similar turbine at the actual wind farm. The optimisation procedure is performed for the three anemological regions as well for the 10 individual sites, and it is found that the results are very similar, indicating that using a clustering methodology could be a useful way of reducing the overall computational time required for the optimisation procedure. In this study, the results presented did not include the efficient frontier as is customary for mean-variance studies, and instead the minimum variance, maximum energy and minimum coefficient of variance portfolios are given special attention. The optimisation procedure was repeated using a different wind turbine power curve (Enercon E48/800, rated power of 800 kW) and confirmed that the results are turbine independent, i.e. the optimised portfolio weights stayed largely the same even when a larger wind turbine power curve was used.

Roques *et al*. [72] performed a study on the optimal wind power deployment in Europe using the mean-variance portfolio approach in 2009. The paper also gives a brief review of where mean-variance portfolio theory had been utilised in other energy planning studies outside of wind farm location planning. This study used historical hourly wind production data from five countries, namely Austria, Denmark, France, Germany and Spain for the period from 2006 until 2007. The study

considered both unconstrained portfolios and constrained portfolios where national wind resource potential and transmission constraints were taken into account, with the view to optimising the wind farm capacity allocation of 2020. As in the study by Hansen [66], this study also investigated the optimisation of wind farm locations to cover peak demand hours by applying the procedure to a subset of the time series data, thereby contributing to system reliability. Although the constrained portfolios reduce the potential for wind power variance minimisation, the authors conclude that there is still a lot of room for variance reduction, especially compared to the actual projected wind farm allocations for 2020 in the respective countries. The choice of whether to minimise the overall variance of wind power or just the variance in peak hours also had a considerable effect on the optimal solutions and the authors suggest that policy makers should consider which objective is more relevant. The paper recommends relieving cross-border network constraints and improving the integration of European electricity markets so as to allow for the maximum reduction of wind power variability through geographic diversification.

In 2010, Degeilh and Singh [17] presented a precise mathematical formulation of using mean-variance portfolio theory for wind farm location optimisation, along with a comprehensive small-scale case study in Texas where several reliability impacts are also investigated. The study considered the optimal allocation of 40 3 MW wind turbines across seven positively correlated sites and seven sites with minimal correlation. The study simulated wind power time series using the Vestas V90 3.0 MW wind turbine power curve and three years of wind data from 30 000 sites in the Western Wind and Solar Integration Study (WWSIS). This was one of the first studies that used mesoscale wind data comprising many sites over a large area. Reliability impacts, such as the loss of load probability (LOLP) were investigated using the 1996 IEEE RTS model in combination with Monte Carlo methods to account for mechanical and electrical failures of wind turbines. This paper also proposed the idea of incorporating the load data into the mean-variance procedure, effectively attempting to minimise variance of the residual load, i.e. the load that remains after the combined wind power output has been subtracted. In the paper however, the authors state that unless the simulated wind power profiles are shown to have a strong positive correlation with the load, the optimisation procedure effectively reduces to the mean-variance problem without considering load.

Models based on mean-variance portfolio theory has been developed by Rombauts *et al.* [73] that take into account cross-border transmission-capacity constraints in Europe. This work build on the work done by Roques *et al.* [72] in two ways. The first is that cross-border capacities are modelled more explicitly so that the electrical power flows stemming from wind-power production can be analysed. The second improvement is that different datasets within countries are used instead of datasets aggregated by country. This study also differed from other studies in that it proposed that the risk component be defined as the variance of hourly wind power differences, instead of the usual variance of cumulative wind power output. This is simply achieved by taking the difference (differential) of the wind power output signal from the time series. The authors present three models that consider the cases when cross-border transmission-capacity is zero, infinity and a certain limited value. The case study defined three fictitious countries, namely country A, B and C, that utilised historical wind data from the Dutch meteorological service, converted to wind power using a Vestas 112 3 MW wind turbine power curve. The case study considers the optimal allocation of 12000 MW, with the constraint that 5000 MW, 3000 MW and 4000 MW needed to be installed in country A, B and C respectively. In the third model, where cross-border transmission constraints were considered, the transmission constraints were defined as 200 MW between A and B, 100 MW between A and C and 300 MW between B and C (and vice versa). Results indicate that the transmission constraints increase the minimum standard deviation (variability) in hourly wind power differences by a factor of $\sqrt{3}$. This study revealed some interesting insights into the role of cross-border transmission constraints on wind farm location optimisation, but the major shortcomings of the study are the

fictitious nature of the case study and that the rest of the power system components, as well as transmission losses are ignored.

In 2015, mean-variance portfolio theory has also been used to simultaneously optimise wind farm and concentrated solar power station locations in Spain and Portugal by Thomaidis *et al*. [74]. The authors present a brief review of both the pieces of literature that are supportive and pessimistic about the potential of wind power production and the role of spatial diversification. The lack of transmission infrastructure is highlighted as a major constraint to geographically diverse wind farm portfolios and references are also included that draw attention to the inter-annual variability of wind power production. It is stated that wind and solar energy often have complementary profiles and that the literature is sparse on the potential of this meteorological pattern to reduce the risk of renewable energy supply. The viability of including concentrated solar power in the mean-variance optimisation procedure is thus investigated. The study employs the WRF mesocale method to derive three years (2008–2010) of wind speed and solar irradiance data for 2237 sites in the southern part of the Iberian Peninsula on a 9 km spatial resolution. Wind power simulations are achieved using the Vestas V90 2 MW wind turbine power curve. The concentrated solar power plants are modelled as parabolic trough systems according to a model developed by Zhang *et al*. [75], and more details about the concentrated solar power simulations are given in a previous paper by some of the same authors [76]. Special attention is given to the procedural implementation of the mean-variance procedure, namely the Niedermayer and Niedermayer variant of the critical line method, which is particularly efficient when solving large-scale portfolio selection problems. The authors also mention that the original spatial resolution of the WRF mesocale model was reduced from 3 km to 9 km, and the energy generation for the wind and concentrated solar sources were averaged across each day in order the reduce the computational burden of the optimisation procedure. This study thus considers variance in daily renewable energy generation and not on an hourly scale like most of the previous studies. The special procedural implementation of the optimisation procedure and the spatial and temporal resolution reduction point to the difficulties encountered when the mean-variance problem becomes sufficiently large. The case study does not specify the size of renewable energy generating capacity considered, and it is therefore assumed to be an arbitrary capacity that can be scaled up. In the results section the outcomes of a wind only scenario is compared with a wind and concentrated solar power combined scenario, with a focus on maximum return, minimum variance and minimum coefficient of variation portfolios. The efficient frontiers for wind only and combined portfolio scenarios are the same for high values of capacity factor (30% and above), which simply illustrates that wind farms exist that have higher capacity factors than concentrated solar power plants and that choosing a high return value will result in a portfolio made up exclusively of wind farms whether concentrated solar plants are considered or not. This is not to say that concentrated solar power plants can not contribute to increased renewable energy supply security, it only highlights the fact that the combined capacity factor will be lower when concentrated solar power plants are considered. The minimum coefficient of variation portfolios for the two scenarios best illustrate the effect of considering concentrated solar power plants in the mean-variance procudure, with the coefficient of variation reducing from 0.52 in the wind only scenario (16.71 standard deviation as % of capacity, 32.42% capacity factor), to 0.22 in the combined scenario (5.61 standard deviation as % of capacity, 25.49% capacity factor). Out of the 2237 sites considered, only 34 wind power sites and 42 concentrated solar power sites play any role in the efficient frontiers (defined as having a non-zero weight in at least one solution on the efficient frontier), which the authors regard as encouraging when considering the practicality of the solutions. The authors also note that some low capacity factor wind power sites are included in the efficient frontier solutions, which might not be financially feasible in any real-world scenario. It is suggested that a similar study could be conducted on a European scale, but that a dimensionality-reduction method would be essential. It is suggested that clustering techniques, such as those

employed by Zagouras *et al.* [77], is investigated as a means to make large scale mean-variance studies realisable.

2.6.3 Other Wind Farm Location Optimisation Methodologies

There are several studies found in literature which also focus the location and size optimisation of wind farms, but do not use the mean-variance optimisation procedure. These studies either use other financial portfolio optimisation methods, novel variance minimisation methods or pursue a different optimisation goal altogether.

Grothe and Schnieders [21] presented a study in 2010 which focused on a copula theory method to simulate wind speed data and to distribute wind farm capacity optimally. Instead of minimising the variance of the cumulative wind farm output as in the mean-variance method, the value-at-risk (VAR) is optimised, i.e. the low power output value which has a certain probability of occurring, also referred to as tail risks in finance theory, is maximised. The probability, α, is specified by the user, and the α-quantile is maximised so that $(1-\alpha)\cdot 100\%$ of cumulative power outputs are above the α-quantile. A case study for Germany was conducted, considering two scenarios with the α values considered ranging from 0.01 to 0.12. In the first scenario the size and location of the existing capacity is ignored and it is assumed that the capacity can be relocated, which is not a realistic assumption, but is simply useful for comparing the performance of the optimal allocation with that of the existing capacity. In the second scenario the existing capacity is included and optimally expanded by 40%, with the new capacity being placed in optimal locations. The optimal portfolios were constructed using the wind time series modelled by the copula functions which had a time resolution of 24 hours. The optimal portfolios were then evaluated using measured wind speed time series which had daily and hourly frequencies. The wind speed time series were converted to wind power time series by scaling them to the correct height and then implementing a piecewise-defined function approach to simulate the performance of a GE 1.5 MW turbine. The case study also considered whether offshore wind farm locations can be considered or not and what effect that has on the optimal portfolios. Results indicate that there is not enough wind farm capacity in the north of Germany, especially considering offshore sites. Expanding the existing capacity by 40% would entail placing most of the new capacity in this northern region and could increase the power output available at a certain probability in the order of 100%. Even though the modelled time series had a time resolution of 24 hours, the resulting optimal portfolios were shown to increase the VAR at an hourly scale as well.

A robust optimisation approach to wind farm diversification was presented by Liu *et al*. [78] in 2013. This paper assessed the work and case study done by Degeilh and Singh [17], discussed in section 2.6.2, as well as a case study from the Netherlands. Their criticism of the mean-variance method included the fact that the procedure is sensitive to the input data, specifically the mean and covariance matrix. In order to make the wind farm diversification procedure more robust, the authors present a conditional value-at-risk (CVAR) approach. The conditional value-at-risk, also referred to as the expected shortfall, is the mean value of a portfolio returns that fall below a probability, α, on the probability distribution. Beyond the CVAR optimisation, the authors also introduce the methodology to produce robust portfolios, where the assumption is that the probability distribution of wind is not known *a priori*, but is instead determined from the candidates of a set of distributions using box uncertainty and ellipsoidal uncertainty measures. The exact probability distribution might not be known due to the limited availability of data. The mathematical formulation of the complete optimisation approach is described in detail, after which the case studies are presented. In the case study from the Netherlands, 10 years (2001-2010) of daily mean wind speed data from 40 meteorological stations were converted to wind power time series using a piecewise-defined function approach to simulate the performance of a typical wind turbine with a rated power of 1.5 MW. The results confirm that the robust portfolios slightly outperform the nominal portfolios, especially as the

pre-defined uncertainty measure increases. In the Degeilh and Singh [17] case study the robust portfolio results in a slightly larger variance than the mean-variance portfolio, 395.22 MW and 381.15 MW respectively. As in Degeilh and Singh [17], an IEEE RTS model combined with Monte Carlo simulation was also employed to test wind power reliability statistics such as loss of load expectation (LOLE) and expected energy not supplied (EENS). Results indicate that the CVAR portfolio performs slightly better than the mean-variance portfolio in terms of the reliability statistics.

Reichenberg *et al*. [23] presented a wind farm location optimisation study in the Nordic countries and Germany in 2013 which focused exclusively on attaining a portfolio with the minimum coefficient of variation. Instead of applying the mean-variance approach, the authors presented an iterative approach to arrive at the optimal portfolio. At each step a simulated wind time series, i.e. a potential wind farm site, is added to the portfolio if it results in the lowest combined coefficient of variation. The weakness of this approach is that the decision to add sites to the portfolio is binary and there is no optimal weight assigned as in the mean-variance approach. The case study used four years (2006-2009) of wind speed data from 300 sites that was produced using a HIRLAM mesoscale model, with a spatial resolution of 11 km. The wind turbine power simulation method is not provided, and instead the reader is referred to a large scale wind power integration report from where the method was attained. Similar to previous studies, this paper also considered two scenarios where in the first it is assumed that there is no existing wind farm capacity and in the second that the new wind farm capacity has to complement the actual existing capacity. In the scenario where no current capacity is assumed, the optimal coefficient of variation of the wind capacity portfolio was 0.54, which is significantly less than the 0.91 that was calculated for the existing capacity. The study found that the variations in wind power output, considering the existing capacity, can be reduced by about 33% by considering the optimal future allocations.

Schmidt *et al*. [79] presented a study on the potential of the diversification of wind farms in Austria in 2012. The Austrian wind atlas does not provide time series wind speed data that is necessary for a study like this, therefore the study used wind speed Weibull distribution data from the wind atlas in conjunction with measured wind speed data from meteorological stations to construct wind time series using the Iman Conover method. A GIS study eliminated sites that are unsuitable for wind farm siting (due to factors such as land use and a localised cost of energy higher than the current feed in tariff), resulting in 4226 potential wind turbine sites. Along with the wind atlas data for the eligible sites, wind speed data for 2008 from 65 reference meteorological stations were used to construct the wind time series. The wind time series were converted to wind power time series using a generic wind turbine power curve with a rated power of 2 MW. More details about the GIS study and the wind power simulation are provided in another paper by the same authors [80]. The case study considered the optimisation of three models, which attempted to maximise investor profit, minimise hourly variation and minimise seasonal variation respectively. This was achieved by constructing custom cost functions, with the minimum annual energy production and variance given as constraints. The authors indicate that different values of minimal variance were implemented to ascertain feasible variance values. There is no variable controlling the overall capacity to be assigned, only the annual energy to be produced. The case study considered the allocation of wind farms to produce at least 5 TWh of energy annually in each of the three models. Results indicate that the minimum hourly variation model yielded an hourly standard deviation of 320 MW compared to 366.8 MW for the minimum seasonal variation model and 383.7 MW for the maximum profit model. The spatial diversity of the minimum hourly variation model was the highest, with 59 installed sites compared to 26 for the minimum seasonal variation model and 11 for the maximum profit model. The minimum seasonal variation model, which attained a minimum seasonal variability of 7.5 GWh, presented the most installed capacity with 1820 MW compared to 1795 MW for the minimum hourly variation model and 1679 MW for the maximum profit model. The authors conclude that there seems to be a

trade-off between lower seasonal variability and lower hourly variability. Even though the paper references other studies that used the mean-variance method, it is not abundantly clear what advantages the method presented in this paper are over the mean-variance method.

A method to distribute wind farm capacity optimally was presented by Lowery and O'Malley [20] in 2014. Wind data from the MERRA dataset, obtained to facilitate a case study across Ireland, were interpolated to increase the spatial resolution and scaled to the correct height using the log wind profile. The constants in the log wind profile were calculated using wind speed data from different heights. A piecewise-defined function approach was used to simulate a wind power time series, with the parameters of the piecewise-defined function being derived from measured wind farm data from 62 actual wind farms. For the optimisation procedure, the authors constructed a custom objective function by concatenating three objectives, namely variance, mean power output and cost and then assigning a weight to each objective. Different costs were defined for onshore and offshore wind farms. The authors then minimised the objective function using a constrained optimisation by linear approximation (COBYLA) method, which is an optimisation method utilised when the derivative of the objective function is not known. The authors report that for this case study the optimisation problem took between 3 and 4.5 hours to solve, which can generally be viewed as inferior to the mean-variance procedure which can be solved in a matter of minutes depending on the size of the case study. When the cost objective was omitted from the objective function, the wind farm capacity was almost exclusively distributed offshore. When cost was taken into account, no offshore locations were included. It is not immediately clear what benefits this method presents over the mean-variance method, if any. There is also no efficient frontier to examine all available optimal portfolios, instead just a handful of optimal solutions based on the user-defined weights in the objective function was used.

Leenman and Phillipson [81] presented a novel method to distribute wind farms in order to reduce transmission losses on the high voltage power grid considering regional load profiles. This is quite different from the other wind farm location studies discussed above. In the literature, this kind of study falls under Transmission and Generation Expansion Planning (TGEP), with this being a special variant, namely stochastic generation expansion planning. The losses that occur on the high voltage power grid are proportional to how far the power has to flow from where it is generated. Wind farms are typically located according to the wind resource and not necessarily close to load centres, and as such there is the potential for increased transmission losses. The authors present a novel three-step procedure for optimal wind farm placement. First, the DC power flow model is applied to the network structure and the load data. Secondly, the potential wind power profiles are simulated using measured wind speed data. Thirdly, the stochastic optimisation procedure is solved using a simple heuristic method. The paper presents an overview of power grids and derives a simplified power flow model, with the simplifications justified in order to facilitate the mathematical programming needed for the optimisation. The optimisation methodology is explicitly formulated in sufficient detail, after which the authors also describe how the approach can be adapted so that it can be solved by standard optimisation software. Network flow duality is utilised to arrive at a nonlinear programming problem, which is solved by a heuristic method as the investigation of rigorous solution algorithms for nonlinear programming problems falls outside the scope of this work. A Dutch case study is presented, where 10 years (2001-2010) of wind data from 50 measurement stations is used. Wind power time series are simulated using a completely linear piecewise-defined function approach to approximate a typical 2.5 MW wind turbine. In the case study, the Netherlands is clustered into five distinct wind zones, with the regional load being aggregated in these distinct wind zones for the DC power flow model. The optimal locations of wind farms (stochastic generating) is compared with that of deterministic generating units of varying size and overall capacity. The authors come to several conclusions, including the confirmation that optimal deterministic unit placement has a much larger

effect on reducing transmission losses than stochastic generating units such as wind turbines, which is to be expected. However, it is noted that there exists a non-trivial relation between the locations of wind turbines and transportation losses, although this relation only becomes relevant at high penetration and might be more pronounced in countries with large power networks such as the United States or Australia. This study also compares its distribution strategy with the mean-variance method and concludes that at current low levels of wind energy penetration, locating wind farms to minimise transmissions losses might be advisable, whereas at large levels of penetration (specified as 30% or more) the spatial diversification achieved by mean-variance optimisation could potentially become more important.

2.6.4 Summary and Critique

Several wind farm location optimisation studies that are found in the literature have been presented. The majority of papers use a variant of mean-variance portfolio optimisation for wind farm diversification, although there are ample examples of studies that have employed other methods.

In terms of the studies that have utilised mean-variance optimisation, the majority of the studies use measured data pertaining to specific locations instead of mesoscale wind data which covers a large geographical area. Although measured wind speed is slightly more accurate than mesoscale model wind data, it is generally accepted that mesoscale wind data fully capture the daily and seasonal cycles observed in a given location, which is the critical component considered in mean-variance optimisation. Therefore using measured data from the available weather stations has the potential to underestimate the full potential of mean-variance approach, as not all potential wind farm locations in a given area are considered. The time resolutions used in the studies also varied according to the data that was available, ranging from hourly to daily averages, which makes it difficult to compare the obtained results as different variations in wind power output are being optimised. Several studies mention the possibility of including solar power in the mean-variance procedure, but only two papers follow through on this, one including solar photovoltaic power simulations [69] and the other concentrated solar power simulations [74]. The sizes of the case studies are also generally quite small, far below the capacity of wind farms which might be installed on a national scale. There are two problems with the mean-variance method that arises as the problem size is scaled up, namely the computational burden of the optimisation procedure and the practicality of the solutions on the efficient frontier. Neither of these problems are fully addressed in any of the studies, although in the small case study presented by Cassola *et al*. [70] a time series clustering approach based on the measured wind speeds is implemented and mooted as a possible solution to the increasing computational burden that a larger study might present. Although time series clustering is not implemented in the study by Thomaidis *et al*. [74], the authors also propose in their conclusion that these techniques could aid the mean-variance optimisation procedure. There also is a strong case to be made for the wind power output to match the given load profile. In pursuit of this goal, two of the studies [66][72] have implemented the mean-variance approach on a subset of the time series data, effectively minimising the variance of wind power output during peak hours. Degeilh and Singh [17] proposed that the load time series could be incorporated into the mean-variance optimisation procedure, but that unless the wind power profiles exhibited significant correlations with the load, the exercise would amount to very little gain, and as such this formulation was not implemented in their study.

In terms of studies that utilised methods other than the mean-variance optimisation, two studies [7, 36] also implemented optimisation methods from finance theory, namely the VAR and CVAR optimisation methods. Both of these methods minimise tail risks, which translates to the probability of low wind power output when considering wind farm diversification. Occurrences of low wind power output will typically have to be covered by peaking plants which run on more expensive fuels

than other plants. The weaknesses of these approaches lie in the fact that the probabilities of high power output are not considered, which also present financial implications such as increased cycling of conventional generation or curtailment of wind power output. These portfolio optimisation approaches also present various challenges as the size of the case study and datasets become sufficiently large. Three other wind farm location optimisation methods have been presented [23, 79, 20], although it seems that they pursue the same goals as mean-variance optimisation and it is not clear what advantages they provide over mean-variance optimisation, if any. They generally present longer run times and less clarity on the variability reduction potential on offer. One study has been presented that locate wind farm capacity to minimise transmission losses on the high voltage power grid [81], but the authors of this study conclude that it is more suited when penetrations of wind farm capacity are below 30%, i.e. when wind contributes less than 30% of the overall energy in a given timeframe.

2.7 Time Series Clustering

2.7.1 Overview

Time series clustering has been suggested as a possible addition to the mean-variance optimisation procedure (applied to renewable energy integration), but only implemented in one small-scale case study [70] where the time series clustering was done on the wind speeds and not the wind power output. This section gives an introduction to time series clustering, the different methods and validation measures, as well as examples in literature where time series clustering has been used in renewable energy integration studies and mean-variance portfolio studies.

2.7.2 Introduction to Time Series Clustering

Time series clustering is an established field of data mining [82]. It is an unsupervised classification which attempts to order unlabelled time series into groups of time series data which share common behaviours or features. The intended outcome of a time series clustering procedure is to end up with clusters where time series within the same cluster are as similar as possible, while at the same time being as dissimilar from the time series associated with other clusters. In 2005 Liao [83] published a review paper on the clustering of time series data, with another review published by Aghabozorgi *et al.* [82] in 2015.

Traditionally the main challenges with time series clustering have been the high dimensionality, the presence of noise and the high feature correlation. There are different approaches to time series clustering. The approaches to time series clustering have been separated into three groups, namely raw-data-based, feature-based and model-based clustering by Liao [83] as can be seen in Fig. 2.30.

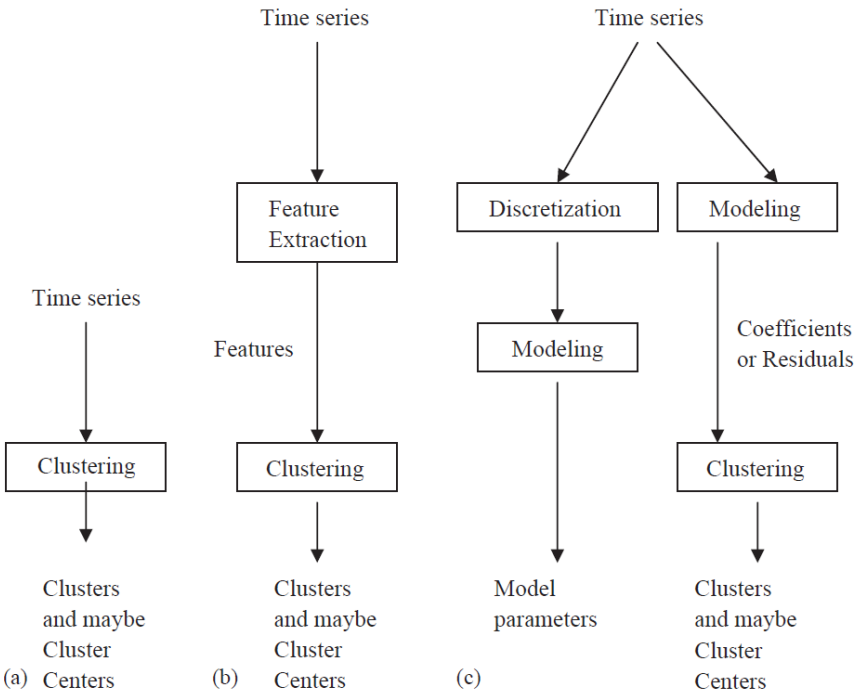

Fig. 2.30 The three different approaches to time series clustering as presented by Laio [83]**.**

In 2001, Halkidi *et al*. [84] published a paper on cluster validation measures in which they summarised the steps of the clustering process as can be seen in Fig. 2.31. This summary is also applicable to time series clustering. First, the selected feature is extracted, which depends on the data in question and the intended application of the clustering result. Next, several clustering methods are applied to the data. In determining the appropriate type of clustering algorithm to use, it is generally suggested to apply several algorithms and then determine the best one for the given case by considering several standard cluster validation measures. After the appropriate clustering method is selected (along with an appropriate number of clusters to use), the final clusters are derived and interpreted.

The focus of this investigation is on the similarity of the hourly power output time series of wind and solar photovoltaic plants in different geographical locations, therefore the raw-data-based approach is investigated. If different regions were to be clustered according to diurnal or seasonal features, feature-based and model-based clustering could be of more use. In raw-data-based time series clustering, it is necessary to specify a similarity measure, which is explained further below.

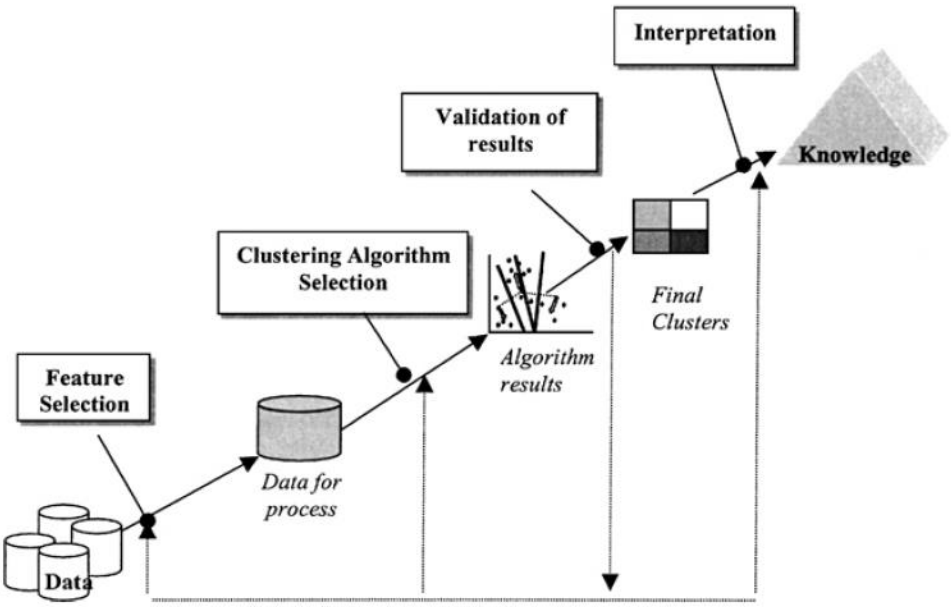

Fig. 2.31 The steps of the clustering process in the study by Halkidi et al. [84]**.**

2.7.3 Similarity Measures

The similarity measure, also sometimes referred to as the distance measure or dissimilarity measure, determines how the similarity between two time series is measured, and is chosen based on the characteristics of the input data and the intended application of the cluster results. The similarity measure determines whether similarity in time, similarity in shape or similarity in change will be targeted. Typical similarity measures used in time series clustering include Lp-norm distance (also known as the Mikowski distance), Dynamic Time Warping distance (DTW), Longest Common Subsequence (LCSS) distance and the Pearson's correlation factor.

2.7.4 Clustering Methods

Different clustering methods exist to cluster time series data. Several complex clustering algorithms have been proposed, but the basic clustering algorithms can be classified as either hierarchical or partitional.

2.7.4.1 Hierarchical Methods

Hierarchical clustering is a clustering method in which a series of partitions takes place that result in nested clusters organised as a hierarchical tree that can easily be visualized using a dendrogram. It is not necessary for the user to specify the number of clusters *a-priori*.

2.7.4.2 Partitional Methods

Partitional clustering divides the datasets into a user-specified number of subsets. There are many different types of partitional clustering methods, of which the k-means algorithm is the most widely used.

2.7.4.3 Other Methods

Many other types of clustering algorithms that have been suggested for time series data include fuzzy c-means clustering, density-based clustering and self-organising maps. Clustering methods are an active research field and several different approaches have been suggested in recent years [82].

2.7.5 Cluster Validation Measures

Cluster validation measures are used to determine the quality of a clustering result. Many cluster validation measures have been proposed and reviewed in the literature by Arbelaitz *et al*. [85]. There is no single clustering method which performs optimally for all types of data. The main purpose of the cluster validation measures is to aid the user in selecting the appropriate clustering method that best fits the specific dataset, as well as to provide insight into how many clusters might be appropriate.

2.7.6 Time Series Clustering in Renewable Energy Research

Time series clustering has been used in many renewable energy studies, some of which will briefly be described here. Burlando *et al*. [71] used time series clustering techniques to identify anemological regions and wind regimes on the isle of Corsica in France. Wind speed data from ten weather stations were used in the study. Three distance measures were combined with five hierarchical clustering methods to form a total of 15 clustering technique combinations. The results of this study was used by Cassola *et al.* [70] to perform a small mean-variance wind farm optimisation procedure. The weather stations and one of the dendrograms from a hierarchical clustering procedure can be seen in Fig. 2.32.

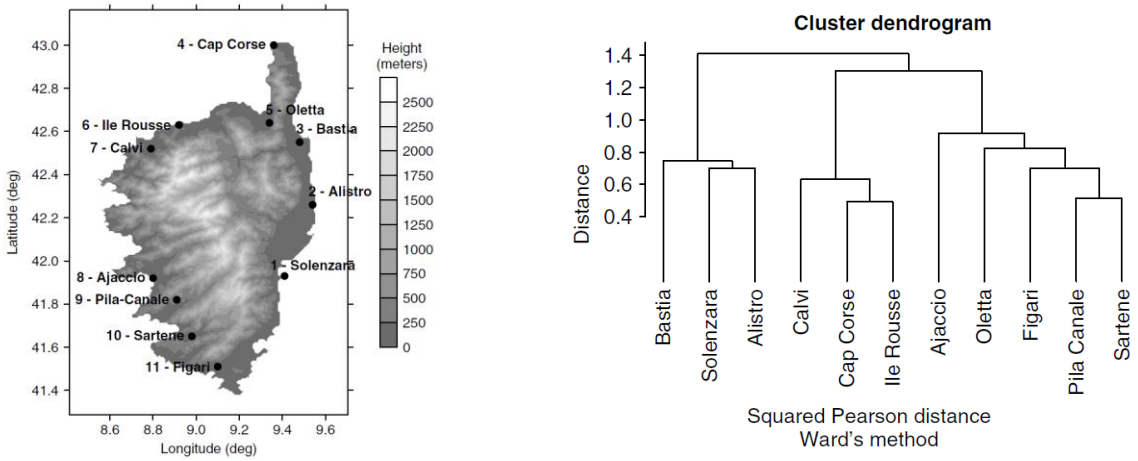

Fig. 2.32 The weather stations on the isle of Corsica (left) and an example of a clustering result (right) from the study by Burlando et al. [71]**.**

Vallée *et al*. [86] used a feature-based time series clustering technique to cluster 94 wind regions in Europe with similar statistical behaviour in order to perform adequacy evaluation studies for wind farms. The authors employed a fast incremental algorithm to cluster the features extracted from the time series, which was compared with the classic k-means clustering method. The Pearson coefficient was specified as the similarity measure. The results of the fast incremental clustering can be seen in Fig. 2.33.

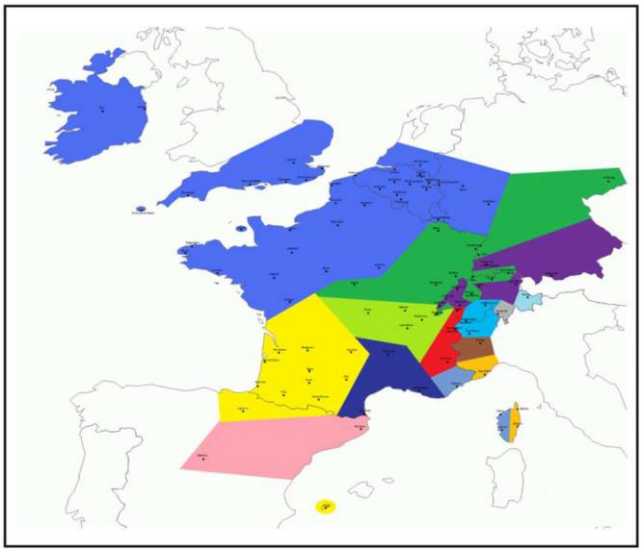

Fig. 2.33 The results of the fast incremental clustering of wind parks in Europe by Vallée et al. [86]**.**

Zagouras *et al*. [77] used clustering techniques to determine coherent zones of Global Horizontal Irradiance (GHI) for a utility scale territory in California for solar photovoltaic capacity planning purposes. The k-means clustering method was used to cluster the gridded irradiance data that was obtained from satellite observations, in conjunction with a principal component analysis based dimensionality reduction method. Two cluster validation measures were used to verify the quality of the clustering result, as well as to ascertain the appropriate number of clusters to use. Some of the coherent solar microclimate zones are shown in Fig. 2.34.

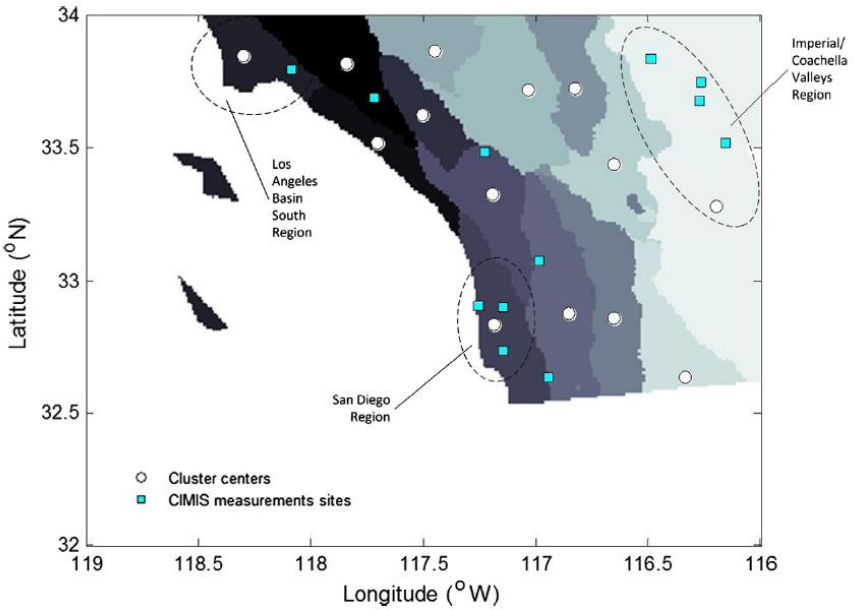

Fig. 2.34 Coherent solar microclimate zones obtained through time series clustering in the study by Zagouras et al. [77]**.**

2.7.7 Time Series Clustering combined with Mean-Variance Portfolio Theory

Time series clustering has been employed in conjunction with stock portfolio optimisation in the literature.

Tola *et al*. [87] used the k-means clustering method to cluster historical time series of stocks in order to improve reliability of share portfolios in terms of the ratio between predicted and realized risk. The authors used the historical daily returns of 1071 selected stocks on the New York Stock Exchange during the period 1988–1998 in the study. The time series were partitioned into two subsets. The first subset was used to cluster the time series, with the clustered daily return time series being used as an input to the mean-variance portfolio optimisation procedure, and compared to an unclustered mean-variance result as well as an approach involving random matrix theory filtering. These initial results represented the predicted risk, with the unclustered solution displaying the lowest predicted risk. The mean-variance optimisation results were then applied to the second subset in order to determine the realised risk. The clustered solutions displayed the lowest realised risk, as can be seen in Fig. 2.35.

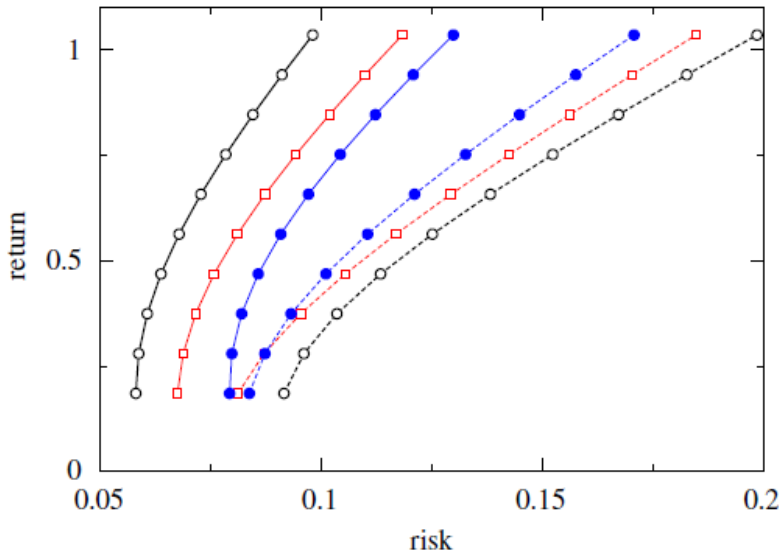

Fig. 2.35 Predicted risk (solid lines) and realised risk (dotted lines) for the unclustered mean-variance results (black), the random matrix theory results (red) and the clustered mean-variance result (blue) in the study by Tola et al. [87]**.**

Nanda *et al*. [88] employed several clustering methods to cluster stocks on the Bombay Stock Exchange (BSE). The authors used k-means clustering, self-organising maps and fuzzy c-means clustering methods to cluster the historical return time series. After consulting several clustering validation measures, it was concluded that the k-means clustering method resulted in the best clustering result. Time series from different clusters were selected to be used in a mean-variance optimisation, with the results being that the inputs from the clusters performing better when compared to the BSE index.

3 Renewable Energy Simulation

3.1 Overview

This section provides the mathematical formulation of the wind power and solar photovoltaic power simulations that were performed in this study. The wind power simulations are performed using a multi-turbine power curve approach developed by Norgaard and Holtinen [22], while the solar photovoltaic power simulations are performed using a simplified approach that is adapted from the textbook by Masters [14] and the PV Watts simulator that was developed by the National Renewable Energy Laboratory (NREL) [28].

3.2 Wind Power Simulation

3.2.1 Multi-turbine Power Curve

The multi-turbine power curve approach by Norgaard and Holtinen [22] was used to simulate the wind power time series from the wind speed time series and a wind turbine power curve. This method was developed to more accurately simulate the wind power from multiple wind turbines located in a relatively large area, for which only a single wind speed time series is available. The method is detailed below in four steps as follows:

Step 1 The first step is to perform a block averaging procedure on the wind speed time series. The number of points to include in the block average procedure, B, is given by [22]:

$$B = \frac{\left(\frac{D}{\mu_w}\right)}{\Delta t} \tag{3.1}$$

where D is the spatial resolution of the wind speed time series data, μ_w is the mean wind speed and Δt is the time resolution of the time series data.

The block averaged wind speed a_j at every point in time j is then given by [22]:

$$a_j = \frac{1}{B+1} \sum_{i=j-\frac{B}{2}}^{j+\frac{B}{2}} w_i \tag{3.2}$$

where w_i is the wind speed at the ith point in time in the original wind speed time series. The block averaging procedure is implemented to account for the spatial "memory effect" of the winds propagating over the specific area with a wind speed similar to the average wind speed of the site [22].

Step 2 A discrete multi-turbine power curve is constructed from a discrete single turbine power curve and a normalised Gaussian distribution. The jth discrete point in the multi-turbine power curve Pm_j is given by [22]:

$$Pm_j = \sum_i \left(Ps_{j+i} \times G_i \right) \tag{3.3}$$

where Ps_j is the jth discrete point in the single-turbine power curve and G_i is the i^{it} discrete point on the Gaussian distribution. In this investigation the type of single-turbine power

curve to be used depends on the average wind speed of the site and is described in section 3.2.2. The single turbine power curve is effectively convoluted with the Gaussian distribution as shown in Fig. 3.1. The Gaussian distribution has a standard deviation, σ, that depends on the assumed wind intensity, I, and the spatial resolution of the wind speed time series, D, as shown in Fig. 3.2. In this investigation a wind speed intensity of 10% was assumed for all sites. The actual standard deviation of the Gaussian distribution is obtained by multiplying the normalised standard deviation by the mean wind speed of the site, μ_w. The offset of the Gaussian distribution is initially zero and is adjusted as described in the next step. The Gaussian distribution represents the probability distribution function of the wind speeds present at individual wind turbines at different locations in the given area.

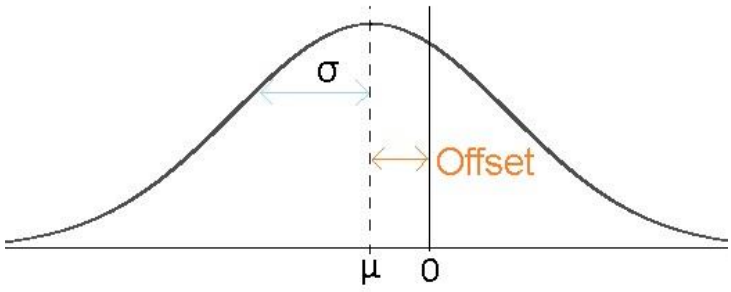

Fig. 3.1 Gaussian distribution.

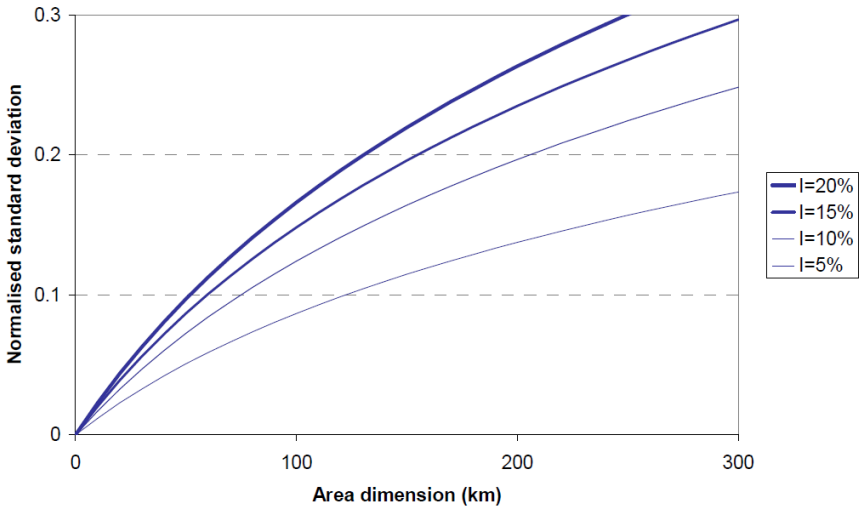

Fig. 3.2 The normalised standard deviation of the Gaussian distribution used to construct the multi-turbine power curve as a function of the spatial resolution of the wind speed time series and the wind speed intensity [22]**.**

Step 3 As described in step 2, the offset of the Gaussian distribution is initially set to zero. In order to find the correct offset, the single-turbine power curve is applied to the complete wind speed time series in order to calculate a total energy yield. The multi-turbine power curve constructed with the Gaussian distribution with zero offset is also applied to the complete time series and will necessarily overestimate the energy yield. Norgaard and Holtinen recommend that the offset be adjusted until the energy yield from the multi-turbine power curve equals the energy yield from the single-turbine power curve. In this investigation the offset was adjusted further until the energy yield from the multi-turbine

power curve equalled 90% of the energy yield from the single-turbine power curve. This is justified by the results from a study performed by Harman [89], which found that real-world power generation results are slightly overestimated when using the single-turbine power curves as given by the manufacturers due to different environmental and wind conditions.

Step 4 Once the correct offset has been determined in step 3, the multi-turbine power curve is applied to the block-averaged wind speed time series to generate the simulated wind power time series.

3.2.2 Turbine Selection

It is unrealistic to use the same turbine model for every site, as different turbine models are specifically designed to perform optimally in different wind speed ranges. As such, three different wind turbine models with the same nameplate capacity (2 MW) from the same manufacturer (Vestas) had been selected to model the wind power in this investigation. The criterium for the type of wind turbine to use is simply the average wind speed of the site, μ_w, as shown in Table 3.1, and has been selected based on information provided by the manufacturer [90].

Table 3.1 Wind turbine models with respective average wind speeds.

Site Average Wind Speed	**Wind Turbine Model**
$\mu_w \leq 6.5$m/s	Vestas V110-2.0 MW IEC IIIA
6.5m/s < $\mu_w \leq 8.5$m/s	Vestas V100-2.0 MW IEC IIB
$\mu_w > 8.5$m/s	Vestas V90-2.0 MW IEC IIA/IEC IIIA

An example of the multi-turbine power curve method applied to the Vestas V100-2 MW wind turbine is shown in Fig. 3.3.

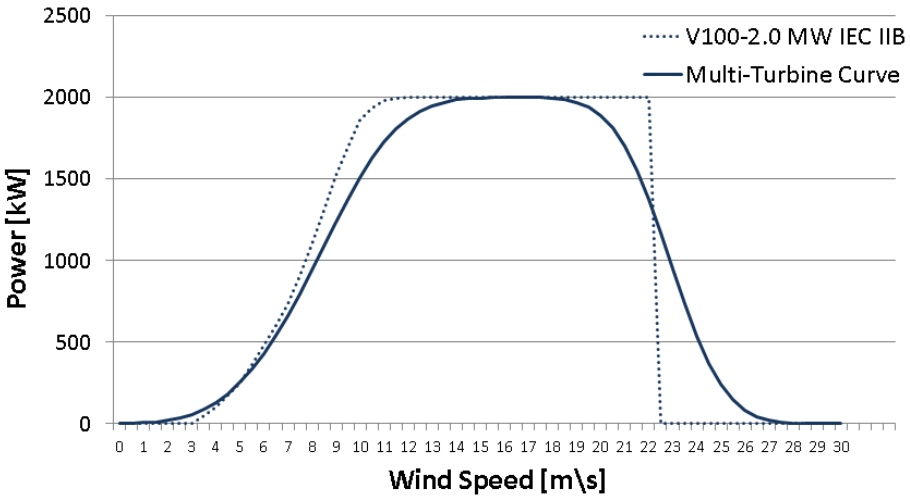

Fig. 3.3 Example of the multi-turbine power curve as applied to a single wind turbine power curve.

3.3 Solar Photovoltaic Power Simulation

The solar photovoltaic power simulations are done at every time step using ambient temperature data and irradiance data using a methodology that is adapted from the textbook by Masters [14] and the

PV Watts simulator [28] by NREL. The solar irradiance is taken as the total irradiance inclined on cell and consists of the direct irradiance, diffuse irradiance and reflected irradiance components.

First, the cell temperature, T_{Cell}, is calculated using the ambient temperature and solar irradiance as follows [14]:

$$T_{Cell} = T_{Amb} + \left(\frac{NOCT - 20}{0.8} \right) \cdot I \tag{3.4}$$

where T_{Amb} denotes the ambient temperature, I denotes the solar irradiance inclined on the photovoltaic panel [kW/m^2], $NOCT$ is the nominal operating cell temperature and is selected as 45 °C in this investigation. The $NOCT$, which is usually provided by the solar photovoltaic panel manufacturer, is the expected cell temperature in a module when the ambient temperature is 20 °C and the solar irradiation is 0.8 kW/m^2 [14].

The derating effect of temperature, η_{Temp}, is given by [28]:

$$\eta_{Temp} = \frac{1 + \gamma \cdot (T_{Cell} - T_{Ref})}{I_{Ref}} \tag{3.5}$$

where γ is the temperature coefficient, T_{Ref} is the reference temperature and I_{Ref} is the reference irradiance. In this investigation, a temperature coefficient of -0.47%/°C is selected, which is typical of a standard solar panel module [28]. The reference temperature and reference irradiance is selected as 25 °C and 1 kW/m^2 respectively.

The DC power, P_{DC}, is calculated as follows [28]:

$$P_{DC} = I \cdot P_{Rated} \cdot \eta_{Temp} \tag{3.6}$$

where P_{Rated} is the nameplate direct current power rating of the photovoltaic panel, selected as 2 MW in order to be of the same magnitude as the wind turbine time series simulation models in section 3.2.

The DC power that the solar photovoltaic panel generates is then converted to AC power using an inverter, with the inverter efficiency, $\eta_{Inverter}$, calculated as follows [28]:

$$\eta_{Inverter} = \frac{\eta_{nom}}{\eta_{ref}} - 0.0162 \cdot \zeta - \frac{0.0059}{\zeta} - 0.0142 \tag{3.7}$$

where η_{nom} is the nominal efficiency of the inverter, η_{ref} is the reference inverter efficiency and ζ is the load fraction, calculated simply as the DC power at that time step divided by the rated power, P_{DC}/P_{Rated}. The nominal efficiency and the reference inverter efficiency are given as 0.96 and 0.9637 respectively. The reference inverter efficiency was calculated by examining actual inverter performance data from the California Energy Commission [28].

A graph of the inverter efficiency, as it depends on the load factor, is given in Fig. 3.4. It is clear that the inverter typically reaches the nominal efficiency at load factors of approximately 0.3 and higher.

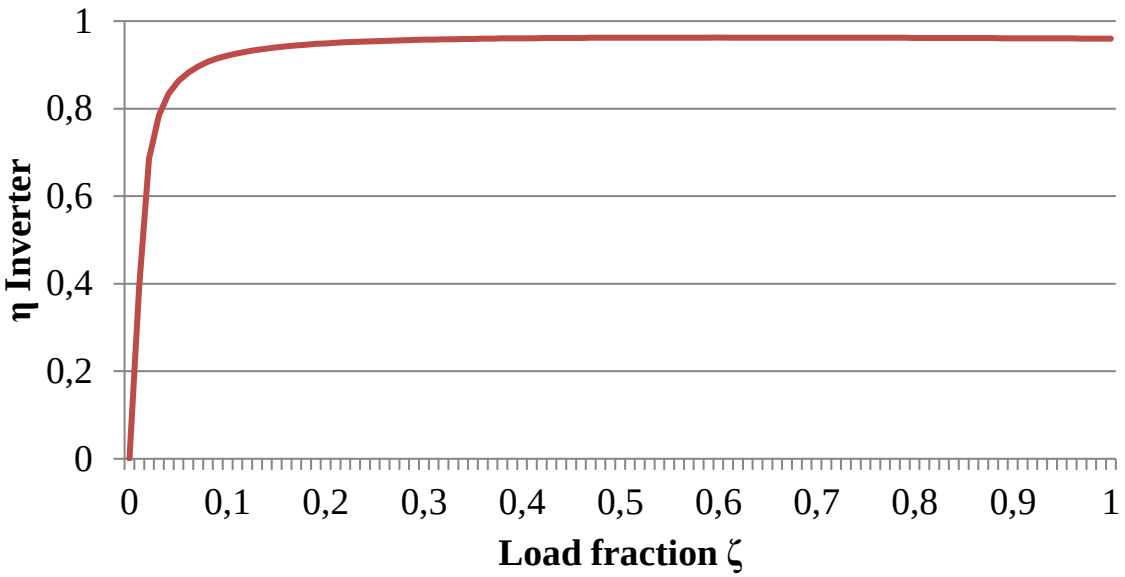

Fig. 3.4 Graph of inverter efficiency versus load factor obtained from equation (3.4).

Finally the AC power, P_{AC}, is calculated as

$$P_{AC} = \begin{cases} P_{DC} \cdot \eta_{Inverter} : 0 < P_{DC} < P_{Rated} \\ P_{Rated} \cdot \eta_{nom} : \quad P_{DC} \geq P_{Rated} \\ 0 \qquad : \qquad P_{DC} = 0 \end{cases} \tag{3.8}$$

In standard cases, the AC power is equal to the DC power multiplied by the inverter efficiency. When the calculated DC power is greater than the rated DC power, the AC power is simply calculated as the rated DC power times the nominal efficiency of the inverter.

For the sake of simplicity, many other sources of losses have not been taken into account, including but not limited to effects from soiling, shading, wiring and ageing.

4 Time Series Clustering

4.1 Overview

Time series clustering has been suggested in the literature as a method of improving the mean-variance optimisation procedure. The justification for using time series clustering is given in section 5.6, which stems from the mean-variance optimisation formulation.

Time series clustering is an established field of data mining. It is an unsupervised classification which attempts to order unlabelled time series into groups of time series data which share common behaviours or features. Traditionally the main challenges with time series clustering have been the high dimensionality, the presence of noise and the high feature correlation [83]. There are also different approaches to time series clustering which have been separated into three groups, namely raw-data-based, feature-based and model-based clustering. As the focus of this investigation is on the correlation of the hourly power output profiles of different geographical locations, the raw-data-based approach is applied.

This section will give an overview of the complete time series clustering methodology used in this investigation. The elements in time series clustering include the similarity measure, distance matrix, clustering method and cluster validation measures.

4.2 Similarity Measure

The similarity measure determines how similar two time series are to each other. The type of similarity measure that is used determines whether similarity in time, similarity in shape or similarity in change will be targeted.

The Euclidian distance similarity measure is used in this investigation to quantify the similarity between two time series. Suppose vectors **X** and **Y** are *L*-dimensional and represent two time series:

$$\begin{aligned}\mathbf{X} &= \begin{bmatrix} X_1 & X_2 & X_3 & \dots & X_L \end{bmatrix}^{\mathrm{T}} \\ \mathbf{Y} &= \begin{bmatrix} Y_1 & Y_2 & Y_3 & \dots & Y_L \end{bmatrix}^{\mathrm{T}}\end{aligned} \tag{4.1}$$

Then the Euclidian distance, $\mathrm{D}_E(\mathbf{X},\mathbf{Y})$ between the two vectors is formulised as follows [83]:

$$D_E(\mathbf{X},\mathbf{Y}) = \sqrt{\sum_{i=1}^{L}(X_i - Y_i)^2} \tag{4.2}$$

The Euclidian distance is a specific version of the $\mathrm{L_q}$-norm distance, also known as the Minkowski distance, $\mathrm{D}_{L_q}(\mathbf{X},\mathbf{Y})$, which is given by [83]:

$$D_{L_q}(\mathbf{X},\mathbf{Y}) = \left(\sum_{i=1}^{L}(X_i - Y_i)^q\right)^{\frac{1}{q}} \tag{4.3}$$

where q is usually selected as 1 (Manhattan distance) or 2 (Euclidian distance). This similarity measure examines values observed at corresponding points in time, effectively treating observations in a single time series at different points in time as if they were independent [91]. This is a desirable characteristic in this application, as it is the intention so cluster simulated power output time series by comparing their values at a given time independent from values right before or after, in order to construct a centroid that best represents the power output time series of that cluster. For example, if

two potential wind farm sites are clustered together, one with strong power output values during 15:00 to 17:00 and one with strong power output values between 17:00 and 19:00, the one potential site would be contributing during peak load times while the other would not, and the resulting centroid would lose a lot of that information. There are similarity measures that could account for time stretching and time shifting formations such as this, if this fits with the intended application.

4.3 Distance Matrix

The distance matrix is a symmetrical matrix that captures the distance between every vector and stores it in the off-diagonal elements. The diagonal contains all zeros as the distance between a vector and itself is zero. The distance matrix stores the similarity between every time series that is included in the investigation and serves as an input to the clustering method.

Suppose another *L*-dimensional vector **Z**, in conjunction with the previous vectors **X** and **Y**:

$$\mathbf{Z} = \begin{bmatrix} Z_1 & Z_2 & Z_3 & \dots & Z_L \end{bmatrix}^{\mathrm{T}} \tag{4.4}$$

then using the Euclidian distance measure will result in a distance matrix between the three vectors that looks as follows:

$$\text{Distance Matrix} = \begin{bmatrix} D_E(\mathbf{X},\mathbf{X}) = 0 & D_E(\mathbf{X},\mathbf{Y}) & D_E(\mathbf{X},\mathbf{Z}) \\ D_E(\mathbf{Y},\mathbf{X}) & D_E(\mathbf{Y},\mathbf{Y}) = 0 & D_E(\mathbf{Y},\mathbf{Z}) \\ D_E(\mathbf{Z},\mathbf{X}) & D_E(\mathbf{Z},\mathbf{Y}) & D_E(\mathbf{Z},\mathbf{Z}) = 0 \end{bmatrix} \tag{4.5}$$

The distance matrix serves as an input to the clustering methods. After the distance matrix has been computed, the different time series can effectively be viewed as data points, with distances between them specified by the distance matrix. As such, in the following section reference will be made to data points, with the i^{th} coordinate of the data point being analogues to the i^{th} value in the time series.

4.4 Clustering Methods

The clustering method determines how the cluster operation will be performed. In determining the type of clustering method to use, it is generally suggested to apply several algorithms and then determine the best option for the given case, using cluster validation methods. Several clustering methods have been considered in this investigation. Basic clustering algorithms can be classified as either hierarchical or partitional.

4.4.1 Hierarchical Methods

Hierarchical clustering makes use of clustering steps that result in nested clusters organised as a hierarchical tree that can easily be visualised using a dendrogram, as can be seen in Fig. 4.1. It is therefore not necessary for the user to specify the number of clusters beforehand.

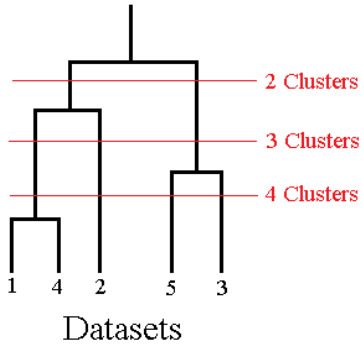

Fig. 4.1 Example of a dendrogram.

In hierarchical clustering, the clustering steps can be done in two directions:

- Agglomerative: All the data points start as their own cluster, and clusters are then grouped at each step according to the distances between the clusters. This is referred to as the "bottom up" approach.
- Divisive: All the data points start as one cluster, and clusters are then split at each step according to the distances between the clusters. This is referred to as the "top down" approach.

The distances between different clusters depend on the type of hierarchical clustering method, as can be seen in an example in Fig. 4.2 (where only two dimensions are plotted and each data point represents a time series) with the distance between points being the similarity measure (the Euclidian distance in this investigation). The cluster centroids represent the average coordinates of all the data points assigned to the respective cluster. If an agglomerative hierarchical clustering is used, the next step would be to combine two of the three clusters. If the average distance between points was considered (centroid distance), cluster 2 and cluster 3 would be combined, but if the maximum distance was considered, cluster 1 and cluster 2 would be combined as the maximum distance between a point in cluster 2 and cluster 3 is greater than the maximum distance between point in cluster 1 and cluster 2.

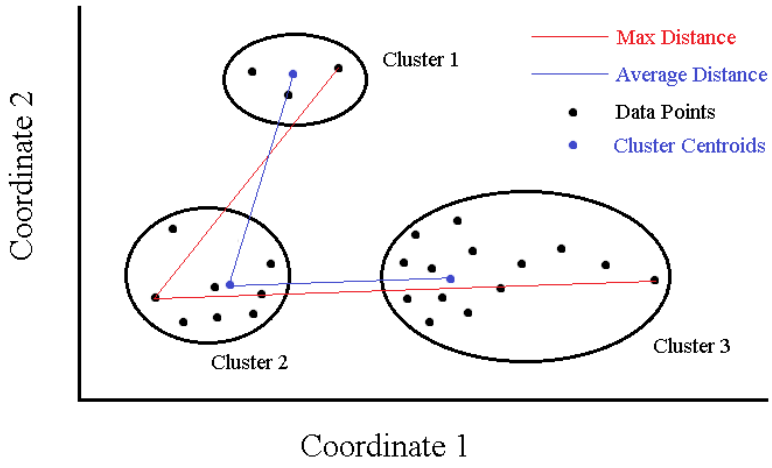

Fig. 4.2 Example of hierarchical clustering.

The agglomerative hierarchical clustering algorithms considered in this investigation include complete-linkage, average-linkage and Ward's method hierarchical clustering.

4.4.1.2 Complete-linkage

The complete-linkage clustering method attempts to find similar clusters. The two data points that represent the maximum distance between two clusters are used as the distance metric.

4.4.1.3 Average-linkage

The average-linkage clustering method attempts to find clusters with similar variances. The average distance between the data points in different clusters is used as the distance metric.

4.4.1.4 Ward's Method

Ward's method, which is also known as the minimum variance method, attempts to minimise information loss when clustering. At each step, it groups the two elements whose grouping would induce the least increase in their sums of square difference from the mean [83]. The Ward distance metric $d_W(C_m, C_n)$ is given by [92]:

$$d_W(C_m, C_n) = \frac{|C_m||C_n|}{|C_m|+|C_n|}\left\|\bar{x}_m - \bar{x}_n\right\|^2 \tag{4.6}$$

where $|C_m|$ and $|C_n|$ represent the number of elements in cluster C_m and C_n respectively, and $\bar{x}_m$ and $\bar{x}_n$ represent the centroids of the respective clusters.

4.4.2 Partitional Methods

Partitional clustering divides the datasets into a user-specified number of subsets. One partitional method has been considered in this investigation, namely the partitioning around medoids (PAM) methodology, which is generally viewed as a more robust version of the well-known k-means algorithm [82].

4.4.2.1 Partitioning Around Mediods

The PAM method requires that the number of clusters, p, be specified beforehand. The clustering method contains four steps which are detailed below [93]:

1. Initialisation is performed. Randomly assign p of the data points as the mediods.
2. Assign each data point to the mediod closest to it.
3. Perform an update swap for each mediod p and each data point associated with mediod p. The cost of the configuration, represented by the average dissimilarity of the data point to all the other data points associated to p, is calculated. A new medoid data point, with the lowest cost, is selected.
4. Repeat the assignment and update steps, i.e. step 2 and step 3 above, until no new assignments are made.

4.5 Cluster Validation Methods

The cluster validation measures are used to judge to the quality of a clustering result and to justify the use of certain clustering methods over others, as well as the appropriate number of clusters to be used. Several cluster validation methods have been considered.

Four cluster validation metrics have been applied in validating the performance of the clustering algorithms in this investigation. These include the average between cluster distance, the average within cluster distance, the average silhouette widths and the Caliński-Harabasz index.

4.5.1 Average Between Cluster Distance

The average between cluster distance represents the average sum of the square distance between data points clustered together in different clusters. A higher average between cluster distance is desirable as this indicates better separation between clusters.

4.5.2 Average Within Cluster Distance

The average within cluster distance represents the average sum of the square distance between time series clustered together in a single cluster. A lower average within cluster distance is desirable as this indicates less separation between data points in a single cluster.

4.5.3 Average Silhouette Width

The silhouette width of a data point is a measure of the membership strength of that data point to its assigned cluster. It is based on the average distance a_{x_t} between each data point x_t of a cluster C_m to every other data point in that cluster, and b_{x_t}, the minimum value of the average distance between that data point and the data point belonging to all other clusters. The average silhouette width is defined as [85]:

$$\text{average silhouette width} = \frac{1}{T}\sum_{k=1}^{K}\sum_{x_t \in C_k}\frac{b_{x_t} - a_{x_t}}{\max(b_{x_t}, a_{x_t})} \tag{4.7}$$

where T denotes the number of data points and K denotes the number of clusters. Note that the difference between b_{x_t} and a_{x_t} is normalized by their maximum value. The average silhouette width metric results in a score between -1 and 1, where -1 one indicates a very poor clustering and 1 represents a very good clustering.

4.5.4 Caliński-Harabasz Method

The Caliński-Harabasz (CH) index calculates the ratio between cohesion and separation, where cohesion is based on the distances from the points in a cluster to its centroid and the separation is based on the distance from the centroids to the global centroid, i.e. the centroid of all the data points [94]. It is defined by the relationship:

$$\text{Caliński-Harabasz index} = \frac{Tr(S_B)/(K-1)}{Tr(S_W)/(T-K)} \tag{4.8}$$

with

$$Tr(S_B) = \sum_{k=1}^{K} T_k \left\| \bar{x}_k - \bar{x} \right\|^2 \tag{4.9}$$

and

$$Tr(S_w) = \sum_{k=1}^{K} \sum_{x_t \in C_k} \left\| x_t - \bar{x}_k \right\|^2 \tag{4.10}$$

where T denotes the number of data points, K denotes the number of clusters, S_B and S_W denote the traces of the between-class and the within-class scatter matrices respectively, T_k denotes the number of number of data points in cluster k, x_t denotes a data point in cluster k, $\bar{x}_k$ denotes the centroid of cluster k and $\bar{x}$ denotes the centroid of all the data points. The CH index is normalised to account for the increasing number of clusters. The objective of the CH method is to determine a number of clusters K that maximises the CH index. This implies maximising the ratio of $Tr(S_B)$ and $Tr(S_W)$, i.e. the ratio of between cluster scatter and within cluster scatter.

4.6 Determining the Number of Appropriate Clusters

There is no definitive way to determine the number of clusters that is appropriate for a given dataset. It is suggested that the results of the cluster validation measures are consulted. The number of clusters is typically chosen to represent a point where increasing the number of clusters yields diminishing returns in the cluster validation measures, as formalised in the L-method [95].

4.6.1 Wind Time Series

The wind power time series show significant variance between different time series, and as such it has been decided that the average centroid error will be consulted in order to determine the optimal number of clusters. The number of clusters is chosen so the centroids display an average centroid error of less than 10%. The average centroid error is formulised as follows:

A centroid data time series, $\bar{x}_k$, is calculated for each cluster and the total error at each point in time i between the centroid time series and every time series x_t in the cluster C_k is summed and averaged to calculate the average centroid error. The average centroid error is defined by the relationship:

$$\text{average centroid error} = \frac{1}{L \cdot T} \sum_{k=1}^{K} \sum_{x_t \in C_k} \sum_{i=1}^{L} \left| \bar{x}_{ki} - x_{ti} \right| \tag{4.11}$$

where L denotes the number of length of the time series, T denotes the number of time series, K denotes the number of clusters and $\bar{x}_{ki}$ and x_{ti} represents the ith record of centroid $\bar{x}_k$ and time series x_t respectively.

4.6.2 Solar Photovoltaic Time Series

The solar photovoltaic power time series show more correlation than wind power time series, and as such it is decided that all the cluster validation measures will be inspected using the L-method, in order to ascertain how many clusters might be appropriate.

The L-Method [95] attempts to find the K best number of clusters by fitting 2 linear models to the left hand side and right hand side of a cluster validation method dataset and determining a point c such that the total root mean square of the linear models is minimized. The cluster validation method's values, each corresponding to a number of clusters, is split into two groups such that the left hand group L_C has values {2,…, c} and right hand group R_C has values {c,…, b}, where b represents the maximum number of clusters. After a linear model is fitted to each group using linear regression, the total root-mean-square error ($RMSE_T$) is given by the relationship:

$$\text{RMSE}_T = \frac{c-1}{b-1}\text{RMSE}_L + \frac{b-c}{b-1}\text{RMSE}_R \tag{4.12}$$

The RMSE of the left and right hand groups, RMSE_L and RMSE_R respectively, are weighted proportional to the lengths of L_C and R_C. The crucial point is found by finding the value c that minimizes RMSE_T.

5 Mean-Variance Optimisation

5.1 Overview

In mean-variance portfolio theory, an investor seeks to minimise risk for a preferred yield when investing shares on the stock market [96]. This problem equates well with the problem of locating wind generation capacity with the view to maximise the cumulative power contribution whilst minimising variability and has been applied extensively in the literature in this regard.

This section will give an introduction and mathematical formulation to mean-variance portfolio theory. This section will also introduce the addition of solar photovoltaic power time series and load time series into the optimisation problem. Studies in the literature have suggested that solar photovoltaic power and load data be incorporated, but no study has actually implemented this. Some studies has also suggested that clustering techniques be incorporated into the optimisation procedure. The incorporation will be justified at the end of this section.

5.2 Introduction to Mean-variance Portfolio Theory

Mean-variance portfolio theory, which was first proposed by Markowitz in 1952 [65], provides a mathematical framework to select a portfolio of assets, each with an associated historical return time series, that minimises the risk of the combined portfolio. The investor provides a desired mean return on his portfolio, which acts as a constraint in the optimisation problem, and the optimisation is solved such that an optimal weight of each asset is found that results in a cumulative return with minimum variance. The portfolio return column vector, **R**, is defined as:

$$\mathbf{R} = w_1\mathbf{H}_1 + w_2\mathbf{H}_2 + w_3\mathbf{H}_3 + \ldots + w_t\mathbf{H}_t + \ldots + w_T\mathbf{H}_T \tag{5.1}$$

where $\mathbf{H}_t$ denotes the historical return of asset t, w_t denotes the weight of asset t and T is the total number of assets. Each historical return vector looks as follows:

$$\mathbf{H}_t = \begin{bmatrix} H_1 & H_2 & H_3 & \ldots & H_i & \ldots & H_L \end{bmatrix}^{\mathrm{T}} \tag{5.2}$$

where H_i is the return at time i and L is the length of the historical return vector (time series).

The optimisation problem is formulised as follows [96]:

$$\min_{w_t=(w_1,w_2,w_3,\ldots,w_T)} \operatorname{var}(\mathbf{R}) = \sum_{j=1}^{T}\sum_{l=1}^{T} w_j w_l \sigma_{jl} \tag{5.3}$$

such that

$$\sum_{t=1}^{T} w_t \mu_t = \mu_{\text{Desired}}, \tag{5.4}$$

$$\sum_{t=1}^{T} w_t = w_{\text{Total}} \tag{5.5}$$

and

$$\min_t \le w_t \le \max_t, t \in [1\ldots\mathrm{T}] \tag{5.6}$$

where w_t is the decision variable that results in a minimised cost function, $\text{var}(\mathbf{R})$, which is the variance of cumulative portfolio return vector $\mathbf{R}$. Variable T is the total number of assets, σ_{jl} denotes the covariance between the return time series $\mathbf{H}_j$ and $\mathbf{H}_l$ of asset j and l, μ_t is the mean value of return time series $\mathbf{H}_t$ of asset t, μ_{Desired} is the desired mean return of the cumulative portfolio, w_{Total} is the total weight that can be assigned and $\min_t$ and $\max_t$ are the minimum and maximum weight respectively that can be assigned to asset t.

The total weight, w_{Total}, is normally specified as 1, which results in the weights assigned to assets, w_t, falling between 0 and 1 subject to their respective minimum and maximum weights, $\min_t$ and $\max_t$.

Equation (5.3) can alternatively be written as follows:

$$\min_{\mathbf{w}=\begin{bmatrix} w_1 & w_2 & w_3 & \dots & w_T \end{bmatrix}^{\mathrm{T}}} \text{var}(\mathbf{R}) = \mathbf{w}^{\mathrm{T}} \sum \mathbf{w} \tag{5.7}$$

where $\mathbf{w}$ is a $T \times 1$ vector that represents the weights of each asset, Σ is the covariance matrix and $\mathbf{w}^{\mathbf{T}}$ indicates the transpose of vector $\mathbf{w}$ (which is not to be confused with w_t, which indicates the T^{th} element of column vector $\mathbf{w}$). The covariance matrix, Σ, is positive semi-definite, which means that $\mathbf{w}^{\mathbf{T}}\Sigma\mathbf{w}$ is non-negative for every non-zero column vector $\mathbf{w}$ of T real numbers.

Covariance is a measure of how two random variables, X and Y, vary together, and is calculated as follows [97]:

$$\text{cov}(X,Y) = \sigma_{XY} = \frac{1}{L}\sum_{i=1}^{L}(X_i - \overline{X})(Y_i - \overline{Y}) \tag{5.8}$$

where L is the length of the random variables and $\bar{X}$ and $\bar{Y}$ represent the mean values of X and Y respectively.

The covariance calculation can also be written as:

$$\text{cov}(X,Y) = \text{E}[(X - \text{E}[X])(Y - \text{E}[Y])] \tag{5.9}$$

where E[ ] represents the expected (mean) value function.

The covariance matrix, Σ, which is also known as the dispersion matrix or variance–covariance matrix [96], contains the variance of each random variable in its diagonal and the covariance between the random variables in the off-diagonal elements:

$$\Sigma = \begin{bmatrix} \text{var}(X) & \text{cov}(X,Y) \\ \text{cov}(Y,X) & \text{var}(Y) \end{bmatrix} \tag{5.10}$$

with $\text{cov}(Y,X) = \text{cov}(X,Y)$.

The mean-variance portfolio theory formulation translates to a quadratic programming problem. Quadratic programming problems are formulated as follows [98]:

An n-dimensional vector, $\mathbf{x}$, is found that will

$$\text{minimise}\,\frac{1}{2}\mathbf{x}^{\mathrm{T}}\mathbf{Q}\mathbf{x}+\mathbf{c}^{\mathrm{T}}\mathbf{x} \tag{5.11}$$

subject to m constraints in the form

$$\mathbf{A}\mathbf{x} \leq \mathbf{b} \tag{5.12}$$

where $\mathbf{c}$ is a real-valued n-dimensional vector, $\mathbf{Q}$ is a symmetric real-valued $n \times n$-dimensional matrix, A is a real $m \times n$-dimensional matrix and $\mathbf{b}$ is an m-dimensional real vector. The notation $\mathbf{Ax} \leq \mathbf{b}$ means that every entry of the vector $\mathbf{Ax}$ is less than or equal to the corresponding entry of the vector $\mathbf{b}$.

When observing equation (5.7) and the linear constraints in equation (5.4)-(5.6), it is clear that the mean-variance optimisation problem takes the form of a quadratic programming problem with the vector $\mathbf{c}$ specified as a zero column vector.

The mean-variance problem can be solved for different given desired mean returns, μ_{Desired}, to yield a set of solutions known as the efficient frontier. Every point on the efficient frontier represents a portfolio with a minimum variance for the given desired mean return as can be seen in Fig. 5.1. The extreme points on the efficient frontier to the far left and far right represent portfolios that are made up exclusively of one asset with the lowest and highest returns respectively (in the absence of constraints that limit the weight of individual assets).

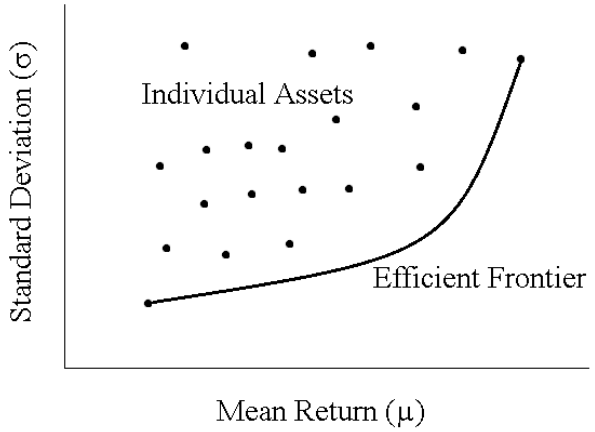

Fig. 5.1 The efficient frontier in the mean-variance portfolio optimisation problem.

5.3 Mean-variance Portfolio Theory Mathematical Formulation with Wind Power

Mean-variance portfolio theory will be formalised here as applied to wind farm location optimisation. Potential wind farm sites, x, are viewed as assets (t in section 5.2) and simulated or measured historical wind data sets are used to simulate theoretical wind turbine power time series using a given wind turbine power curve for each of the potential locations. The simulated wind power time series, $\mathbf{P}_x$, is equated to historical return time series ($\mathbf{H}_t$ in section 5.2). The covariance between proposed wind farm locations (equated to risk) is minimised for different capacity factors (equated to mean portfolio return).

The mathematical formulation of the optimisation problem is similar to section 5.2:

$$\min_{w_x=(w_1,w_2,w_3,\ldots,w_N)} \operatorname{var}(\mathbf{W}) = \sum_{j=1}^{N}\sum_{l=1}^{N} w_j w_l \sigma_{jl} \tag{5.13}$$

such that

$$\sum_{x=1}^{N} w_x \mu_x = \mu_{\text{Desired Wind}}, \tag{5.14}$$

$$\sum_{x=1}^{N} w_x = w_{\text{Total Wind}} \tag{5.15}$$

and

$$0 \le w_x \le \max_x, x \in [1\ldots\text{N}] \tag{5.16}$$

where w_x is the number of turbines at site x, $\operatorname{var}(\mathbf{W})$ is the variance of the cumulative wind power output vector $\mathbf{W}$, N is the total number of potential wind farm sites, σ_{jl} is the covariance between the wind power time series $\mathbf{P}_j$ and $\mathbf{P}_l$ of site j and l, μ_x is the mean wind power output $\mathbf{P}_x$ of site x, $\mu_{\text{Desired Wind}}$ is the desired mean wind power output of the cumulative wind power output $\mathbf{W}$ from all sites, $w_{\text{Total Wind}}$ is the total number of wind turbines that can be assigned and $\max_x$ is the maximum number of turbines that can be assigned to site x.

In equation (5.16), instead of a 0, a $\min_x$ term (minimum number of turbines) can be included for two reasons:

- If there is a minimum number of turbines that is specified to be built on a certain site (this might lead to a sub-optimal solution).
- If the mean-variance optimisation is performed with existing wind farm capacity in mind, the historical or simulated wind power time series of the existing wind farm capacity would be included and the existing capacity would be specified as the $\min_x$ term.

The capacity factor of the cumulative wind power output is simply the mean cumulative wind power output divided by the total capacity as follows:

$$\text{capacity factor} = \frac{\mu_{\text{Desired Wind}}}{w_{\text{Total Wind}}} \tag{5.17}$$

Therefore solving for different values of $\mu_{\text{Desired Wind}}$ yields the efficient frontier. Solutions on the efficient frontier representing a mathematically optimal mix of wind farm capacities and locations with a minimum level of variance for a given overall capacity factor.

When performing the mean-variance optimisation with wind farms, the wind turbine power curves that are used to simulate the wind power time series should satisfy one of two criteria:

- The wind turbine power curves should have the same rated power.
- If the wind turbine power curves don't have the same rated power, the wind turbine power curves should all be normalised to a selected rated power, with the total assigned capacity decision variable (w_x, number of turbines) resulting from the optimisation procedure being scaled using the same respective normalising factor.

This is to ensure that the trivial solution is avoided where wind power capacity is assigned to the site where a wind turbine with a higher rated capacity is used.

5.4 Mean-variance Formulation with Wind Power and Solar Photovoltaic Power

When incorporating solar photovoltaic power into the mean-variance optimisation problem, it is possible to treat the potential solar photovoltaic sites just as potential wind farm sites and perform the optimisation just as in section 5.3, with the variance of the total renewable power output being minimised. However, this would cause some confusion with the mean power output variable, μ_{Desired}, as wind farms and solar photovoltaic farms typically have very different capacity factors. wind farms typically display capacity factors larger than 25%, whereas solar photovoltaic farms typically display capacity factors of 18% to 25%. The μ_{Desired} variable would now represent the mean renewable power output. Solving the mean-variance optimisation problem in the usual way would lead to solutions on the lower end of the efficient frontier being dominated by solar photovoltaic farm capacity and solutions to the higher end being dominated wind farm capacity. This is obviously not desirable, as the objective should be to have a high capacity factor wind farm portfolio that is supported by solar photovoltaic power. This can be solved by setting up the linear constraints in a slightly different way. The approach that is defined here considers the total wind farm capacity that is to be assigned and the desired overall wind farm capacity factor, and simply allows the optimisation procedure to supplement the wind power output with solar photovoltaic power output in order to minimise the variance of the total renewable power output, with several optional constraints related to the solar photovoltaic power capacity.

First, the total renewable power output is defined as:

$$R_i = \sum_{x=1}^{N} W_i^x + \sum_{y=1}^{M} S_i^y \tag{5.18}$$

where R_i is the total renewable power output at time i, N is the number of wind farms, W_i^x is the wind power output at wind farm x at time i, M is the number of solar photovoltaic farms, S_i^y is the solar photovoltaic power output at solar photovoltaic farm y.

Combining the total renewable power output at all times i, results in the total renewable power output vector $\mathbf{R}$ of length L:

$$\mathbf{R} = \begin{bmatrix} R_1 & R_2 & R_3 & \dots & R_L \end{bmatrix}^{\mathrm{T}} \tag{5.19}$$

The mean-variance problem is then formulised as follows:

$$\min_{w_x = (w_1, w_2, w_3, \dots, w_{N+M})} \operatorname{var}(\mathbf{R}) = \sum_{j=1}^{N+M} \sum_{l=1}^{N+M} w_j w_l \sigma_{jl} \tag{5.20}$$

such that

$$\sum_{x \in \text{Wind}}^{N} w_x \mu_x = \mu_{\text{Desired Wind}}, \tag{5.21}$$

$$\sum_{x \in \text{Solar}}^{M} w_x \mu_x \geq \mu_{\text{Min Desired Solar}}, \tag{5.22}$$

$$\sum_{x \in \text{Wind}}^{N} w_x = w_{\text{Total Wind}}, \tag{5.23}$$

$$\sum_{x \in \text{Solar}}^{M} w_x \leq w_{\text{Max Total Solar}} \tag{5.24}$$

and

$$0 \leq w^x \leq \max^x, x \in [1...\text{N+M}] \tag{5.25}$$

where w_x is the number of turbines or solar photovoltaic capacity at site x, var($\mathbf{R}$) is the variance of cumulative renewable power output, N is the total number of potential wind farm sites, M is the total number of potential solar photovoltaic farm sites, σ^{jl} is the covariance between the power time series of site j and l, μ_x is the mean power output of site x. The sites included in the optimisation procedure are classified as either potential wind farm sites ($x \in$ Wind) or potential solar photovoltaic farm sites ($x \in$ Solar). The desired mean wind farm output, $\mu_{\text{Desired Wind}}$, and the total wind farm capacity (number of wind turbines) to be allocated, $w_{\text{Total Wind}}$, is specified by the user. Equation (5.22) and (5.24) are optional constraints that control the minimum overall solar photovoltaic farm power output, $\mu_{\text{Min Desired Solar}}$, and the maximum solar photovoltaic farm capacity that can be allocated, $w_{\text{Max Total Solar}}$. As before, $\max_x$ is the maximum number of turbines or solar photovoltaic farm capacity that can be assigned to any one individual site x.

Similar to the wind turbine power curve scaling procedure in section 5.3, the simulated solar photovoltaic power time series would typically be scaled to the selected rated power of the wind turbine power curve in order to have decision variables ($w_1, w_2, w_3, \ldots, w_{N+M}$) that refer to the same capacity, although this is not necessary with the formulation of the constraints given above due to the separation of wind capacity and solar photovoltaic capacity constraints. For example, if a simulated power time series of a 2 kW solar photovoltaic panel is included in conjunction with simulated power time series of 2 MW wind turbines, the simulated power time series of the 2 kW solar photovoltaic panel would be scaled to 2 MW so that the decision variables could be compared as is.

5.5 Mean-variance Formulation with Wind Power, Solar Photovoltaic Power and Load

In section 5.3 and 5.4 the variance or the total wind power output and the variance of the total renewable power output was minimised respectively. As renewable power plants have no fuel costs and don't emit any greenhouse gases, they are usually given priority dispatch over conventional generation plants and are only curtailed in extreme events. This effectively means that the conventional generation fleet has to meet the residual load, i.e. the load minus the contribution of renewables. It is therefore intuitive to want to minimise the variance of the residual load in order to maximise the use of cheaper and more efficient base-load and load-following plants over peaking power plants.

Incorporating the load time series into the mean-variance formulation was suggested (but not implemented) by Degeilh and Singh [17]. The authors considered only wind farm capacity and load, and proposed that unless the wind farm time series showed considerable correlation with the load, the incorporating the load time series has a very small effect. In the case of wind power only, where the cumulative wind power output, $\mathbf{W}$, is the weighted total of the power time series of the individual sites $\mathbf{P}_x$:

$$\mathbf{W} = w_1\mathbf{P}_1 + w_2\mathbf{P}_2 + w_3\mathbf{P}_3 + \ldots + w_x\mathbf{P}_x + \ldots + w_N\mathbf{P}_N \tag{5.26}$$

and the weight vector $\mathbf{w}$ is consists of the respective weights:

$$\mathbf{w} = \begin{bmatrix} w_1 & w_2 & w_3 & \dots & w_N \end{bmatrix} \tag{5.27}$$

the variance of the cumulative wind power output is:

$$\begin{aligned} \text{var}(\mathbf{W}) &= \mathbf{w}^{\mathrm{T}} \sum \mathbf{w} \\ &= \mathbf{w}^{\mathrm{T}} \begin{bmatrix} \text{var}(\mathbf{P}_1) & \text{cov}(\mathbf{P}_1, \mathbf{P}_2) & \cdots & \text{cov}(\mathbf{P}_1, \mathbf{P}_N) \\ \text{cov}(\mathbf{P}_2, \mathbf{P}_1) & \text{var}(\mathbf{P}_2) & \cdots & \text{cov}(\mathbf{P}_2, \mathbf{P}_N) \\ \vdots & \vdots & \ddots & \vdots \\ \text{cov}(\mathbf{P}_N, \mathbf{P}_1) & \text{cov}(\mathbf{P}_N \mathbf{P}_2) & \dots & \text{var}(\mathbf{P}_N) \end{bmatrix} \mathbf{w} \\ &= \sum_{x=1}^{N} {w_x}^2 \, \text{var}(\mathbf{P}_x) + 2 \sum_{x<y} w_x w_y \, \text{cov}(\mathbf{P}_x, \mathbf{P}_y) \end{aligned} \tag{5.28}$$

Degeilh and Singh [17] showed that when the load is included in the variance formulation, the variance of the residual load reduces to:

$$\begin{aligned} \text{var}(\mathbf{L} - \mathbf{W}) &= \text{var}(\mathbf{L}) + \text{var}(\mathbf{W}) - 2\,\text{cov}(\mathbf{L}, \mathbf{W}) \\ &= \text{var}(\mathbf{L}) + \sum_{x=1}^{N} {w_x}^2 \, \text{var}(\mathbf{P}_x) + 2 \sum_{x<y} w_x w_y \, \text{cov}(\mathbf{P}_x, \mathbf{P}_y) - 2 \sum_{x=1}^{N} w_x \, \text{cov}(\mathbf{L}, \mathbf{P}_x) \end{aligned} \tag{5.29}$$

The formulation of the variance of the residual load thus contains four terms. The first term, $\text{var}(\mathbf{L})$, is fixed. The second term, the variances of the power outputs of individual sites $\text{var}(\mathbf{P}_x)$, is controlled by a squared variable ${w_x}^2$. The third term, the covariances between power outputs of individual sites $\text{cov}(\mathbf{P}_x, \mathbf{P}_y)$, is controlled by a cross product variable $w_x w_y$. The last term, the covariances between the load and the power output of individual sites, $\text{cov}(\mathbf{L}, \mathbf{P}_x)$, are controlled by a single degree variable w_x. Due to the nature of these controlling variables, Degeilh and Singh [17] proposed that the last term, which captures the interaction between the load and the power output of individual sites, contributes much less to variance than the second and third terms, and that unless the power output of individual sites showed considerable correlation with the load, the mean-variance optimisation would essentially reduce to the case where the load was not included.

However, it is hypothesised that when both the wind power time series and solar photovoltaic power time series are used in conjunction with the load time series, the combined power profiles of wind farms and solar photovoltaic farms might show good correlation with the load, and an optimal ratio of wind farm capacity to solar photovoltaic farm capacity could be obtained. This technique takes into account the shape of the daily load profile and could result in a more country specific distribution of renewable power capacity. The mathematical formulation will now follow.

The residual load is given by

$$L_i^R = L_i^T - R_i \tag{5.30}$$

where L_i^R is the residual load at time i, L_i^T is the total load and R_i is the total renewable power output.

Combining the residual load at all times i, results in the residual load vector $\mathbf{L}^R$ of length L:

$$\mathbf{L}^R = \begin{bmatrix} L_1^R & L_2^R & L_3^R & \dots & L_L^R \end{bmatrix}^{\mathrm{T}} \tag{5.31}$$

The mean-variance problem is then formulised as follows:

$$\min_{w^x=(w_1,w_2,w_3,\ldots,w_{1+N+M})} \operatorname{var}(\mathbf{L}^R) = \sum_{j=1}^{1+N+M} \sum_{l=1}^{1+N+M} w_j w_l \sigma_{jl} \tag{5.32}$$

such that

$$w_1 = 1, \tag{5.33}$$

$$\sum_{x\in\text{Wind}}^{N} w_x \mu_x = \mu_{\text{Desired Wind}}, \tag{5.34}$$

$$\sum_{x\in\text{Solar}}^{M} w_x \mu_x \geq \mu_{\text{Min Desired Solar}}, \tag{5.35}$$

$$\sum_{x\in\text{Wind}}^{N} w_x = w_{\text{Total Wind}}, \tag{5.36}$$

$$\sum_{x\in\text{Solar}}^{M} w_x \leq w_{\text{Max Total Solar}} \tag{5.37}$$

and

$$0 \leq w_x \leq \max_x, x \in [2\ldots1+\text{N+M}] \tag{5.38}$$

This formulation is similar to the formulation in section 5.4, except that the load time series is included as the first time series in conjunction with the negative of the wind power time series and solar photovoltaic power time series, meaning that w_1 is the decision variable that refers to the load time series. As can be seen in equation (5.33), this decision variable is set to one. This leaves the optimisation procedure with decision variables $w_2,\ldots,w_{1+N+M}$ to assign to the negative wind power time series and negative solar photovoltaic power time series in order to minimise the variance of the residual load.

5.5.1 Load Time Series Pre-processing (Detrending)

Any multi-year load time series that is obtained from actual data is likely to display annual growth or decline trends in the load. It is therefore necessary to remove the annual trend from the load before including the load time series in the mean-variance optimisation procedure, resulting in a load time series where every year of load data has the same mean value. Failing to remove the annual trend would in all likelihood invalidate the results of the optimisation procedure as sites with coincidental low power output in lower load years might be preferred to the actual optimal solution, with the same occurrence possible for higher load years and sites with coincidentally higher power output during those years.

In this investigation, it has been decided to remove the seasonal trend from the load data as well when it is used in the mean-variance optimisation procedure. The goal of the mean-variance optimisation procedure is ultimately to minimise the variance of the residual load around the mean, and therefore a constant mean load is required throughout the year. It is hypothesised that leaving the seasonal trend in the load data would only be useful if renewable power sources with extremely seasonal variability are included in the optimisation problem, which is not the case here. It is therefore left as a future research question. It is important to keep in mind that the standard deviation of the residual load

obtained in this investigation refers to the standard deviation of the residual load with its seasonal trend removed, whereas the load data with its seasonal trend still intact (which represents the real world scenario) is used to calculate all the key performance indicators.

5.6 Time Series Clustering Justification

The quadratic programming problem allows for a ceiling constraint for each site, $\max_x$, but not a floor constraint. This implies that, while upper limits can be imposed on the capacity assigned to individual locations, the lower limit equates to zero (when there is no minimum capacity that is assigned or there is no existing capacity on that site). It is therefore impossible to assign a minimum capacity that would justify the fixed cost infrastructure needed to support a wind farm or solar photovoltaic farm on that site. This is problematic because the solutions on the efficient frontier often assign low capacities to certain sites, which makes part of the solution unfeasible in the face of practical and economic considerations. The capacities are furthermore assigned to exact coordinates, depending on the spatial resolution of the input data, yielding a very rigid solution when factors such as land use, grid connection capacity, etc. have not been taken into account. There is no clear site selection alternatives should a specific site be disqualified based on these considerations and the optimisation has to be performed again with the adjusted constraints.

The optimisation strategy can be combined with time series clustering, thereby optimising the distribution of wind power capacity in terms of geographical areas with similar wind power profiles rather than individual potential wind farm sites. In order to define geographical areas with similar wind power profiles and solar photovoltaic power profiles, potential wind farm sites and solar photovoltaic sites are clustered according to the temporal similarity of the associated simulated power time series. An averaged power profile, referred to as a centroid, is derived for each cluster by averaging the power at each time instant for all locations assigned to that cluster. The total wind power capacity, supplemented by solar photovoltaic power capacity, is then optimally distributed amongst the clusters with the mean-variance portfolio methodology, using the centroids as an input.

6 Key Performance Indicators related to Renewable Power Integration

6.1 Overview

In order to compare the results of the optimisation procedure, it is necessary to select several key performance indicators. This section provides the mathematical formulations and the reasoning behind the selection of the key performance indicators.

Before the key performance indicators are formulised, several variables are introduced that will be used throughout this section. The total renewable power, R_i, which is the total wind power output and solar photovoltaic power output at a given time, is given by:

$$R_i = \sum_{x=1}^{N} W_i^x + \sum_{y=1}^{M} S_i^y \tag{6.1}$$

where N is the number of wind farms, W_i^x is the wind power output at wind farm x at time i, M is the number of solar photovoltaic farms, S_i^y is the solar photovoltaic power output at solar photovoltaic farm y.

The residual load, which is the load minus the renewable power output, is given by

$$L_i^R = L_i^T - R_i \tag{6.2}$$

where L_i^R is the residual load at time i and L_i^T is the total load at time i.

6.2 Standard Deviation of Renewable Power Output/Residual Load

The goal of the mean-variance optimisation is to minimise the variance of the combined input time series. In the case where only the wind power is included in the mean-variance formulation, the variance of the cumulative wind power output is minimised. In the case where solar photovoltaic power is included, the variance of the cumulative renewable power output is minimised. If load is also included in the procedure, the variance of the residual load time series is minimised.

In each of the formulations of the mean-variance procedure, the standard deviation, s, of any time series x, is calculated as follows [97]:

$$s = \sqrt{\frac{1}{L-1}\sum_{i=1}^{L}(x_i - \bar{x})^2} \tag{6.3}$$

where L is the length of time series x and $\bar{x}$ is the mean of time series x.

6.3 Mean Absolute Load Ramp Rate

The mean absolute load ramp rate provides a measure of the intra-hour differences in load. It is expected that larger penetrations of renewables will increase the variability of the residual load and thereby also increase the intra-hour differences in load that will cause conventional generators to cycle more and increase the need for peaking power plants. The mean absolute load ramp rate is defined as follows:

$$\text{Mean Absolute Ramp Rate} = E\left[\left|\frac{d}{dt}(L)\right|\right] \tag{6.4}$$

where L is either the load time series or the residual load time series, $\frac{d}{dt}$ is the differential and $E[\,]$ is the expected value (mean).

6.4 Capacity Credit

In order to approximate the capacity credit, the Garver approximation-based method is used, as discussed in section 2.5.2.3. Instead of considering the full load and residual load datasets, the Garver capacity value formulation considers two different subsets of the residual load data, H_1 and H_2, which represents the highest α% of loads and residual loads respectively. This is similar to the approach employed by Madaeni *et al.* [56], and is reported to provide a better approximation of the true capacity credit because the peak load periods are isolated. The Garver α% highest load capacity value is given by [56]:

$$\text{Garver } \alpha\% \text{ Highest Load Capacity Value} = m \cdot \ln\left(\frac{\sum_{i \in H_1} \frac{e^{L_i^T}}{m}}{\sum_{i \in H_2} \frac{e^{L_i^R}}{m}}\right) \tag{6.5}$$

where m is the system characteristic, L^T and L^R are the load time series and the residual load time series respectively, i represents the ith data point in the time series with L data points. Because detailed generating unit data of the Eskom fleet is unavailable, the system characteristic m is assumed to be 4% of peak load as is consistent with the literature [8]. In this investigation α is selected as 5%, which is a compromise between the lower percentage that would be considered in the case of solar photovoltaic power only and the higher percentage that would be considered in the case of wind power only.

The capacity credit is calculated from the capacity value and the nameplate capacity of the installed renewable power plants as follows:

$$\text{capacity credit} = \frac{\text{capacity value}}{\text{nameplate capacity}} \tag{6.6}$$

The capacity credit can be calculated for the wind farm capacity or solar photovoltaic farm capacity separately, or a combined capacity credit can be calculated.

6.5 Generator Capacity by Type

The goal of the generator capacity by type metric is to use a high-level statistical approach to estimate the size and type of generators that will be needed to supply the load/residual load. This approach was described in the study by Tarroja *et al*. [60], and is discussed in more detail in section 2.5.2.4. The approach is formulised as follows:

Each of three type of generators, namely base-load, load-following and peaker plants are assigned a duration period length, which represents the typical average time that the specific type of generator will be online. The duration period lengths are given in Table 6.1.

Table 6.1 Generator Type Duration Period Lengths [60]**.**

Generator Type	Duration Period Length	Typical generator types
Peaker	≤5 h	Natural-gas brayton cycle Reciprocating engines
Load-following	6-168 h	Natural-gas combined cycle Natural-gas rankine cycle Natural-gas brayton cycle
Base-load	169+ h	Nuclear rankine cycle Coal-powered rankine cycle Gasified coal-powered combined cycle

Next, the base-load, load-following and peaker plant totals are initialised to 0 MW. Generator duration lengths are obtained by examining the residual load time series at different power levels which are increased by equal increments, P_{inc}, from zero. P_{inc} is specified as 10 MW in this study similar to the study by Tarroja *et al*. At each power level, the periods of generator operation at or above that power level are located and each of their duration recorded. A graphical representation of this process is presented in Fig. 6.1. The generator duration lengths (t1, t2, t3, …) are grouped according to duration period lengths of the different type of generators. P_{inc} is then divided into three parts in the same proportion as the generator duration length groupings and added to the base-load, load-following and peaker plant totals.

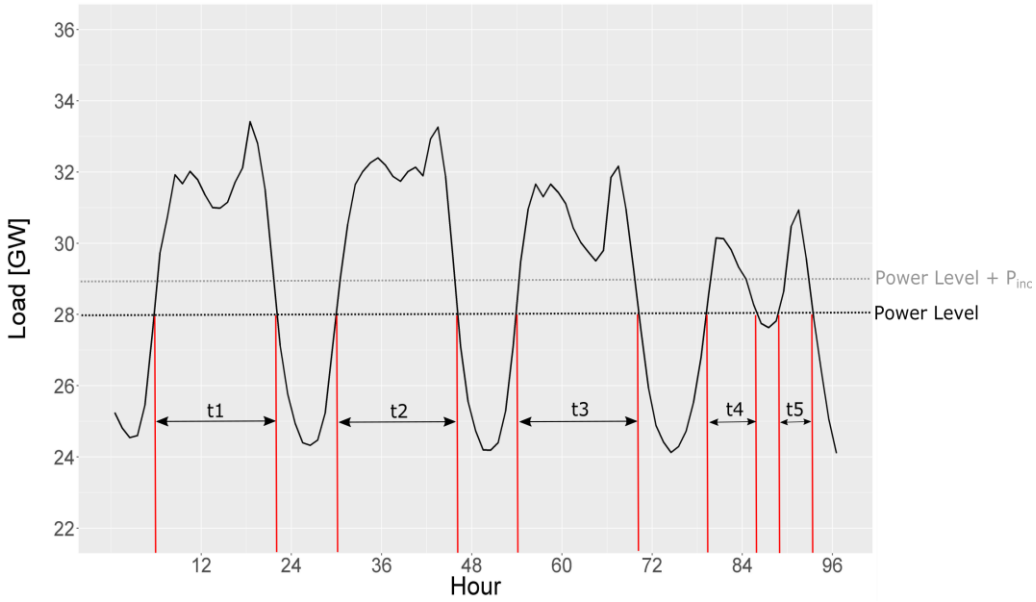

Fig. 6.1 Visualisation of the generator duration counts metric (adapted from Tarroja et al. [60]***).***

A similar example to the one that was provided in the literature review in section 2.5.2.4, will now be provided here to clarify the procedure. If at 28 GW, zero of the generator duration lengths are longer than 168 hours, two thirds of the generator duration lengths are between 6 hours and 168 hours and the remaining third of the generator duration lengths are less than 6 hours, 0 MW will be added to the base-load total, 6.66 MW will be added to the load-following total and 3.33 MW will be added to the peaker total. In effect this means that the marginal demand at between 28 GW and 28.01 GW will be served by load-following plants 66.6% of the time and by peaker plants 33.3% of the time. After this process is repeated for successive power levels up until the maximum value of the net load signal, the totals for the different types of generators are obtained.

The generator capacity by type metric is applied to the load before subtracting any renewable power, and then applied to the residual load obtained from optimised renewable distributions to ascertain the different types of capacity that will be needed in the future to meet the load with different penetrations of renewable power plants.

7 Data Acquisition and Processing

7.1 Overview

The data that was required to perform the renewable energy simulations and optimisation procedures were obtained from different sources. This section details the sources and acquisition of all the relevant data.

7.2 Grid GIS Data

In order to collect the data that is necessary for renewable energy simulation, it is necessary to know the location of high voltage power lines in South Africa. It is unlikely that renewable power plants will be built far away from the grid, and as such the physical location of the grid will dictate where data for renewable energy simulation should be collected.

Geographic information system (GIS) files of the South African high voltage grid (88 kV up to 765 kV) was obtained from Eskom and can be seen in Fig. 7.1. The GIS files include existing lines, as well as planned lines that will be built in the next 15 years from the time of this study.

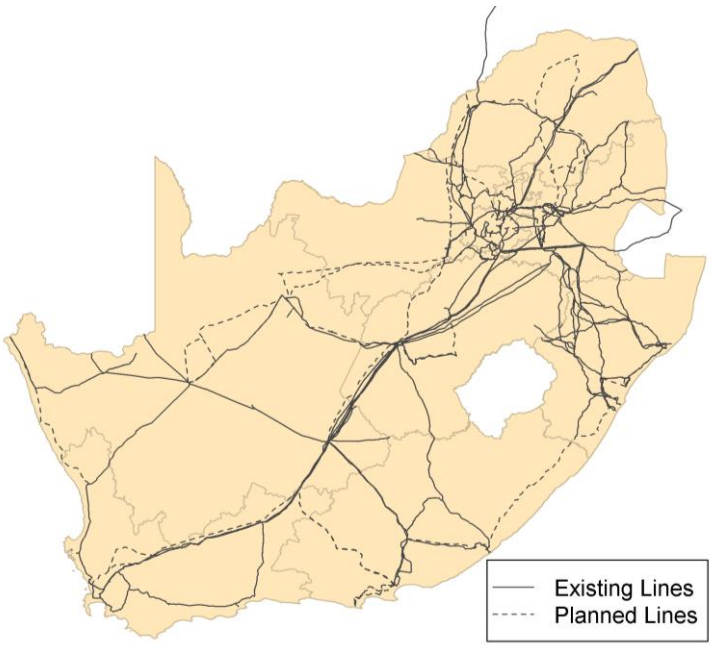

Fig. 7.1 Existing and planned high voltage power lines in South Africa.

7.3 Wind Data

Wind speed data was obtained from the WASA project (described in section 2.4.2.2). The WASA project includes hourly wind speed and wind direction time series data from 1 Jan 1990 until 31 Dec 2012. The dataset includes 527 time series, each falling on a 27 km x 31 km grid, for a large area covering parts of the Northern Cape, Western Cape and Eastern Cape. Only sites within 50 km from the existing and planned high voltage network were included in the study, as can be seen in Fig. 7.2. Any datasets that were offshore were also excluded. This resulted in 402 sites that would be included in the study.

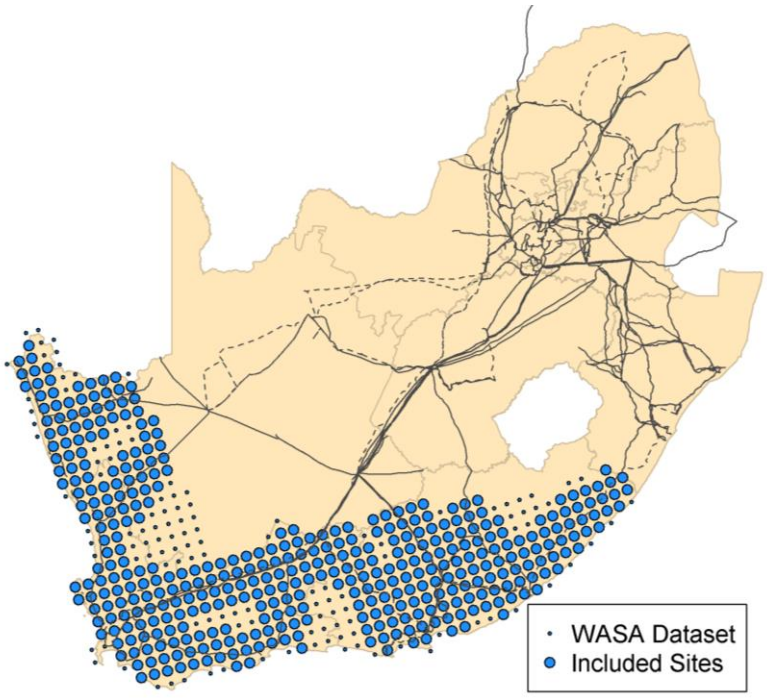

Fig. 7.2 Complete WASA dataset and sites included in the study.

7.4 Solar Photovoltaic Data

7.4.1 Solar Irradiance Data

Solar irradiance data was obtained from the SoDa service (described in section 2.4.3). The SoDa service allows the user to select the coordinates of the data that the user requires. A 40 km x 40 km grid was drawn across South Africa and solar irradiance data was collected for all grid points that fall within 50 km from the existing and planned high voltage network, which resulted in 590 solar irradiance time series datasets, as can be seen in Fig. 7.3.

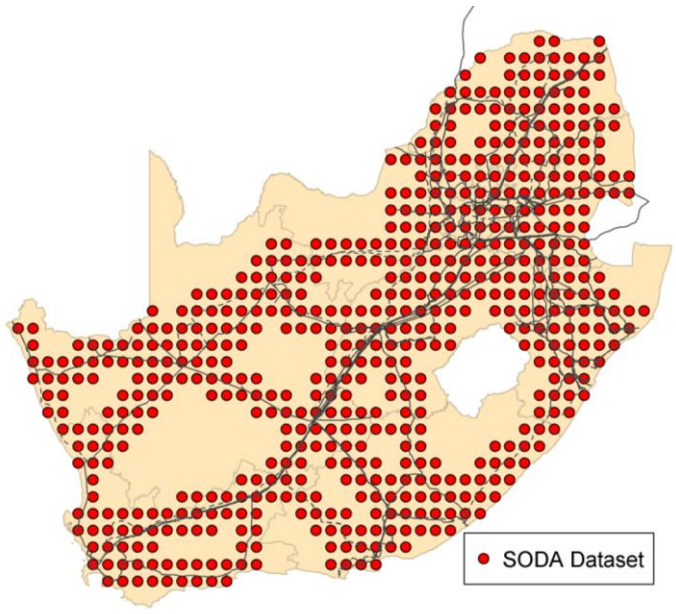

Fig. 7.3 SoDa dataset that was collected for this study.

The type of solar radiation data that was collected was the inclined irradiance, which consists of three components, namely the direct irradiance, diffuse irradiance and the reflected irradiance. The three components combined give the total inclined irradiance, also referred to as the global inclined irradiance. Each dataset was downloaded with the optimum angle corresponding with the optimal solar photovoltaic angle map provided by the Department of Environmental Affairs [99] as shown in Fig. 7.4. The optimal solar photovoltaic angle represents the tilt angle of the solar photovoltaic panel that would result in the maximum annual energy generation. It was assumed that the solar photovoltaic panels face north. The irradiance data that was downloaded represented hourly data from 1 February 2004 until 31 December 2012.

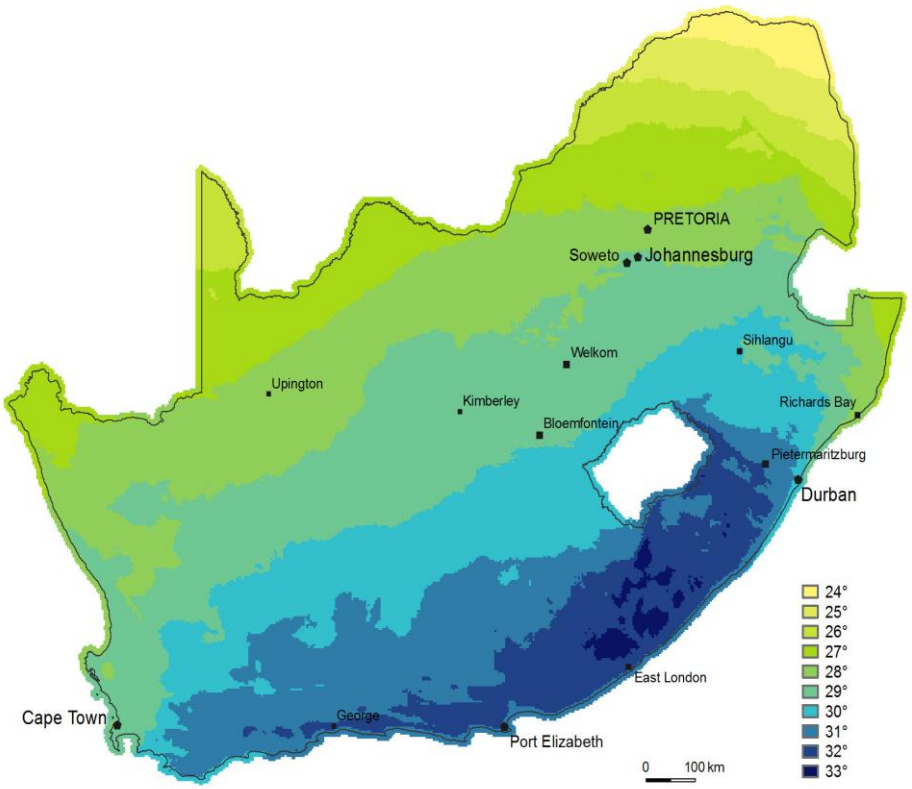

Fig. 7.4 ***Optimal solar photovoltaic angle map from the Department of Environmental Affairs*** [99]**.**

7.4.2 Temperature Data

Temperature data was obtained from the South African Weather Service (SAWS). It was not possible to obtain temperature data from all the weather stations. A total of 38 weather stations were selected that fell along the high voltage electricity grid, as can be seen in Fig. 7.5. The requested temperature data spanned from 1 January 2005 until 31 December 2012. Unlike the wind speed data and solar irradiance data however, many of the temperature time series contained significant quantities of missing data.

Fig. 7.5 Selected weather stations (from SAWS) for temperature data acquisition.

In order to replace the missing data in the temperature records, a linear regression technique was used. A linear model was constructed for each temperature time series that was trained with the known values and the corresponding temperature records from the nearest four temperature stations. This linear model was then used to fill in the missing values.

7.5 National Load Data

Hourly national load data was obtained from Eskom for the period from 1 January 2000 until 31 March 2015. The peak load in South Africa typically occurs in winter, and the winter and summer load profiles have markedly different shapes as can be seen in Fig. 7.6.

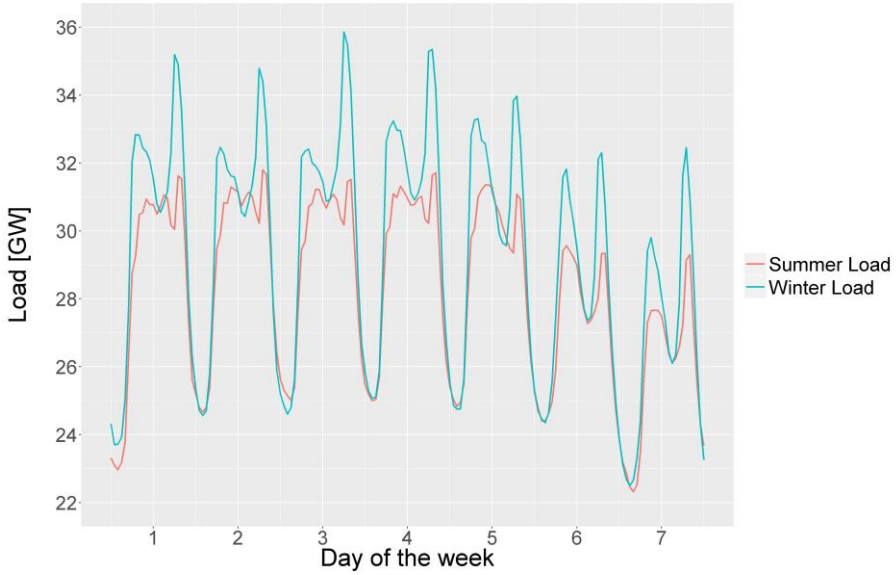

Fig. 7.6 Typical week of summer and winter load.

The load data contained significant annual growth and decline trends. In order to use the load time series in the mean-variance optimisation procedure, it was necessary to remove the annual and seasonal trends as discussed in section 5.5.1. In order to calculate the key performance indicators, only the annual trend is removed, which maintains the higher mean values that is observed during winter months.

Removing the annual trend effectively caused the entire load time series to resemble the peak load year, which in this case was 2007, along with the random fluctuations that occurred in each year. Throughout the case studies in the results section, reference is made to the current load. This is a reference to the key performance indicators as applied to the detrended load data without any renewable power subtraction.

7.6 Overlap of Data

The period that wind data, solar radiation data, temperature data and load data overlapped was from 1 Jan 2005 until 31 Dec 2012. This represented eight years of hourly data and was deemed sufficient to account for the inter-annual variability of wind power and the relationship between weather phenomena and load. The leap days in 2008 and 2012 were removed, leaving 70 080 hourly records (8 years x 365 days x 24 hours). All the case studies were performed using this subset of time series data.

8 Software Implementation

8.1 Overview

The complete methodology was implemented using two software packages, namely Matlab and R Studio. Matlab was used for the initial data cleaning and renewable energy simulation, due to its speed. The time series clustering, mean-variance optimisation, key performance indicator calculations and GIS file outputs were performed in R Studio due to the availability of a range of packages that facilitated the above-mentioned procedures. An overview of the software implementation can be seen in Fig. 8.1.

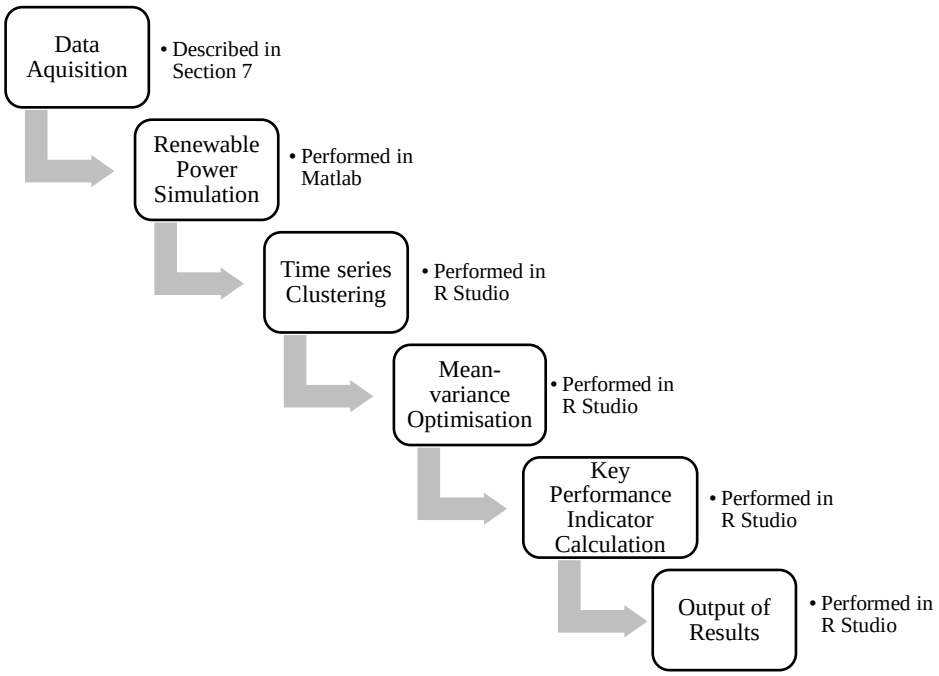

Fig. 8.1 Overview of the software implementation.

This section gives an overview of the software programs and the software implementation, including the workflow and the respective Matlab and R packages that were used.

8.2 Renewable Power Time Series Simulation in Matlab

Matlab is a numerical computing environment that contains a proprietary object-oriented programming language. Matlab is used in academia and industry across a wide range of topics including science, engineering and economics [100]. Matlab was chosen for the data cleaning and renewable power simulation due the speed of Matlab code computation, which stems from the efficient use of vector and matrix calculus inherent in the programming language. Matlab code can either be entered into the command window, or saved as a script in the Matlab editor. In the following part of this section, each flowchart represents a separate Matlab script.

8.2.1 Wind Power Simulation

The wind power time series are simulated using the wind speed data and the methodology described in section 3.2. The flowchart for this process can be seen in Fig. 8.2. The input and output data are stored as CSV files (Comma Separated Values).

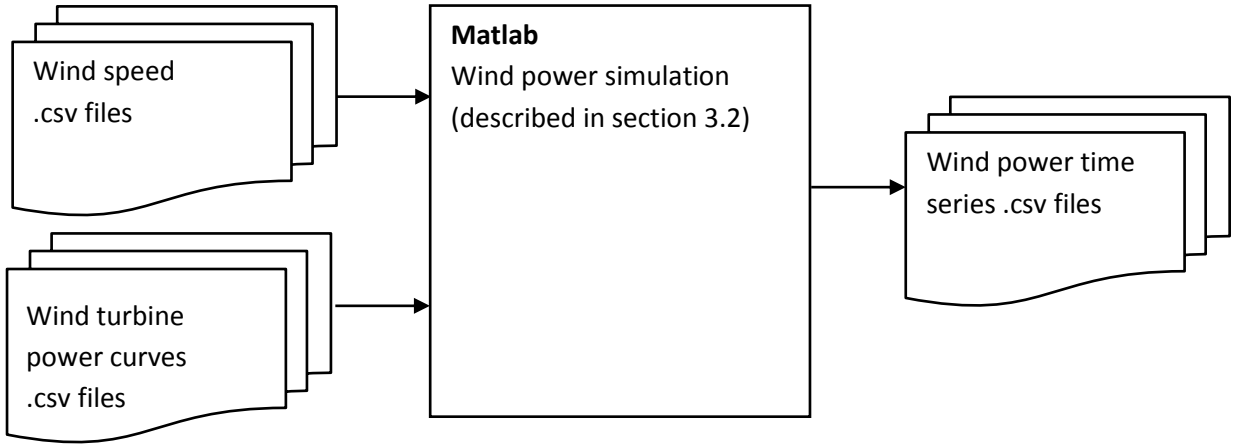

Fig. 8.2 Flowchart of the wind power simulation procedure in Matlab.

The curve-fitting toolbox in Matlab is used to convert discrete data points for the single wind turbine power curve and the multi-turbine power curve into a function that can be applied to any analogue wind speed.

8.2.2 Solar Photovoltaic Simulation

The first step in the solar photovoltaic power simulation is to condition the temperature data using the method described in section 7.4.2. By conditioning it is meant that missing data is calculated using a linear regression method by considering the four closest stations whose data is not missing. The flowchart for this process can be seen in Fig. 8.3. The input and output data are stored as CSV files.

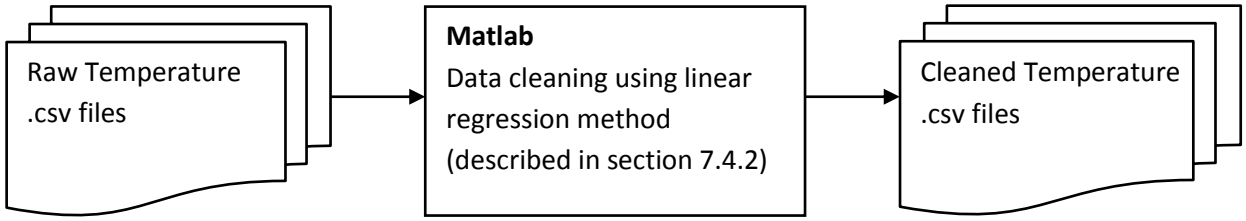

Fig. 8.3 Flowchart of the temperature data cleaning procedure in Matlab.

The next step is to simulate the solar photovoltaic power time series using the conditioned temperature data and the solar radiation data with the method described in section 3.3. The flowchart for this process can be seen in Fig. 8.4. The input and output data are stored as CSV files.

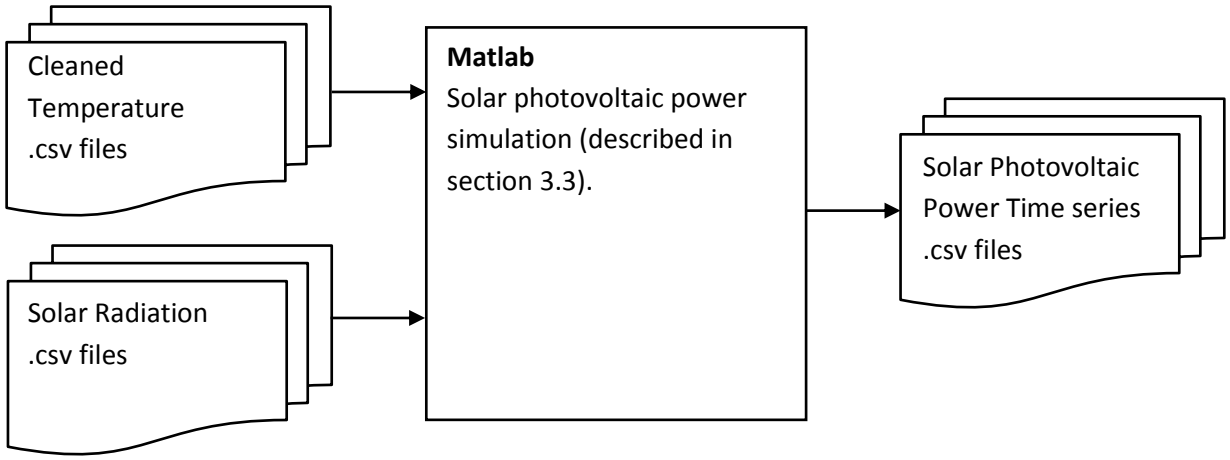

Fig. 8.4 Flowchart of the solar photovoltaic power simulation procedure in Matlab.

8.3 Time Series Clustering, Mean-variance Optimisation and Key Performance Indicator Calculation in R Studio

R Studio is an open-source integrated development environment for the R programming language. The R programming language is an implementation of the S programming language and is most often used for data mining, optimisation and statistical analysis [101]. R implementations are highly extensible through various packages to which a very active R community contribute. R was chosen for the time series clustering, mean-variance optimisation and the key performance indicator calculations for two reasons:

- The availability of R packages that can facilitate time series clustering procedures, optimisation procedures and GIS file plotting and editing.
- The ability of R to perform high-quality data visualisation.

Similar to Matlab, R code can either be entered into the command window, or saved as a script using the R studio editor. The time series clustering, mean-variance optimisation and key performance indicator calculations were all implemented in a single R script. The flowchart for the R script can be seen in Fig. 8.5. The inputs are the renewable energy simulations that were performed in section 8.2 and are in comma-separated-value (CSV) format. The output of the R script is graphs of the key performance indicators and GIS files that represent the clustered areas with their associated optimal renewable energy capacity.

8.3.1 Flowchart of the Complete R Studio Script

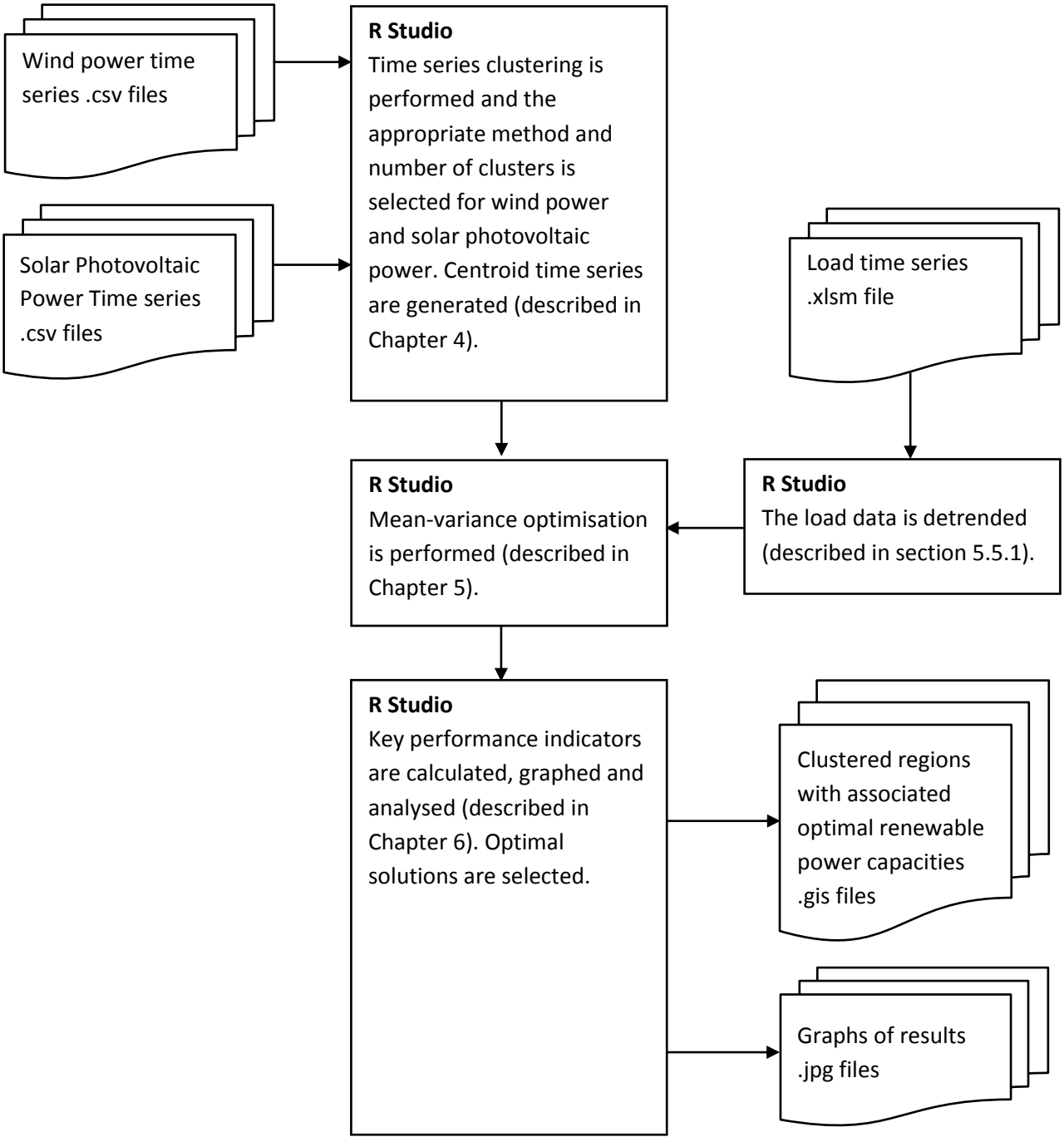

Fig. 8.5 Flowchart of the time series clustering, mean-variance optimisation and key performance indicator calculation in R Studio.

8.3.2 R Packages Used

Table 8.1 contains each external R package that was used in the study, as well as the purpose for which it was used. Table 8.1 does not list packages that are included in the base R distribution.

Table 8.1 Summary of R packages used in this study (excluding base R packages).

Package Name	**Description**	**Purpose in this study**
ggplot2	A package that implements a novel plotting system in R that is based on the grammar of graphics methodology by Leland Wilkinson.	Used to plot various results.
quadprog	A package that contains a quadratic programming algorithm.	Used to perform the mean-variance optimisation (quadratic programming).
cluster	A package that contains several well-known clustering algorithms	Used to perform the PAM clustering method.
fpc	Flexible Procedures for Clustering. A package that contains various methods for clustering and cluster validation.	Used to perform the average silhouette width and Caliński-Harabasz index cluster validation measures.
sp	A package providing classes and methods for spatial data.	Used to import, manipulate and export spatial data.
rgeos	Interface to The Geometry Engine Open Source (GEOS), a free program library in C ++ for handling two- and 2.5-dimensional geometries	Used to manipulate spatial data.
alphahull	A package that contains functions to compute the alpha-shape and alpha-convex hull of a given sample of points in a plane.	Used to create alpha hull shapes (GIS files) for clustered regions.

9 Case Studies and Results

9.1 Overview

The chapter provides the results obtained using the complete methodology on a South African case study. The wind speed data, solar irradiance data and temperature data time series has been used to simulate wind power time series and solar photovoltaic time series. The simulated power time series has been clustered using time series clustering techniques. The clustered wind and solar photovoltaic time series have been used in conjunction with load data in mean-variance optimisation procedures to optimise the distribution of renewable power capacity in four different case studies that use the key performance indicators to assess the results. Hourly data from 1 January 2005 until 31 December 2012 (excluding leap year days) is used.

This chapter is divided into four parts:

- Section 9.2: The results of the renewable power simulation procedures is presented.
- Section 9.3–9.4: The results of the time series clustering applied to the simulated wind power time series and solar photovoltaic time series.
- Section 9.5–9.8: The results of four case studies which investigated the use of clustered wind and solar photovoltaic time series in conjunction with mean-variance optimisation. Table 9.1 provides a summary of the four case studies that have been performed.
- Section 9.9: Several investigations have been performed that pertains to the work which is not included in this thesis. A brief overview of the results is given in this section.

Table 9.1 Summary of Case Studies

Case Study	Description	Summary
1	Different Formulations of Mean-variance Optimisation	In the literature mean-variance portfolio theory has been applied to minimise the variance of wind power. This case study examines the effect of including the solar photovoltaic power time series and the load time series in the optimisation procedure.
2	REIPPPP Round 1-3 vs. Optimisation (Unclustered and Clustered)	This case study compares the optimisation procedure (considering wind power, solar photovoltaic power and load) with the wind farm and solar photovoltaic farm allocation in the REIPPPP, in order to quantify the benefits of the optimisation procedure when compared with a real world allocation in South Africa. This case study also justifies the use of time series clustering by examining the effect that time series clustering has on the results of the optimisation procedure when compared to the unclustered optimisation as found in the literature.
3	Optimal Future Penetrations of Wind and Solar Photovoltaic Power in South Africa	This case study uses the optimisation procedure to allocate a range of future penetrations of wind power capacities with complementing solar photovoltaic power capacities in South Africa, in order to study the effect that increasing penetrations of renewable energy will have on the conventional generating capacity requirements and to determine an optimal ratio of wind to solar photovoltaic power capacity.
4	Optimal Distribution of 14 GW of Wind Power with Complementing Solar Photovoltaic Power Compared to Random Distributions	This case study compares one of the results from case study 3, namely the optimised distribution of 14 GW of wind power capacity with complementing solar photovoltaic power capacity, with random distributions of renewable power capacity. This case study is intended to quantify the benefit that the optimisation procedure will have when doing long-term planning of a realistic size of wind farm and solar photovoltaic farm penetration in South Africa.

9.2 Wind and Solar Photovoltaic Power Simulation in South Africa

9.2.1 Overview

This section provides the results of the wind power and solar photovoltaic farm simulations (described in Chapter 3). In total 402 wind power time series simulations and 590 solar photovoltaic time series simulations have been performed.

9.2.2 Wind Power Simulations

Fig. 9.1 shows a map of the wind turbine type that has been used at each potential wind farm site to perform the simulation. As described in section 3.2, the wind turbine selection depended on the mean wind speed at each site.

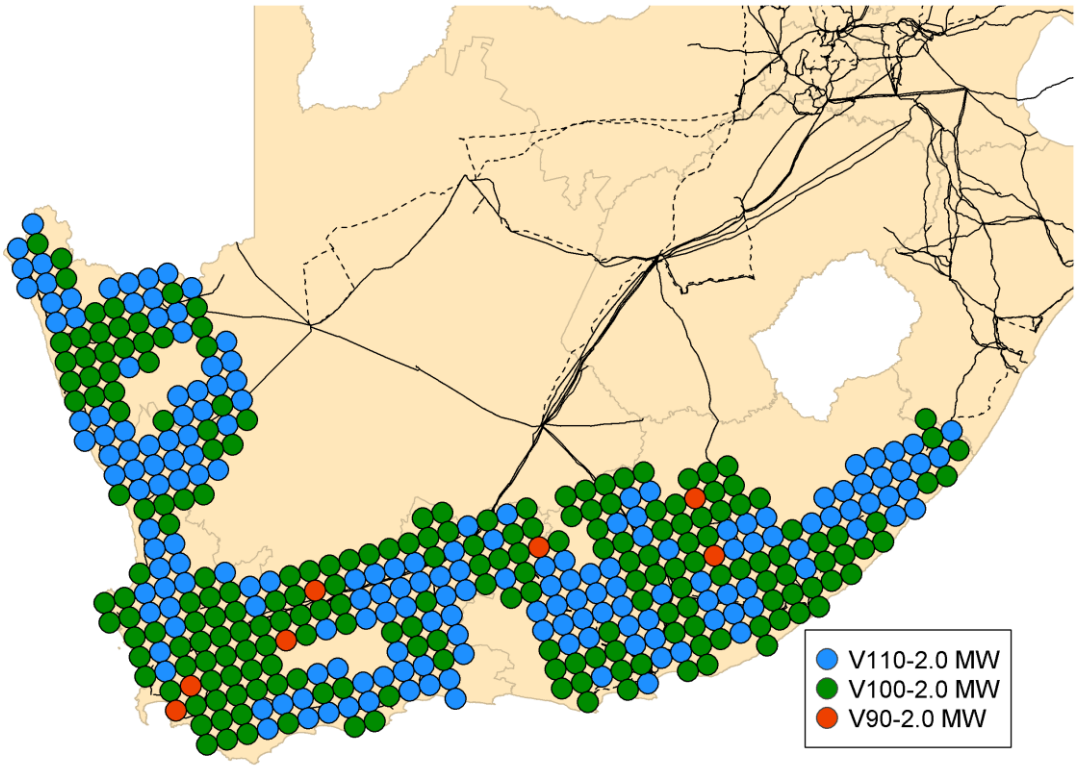

Fig. 9.1 Turbine types used to simulate wind power time series (all from the Vestas 2 MW platform).

Fig. 9.2 shows a map of the simulated capacity factors achieved at each potential wind farm site.

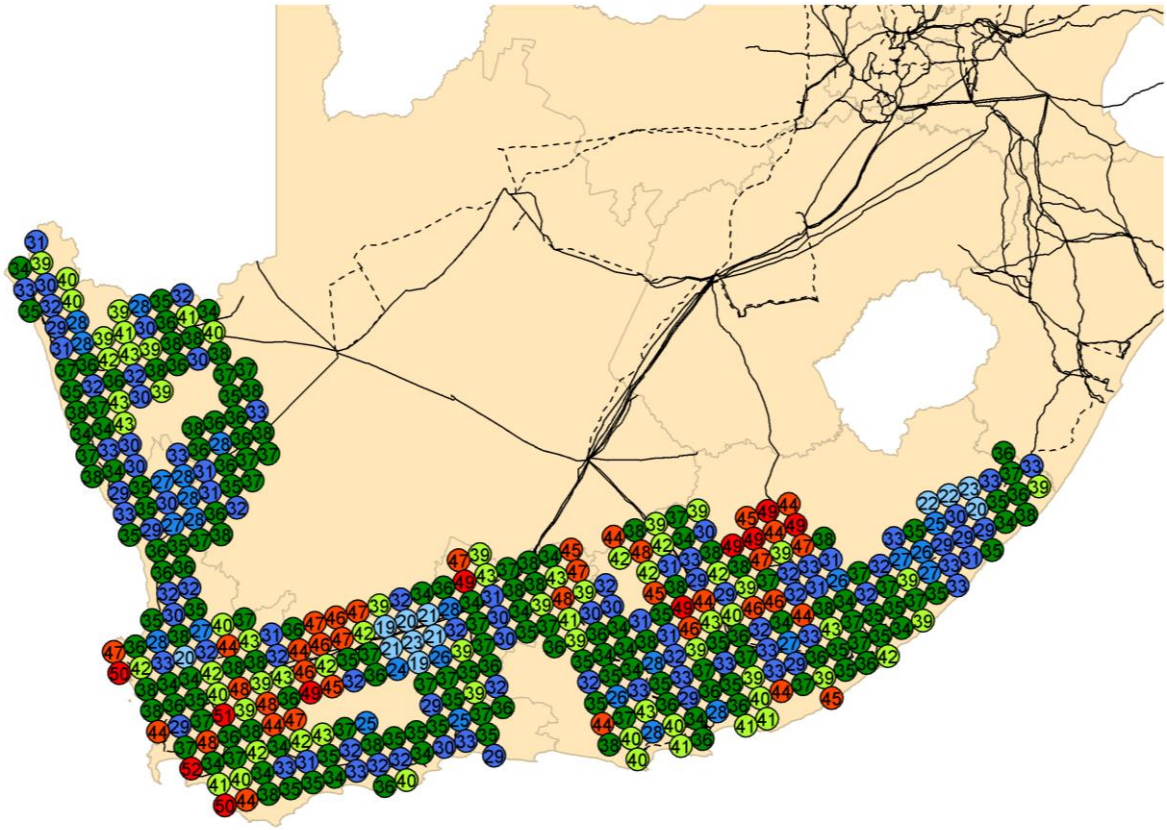

Fig. 9.2 Simulated Wind Power Capacity Factors.

Fig. 9.3 shows a histogram of the simulated capacity factors achieved. It is clear that most potential wind farm sites have a capacity factor of 30% or more. As described in section 3.2, wake effects have not been taken into account and an availability of 100% is assumed. As such, it is expected that the simulated capacity factors are slightly higher than their real life counterparts (hypothesised to be in the order of 3 to 5 percentage points due to the exclusion of factors such as wake effects [89]).

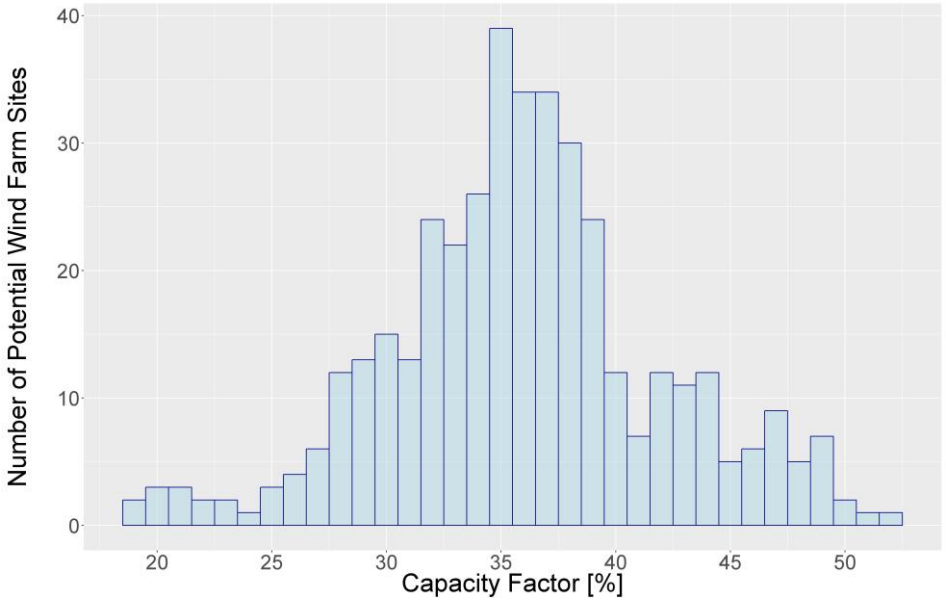

Fig. 9.3 Histogram of the 402 capacity factors achieved in the wind power time series simulation.

9.2.3 Solar Photovoltaic Power Simulations

Fig. 9.4 provides a map of the simulated capacity factors achieved at each potential solar photovoltaic farm site.

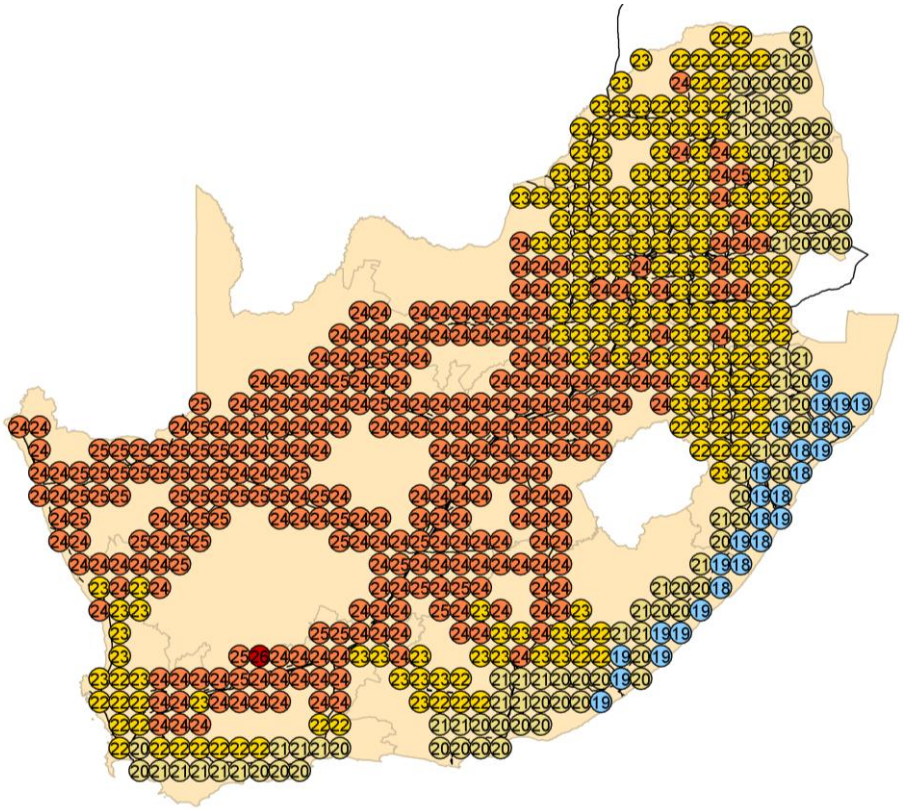

Fig. 9.4 Simulated Solar Photovoltaic Power Capacity Factors.

Fig. 9.5 provides a histogram of the simulated capacity factors achieved. Most sites exhibit a capacity factor of between 22% and 25%. It is hypothesised that this shows good agreement with actual utility-scale solar photovoltaic farm capacity factors.

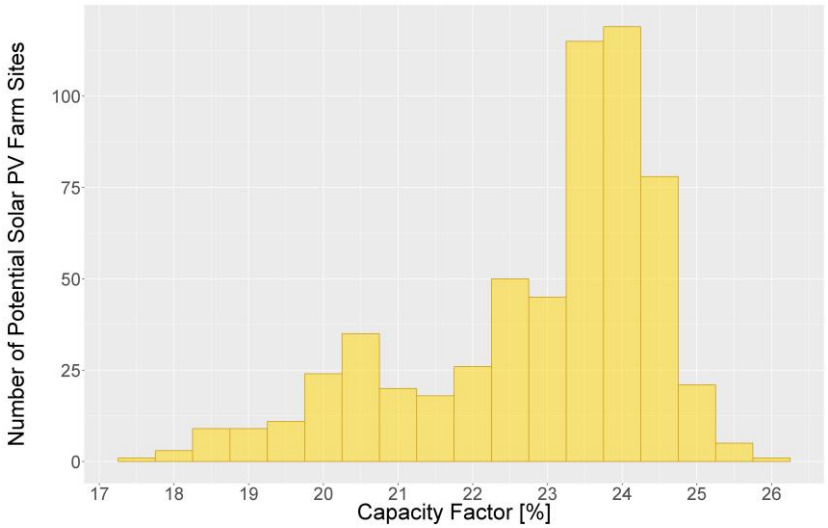

Fig. 9.5 Histogram of the 590 capacity factors achieved in the solar photovoltaic power time series simulation.

9.3 Clustering Potential Wind Farm Sites in South Africa

9.3.1 Overview

This section presents the results of the clustering techniques as applied to the simulated wind power time series (described in Chapter 4). By examining the cluster validation measures, it is proposed that Ward's method of hierarchical clustering performs slightly better than other clustering methods, and that clustering the 402 potential wind farm sites into 69 clusters yields an average centroid error of less than 10%. In addition, the clustering steps are visualised and the clustering result with 69 clusters is inspected.

9.3.2 Euclidian Distance Matrix

The calculated Euclidian distances between the simulated wind power time series is briefly overviewed so as to serve as a yardstick for the "average distance between" and "average distance within" cluster validation techniques in the following section.

A subset of the Euclidian distance matrix for the wind time series can be seen in Table 9.2, where only the first five time series have been considered. It is necessary to keep in mind that each time series ranges between 0 kW and 2000 kW, and that each time series has 70 080 records.

Table 9.2 Subset of the Euclidian distance matrix for the simulated wind time series.

Time Series	**1**	**2**	**3**	**4**	**5**
1	0	133237.2	137493.2	150727.5	105629.6
2	133237.2	0	156048.3	126962.7	120659.9
3	137493.2	156048.3	0	176281.4	157905.6
4	150727.5	126962.7	176281.4	0	133408.4
5	105629.6	120659.8	157905.6	133408.4	0

A box and whisper diagram for the Euclidian distances between the simulated wind power time series is given in Fig. 9.6. It can be seen that 50% of the Euclidian distances fall between approximately 188 000 and 232 000, with a median of approximately 213 000.

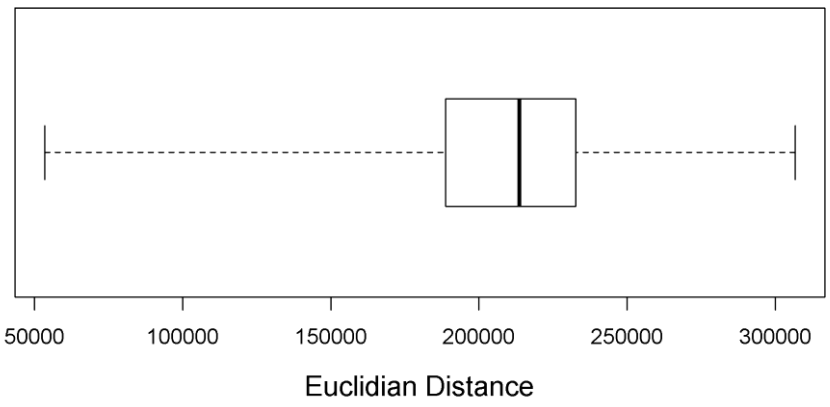

Fig. 9.6 Box and whisker diagram for the Euclidian distances between the simulated wind power time series.

9.3.3 Cluster Validation Measures

The results of the four cluster validation methods will now be presented. Fig. 9.7 presents the average Euclidian distance between the clusters. It is expected that as the number of clusters increase, the average distance between clusters decreases, although for a given number of clusters a higher average distance between clusters is desirable. It can be seen that the Ward's method and PAM method show similar results, with slightly lower distances between different clusters than the complete-linkage method. The average-linkage method performs the best overall.

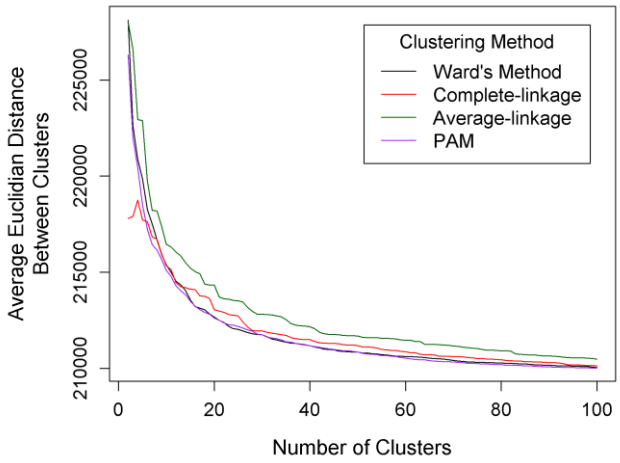

Fig. 9.7 Comparison of average Euclidian distance between clusters for different clustering methods and different number of clusters in the wind power time series clustering procedure.

Fig. 9.8 presents the average Euclidian distance within the clusters. Again the Ward's method and PAM method show similar results, with slightly lower distances within clusters than the other methods, which is desirable. At approximately 65 clusters or more, Ward's method displays measurably lower average distances within the clusters compared to the PAM method.

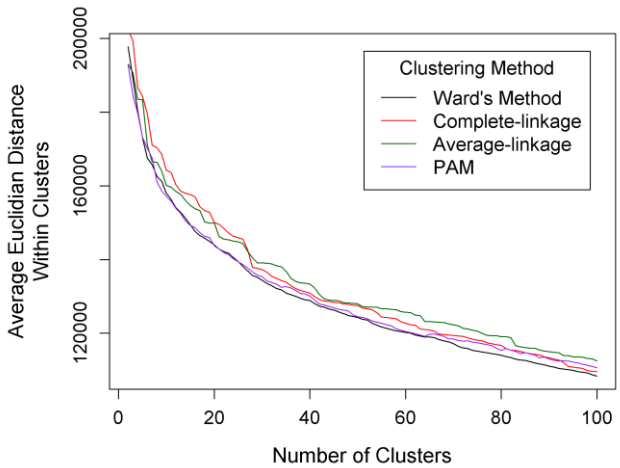

Fig. 9.8 Comparison of average Euclidian distance within clusters for different clustering methods and different number of clusters in the wind power time series clustering procedure.

Fig. 9.9 presents the average silhouette widths of the time series associated with the respective clusters. As stated before, the average silhouette width metric is a measure of the membership strength of time series to their respective clusters and is based on the pairwise difference of between and

within-cluster distances [94]. It results in a score between -1 and 1, where -1 one indicates very poor clustering and 1 represents very good clustering. The results indicate that all of the clustering methods resulted in fairly average clustering results. Ward's method clustering and average-linkage clustering provide the best clusters across the range of cluster numbers. A higher average silhouette width score would require a greater difference between the between and within-cluster distances, which is not a property of the simulated wind power time series as all the time series are bound by the same range. It is seen, however, that as the number of clusters increase, the average silhouette width increases, which suggests using more clusters rather than fewer clusters results in a better clustering.

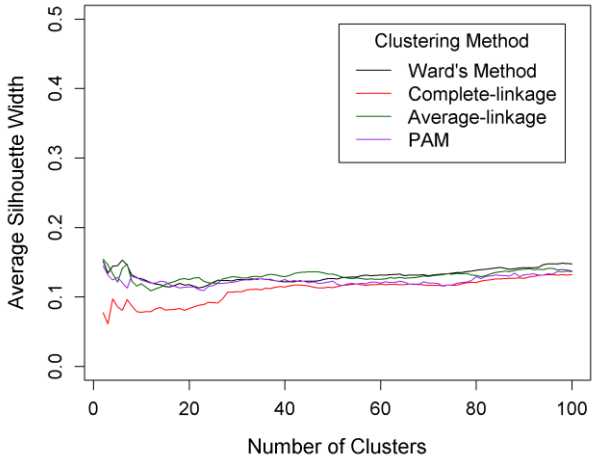

Fig. 9.9 Comparison of average silhouette width for different clustering methods and different number of clusters in the wind power time series clustering procedure.

Fig. 9.10 displays the result of the Caliński-Harabasz (CH) index. As stated before, the CH index calculates the ratio between cohesion and separation, with a higher ratio preferable. As the number of clusters increases, the ratio between cohesion and separation deteriorates. At every given number of clusters, Ward's method displays a slightly higher CH index compared to the other clustering methods.

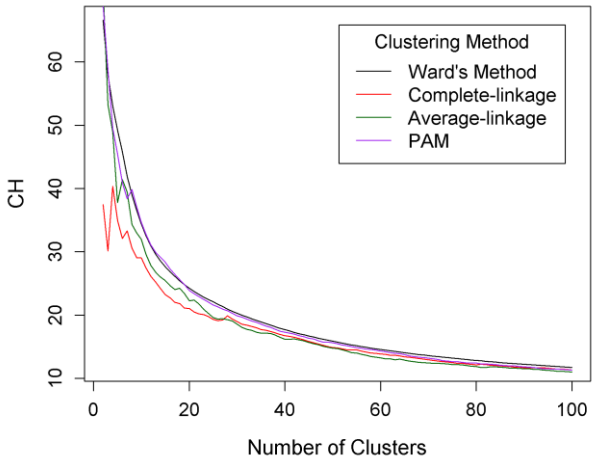

Fig. 9.10 Comparison of Caliński-Harabasz (CH) index for different clustering methods and different number of clusters in the wind power time series clustering procedure.

From the cluster validation measures it can be observed that Ward's method of hierarchical clustering marginally outperforms the other clustering methods. Ward's method is the best performer in the

average Euclidian distance within the clusters metric and the Caliński-Harabasz index. It is therefore henceforth the preferred clustering methodology for simulated wind power time series. The choice of Ward's method also makes sense for the intended purpose of this clustering result, namely to create a centroid time series to use as an input to the mean-variance optimisation procedure. Ward's method specifically attempts to minimise the variance within clusters, leading to centroids that better represent their original time series origins.

9.3.4 Visualisation of the Clustering Steps

In the previous section it was determined that Ward's method for hierarchical clustering is preferred when clustering simulated wind power time series. It is informative to examine how the clustering method functions, and as such a brief look at the clustering steps is provided here.

Fig. 9.11 visualises the clustering steps for two to seven wind time series clusters. When observing Fig. 9.11, the result of the hierarchical agglomerative ("bottom-up") approach is clear. At each clustering step, the cluster with the highest Ward's distance between its respective time series is split into a further two clusters.

When considering the result where only two clusters are used, it is clear that the simulated wind time series in the Northern Cape region is most different from the rest of the simulated wind time series.

When three clusters are specified, the coastal region in the Eastern Cape is separated from the inland Eastern Cape and Western Cape time series.

Specifying four clusters does not result in as clean a separation as before, as selected inland sites are assigned to their own clusters, most likely signifying the effect of higher simulated wind power at these sites (this can be confirmed by considering the simulated capacity factor map in Fig. 9.2). This process continues at each clustering step.

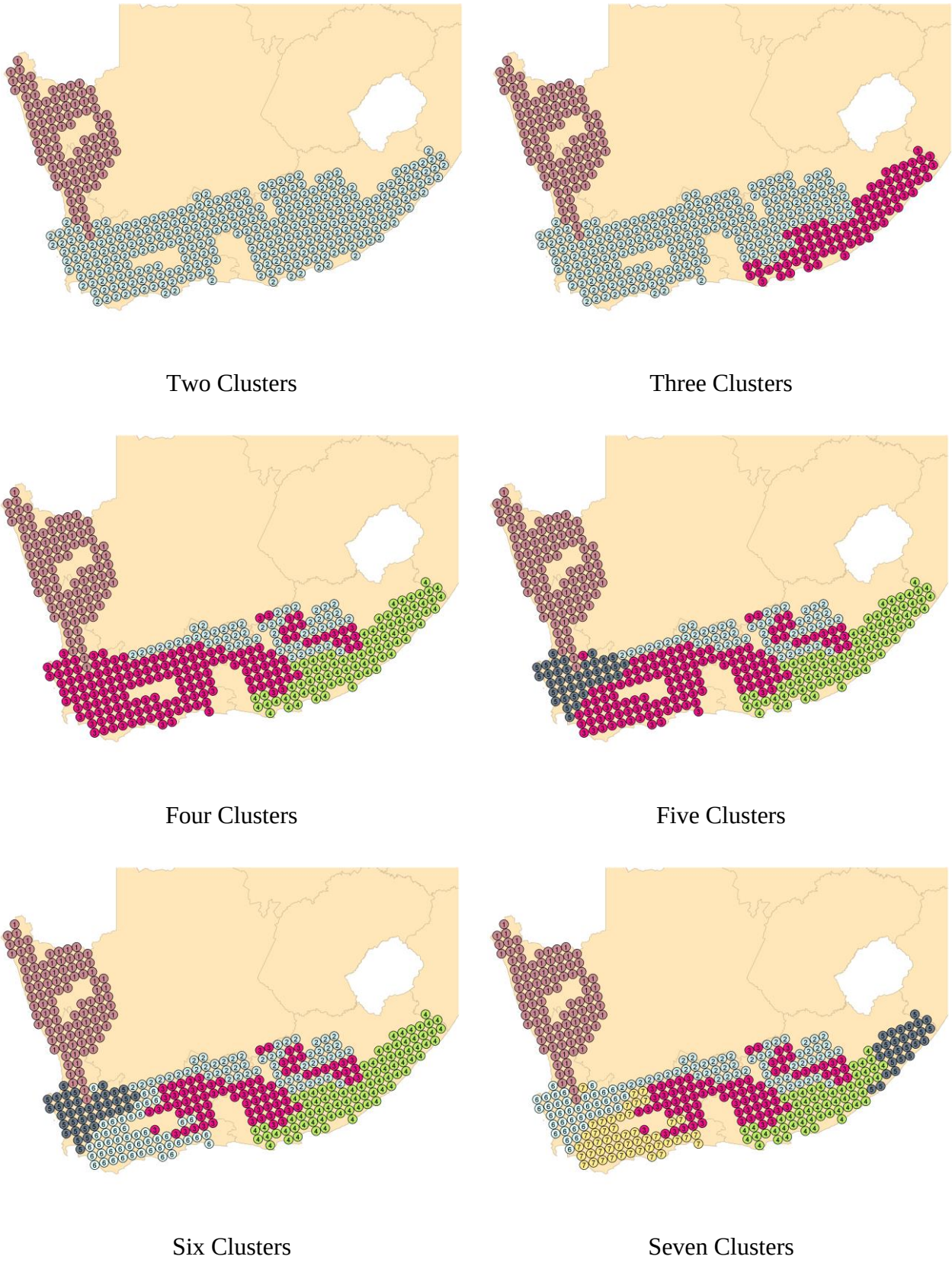

Fig. 9.11 Visualisation of the clustering steps in the Ward's method for hierarchical clustering for two to seven simulated wind time series clusters.

9.3.5 Appropriate Number of Clusters

The appropriate number of clusters for the simulated wind time series is determined by considering the average centroid error. The centroid represents the average value at every time step of all the time series that are assigned in the same cluster. An example of a centroid time series can be seen in Fig. 9.12, where the centroid has been calculated for six time series in the same cluster and displayed for one week.

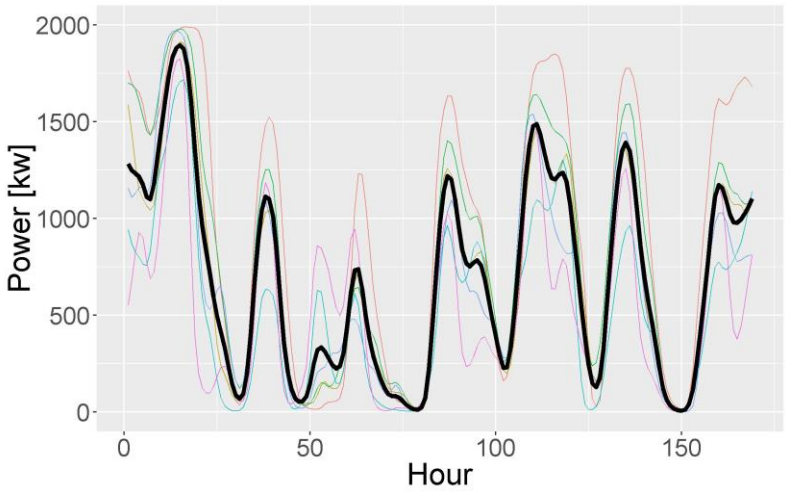

Fig. 9.12 Example of a centroid time series (thick black line) of six simulated wind power time series in the same cluster.

The number of clusters is chosen in such a way that the average centroid error is less than 10%, as can be seen in Fig. 9.13. It is therefore proposed that 69 clusters be used for the simulated wind power time series.

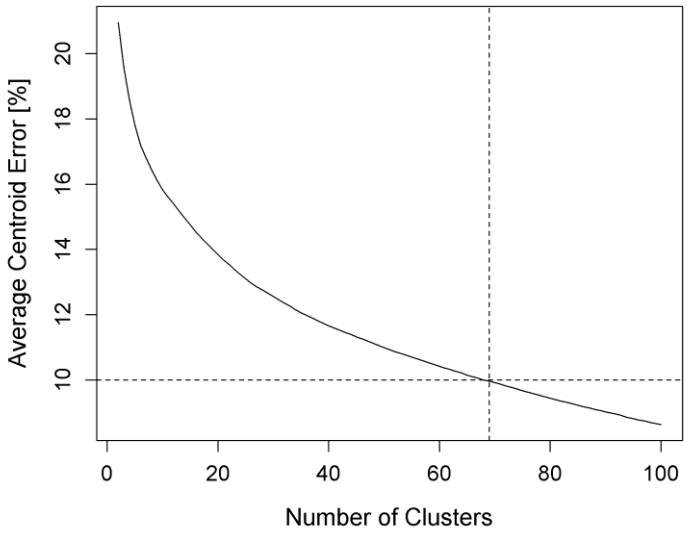

Fig. 9.13 Average centroid error using Ward's method of hierarchical clustering on the wind time series. The dotted lines indicate 69 clusters where the average centroid error is smaller than 10%.

9.3.6 Inspection of the Optimal Clustering Result

The spatial distribution of the optimal simulated wind power time series clustering result, using Ward's method of hierarchical clustering for 69 clusters, can be seen in Fig. 9.14.

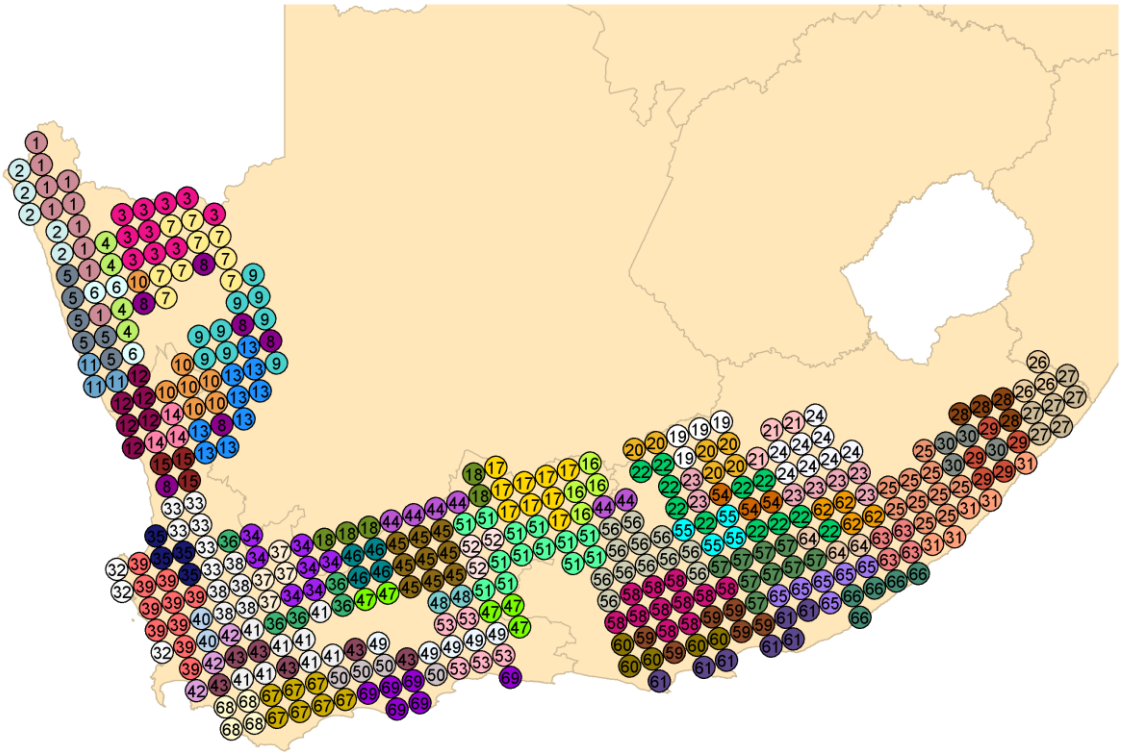

Fig. 9.14 Spatial distribution of wind site clusters obtained using Ward's method for 69 clusters.

The average seasonal daily power profiles of a selection of different clusters are inspected in Fig. 9.15. In Fig. 9.15, summer is defined as December to February, autumn is defined as March to May, winter is defined as June to August and spring is defined as September to November.

Cluster 3 (inland Northern Cape region) and cluster 19 (inland Eastern Cape region) have been included to showcase two clusters with their strongest winds during different times of the year. The simulated wind power time series in cluster 3 display their highest average wind power outputs during summer and spring evenings, whereas those in cluster 19 occur during the winter months, with high average wind power occurring throughout the day.

Cluster 47 and cluster 53 have been included to showcase the fact that scattered sites are sometimes included in the same cluster, and that, sites which are close together sometimes display markedly different power profiles. Cluster 47 consists of two sites inland in the Western Cape and three sites on the border between the Eastern Cape and Western Cape, with the two groups relatively far from each other. Cluster 53 consists of two sites inland in the Western Cape and another three sites located on the coast. Cluster 47 displays relatively strong winds throughout the year (with maximums during summer and spring evenings), while cluster 53 clearly shows stronger winds during winter (with maximums in the early hours of the day) and relatively weak winds during the rest of the year.

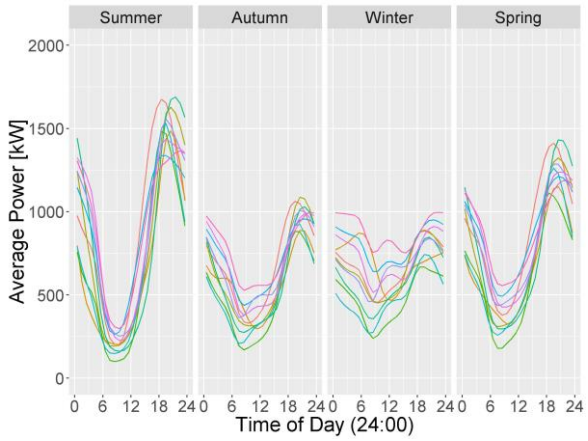

Cluster 3: 10 Sites

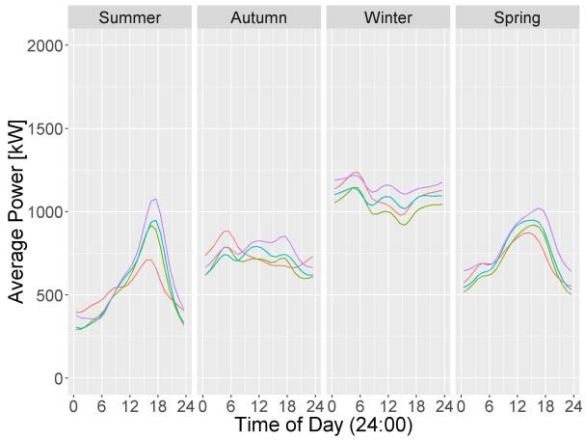

Cluster 19: Four Sites

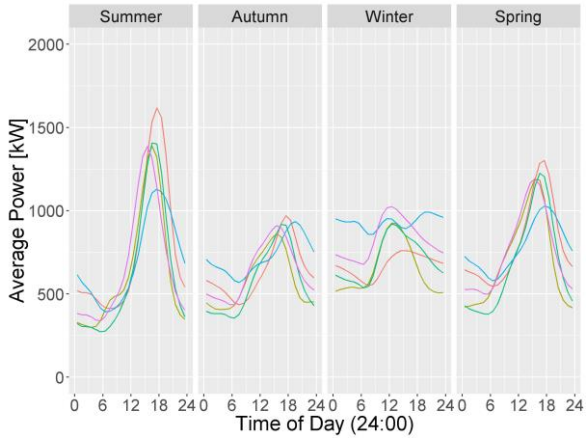

Cluster 47: Five Sites

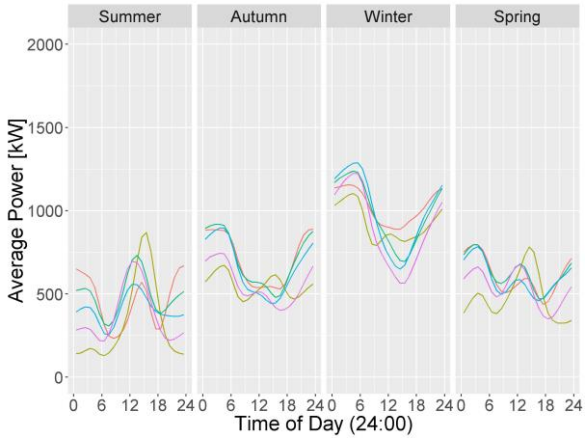

Cluster 53: Five Sites

Fig. 9.15 Seasonal average daily power profiles for a 2 MW turbine for the potential wind farm sites in selected clusters.

9.4 Clustering Potential Solar Photovoltaic Farm Sites in South Africa

9.4.1 Overview

This section presents the results of the clustering techniques as applied to the simulated solar photovoltaic power time series (described in Chapter 4). By examining the cluster validation measures, it is proposed that Ward's method of hierarchical clustering performs slightly better than other clustering methods, and that applying the L-method to the cluster validation measures results in an average recommended number of clusters of 17. Therefore, clustering the 590 potential solar photovoltaic farm sites into 17 clusters is recommended. In addition, the clustering steps are visualised and the clustering result with 17 clusters is inspected.

9.4.2 Euclidian Distance Matrix

The calculated Euclidian distances between the simulated solar photovoltaic power time series are briefly overviewed so as to serve as a yard stick for the "average distance between" and "average distance within" cluster validation techniques in the following section.

A subset of the Euclidian distance matrix for the solar photovoltaic time series can be seen in Table 9.3, where only the first five time series have been considered. It is necessary to keep in mind that each time series ranges between 0 kW and 2000 kW, and that each time series has 70 080 records.

Table 9.3 Subset of the Euclidian distance matrix for the simulated solar photovoltaic time series.

Time Series	**1**	**2**	**3**	**4**	**5**
1	0	25203.41	46493.63	39471.18	34951.21
2	25203.41	0	42110.49	42109.41	38779.19
3	46493.63	42110.49	0	54843.48	51816.6
4	39471.18	42109.41	54843.48	0	32334.84
5	34951.21	38779.19	51816.6	32334.84	0

A box and whisker diagram for the Euclidian distances between the simulated wind power time series is given in Fig. 9.6. It can be seen that 50% of the Euclidian distances fall between approximately 54 000 and 66 000, with a median of approximately 78 000.

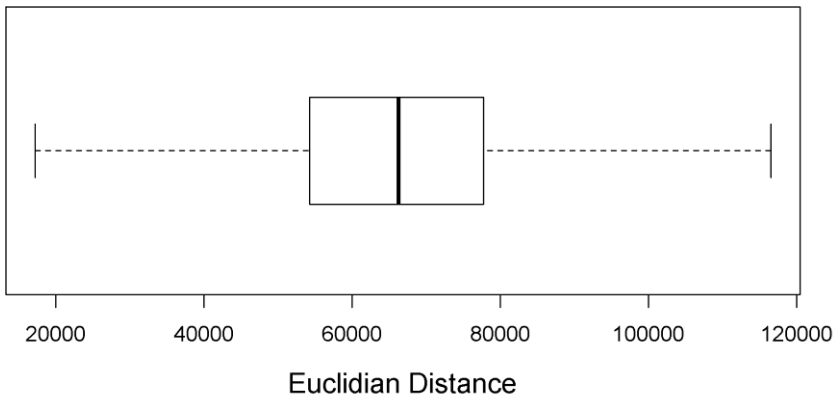

Fig. 9.16 Box and whisker diagram for the Euclidian distances between the simulated solar photovoltaic power time series.

9.4.3 Cluster Validation Measures

The results of the four cluster validation methods will now be presented. Fig. 9.17 presents the average Euclidian distance between the clusters. It is expected that as the number of clusters increase, the average distance between clusters decreases, although for a given number of clusters a higher average distance between clusters is desirable. It can be seen that the complete-linkage and average-linkage methods show a greater average distance between the clusters, outperforming Ward's method and the PAM clustering method. Ward's method does show slightly higher distances between clusters compared to the PAM method.

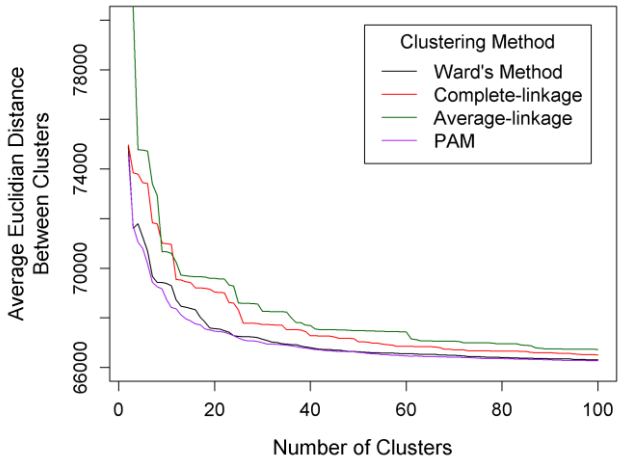

Fig. 9.17 Comparison of average Euclidian distance within clusters for different clustering methods and different number of clusters in the solar photovoltaic power time series clustering procedure.

Fig. 9.18 presents the average Euclidian distance within the clusters. Ward's method and the PAM clustering method show similar results, with lower distances within clusters than the other methods, which is desirable.

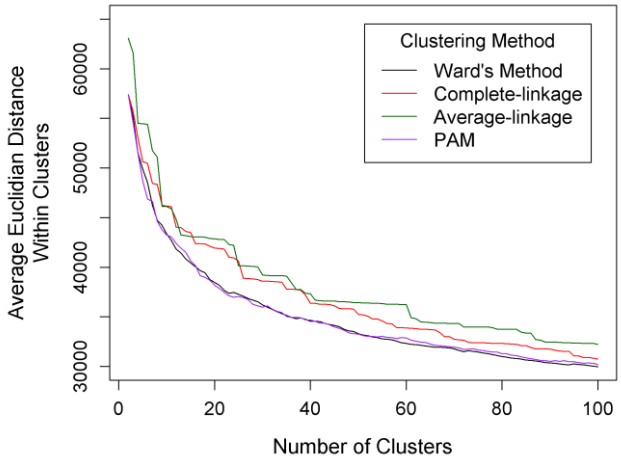

Fig. 9.18 Comparison of average Euclidian distance within clusters for different clustering methods and different number of clusters in the solar photovoltaic power time series clustering procedure.

Fig. 9.19 presents the average silhouette widths of the time series associated with the respective clusters. As stated before, the average silhouette width metric is a measure of the membership strength of time series to their respective clusters, and is based on the pairwise difference of between and within-cluster distances [94]. It results in a score between -1 and 1, where -1 one indicates a very poor clustering and 1 represents a very good clustering. The results indicate that all the clustering methods resulted in fairly average clustering results, with mixed results across the range of cluster numbers. A higher average silhouette width score would require a greater difference between the between and within-cluster distances, which is not a property of the simulated solar photovoltaic power time series as all the time series are bound by the same range. It is seen, however, that as the number of clusters increase, the average silhouette width decreases, which suggests using fewer clusters rather than more clusters results in a better clustering.

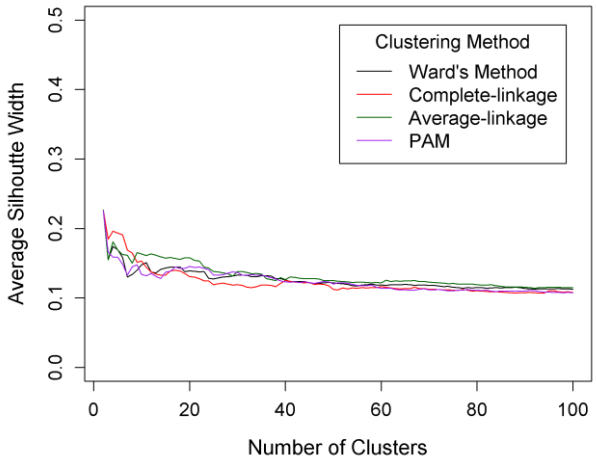

Fig. 9.19 Comparison of average silhouette width for different clustering methods and different number of clusters in the solar photovoltaic power time series clustering procedure.

Fig. 9.20 displays the result of the Caliński-Harabasz (CH) index. As stated before, the CH index calculates the ratio between cohesion and separation, with a higher ratio being preferable. As the number of clusters increases, the ratio between cohesion and separation deteriorates. At every given number of clusters, Ward's method and the PAM clustering method displays a higher CH index compared to the other clustering methods.

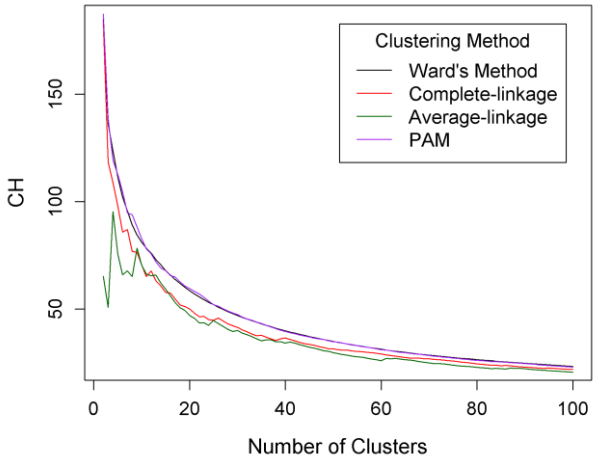

Fig. 9.20 Comparison of Caliński-Harabasz (CH) index for different clustering methods and different number of clusters in the solar photovoltaic power time series clustering procedure.

Ward's method is the best performer in the average Euclidian distance within the clusters metric and the Caliński-Harabasz index, and outperforms the PAM method at lower cluster numbers. It is therefore henceforth the preferred clustering methodology for simulated solar photovoltaic power time series. Similar to the wind power time series case, the choice of Ward's method also makes sense for the intended purpose of this clustering result (see end of section 9.3.3).

9.4.4 Visualisation of the Clustering Steps

Fig. 9.21 visualises the clustering steps for two to seven solar photovoltaic time series clusters using Ward's method of hierarchical clustering.

Fig. 9.21 Visualisation of the clustering steps in the Ward's method of hierarchical clustering for two to seven simulated solar photovoltaic time series clusters.

When observing Fig. 9.11, the result of the hierarchical agglomerative ("bottom-up") approach is clear. At each clustering step, the cluster with the highest Ward's distance between its respective time series is split into a further two clusters.

Considering the case when two and three clusters are selected, it would seem that the biggest differentiator between the solar photovoltaic simulations from different sites is the longitude of the sites. This of course makes sense as it relates to irradiance profile in the different clusters, i.e. the time of sunrise and sunset.

When four clusters are selected, the coastal region in KwaZulu Natal and the north-eastern part of the Eastern Cape is separated into its own cluster. This is because of the lower capacity factors achieved in this region, as can be seen in Fig. 9.4. This region of South Africa has a sub-tropical climate [102] that is characterised by high levels of cloud cover and frequent rains during the summer months, leading to a lower solar-photovoltaic energy yield.

When five and six clusters are selected, the coastal zones and areas bordering the coastal zones are separated from those areas further inland, mainly due to the difference in solar irradiance between these respective areas that is again caused by differences in cloud cover.

Specifying seven clusters separates the north-eastern cluster into two separate clusters.

9.4.5 Appropriate Number of Clusters

The simulated solar photovoltaic time series displayed much lower Euclidian distances between the respective time series than in the case of wind power simulations, leading to much lower average centroid errors. As such, it is decided that the L-method will be applied to all four cluster validation methods (as applied to the result obtained using Ward's method of hierarchical clustering), in order to determine the appropriate number of clusters.

It can be seen in Fig. 9.22 how the L-method is applied to one of the cluster validation measures, namely the average Euclidian distance between the clusters, in order to find a point, c, where the total root-mean-squared error (RMSE) of the left and right linear models are minimised. For this cluster validation measure, using 19 clusters minimises the total RMSE.

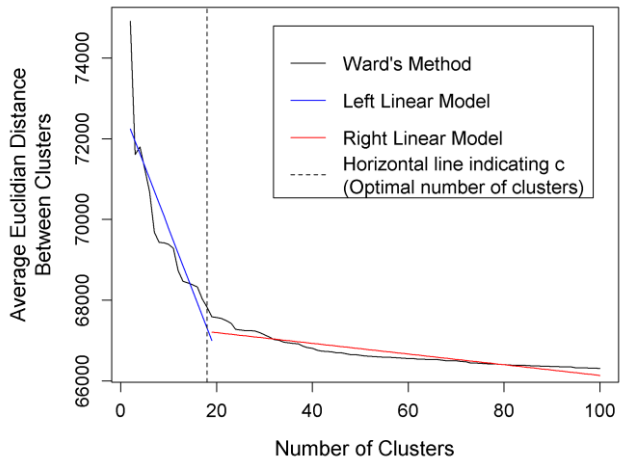

Fig. 9.22 Visualisation of the L-method applied to the average Euclidian distance between clusters using Ward's method of hierarchical clustering. The point c is found to be 19 for this cluster validation measure.

Table 9.4 shows the results of the L-method as applied to all of the cluster validation measures under consideration. The average result of the L-method applied to all the cluster validation measures gives the point, c, as 17. It is therefore proposed that 17 clusters be used for the simulated solar-photovoltaic power time series.

Table 9.4 Results of the L-method Applied to Different Cluster Validation Measures

Cluster Validation Measure	**Point c obtained from the L-method**
Average Euclidian distance between clusters	19
Average Euclidian distance within clusters	20
Average Silhouette Width	8
Caliński-Harabasz Index	21

9.4.6 Inspection of the Optimal Clustering Result

The spatial distribution of the optimal simulated solar photovoltaic power time series clustering result, using Ward's method of hierarchical clustering for 17 clusters, can be seen in Fig. 9.23.

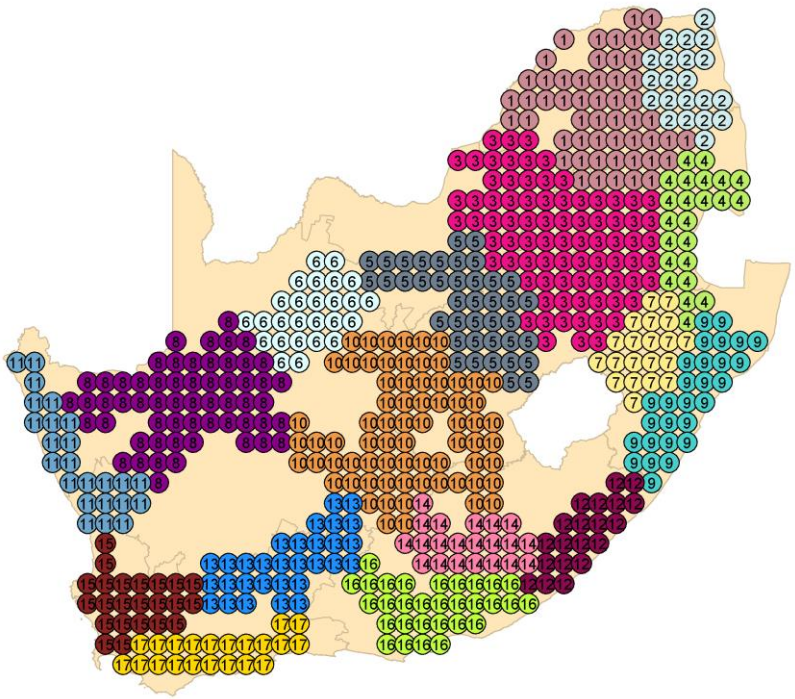

Fig. 9.23 Spatial distribution of solar photovoltaic site clusters obtained using Ward's method for 17 clusters.

The average seasonal daily power profiles of a selection of different clusters are inspected in Fig. 9.24. In Fig. 9.24, summer is defined as December to February, autumn is defined as March to May, winter is defined as June to August and spring is defined as September to November.

Cluster 1 (Limpopo region) and cluster 13 (north-east Western Cape region) have been included to showcase the difference between two clusters. The seasonal daily average profiles of the simulated

solar photovoltaic power time series of both clusters reach similar maximum power outputs during winter, although this represents the strongest power output season for cluster 1 and the weakest power output season for cluster 13. There is also a time shift, with cluster 1 starting power delivery earlier in the day than cluster 13.

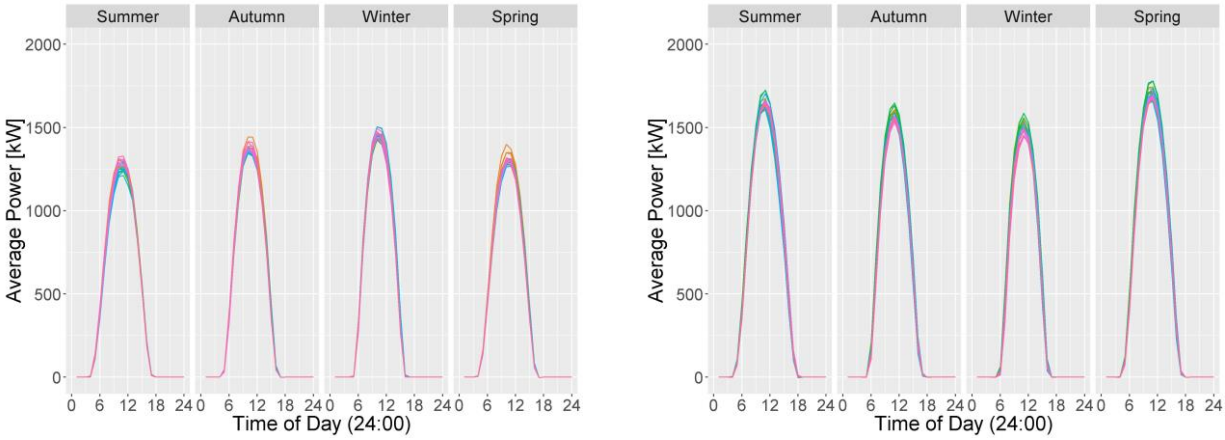

Cluster 1: 53 Sites

Cluster 13: 30 Sites

Fig. 9.24 Seasonal average daily power profiles for a 2 MW solar photovoltaic installation for the potential solar photovoltaic farm sites in selected clusters.

9.5 Case Study 1: Different Formulations of Mean-variance Optimisation

9.5.1 Overview

In the literature, mean-variance portfolio theory has been applied to minimise the variance of wind power. This case study examines the effect of including the solar photovoltaic power time series and the load time series in the optimisation procedure.

The size of the case study is arbitrarily chosen to represent the wind and solar capacities assigned in the IRP 2010 policy document for the year 2030 (see section 2.2.1). Therefore the optimal allocation of 9 200 MW of wind farm capacity and 8 400 MW of solar photovoltaic farm capacity will be considered. It is assumed that the load in 2030 will be the same as in peak load year, 2007. Four scenarios are studied, as summarised in Table 9.5.

Table 9.5 Summary of the four scenarios studied in case study 1.

Scenario	**Data Included in Optimisation**	**Optimisation Target**	**Mathematical formulation**
1	Simulated wind power time series	Minimise variance of cumulative wind power output	Section 5.3.
2	Simulated wind power time series and load time series	Minimise variance of load minus wind power output	Section 5.5 (excluding solar).
3	Simulated wind power time series and simulated solar photovoltaic time series	Minimise variance of cumulative renewable power output	Section 5.4.
4	Simulated wind power time series, simulated solar photovoltaic time series and load time series	Minimise variance of residual load	Section 5.5.

In case study 1, the clustering techniques that have been applied in section 9.3 and section 9.4 are used to cluster the simulated wind time series and simulated solar photovoltaic time series. For each resulting cluster a centroid time series is calculated that is used as an input to the mean variance optimisation procedure. The effect of the time series clustering and the justification of its use are examined in case study 2.

In scenarios 1 and 2, it is assumed that the full 8 400 MW of solar photovoltaic capacity is added to the system. An average time series of all the photovoltaic time series is used to achieve this. In case studies 3 and 4, the solar photovoltaic capacity is allocated by the optimisation procedure.

9.5.2 Mean-Variance Variable Assumptions

All the variable assumptions that are made in case study 1 are shown in Table 9.6.

Table 9.6 Summary of Variable Assumptions in case study 1.

Variable	Meaning	Value
$\mu_{\text{Min Desired Solar}}$	The minimum overall mean solar photovoltaic power output (related to capacity factor)	Not set
$w_{\text{Total Wind}}$	The total wind farm capacity that is to be allocated.	9 200 MW
$w_{\text{Max Total Solar}}$	The maximum solar photovoltaic farm capacity that can be allocated.	8 400 MW
$\max_x, x \in \text{Wind}$	Maximum wind farm capacity that can be assigned to each 27 x 31 km site.	500 MW
$\max_x, x \in \text{Solar}$	Maximum wind farm capacity that can be assigned to each 40 x 40 km site.	1 000 MW

The $\mu_{\text{Min Desired Solar}}$ variable is not set in this case study. It is only necessary when there are sites with very low solar photovoltaic power outputs that need to be limited. The capacity constraints per site, $\max_x$, represent conservative estimates of how much capacity could be built on a single potential wind farm site or solar photovoltaic farm site.

9.5.3 Scenario Efficient Frontiers

The efficient frontiers of each scenario will now be inspected. The efficient frontier shows the minimised target and is obtained by solving the optimisation problem for a range of different values of $\mu_{\text{Desired Wind}}$, the desired mean wind power output, which can be transformed to wind farm capacity factor by dividing by the total wind farm capacity (9 200 MW in case study 1).

9.5.3.1 Scenario 1 Efficient Frontier

The efficient frontier for scenario 1 is shown in Fig. 9.25. The minimisation target, the variance of cumulative wind power output, is plotted on the y-axis and the capacity factor ($\mu_{\text{Desired Wind}}$) is plotted on the x-axis.

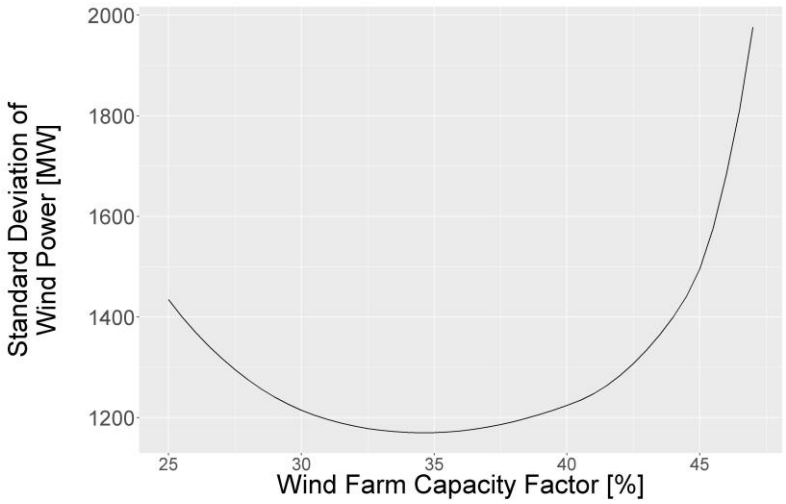

Fig. 9.25 Efficient frontier of scenario 1.

9.5.3.2 Scenario 2 Efficient Frontier

The efficient frontier for scenario 2 is shown in Fig. 9.26. The minimisation target, the variance of load minus wind power output, is plotted on the y-axis and the capacity factor ($\mu_{\text{Desired Wind}}$) is plotted on the x-axis.

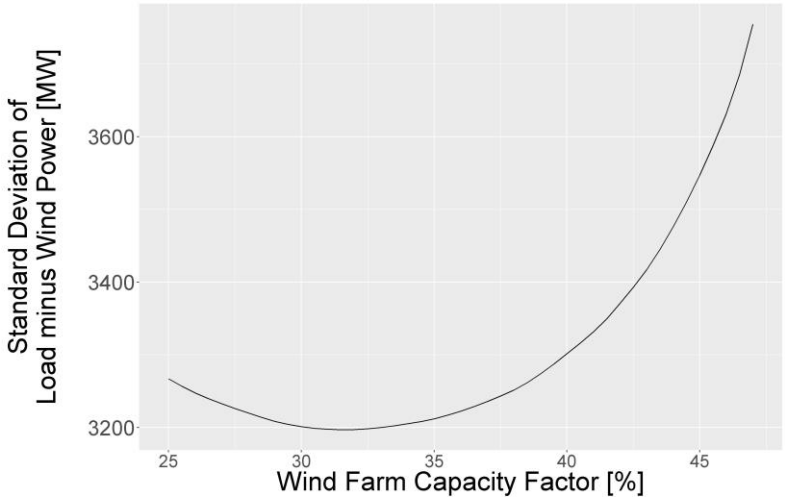

Fig. 9.26 Efficient frontier of scenario 2.

9.5.3.3 Scenario 3 Efficient Frontier

The efficient frontier for scenario 3 is shown in Fig. 9.27. The minimisation target, the variance of cumulative renewable power output, is plotted on the y-axis and the capacity factor ($\mu_{\text{Desired Wind}}$) is plotted on the x-axis.

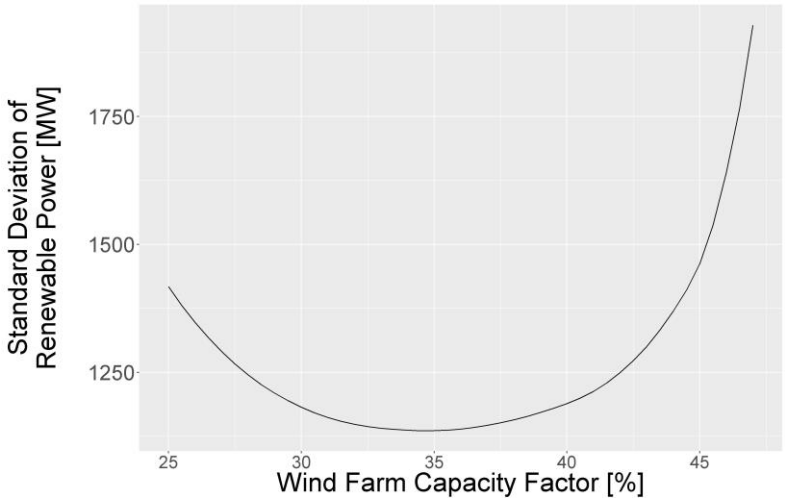

Fig. 9.27 Efficient frontier of scenario 3.

Unlike scenarios 1 and 2, where 8 400 MW of solar photovoltaic capacity was uniformly allocated, the mean-variance optimisation procedure determined the allocation (and therefore the total solar capacity), for every value of $\mu_{\text{Desired Wind}}$, that would minimise the variance of the cumulative renewable power output. This can be seen in Fig. 9.28. The totals are relatively low when compared to the 9 200 MW of wind farm capacity that is added.

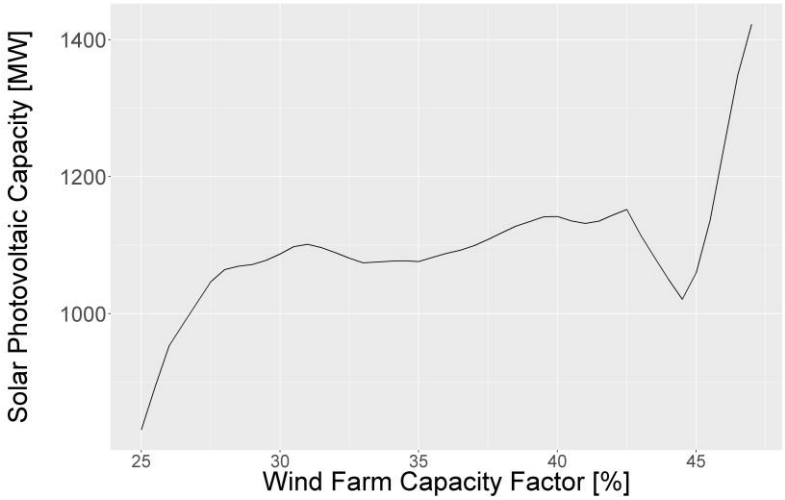

Fig. 9.28 Solar photovoltaic capacity included in efficient frontier solutions of scenario 3.

9.5.3.4 Scenario 4 Efficient Frontier

The efficient frontier for scenario 4 is shown in Fig. 9.29. The minimisation target, the variance of residual load, is plotted on the y-axis and the capacity factor ($\mu_{\text{Desired Wind}}$) is plotted on the x-axis.

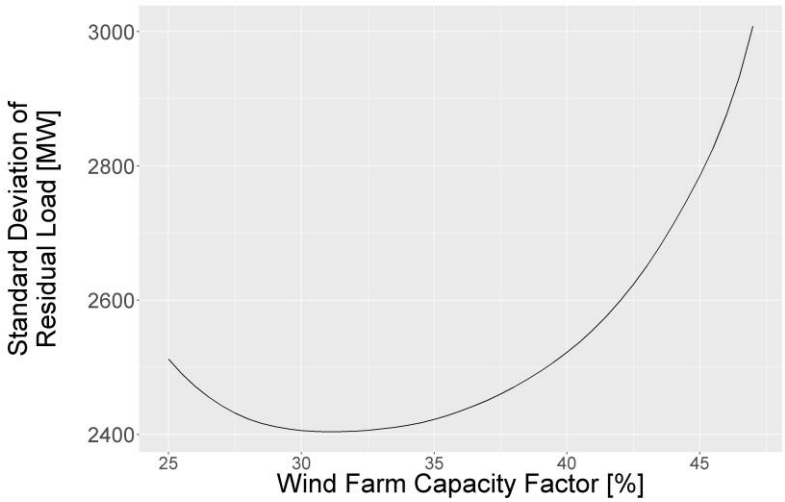

Fig. 9.29 Efficient frontier of scenario 4.

Unlike scenarios 1 and 2, where 8 400 MW of solar photovoltaic capacity was uniformly allocated, the mean-variance optimisation procedure determined the allocation (and therefore the total solar capacity), for every value of $\mu_{\text{Desired Wind}}$, that would minimise the variance of the residual load. This can be seen in Fig. 9.30. A higher overall wind farm capacity factor required a higher capacity of solar photovoltaic farm capacity. Also, the solar photovoltaic farm capacities are considerably higher than those assigned in scenario 3 (in the order of 900 to 1 400 MW).

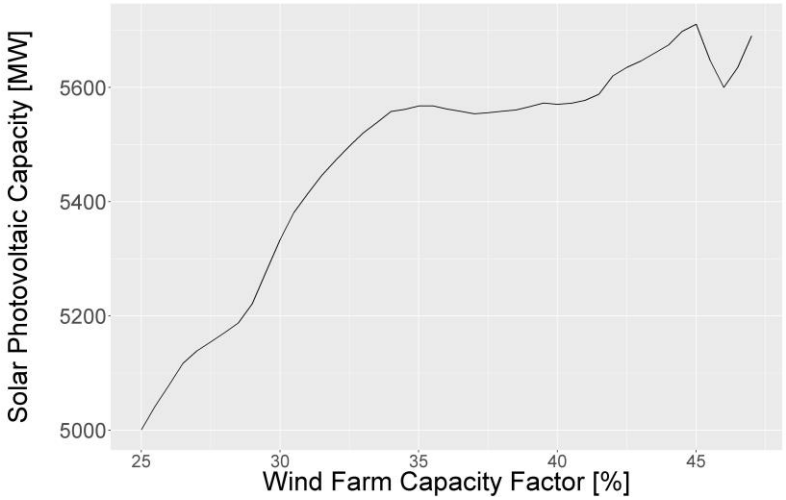

Fig. 9.30 Solar photovoltaic capacity included in efficient frontier solutions of scenario 4.

9.5.4 Comparison of Scenario Performance

The four scenarios will now be compared using the standard deviation of the renewable power output and the standard deviation of the residual load. Fig. 9.31 displays the standard deviations of the renewable power output of the efficient frontier solutions of scenarios 1 to 4. It is important to remember that scenarios 1 and 2 both have 8 400 MW of uniformly distributed solar photovoltaic capacity, while scenario 3 has solar photovoltaic capacity in the order of 900 MW to 1 400 MW and scenario 4 has solar photovoltaic capacity in the order of 5 000 MW to 5 700 MW. Predictably, it is scenario 3 that has the lowest standard deviation of renewable power output as this was its optimisation goal.

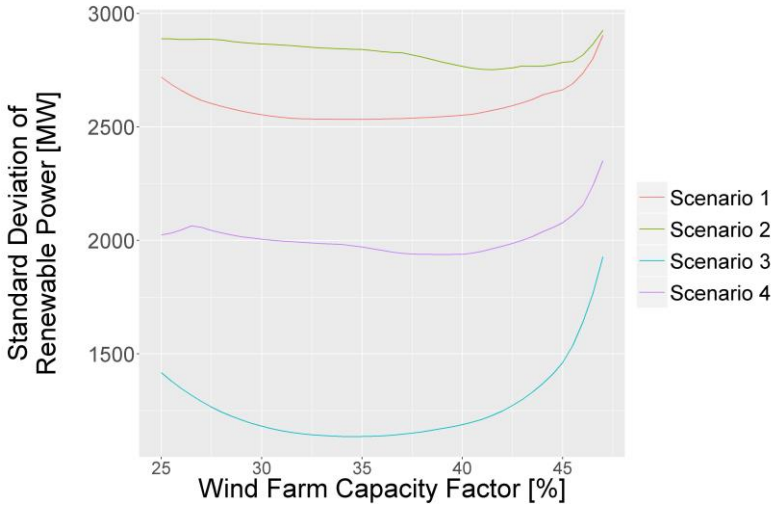

Fig. 9.31 Standard deviations of renewable power outputs of efficient frontier solutions of scenarios 1-4.

The standard deviation of the residual load is arguably of more importance than the standard deviation of the renewable power output, and is shown in Fig. 9.32. Also plotted on Fig. 9.32, is the standard deviation of the current load, i.e. the load time series before any renewable power has been subtracted (with its annual and seasonal trends removed). It is telling that at this level of wind power capacity addition, the standard deviation of the load can actually be reduced significantly if the right optimisation procedure is used to allocate wind farm capacity and solar photovoltaic farm capacity.

It is also possible to see that the solutions obtained in scenario 3 does not in fact reduce the standard deviation of the residual load, meaning that minimising the variance of renewable power output while excluding the load time series data from the optimisation procedure will lead to sub-optimal results. This is mainly due to the low solar allocation in scenario 3, which ignores the correlation that solar photovoltaic power has with the rise and fall of the daily load profile.

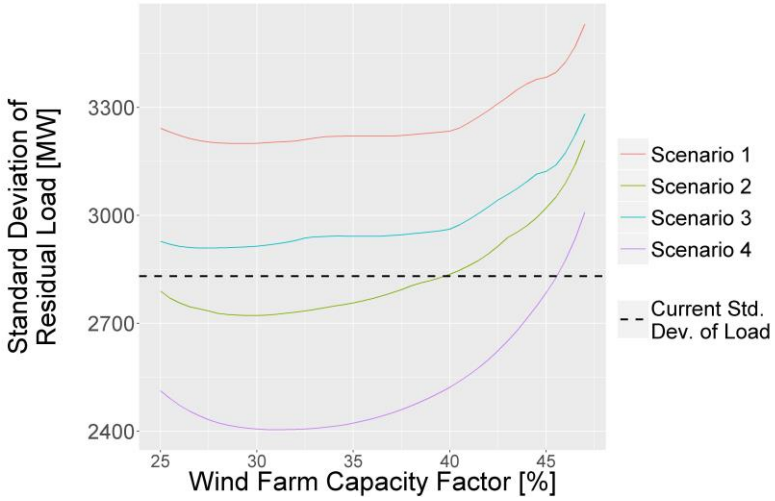

Fig. 9.32 Standard deviations of residual loads of efficient frontier solutions of scenarios 1-4.

9.5.5 Comparison of all Scenario Solutions at 40% Wind Farm Capacity Factor

Every point on the efficient frontier represents a solution which consists of a particular distribution of wind farm and solar photovoltaic farm capacity. The solutions that fall at the 40% wind farm capacity factor level of every efficient frontier for scenarios 1 to 4 is now inspected. The solution at 40% wind farm capacity factor is chosen because it represents a solution with a high wind energy yield, but falls at a point where the minimisation target is still relatively close to its absolute minimum.

Fig. 9.33 shows the spatial distribution of the 9 200 MW of wind farm capacity that is allocated in the 40% wind power capacity factor solution in each scenario. There are similarities between scenarios 1 and 3, where the load time series has not been taken into account. The same can be said for scenarios 2 and 4, where the load time series is taken into account.

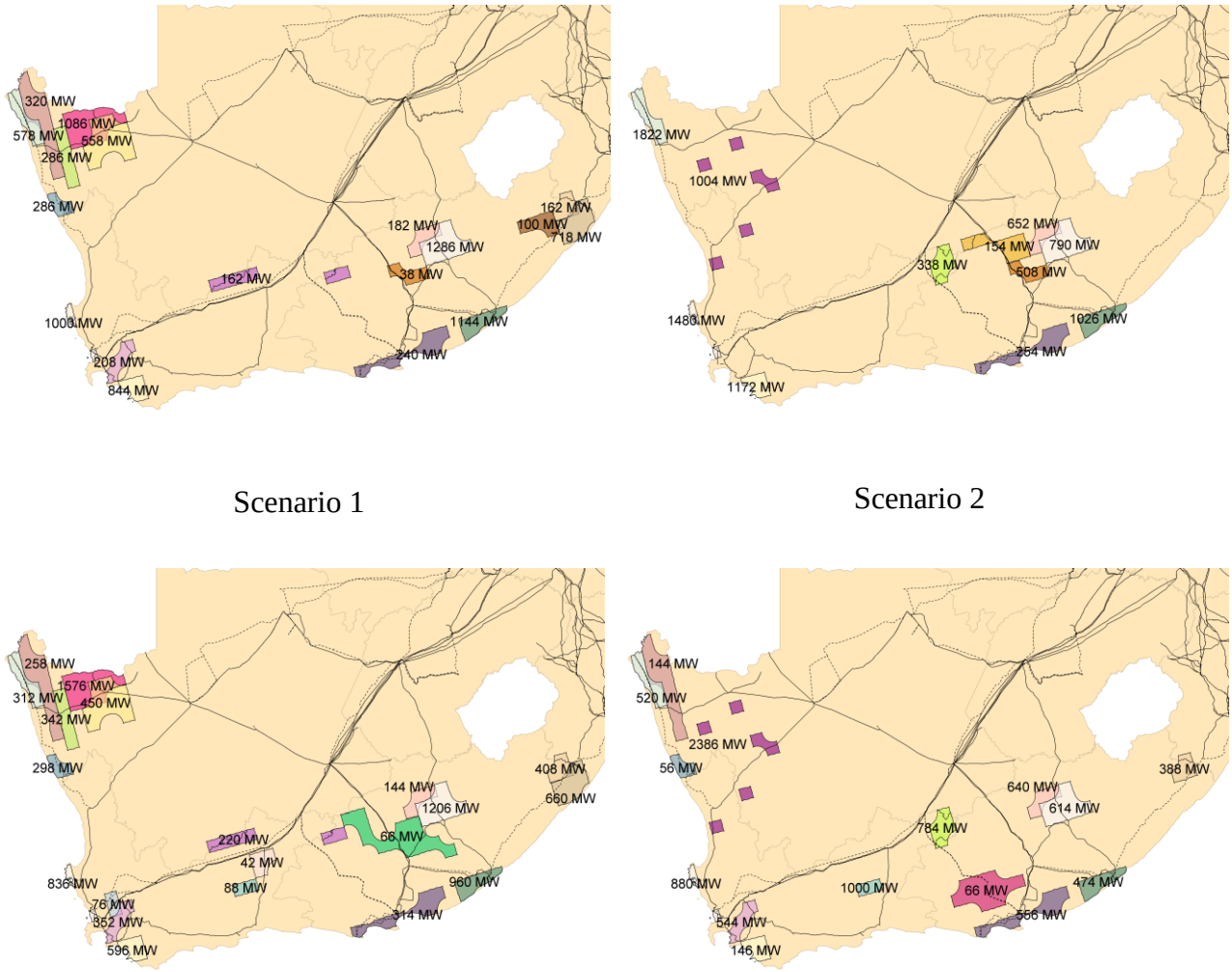

Scenario 1 Scenario 2

Scenario 3 Scenario 4

Fig. 9.33 Spatial distributions of the 9 200 MW of wind farm capacity of 40% wind farm capacity factor solutions on the efficient frontiers of scenarios 1-4.

Fig. 9.34 shows the size and spatial distribution of the solar photovoltaic farm capacity that is present in the 40% wind power capacity factor solution of each scenario. As stated before, a uniform distribution of solar photovoltaic capacity is assumed in scenarios 1 and 2 (note that each site is assigned 14.24 MW, even though this is rounded to 14 MW in Fig. 9.34). The difference between the solar photovoltaic capacity allocation in scenarios 3 and 4 is also clear. Scenario 4 shows that including the load into the optimisation procedure significantly increases the solar photovoltaic capacity, but to the level of 8 400 MW as mandated in the IRP 2011 policy document. The solar photovoltaic capacity in scenario 4 is also mainly allocated in the south-west of the country, possibly as a result of the solar photovoltaic profiles of this region playing a bigger role in meeting the peak load, which stems mainly from the load centres in the north east of the country.

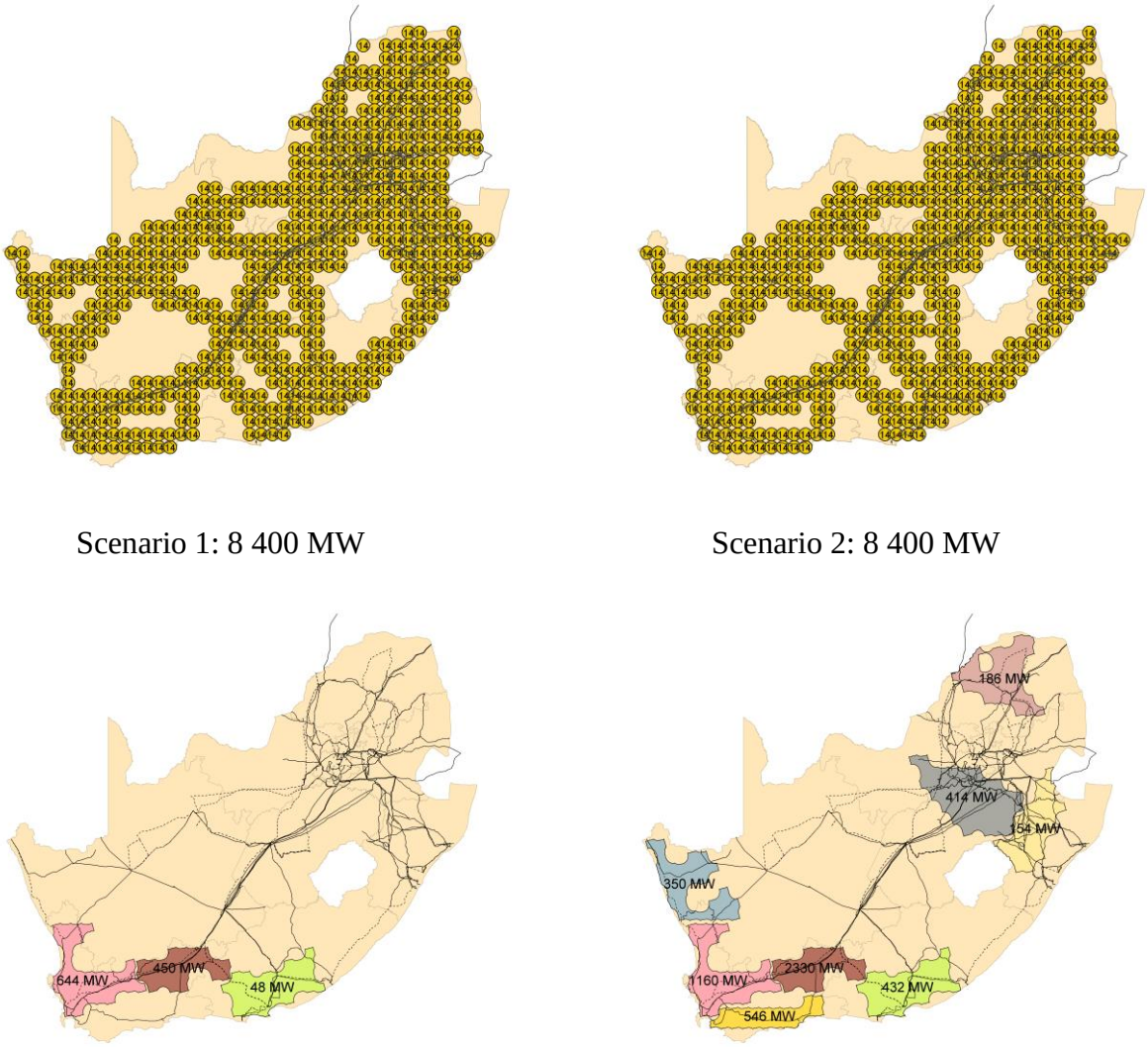

Scenario 1: 8 400 MW

Scenario 2: 8 400 MW

Scenario 3: 1 142 MW

Scenario 4: 5 572 MW

Fig. 9.34 Size and spatial distributions of the solar photovoltaic farm capacity of the 40% wind farm capacity factor solutions on the efficient frontiers of scenarios 1-4.

Fig. 9.35 shows the seasonal average daily power profiles for the renewable power output of the 40% wind farm capacity factor solutions on the efficient frontiers of scenario 1 to 4. From Fig. 9.35 it is clear that scenario 3 minimises the variance of the renewable power output. Also, the seasonal average power profiles of scenarios 1 and 2 look quite similar (both are dominated by the relatively large solar photovoltaic capacity), but we have already seen from Fig. 9.32 that the standard deviation of the residual load in these two cases differ substantially. This could point to the dangers of using daily average profiles for analysis. Scenario 4 results in the "widest" daily power profiles, which optimally covers the load.

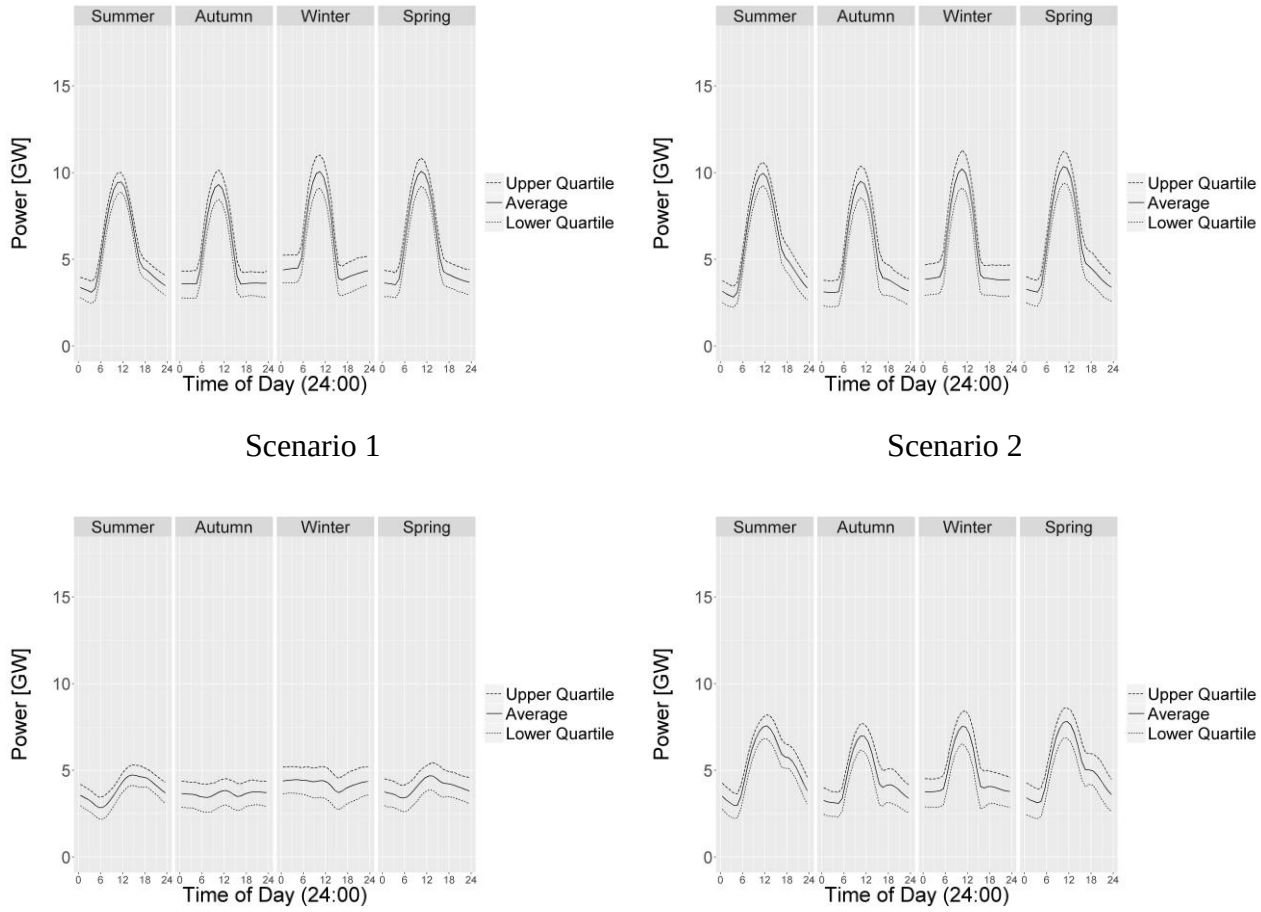

Fig. 9.35 Seasonal average daily power profiles for the renewable power output of the 40% wind farm capacity factor solutions on the efficient frontiers of scenarios 1-4.

9.5.6 Inspection of Scenario 4 solution at 40% Wind Farm Capacity Factor

In section 9.5.4 it was shown that including the wind power time series, solar photovoltaic power time series and load in the optimisation procedure (as in scenario 4), could actually result in a residual load with a lower standard deviation than the original load time series. The scenario 4 solution at 40% wind farm capacity factor is now investigated further.

Fig. 9.36 shows the seasonal average daily wind power profiles for the wind power output of the 40% wind farm capacity factor solution of scenario 4. It can be seen that there is considerably more variance in the wind power output during autumn and winter than during summer and spring. It is hypothesised that this is a characteristic of the wind resource in South Africa. This characteristic will have an effect on the power system as will be shown in the following figures.

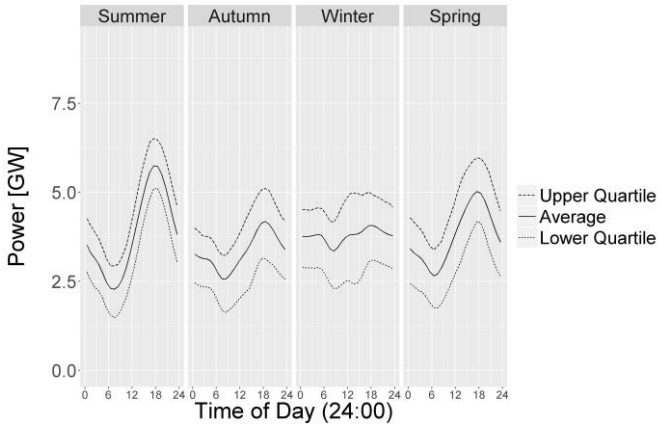

Fig. 9.36 Seasonal average daily wind power profiles for the wind power output of the 40% wind farm capacity factor solution of scenario 4.

Fig. 9.37 shows the load, renewable power and residual load time series for a week in February (summer) 2007 of the 40% wind farm capacity factor solution of scenario 4. It can be seen that the up and down ramps of the residual load is for the most part smaller than that of the load, illustrating the smaller standard deviation of the residual load. It can also be seen that the wind power follows a similar daily cycle on most days, thereby increasing the longer term predictability of the residual load. Where the load was relatively flat during the day, the residual load displays distinct morning and evening peaks on most days.

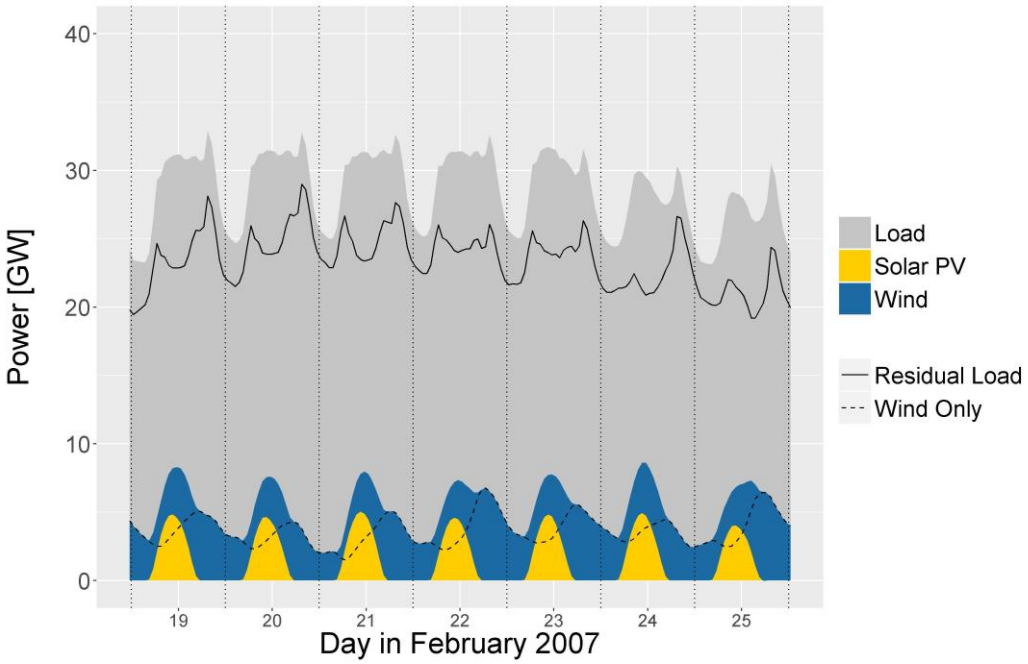

Fig. 9.37 Load, renewable power and residual load time series for a week in February 2007 of the 40% wind farm capacity factor solution of scenario 4.

Fig. 9.38 shows the load, renewable power and residual load time series for a week in July (winter) 2007 of the 40% wind farm capacity factor solution of scenario 4. Here, the wind power output does not follow a similar daily cycle. Instead, higher wind days and lower wind days are clearly visible. On most days the morning peak of the load is considerably reduced, but the evening peak is only slightly reduced. This kind of result will have impacts on power system operation.

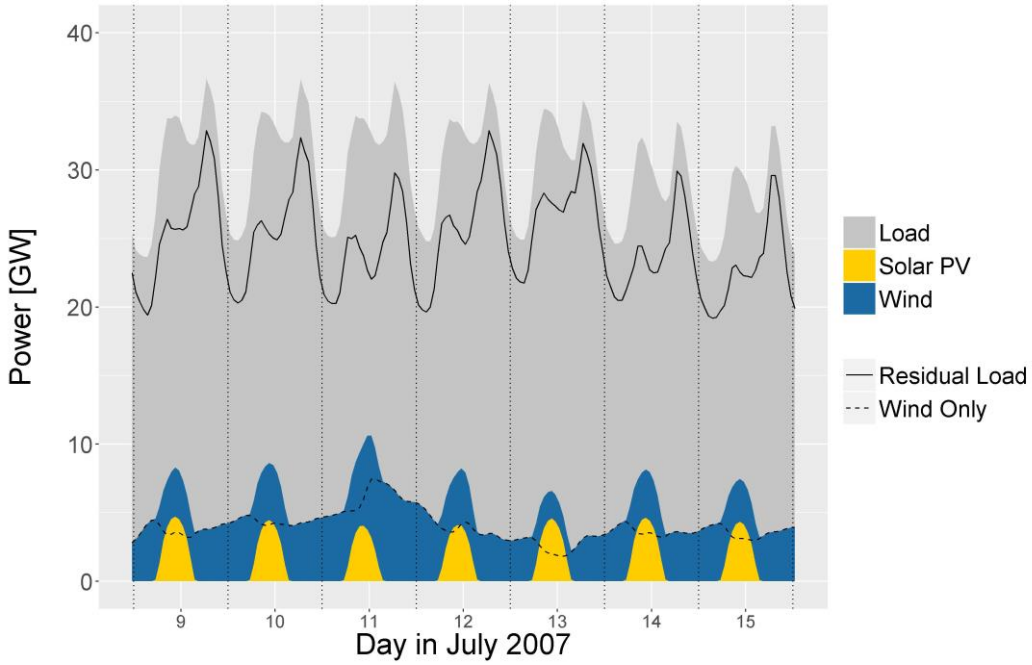

Fig. 9.38 Load, renewable power and residual load time series for a week in July 2007 of the 40% wind farm capacity factor solution of scenario 4.

9.6 Case Study 2: REIPPPP Round 1-3 vs. Optimisation (Unclustered and Clustered)

9.6.1 Overview

This case study compares the optimisation procedure (considering wind power, solar photovoltaic power and load) with the wind farm and solar photovoltaic farm allocation in the REIPPPP, in order to quantify the benefits of the optimisation procedure when compared with a real-world allocation in South Africa. This case study also justifies the use of time series clustering by examining the effect that time series clustering has on the results of the optimisation procedure when compared to the unclustered optimisation as found in the literature.

Wind power simulations were performed for all the wind farm projects in rounds 1 to 3 of the REIPPPP, excluding two wind farms at De Aar in the Northern Cape due to their location falling outside the WASA wind dataset. Therefore, a total of 1 778 MW of wind farm capacity is considered. The method used to simulate the wind power time series is exactly the same as the method described in section 3.2. In each case, the WASA wind speed time series closest to the respective REIPPPP wind farm was used to perform the simulation, using a wind turbine power curve that matches the actual wind turbine power curve. The details of the wind farms that were considered in this case study is given in Table 9.7. The wind turbine power curves that were used for the REIPPPP simulation is shown in Fig. 9.39.

Solar photovoltaic simulations were also done for the solar photovoltaic projects in rounds 1 to 3 of the REIPPPP. Therefore, a total of 1 484 MW of solar photovoltaic farm capacity is considered. The method used to simulate the solar photovoltaic power time series is exactly the same as the method described in section 3.3. In each case, the SoDa irradiance and temperature time series closest to the respective REIPPPP solar photovoltaic farm was used to perform the simulation, assuming a fixed angle installation (i.e. no tracking). The details of the solar photovoltaic farms that were considered in this case study are given in Table 9.8.

Table 9.7 Details of the Wind Farm Projects in REIPPPP Rounds 1-3 (excluding two wind farms at De Aar in the Northern Cape).

Name	REIPPPP Phase	Province	Capacity (MW)	Turbine Model	Hub Height (m)	Turbine Rated Power (MW)	Number of Turbines	Latitude	Longitude
Cookhouse Wind Farm	1	Eastern Cape	138.6	Suzlon S88 2.1 MW	80	2.1	66	-32.81	25.91
Dorper Wind Farm	1	Eastern Cape	100	Nordex N100 2.5MW	80	2.5	40	-31.48	26.45
Jeffreys Bay Wind Farm	1	Eastern Cape	138	Siemens SWT-2.3-108	80	2.3	60	-34.00	24.84
Kouga Wind Farm	1	Eastern Cape	80	Nordex N90 2.5 MW	80	2.5	32	-34.15	24.72
Metrowind Van Stadens Wind Farm	1	Eastern Cape	27	Sinovel SL3000-113	90	3	9	-33.96	25.24
Noblesfontein Gestamp Wind Farm	1	Northern Cape	73.8	Vestas V100 1.8MW	95	1.8	41	-31.70	23.18
Dassiesklip Wind Energy Facility	1	Western Cape	27	Sinovel SL3000-113	100	3	9	-34.23	19.38
Hopefield Umoya Wind Farm	1	Western Cape	66.6	Vestas V100 1.8MW	95	1.8	37	-33.10	18.40
Amakhala Emoyeni Wind Farm	2	Eastern Cape	134.4	Nordex N117 2.4MW	91	2.4	56	-32.75	25.93
Chaba Wind Farm	2	Eastern Cape	21	Vestas V112 3MW	84	3.075	7	-32.59	27.34
Grassridge Wind Project	2	Eastern Cape	61.5	Vestas V112 3MW	84	3.075	20	-33.65	25.59
Tsitsikamma Community Wind Farm	2	Eastern Cape	95	Vestas V112 3MW	94	3.075	31	-34.08	24.50
Waainek Wind Project	2	Eastern Cape	24.6	Vestas V112 3MW	84	3.075	8	-33.33	26.47
Gouda Wind Facility	2	Western Cape	138	Acciona AW-100-3000	100	3	46	-33.26	19.03
West Coast One Wind Farm	2	Western Cape	94	Vestas V90 2MW	80	2	47	-32.83	18.00
Gibson Bay Wind Farm	3	Eastern Cape	110	Nordex N117 3MW	91	3	37	-34.14	24.52
Nojoli Wind Farm	3	Eastern Cape	88	Vestas V100 2MW	80	2	44	-32.77	25.92
Khobab Wind Farm	3	Northern Cape	140	Siemens SWT-2.3-108	99.5	2.3	61	-30.43	19.49
Loeriesfontein 2 Wind Farm	3	Northern Cape	140	Siemens SWT-2.3-108	99.5	2.3	61	-30.40	19.60
Noupoort Wind Farm	3	Northern Cape	80.5	Siemens SWT-2.3-108	99.5	2.3	35	-31.18	25.05

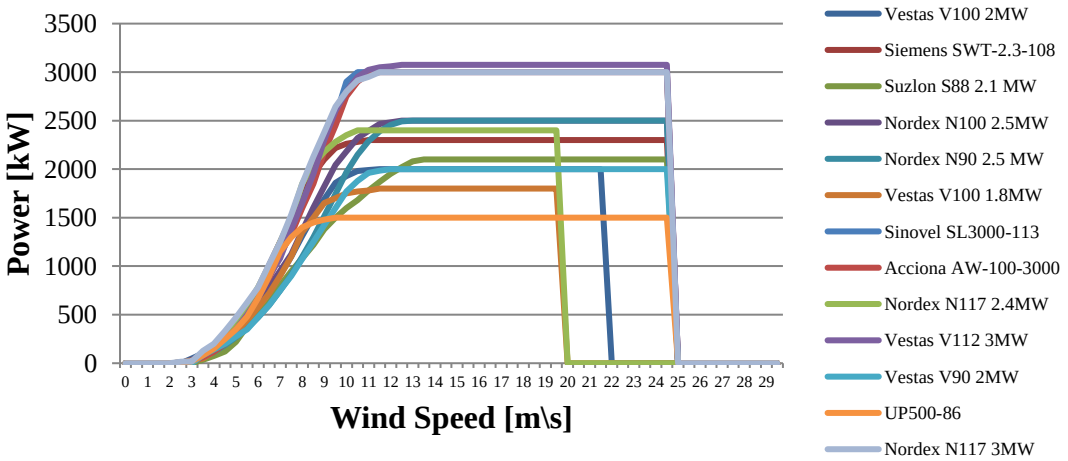

Fig. 9.39 Wind turbine power curves used in the REIPPPP simulation

Table 9.8 Details of the Solar Photovoltaic Farm Projects in REIPPPP Rounds 1-3.

Name	REIPPPP Phase	Province	Capacity (MW)	Longitude	Latitude
Letsatsi Power Company	1	Free State	64	25.92	-28.92
Soutpan Solar Park	1	Limpopo	28	29.25	-22.99
Witkop Solar Park	1	Limpopo	30	29.36	-24.04
RustMo1 Solar Farm	1	North West	6.76	27.42	-25.74
Aries Solar PV Energy Facility	1	Northern Cape	9.65	20.79	-29.50
De Aar Solar PV	1	Northern Cape	48.25	24.03	-30.62
Droogfontein Solar PV Project	1	Northern Cape	48.25	24.76	-28.61
Greefspan PV Power Plant	1	Northern Cape	10	23.31	-29.39
Herbert PV Power Plant	1	Northern Cape	19.9	23.80	-29.00
Kalkbult	1	Northern Cape	72.5	24.14	-30.16
Kathu Solar Energy Facility	1	Northern Cape	75	23.03	-27.61
Konkoonsies Solar	1	Northern Cape	9.65	19.56	-28.89
Lesedi Power Company	1	Northern Cape	64	23.37	-28.31
Mulilo Renewable Energy Solar PV De Aar	1	Northern Cape	9.65	24.01	-30.63
Mulilo Renewable Energy Solar PV Prieska	1	Northern Cape	19.9	22.32	-29.97
Solar Capital De Aar	1	Northern Cape	75	24.10	-30.60
SlimSun Swartland Solar Park	1	Western Cape	5	18.53	-33.35
Touwsrivier CPV Solar Project	1	Western Cape	36	19.93	-33.41
Project Dreunberg	2	Eastern Cape	69.9	26.21	-30.83
Boshoff Solar Park	2	Free State	60	25.19	-28.46
Jasper Power Company	2	Northern Cape	75	23.35	-28.32
Linde Solar Project	2	Northern Cape	36.8	24.66	-31.00
Sishen Solar Facility	2	Northern Cape	74	22.93	-27.58
Solar Capital De Aar 3	2	Northern Cape	75	24.10	-30.60
Upington Solar PV	2	Northern Cape	8.9	21.27	-28.40
Aurora Solar Project	2	Western Cape	9	18.50	-32.64
Vredendal Solar Power Park	2	Western Cape	8.8	18.51	-31.63
Pulida Solar Park	3	Free State	75	24.90	-29.09
Tom Burke Solar Park	3	Limpopo	60	27.99	-23.07
Adams Solar PV 2	3	Northern Cape	75	23.01	-27.38
Mulilo Prieska PV	3	Northern Cape	75	22.32	-30.04
Mulilo Sonnedix Prieska PV	3	Northern Cape	75	22.36	-30.02
Paleisheuwel Solar PV Park	3	Western Cape	75	18.73	-32.42

Case study 2 compares three different distributions of renewable energy capacity as can be seen in Table 9.9. Both an unclustered and clustered optimisation is performed. This is done to justify the use of the clustering procedure, as the unclustered optimisation yields slightly better results, but fails to provide practicable solutions. The unclustered optimisation considers all the simulated power time series (402 wind power time series from the Vestas 2 MW platform and 590 solar photovoltaic time series). The clustered optimisation considers the centroid time series that were calculated using the preferred clustering methodology and appropriate numbers of clusters as discussed in sections 9.3 and 9.4.

Table 9.9 Three distributions that are compared in case study 2.

Distribution Name	**Distribution Details**
REIPPPP	Distributions obtained from REIPPPP
Optimised Unclustered	Distributions allocated by the mean-variance optimisation procedure considering all individual wind and solar photovoltaic time series and load
Optimised Clustered	Distributions allocated by the mean-variance optimisation procedure considering centroid wind and solar photovoltaic time series (calculated using the time series clustering methodology) and load

9.6.2 Mean-Variance Variable Assumptions

All the variable assumptions that are made in case study 2 are shown in Table 9.10.

Table 9.10 Summary of variable assumptions in case study 2.

Variable	**Meaning**	**Value**
$\mu_{\text{Min Desired Solar}}$	The minimum overall mean solar photovoltaic power output (related to capacity factor)	Not set
$w_{\text{Total Wind}}$	The total wind farm capacity that is to be allocated.	1 778 MW
$w_{\text{Max Total Solar}}$	The maximum solar photovoltaic farm capacity that can be allocated.	1 484 MW
$\max_x, x \in \text{Wind}$	Maximum wind farm capacity that can be assigned to each 27 x 31 km site.	500 MW
$\max_x, x \in \text{Solar}$	Maximum wind farm capacity that can be assigned to each 40 x 40 km site.	1 000 MW

The $\mu_{\text{Min Desired Solar}}$ variable is not set in this case study. It is only necessary when there are sites with very low solar photovoltaic power outputs that need to be limited. The capacity constraints per site, $\max_x$, represent conservative estimates of how much capacity could be built on a single potential wind farm site or solar photovoltaic farm site.

9.6.3 Efficient Frontiers

As stated before, the efficient frontiers display the minimisation target on the y-axis and the desired wind farm capacity factor on the x-axis. The efficient frontier for the minimised standard deviation (variance) of residual load of the unclustered and clustered optimisation procedures are shown in Fig. 9.40, as well as the standard deviation of the residual load from the REIPPPP distribution. It can be seen that the unclustered and clustered optimisations performed similarly across the range of desired wind farm capacity factors, with the unclustered optimisation expectedly performing slightly better (achieving a lower standard deviation of residual load). Although the standard deviation of the residual load of the REIPPPP distribution is lower than the standard deviation of the current load, both the optimisations succeed in achieving a significantly lower standard deviation. It is also clear that there is scope for an increased wind farm capacity factor when comparing the REIPPPP distribution with the optimisation results.

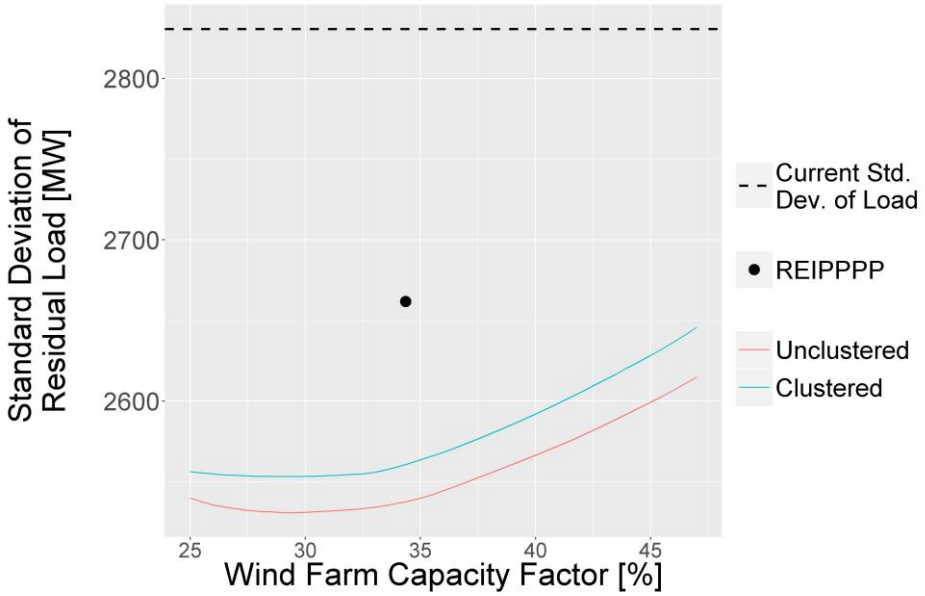

Fig. 9.40 Efficient frontiers of the unclustered and clustered optimisation procedures, as well as the standard deviation of the REIPPPP distribution's residual load.

9.6.4 Comparison of Unclustered and Clustered Solutions at 40% Wind Farm Capacity Factor with REIPPPP

The solutions at 40% wind farm capacity factor will now be compared with the REIPPPP distribution. In Fig. 9.41, the distribution of wind farm capacity in REIPPPP rounds 1 to 3 is shown.

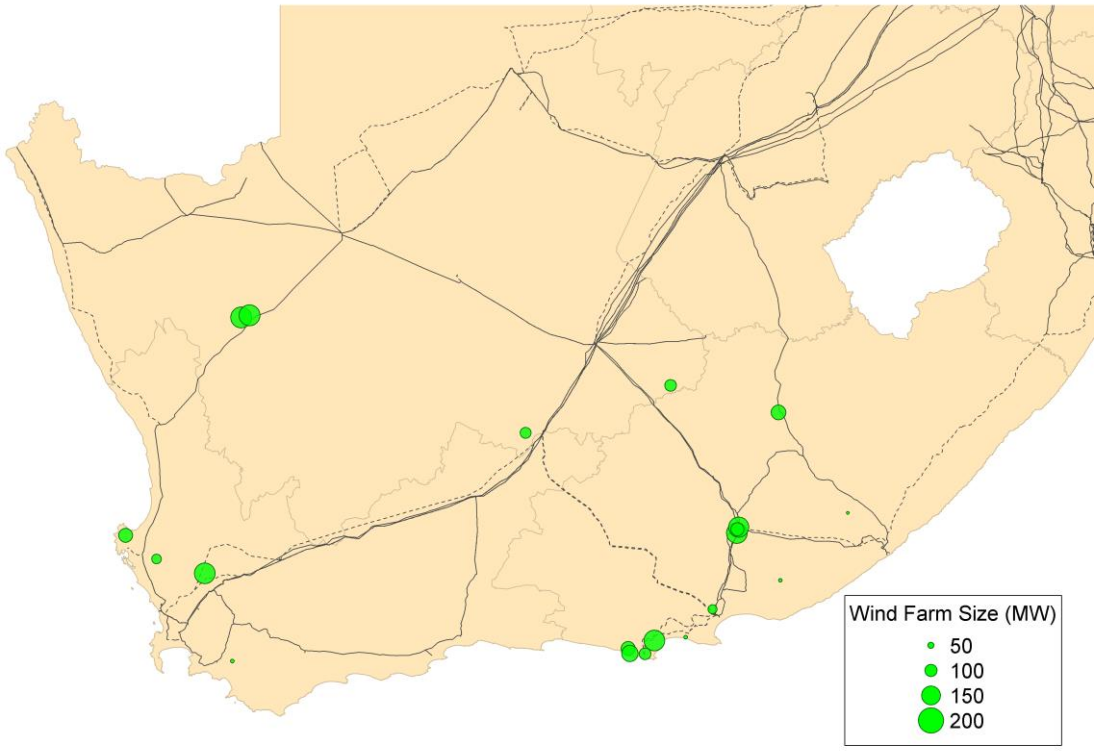

Fig. 9.41 Wind Farm distribution in REIPPPP Rounds 1-3 (excluding two wind farms at De Aar in the Northern Cape).

Fig. 9.42 shows the spatial distribution of the wind farm capacity of the solution at 40% wind farm capacity factor of the unclustered solution. Low capacities are allocated to certain sites, which makes part of the solution unfeasible in the face of practical and economic considerations. The capacities are furthermore assigned to exact coordinates, yielding a very rigid solution when factors such as land use, grid connection capacity, etc. have not been taken into account. There is no clear site selection alternatives should a specific site be disqualified based on these considerations.

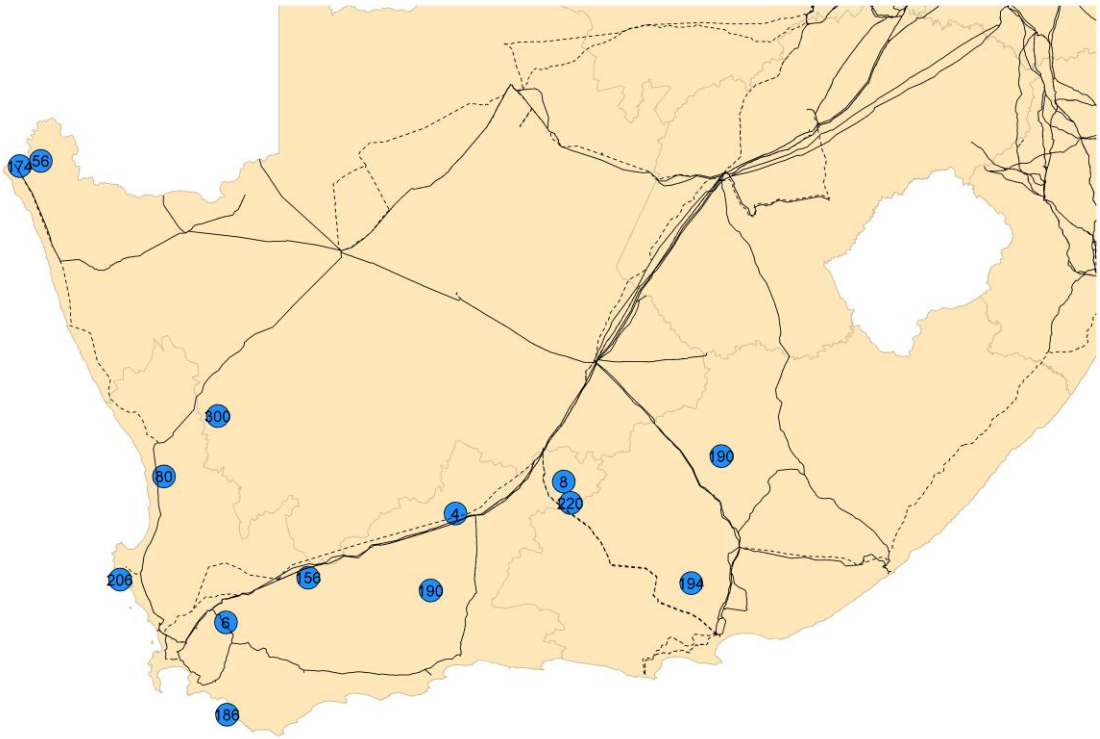

Fig. 9.42 Wind Farm distribution of 1 778 MW of the solution at 40% wind farm capacity factor in the unclustered optimisation.

Fig. 9.43 shows the spatial distribution of the wind farm capacity of the solution at 40% wind farm capacity factor of the clustered solution. As has been confirmed by respective efficient frontiers, the performance of the unclustered and clustered solution is comparable, but the clustered solution is more feasible as it provides a broader range of options to implement the solutions. The capacities are allocated to geographical areas with similar wind power profiles rather than individual potential wind farm sites. The same phenomenon holds true for the solar photovoltaic capacity distribution, which is not shown here. Another consideration is that the unclustered optimisation procedure necessarily contains many more time series and requires more time and memory to solve the optimisation on a standard computer.

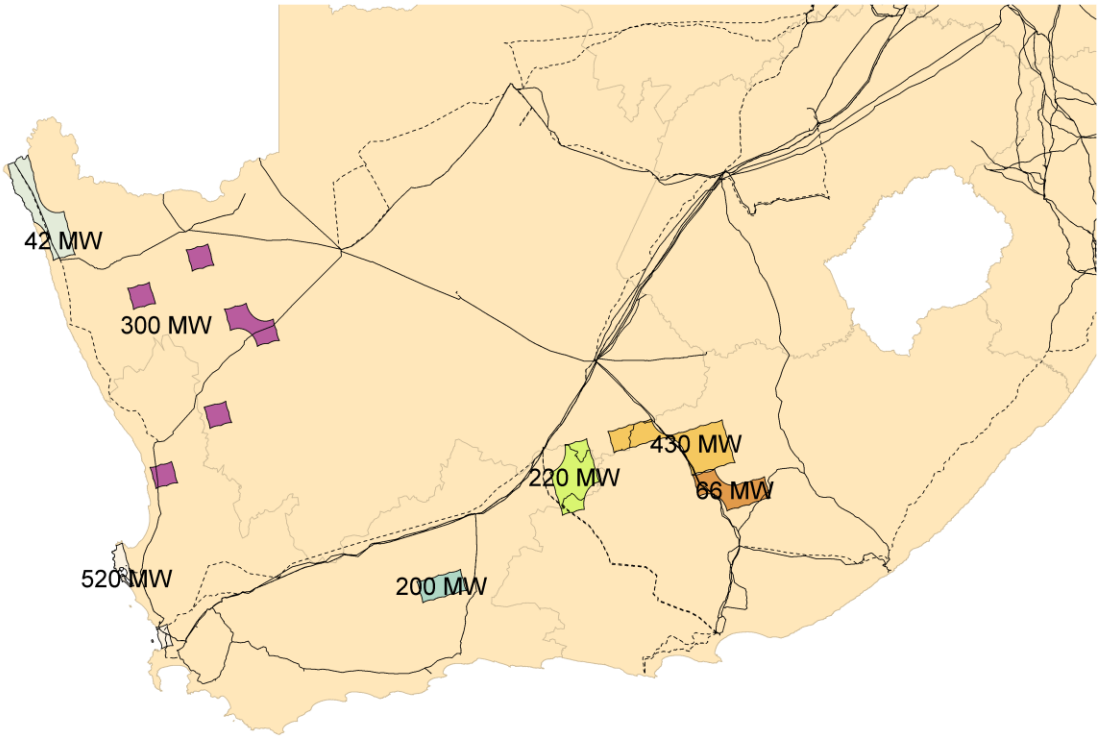

Fig. 9.43 Wind Farm distribution of 1 778 MW of the solution at 40% wind farm capacity factor in the clustered optimisation.

Fig. 9.44 displays a week of load and the residual loads stemming from the clustered solution (at 40% wind farm capacity factor) and the REIPPPP distribution. It serves as an example of the impact of the optimisation procedure. Even at this relatively low penetration of renewable power capacity, it can be seen that the evening peaks are generally much lower with the clustered optimised solution, in the order of 1 000 MW lower than the load, and 500 MW lower than the REIPPPP distribution (on most days).

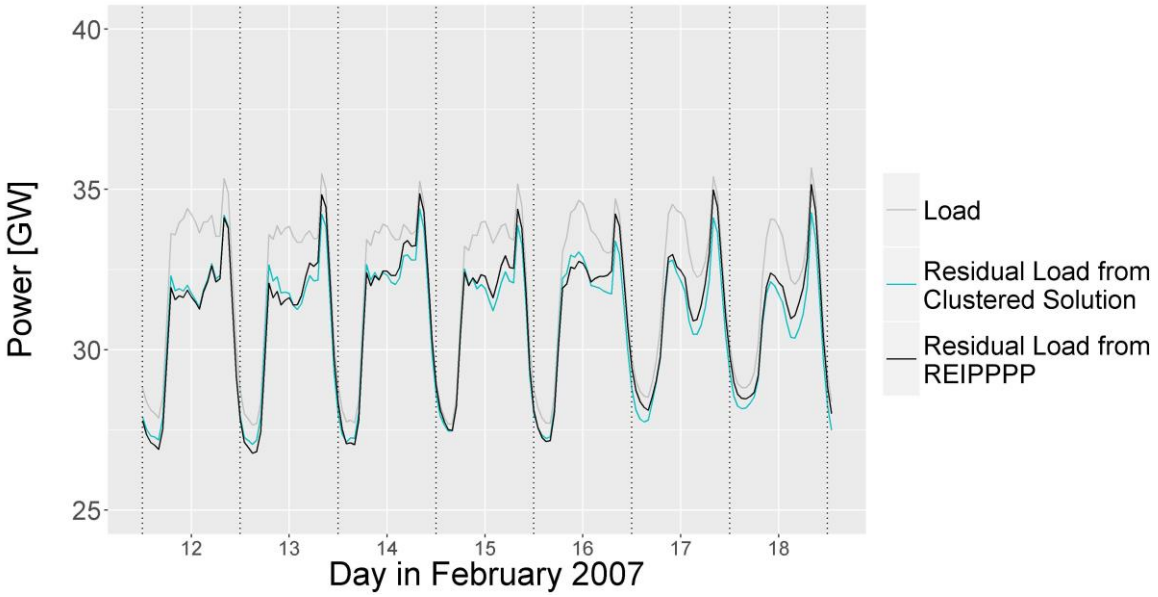

Fig. 9.44 Load and residual load time series from the clustered solution (at 40% wind farm capacity factor) and the REIPPPP distribution for a week in February 2007.

9.7 Case Study 3: Optimal Future Penetrations of Wind and Solar Photovoltaic Power Capacity in South Africa

9.7.1 Overview

This case study uses the mean-variance optimisation procedure to allocate a range of future penetrations of wind power capacity with complementing solar photovoltaic power capacity in South Africa, in order to study the effect that increasing penetrations of renewable energy will have on the conventional generation capacity requirements and to determine an optimal ratio of wind power capacity to solar photovoltaic power capacity.

Similar to case study 1, and unlike case study 2, the constraint that controls the maximum total solar photovoltaic capacity is not set in this case study. This allows the optimisation procedure to allocate as much solar photovoltaic capacity to the specified wind farm capacity in order to minimise the variance of the residual load. This will result in different ratios of solar photovoltaic power capacity to wind power capacity as the wind power capacity increases.

In order to study the effect that increasing penetrations of renewable energy will have on the power system, this case study employs two of the key performance indicators that have not been used before, namely the capacity credit and the generator capacity by type metric.

This case study ignores the existing and planned wind and solar farm capacity in the REIPPPP and assumes the optimisation procedure was used from the beginning to allocate the renewable power capacity. In a real-life study to plan an exact future solution, the existing REIPPPP capacity could be incorporated in the optimisation procedure in the same manner that the load data has been incorporated, i.e. included and constrained with a weight of one. This would result in new capacity complementing the existing capacity in terms of reducing the variance of the existing load. However, the REIPPPP capacity is still sufficiently small, so it is ignored in this case study.

The same load data, which effectively describes the peak load year of 2007 (as discussed in section 7.5), is used for every penetration level of wind power capacity with complementing solar photovoltaic power capacity. This is of course unrealistic, as the load will likely change as future wind and solar photovoltaic power capacity is added to the grid over time. However, it has been kept constant here in order to isolate the effect of increasing renewable power capacities.

9.7.2 Mean-Variance Variable Assumptions

All the variable assumptions that are made in case study 3 are shown in Table 9.11.

Table 9.11 Summary of variable assumptions in case study 3.

Variable	Meaning	Value
$\mu_{\text{Min Desired Solar}}$	The minimum overall mean solar photovoltaic power output (related to capacity factor)	Not set
$w_{\text{Total Wind}}$	The total wind farm capacity that is to be allocated.	1 000 MW to 30 000 MW
$w_{\text{Max Total Solar}}$	The maximum solar photovoltaic farm capacity that can be allocated.	Not set
$\max_x, x \in \text{Wind}$	Maximum wind farm capacity that can be assigned to each 27 x 31 km site.	500 MW
$\max_x, x \in \text{Solar}$	Maximum wind farm capacity that can be assigned to each 40 x 40 km site.	1 000 MW

The $\mu_{\text{Min Desired Solar}}$ variable is not set in this case study. It is only necessary when there are sites with very low solar photovoltaic power outputs that need to be limited. The capacity constraints per site, $\max_x$, represent conservative estimates of how much capacity could be built on a single potential wind farm site or solar photovoltaic farm site.

9.7.3 Optimal Future Penetrations of Wind and Solar Photovoltaic Power

Fig. 9.45 shows the minimised standard deviations of residual load for different penetrations of wind farm capacity with complementing solar photovoltaic power (at different wind farm capacity factors). On the x-axis, the amount of complementing solar photovoltaic power capacity is also indicated, starting at 4.7 GW of solar photovoltaic capacity for 2 GW of wind power capacity and ending at 7.9 GW of solar photovoltaic capacity for 30 GW of wind power capacity. It is clear from Fig. 9.45 that solutions from 35% wind farm capacity factor to 40% wind farm capacity factor display similar results in terms of the standard deviation of residual load across the range of installed wind farm capacities, while opting for a higher wind farm capacity factor solution (41% to 45%) drastically increases the standard deviation of residual load at wind power penetrations above approximately 6 GW. It is also clear that the standard deviation of the current load can be reduced by installing renewable power capacity up to a point depending on the wind farm capacity factor of the solution, e.g. at 40% wind farm capacity factor, approximately 14 GW of wind power capacity with approximately 6.2 GW of solar photovoltaic power capacity can be installed before the standard deviation of the residual load increases above the levels of the current load (this solution is inspected further in case study 4). The standard deviation of the residual load is of course not the only factor to consider when considering power system design, e.g. the residual load with 14 GW of wind power capacity with approximately 6.2 GW of solar photovoltaic power capacity will almost certainly lose the long term predictability of the current load, even though it has a similar standard deviation as the current load.

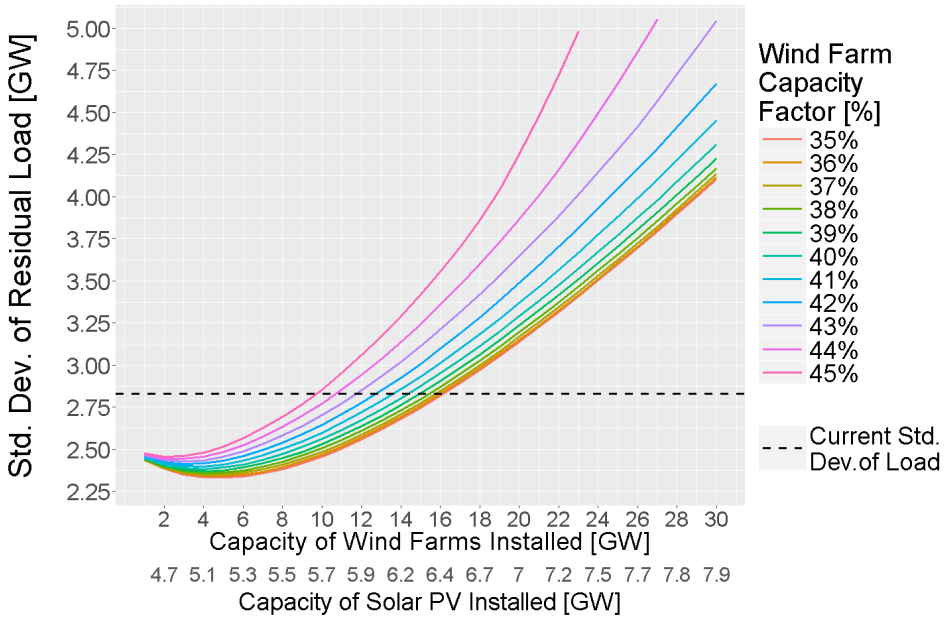

Fig. 9.45 Optimised standard deviations of residual load for different penetrations of wind farm capacity with complementing solar photovoltaic power (at different wind farm capacity factors).

Fig. 9.46 shows the optimal ratios of solar photovoltaic farm capacity to wind farm capacity for different penetrations of wind farm capacity (as a percentage of the total installed renewable power

capacity). This effectively plots the two x-axes on Fig. 9.45 against each other. Initially, solar photovoltaic power is preferred because of its correlation with the daily load profile, but at some point adding more solar photovoltaic power only serves to increase the standard deviation of the residual load. This result points to the need for adequate storage capacity in the future if solar photovoltaic power is to play a bigger role in meeting the load. It is clear from Fig. 9.46 that the solar photovoltaic ratio is fairly independent from the wind farm capacity factor, meaning that the solar photovoltaic ratio depends almost entirely on the nameplate capacity of the installed wind farms.

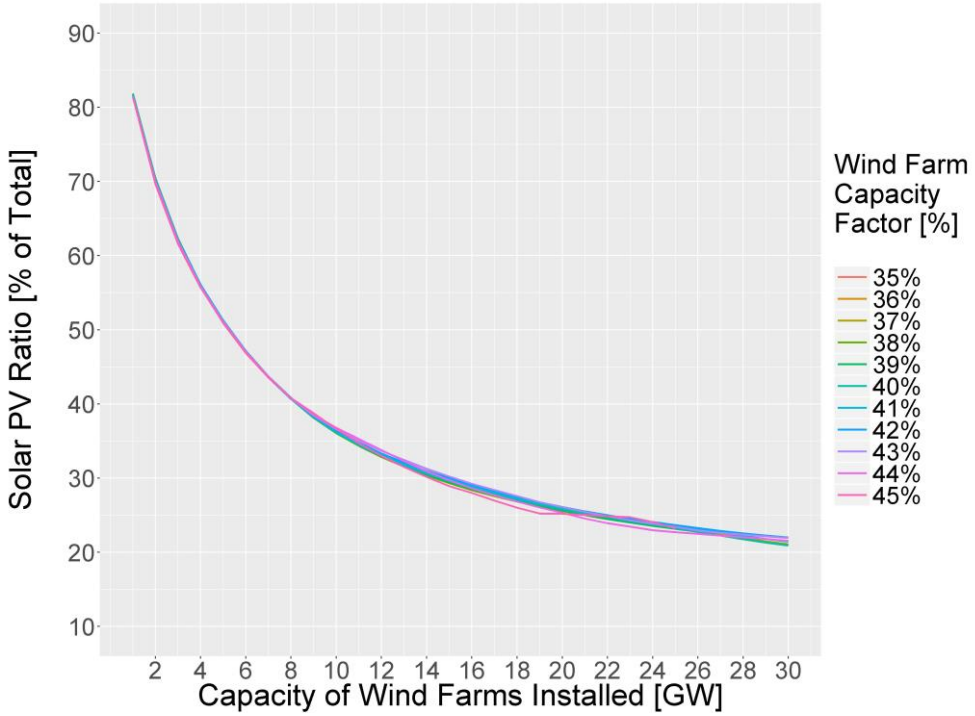

Fig. 9.46 Optimal ratios of solar photovoltaic farm capacity to wind farm capacity for different penetrations of wind farm capacity (at different wind farm capacity factors).

9.7.4 Results of Key Performance Indicators

The capacity credit and the generator capacity by type metric are inspected for optimal future penetrations of wind and solar photovoltaic power.

9.7.4.1 Capacity Credit

The Garver approximation of capacity credit (discussed in section 6.4) is shown in Fig. 9.47. It is clear that the capacity credit is quite low at the lower penetrations of renewable power, mainly due to the high share of solar photovoltaic capacity that is allocated by the optimisation procedure. The capacity credit increases up until approximately 14 GW of wind farm capacity is installed (with approximately 6.2 GW of solar photovoltaic capacity), after which it slowly decreases as the renewable power capacity increases. It is also clear that the solutions with an extremely high wind farm capacity factor (43% and above) experiences a steeper decrease in capacity credit. This is mainly because specifying such a high wind farm capacity factor limits the options of the optimisation procedure in terms of which clusters it can include in the solution, resulting in most of the allocated capacity being assigned to relatively few clusters with high wind farm capacity factors in order to meet the capacity factor constraint, thereby drastically increasing the intermittency of the wind power, which makes it less reliable. The capacity credit approximation thus estimates the capacity credit of

the renewable power portfolio to peak at around 25–28% at about 14 GW of wind farm capacity and 6.2 GW solar photovoltaic farm capacity.

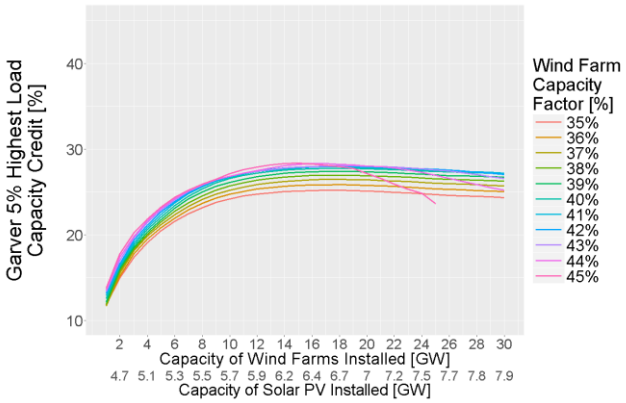

Fig. 9.47 The Garver capacity credit (left) and the Garver 5% highest load capacity credit (right) approximations for optimal future penetrations of wind and solar photovoltaic power capacity

In Fig. 9.47 it can be seen that the solutions at 45% wind farm capacity factor stop at approximately 25 GW. This is simply where the optimisation procedure runs into all the cluster capacity constraints ($\max_x, x \in$ Wind). There exist no solutions at higher penetrations of installed wind farms as the clusters that satisfy the capacity factor constraints have been filled to capacity.

9.7.4.2 Generator Capacity by Type Metric

The results of the generator capacity by type metric is shown in Fig. 9.48 to Fig. 9.51. In Fig. 9.48, the peaker capacity that is required to meet the residual load is shown for the optimal future penetrations of wind and solar photovoltaic solar power capacity. The current peaker capacity requirement is also indicated (which is obtained by applying the generator capacity by type metric to the load data without any renewable power capacity). The peaker capacity is considerably higher than the current peaker requirement even at low wind farm capacities, mainly due to the high initial solar photovoltaic capacity. The solar photovoltaic capacity typically displaces load-following capacity in favour of peaker capacity, because where load-following capacity would have been used throughout the day the solar photovoltaic power now covers the load during morning, midday and afternoon but requires peaker capacity for the early morning and late evening peak load periods. It is interesting to note that the peak capacity requirement does not really increase even as renewable power capacity increases.

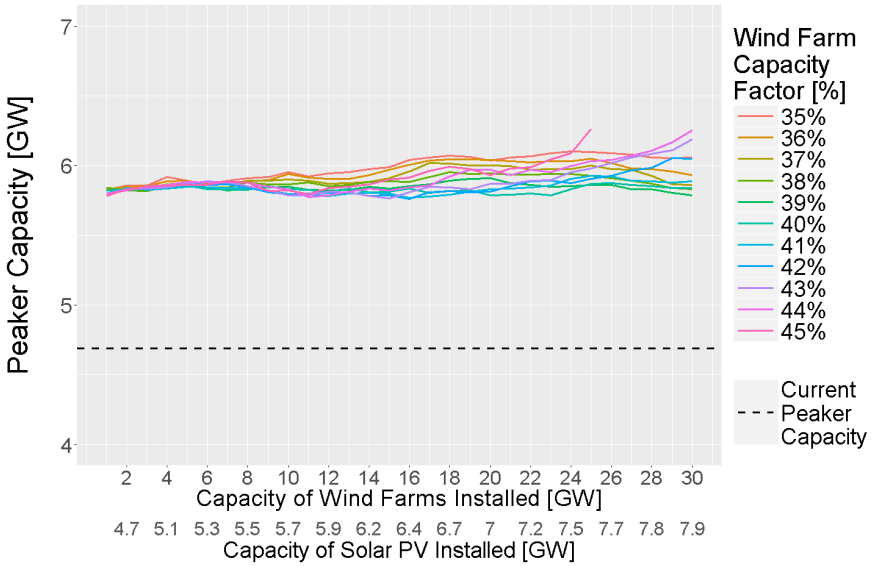

Fig. 9.48 Peaker capacity requirement for optimal future penetrations of wind and solar photovoltaic capacity.

In Fig. 9.49, the load-following capacity that is required to meet the residual load is shown for the optimal future penetrations of wind and solar photovoltaic solar power capacity, with the current load-following capacity requirement also being indicated. It is clear that an increase in renewable power capacity at these optimal ratios of wind and solar photovoltaic power mainly leads to an increased need for load-following capacity to meet the residual load. At 40% wind farm capacity factor, one could install up to approximately 13 GW of wind farm capacity (with approximately 6.05 GW of solar photovoltaic capacity) before additional load following capacity would be required as compared to the required load following capacity to meet the current load.

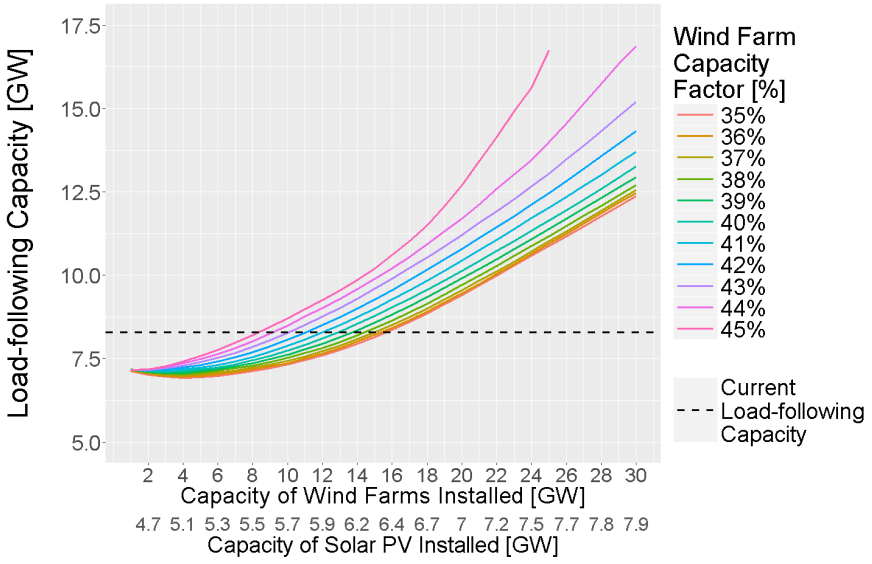

Fig. 9.49 Load-following capacity requirement for optimal future penetrations of wind and solar photovoltaic capacity.

In Fig. 9.50, the base-load capacity that is required to meet the residual load is shown for the optimal future penetrations of wind and solar photovoltaic solar power capacity, with the current base-load capacity requirement also being indicated. It is clear that an increase in renewable power capacity at

these optimal ratios of wind and solar photovoltaic power mainly leads to a decreased need for base-load capacity to meet the residual load.

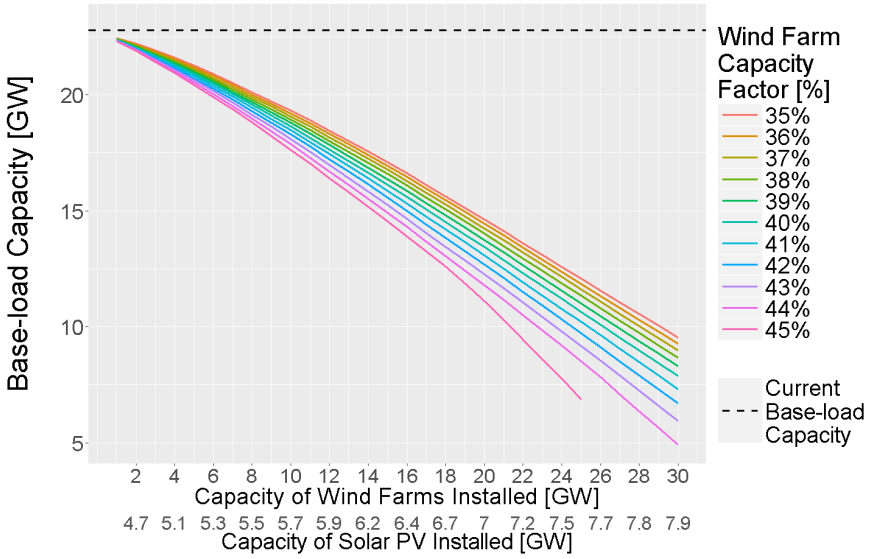

Fig. 9.50 Base-load capacity requirement for optimal future penetrations of wind and solar photovoltaic capacity.

In Fig. 9.51, the total conventional capacity that is required to meet the residual load is shown for the optimal future penetrations of wind and solar photovoltaic solar power capacity, with the current total conventional capacity requirement also being indicated. This provides a general overview of the rate at which the need for conventional generation capacity decreases at the renewable power capacity increases.

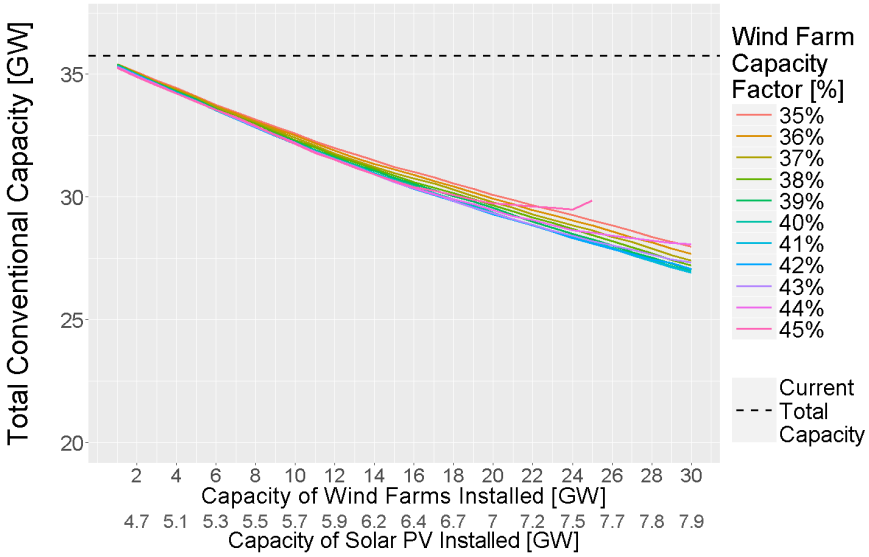

Fig. 9.51 Total capacity requirement for optimal future penetrations of wind and solar photovoltaic capacity.

It is important to remember that the capacity generator by type metric is a high level statistical analysis that attempts to show the general effect that increased renewable power capacity will have on the

capacities and types of conventional generation that is needed to meet the load. The three most important aspects that the capacity generator by type metric ignores are the following:

- Often load-following plants will be ramped up to meet peak load instead of peaker plants, thereby acting as load-following and peaker plants at different times
- The reserve requirements are not included
- The metric does not give any indication of capacity factor, only the nameplate capacity.

Therefore, even though the peaker capacity does not increase significantly in Fig. 9.48, the capacity factor of the peaker plants might well increase (it is impossible to know using this metric). In order to plan for an exact future scenario, a full AC-load flow simulation with marginal pricing information is needed.

9.8 Case Study 4: Optimal Distribution of 14 GW of Wind Power Capacity with Complementing Solar Photovoltaic Power Capacity Compared to Random Distributions

9.8.1 Overview

This case study compares one of the results from case study 3, namely the optimised distribution of 14 GW of wind power capacity (at 40% wind farm capacity factor) with 6.17 GW of complementing solar photovoltaic power capacity, with random distributions of renewable power capacity. This case study is intended to quantify the benefit that the optimisation procedure will have when doing long-term planning of a realistic size of wind farm and solar photovoltaic farm penetration in South Africa.

The solution at 14 GW of wind power capacity (at 40% wind farm capacity factor) with 6.17 GW of complementing solar photovoltaic power capacity has been chosen as it represents the solution where the standard deviation of the residual load is roughly equal to the standard deviation of the load. It is also hypothesised that this level of renewable power capacity represents a reasonable target for South Africa in the medium term (10 to 15 years).

In the absence of an optimisation procedure, it is generally understood that distributing wind and solar photovoltaic power capacity over large areas reduces the variability of the cumulative power output. The random distributions of wind and solar power capacity are meant to represent scenarios where the wind and solar photovoltaic power capacity are spread over large areas in South Africa randomly with regard to the wind and solar resource, only insuring a relatively "spread out" distribution. This is not completely unlike the REIPPPP scenario, where only grid constraints, price and socio-economic development goals play a role in the awarding of power purchase agreements. A total of 3 000 random distributions were generated, with the method for generating the random distributions of wind and solar photovoltaic power capacity being described below in section 9.8.4.

The optimised solution at 14 GW of wind power capacity (at 40% wind farm capacity factor) with 6.17 GW of complementing solar photovoltaic power capacity therefore represents 20.17 GW of renewable power capacity with a solar photovoltaic ratio of 30.6%. The random distributions consider the same total renewable capacity with the solar photovoltaic ratio varying between 20% and 40% in order to highlight any effects that the solar photovoltaic ratio has in terms of the key performance indicators.

9.8.2 Mean-Variance Variable Assumptions

All the variable assumptions that are made in case study 4 are shown in Table 9.12.

Table 9.12 Summary of variable assumptions in case study 4.

Variable	Meaning	Value
$\mu_{\text{Min Desired Solar}}$	The minimum overall mean solar photovoltaic power output (related to capacity factor)	Not set
$w_{\text{Total Wind}}$	The total wind farm capacity that is to be allocated.	14 000 MW
$w_{\text{Max Total Solar}}$	The maximum solar photovoltaic farm capacity that can be allocated.	Not set
$\max_x, x \in \text{Wind}$	Maximum wind farm capacity that can be assigned to each 27 x 31 km site.	500 MW
$\max_x, x \in \text{Solar}$	Maximum wind farm capacity that can be assigned to each 40 x 40 km site.	1 000 MW

The $\mu_{\text{Min Desired Solar}}$ variable is not set in this case study. It is only necessary when there are sites with very low solar photovoltaic power outputs that need to be limited. The capacity constraints per site, $\max_x$, represent conservative estimates of how much capacity could be built on a single potential wind farm site or solar photovoltaic farm site.

9.8.3 Distribution of 14 GW of Wind Power Capacity (at 40% Wind Farm Capacity Factor) and Complementing Solar Photovoltaic Power Capacity

Fig. 9.52 shows the spatial distribution of the 14 GW of wind farm capacity with 40% wind farm capacity factor as determined by the mean-variance optimisation.

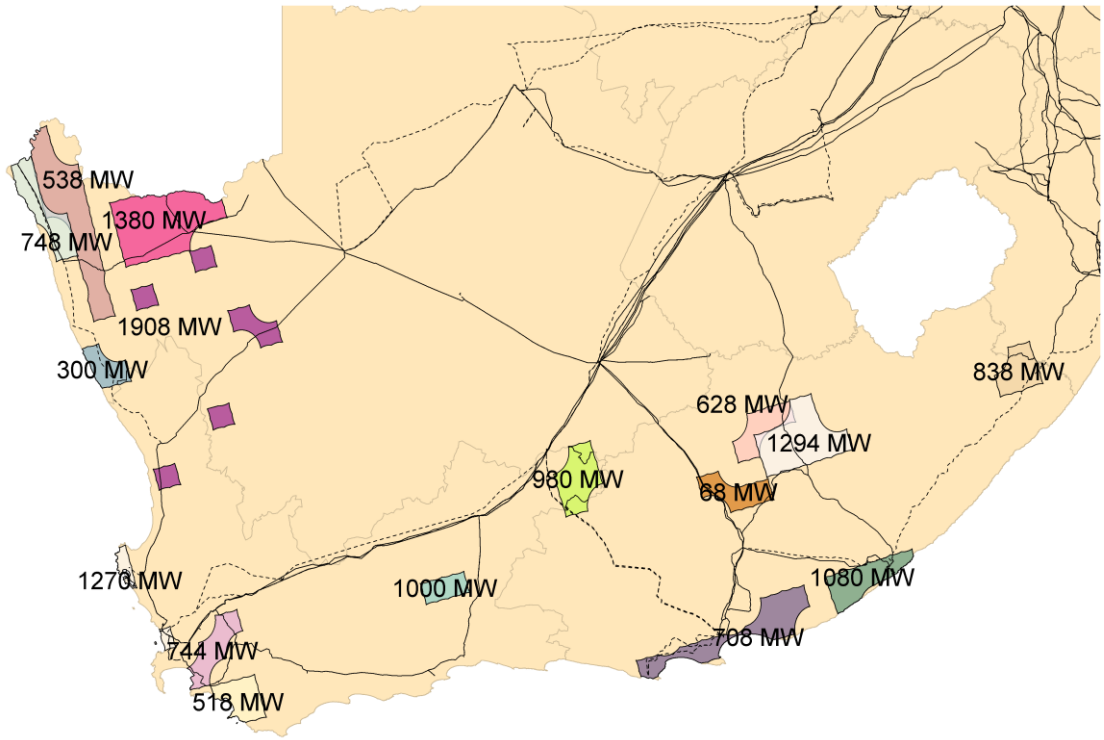

Fig. 9.52 Spatial distributions of the 14 000 MW of wind farm capacity at 40% wind farm capacity factor.

Fig. 9.53 shows the spatial distribution of the 6.17 GW of solar photovoltaic farm capacity, as determined by the mean-variance optimisation, that compliments the wind farm capacity in Fig. 9.52.

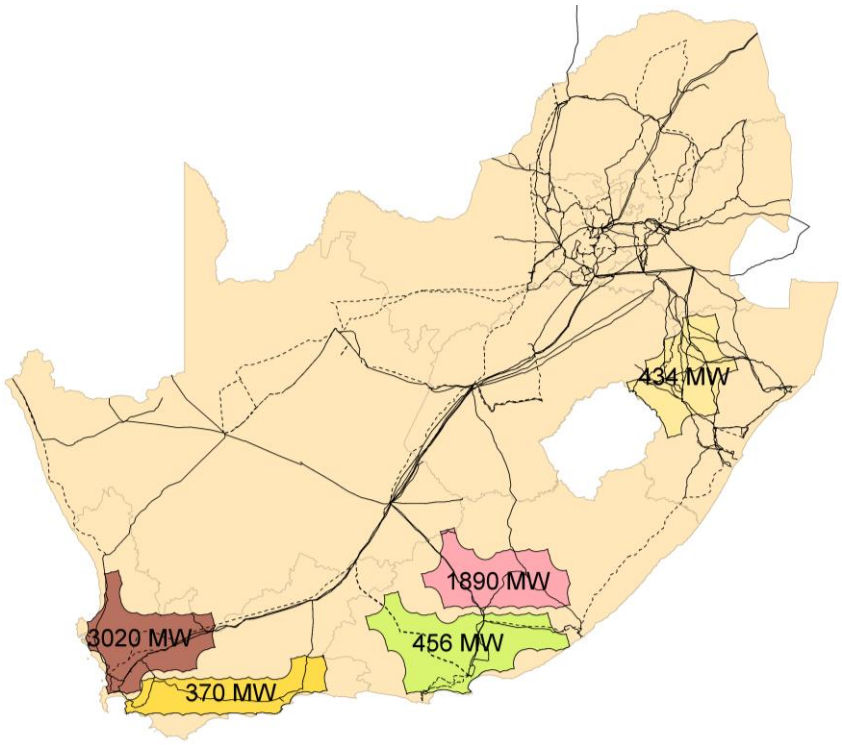

Fig. 9.53 Spatial distributions of the 6 170 MW of solar photovoltaic farm capacity complementing the 14 000 MW of wind farm capacity at 40% wind farm capacity factor.

9.8.4 Random Distributions of Wind and Solar Photovoltaic Power Capacity

This section introduces the method for generating the random distributions of wind farms and solar-photovoltaic farms. All the simulated wind power time series and solar photovoltaic power time series are considered in the random distributions (402 potential wind farm sites and 590 potential solar photovoltaic farm sites).

9.8.4.1 Method for Random Distribution of Renewable Power Capacity

To generate a single random distribution of 20.17 GW of renewable power capacity, several variables are randomly selected from a uniform distribution with an upper and lower limit. The variables that are randomly selected are shown in Table 9.13 and explained further below.

Table 9.13 Summary of variables that are randomly selected in the random distributions of renewable power capacity.

Variable Name	Variable Details	Lower Limit	Upper Limit
$SolarPhotovoltaicRatio$	The solar photovoltaic ratio (as a percentage of total installed renewable power capacity)	20%	40%
$MinWindCapacityFator$	The minimum wind farm capacity factor that qualifies a site to be included in the pool of potential wind farm sites	30%	38%
$MinSolarCapacityFator$	The minimum solar photovoltaic farm capacity factor that qualifies a site to be included in the pool of potential solar photovoltaic farm sites	21%	22%
$AverageLocalWindCapacity$	The average wind farm capacity that is installed per 27 km by 31 km site	150 MW	300 MW
$AverageLocalSolarCapacity$	The average solar photovoltaic farm capacity that is installed per 40 km by 40 km site	100 MW	200 MW

As stated before, the $SolarPhotovoltaicRatio$ is randomly selected between 20% and 40%. Thereafter the wind farm capacity and solar photovoltaic farm capacity are randomly distributed totally independent from each other.

In order to distribute the wind farm capacity randomly, the following seven steps are followed (the steps are repeated for the random solar photovoltaic distribution with its respective variables):

Step 1 The total wind farm capacity to be randomly distributed is calculated as:

$$TotalWindFarmCapacity = 20.17\text{GW} \times (1 - SolarPhotovoltaicRatio) \quad (9.1)$$

Step 2 The $MinWindCapacityFator$ variable is randomly selected between 30% and 38%. Each of the 402 sites with a wind farm capacity factor higher than the $MinWindCapacityFator$ are included in the pool of potential wind farm sites. This variable determines whether the wind farm capacity is consolidated in high yield areas or whether a mix of medium and high wind farm capacity factor sites are included. The $MinWindCapacityFator$ results in a $NumPotentialWindFarmSites$ variable, which simply captures how many of the 402 potential wind farm sites are eligible to be assigned any wind farm capacity.

Step 3 The $AverageLocalWindCapacity$ variable is randomly selected between 150 MW and 300 MW. This variable determines whether the total wind farm capacity is more evenly distributed between the potential wind farm sites or more consolidated between fewer of the potential wind farm sites.

Step 4 Each of the potential wind farm sites is given a chance to be included in the random distribution, with the probability given by:

$$\text{Probability} = \frac{1}{\left(\frac{NumPotentialWindSites}{\left(\frac{TotalWindCapacity}{AverageLocalWindCapacity}\right)}\right)} \tag{9.2}$$

A simple sampling function is used to determine which sites are included in the random distribution with the probability given above.

Step 5 The number of the sites that are included in the random distribution in step 4 results in a $NumRandomWindFarmSites$ variable. A random vector, $\mathbf{X}_{Rand}$, of length $NumRandomWindFarmSites$, with uniformly distributed values between 0 and 1 is generated.

Step 6 Each value in vector $\mathbf{X}_{Rand}$ is divided by the sum of values in $\mathbf{X}_{Rand}$, so that all the values in $\mathbf{X}_{Rand}$ sums to 1.

Step 7 The $\mathbf{X}_{Rand}$ vector is multiplied by $TotalWindFarmCapacity$, so that now $\mathbf{X}_{Rand}$ represents the wind farm capacities of each included wind farm site.

9.8.4.2 Example of Random Distribution of Renewable Power Capacity

An example of the random distribution of wind farm capacity will now be given.

Step 1 The $SolarPhotovoltaicRatio$ is randomly selected as 27.4%. This results in 14.64 GW of wind farm capacity to be randomly distributed.

Step 2 The $MinWindCapacityFator$ is randomly selected as 32.1%. This results in 310 ($NumPotentialWindFarmSites$) out of 402 of the wind farm sites being included in the pool of potential wind farm sites.

Step 3 The $AverageLocalWindCapacity$ is randomly selected as 235.9 MW.

Step 4 Each of the potential wind farm sites are given a probability of

$$\text{Probability} = \frac{1}{\left(\frac{310}{\left(\frac{14.64\ \text{GW}}{0.2359\ \text{GW}}\right)}\right)} \approx 20\% \tag{9.3}$$

The result of the sampling function is that 60 out of the 310 sites are included in the random distribution.

Step 5 The $\mathbf{X}_{Rand}$ vector of length 60 ($NumRandomWindFarmSites$), with uniformly distributed values between 0 and 1 is generated.

Step 6 Each value in vector $\mathbf{X}_{Rand}$ is divided by the sum of values in $\mathbf{X}_{Rand}$, so that all the values in $\mathbf{X}_{Rand}$ sums to 1.

Step 7 The $\mathbf{X}_{Rand}$ vector is multiplied by 14.64 GW ($TotalWindFarmCapacity$), so that now $\mathbf{X}_{Rand}$ represents the wind farm capacities of each included wind farm site. The spatial distribution of $\mathbf{X}_{Rand}$ is shown in Fig. 9.54.

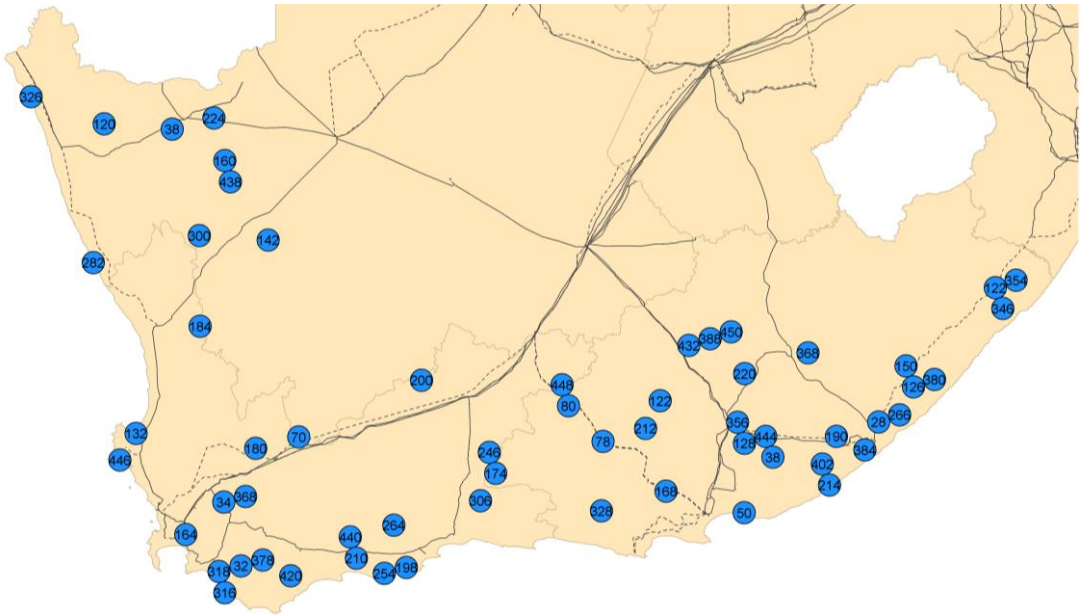

Fig. 9.54 Spatial distribution of the example of a random distribution of wind farm capacity. The values indicate the random wind farm capacities in MW.

The same procedure is followed to generate a random distribution of solar photovoltaic farm capacity to accompany the random distribution of wind farm capacity (with the same $SolarPhotovoltaicRatio$ variable) but is not shown here.

9.8.5 Random Distributions compared to the Efficient Frontier

A total of 3 000 random distributions of wind farms capacity and solar photovoltaic capacity were generated. They are plotted against the efficient frontier in Fig. 9.55. The solar photovoltaic ratio of the random distributions is highlighted so as to highlight its effect on the random distribution performance. The general trend is that among the random distributions, a higher share of wind farm capacity results in a higher standard deviation of the residual load. This is partly because the wind farm capacity has a higher capacity factor than the solar photovoltaic capacity. It is also clear that randomly distributing 20.17 GW of renewable power capacity will certainly increase the standard deviation of the residual load as compared to the standard deviation of the current load (without renewables). The optimised solution at 40% wind farm capacity factor results in a standard deviation of residual load slightly lower than the current load. This optimised solution is further compared to the random distributions below.

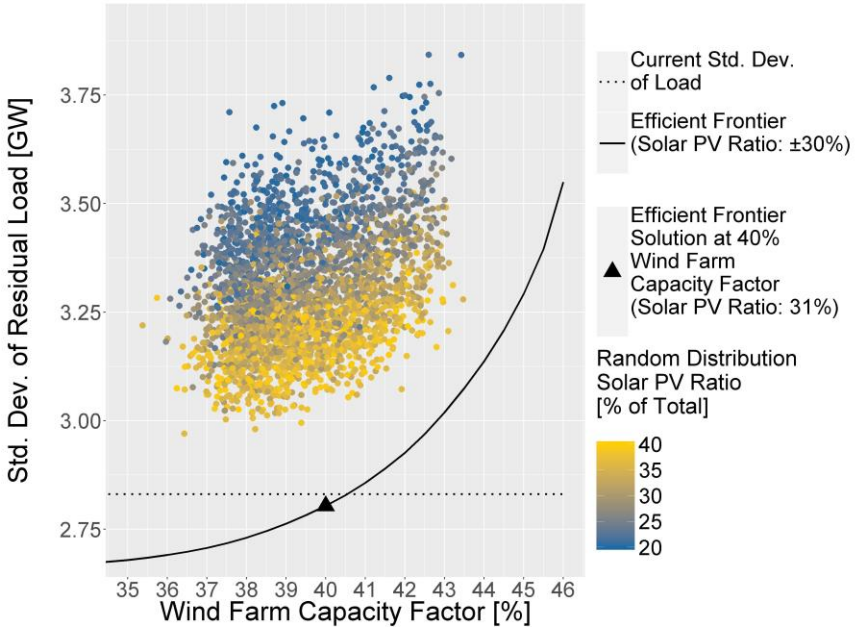

Fig. 9.55 Random distributions of renewable power capacity compared to efficient frontier.

9.8.6 Comparison of Optimised Solution at 40% Wind Farm Capacity Factor with Random Distributions using Key Performance Indicators

Selected key performance indicator metrics were applied to each of the 3000 random distributions, in order to compare their results with the optimised solution at 40% wind farm capacity factor.

9.8.6.1 Mean Absolute Ramp Rate

Fig. 9.56 shows the results for the mean absolute ramp rate of the residual load of the random distributions compared to the optimised solution at 40% wind farm capacity factor. The efficient frontier solution displays the lowest mean absolute ramp rate. When considering the random distributions, it is clear that there is no trend in terms of the solar photovoltaic ratio, and no significant trend in terms of the wind farm capacity factor of the random distributions.

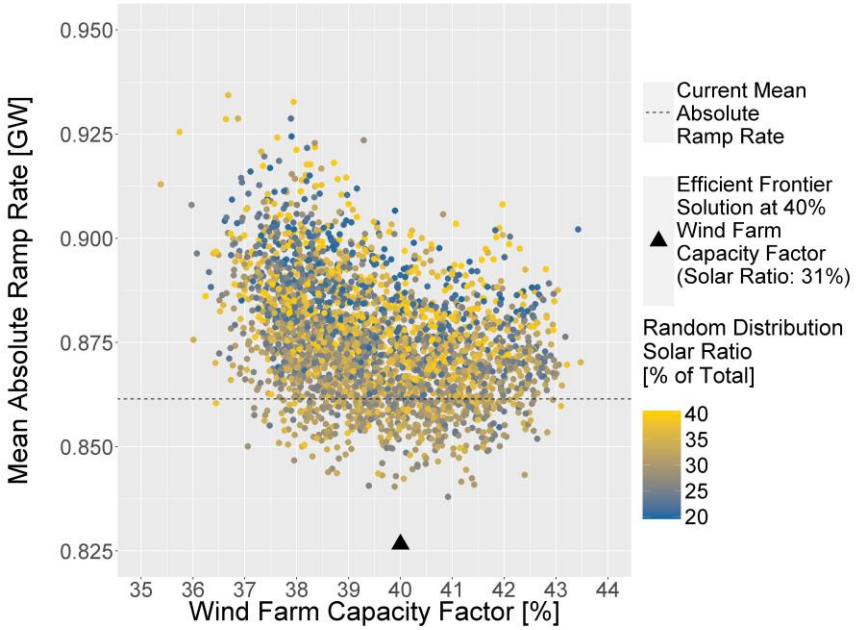

Fig. 9.56 Mean absolute ramp rate of the residual load of the random distributions compared to the optimised solution at 40% wind farm capacity factor.

Fig. 9.57 shows the Garver 5% highest loads capacity credit approximation of the random distributions compared to the optimised solution at 40% wind farm capacity factor. Many of the random distributions display a higher capacity credit than the optimised solution, but this is mainly due to their higher share of wind power capacity. When only the random distributions with a similar solar photovoltaic ratio as the optimised solution is plotted, as shown on the right of Fig. 9.57, it can be seen that the optimised solution performs similarly to the best performing random distributions for the given wind farm capacity factor of 40%.

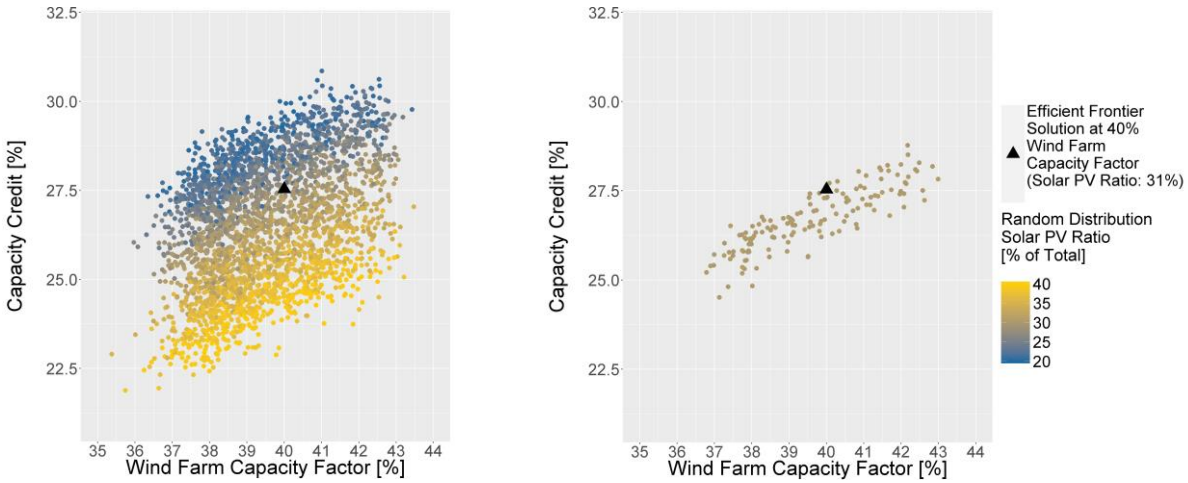

Fig. 9.57 The Garver 5% highest loads capacity credit approximation of the random distributions compared to the optimised solution at 40% wind farm capacity factor. The graph on the right only shows the random distributions with a solar photovoltaic ratio of 30-31%, similar to the optimised solution.

9.8.6.2 Generator Capacity by Type Metric

In Fig. 9.58, the peaker capacity requirement that is required to meet the residual load is shown for the random distributions and the optimised solution at 40% wind farm capacity factor. When considering the random distributions, it is clear that a higher solar photovoltaic ratio results in a higher requirement for peaker capacity. The efficient frontier solution displays a peaker capacity requirement that is slightly above the expected peaker requirement when you compare its solar photovoltaic ratio (approximately 31%) to the random distributions.

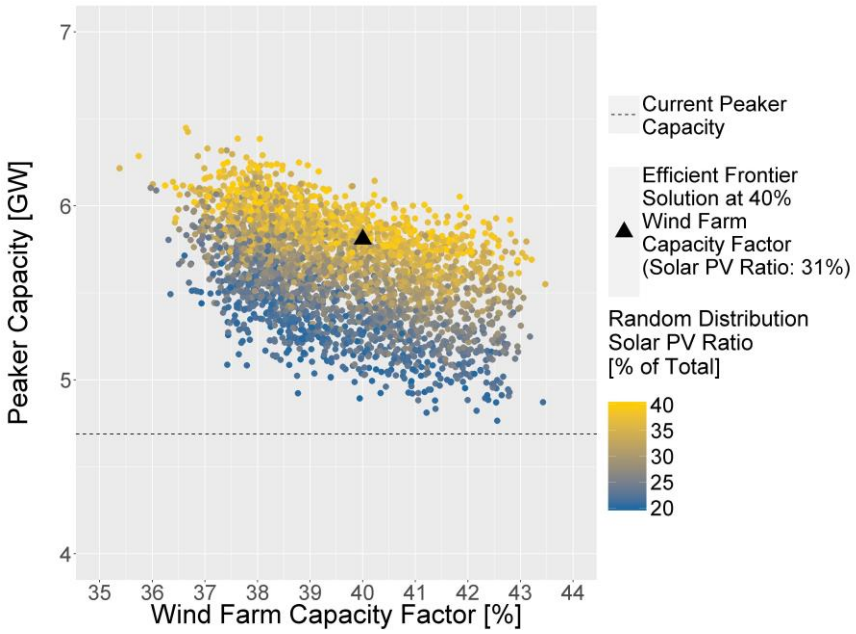

Fig. 9.58 Peaker capacity requirement for the residual load of the random distributions compared to the optimised solution at 40% wind farm capacity factor.

In Fig. 9.59, the load-following capacity requirement that is required to meet the residual load is shown for the random distributions and the optimised solution at 40% wind farm capacity factor. When considering the random distributions, it is clear that a lower solar photovoltaic ratio results in a higher requirement for load-following capacity. The efficient frontier solution displays a load-following capacity requirement that is significantly lower than the random distributions, and only slightly higher than the current load-following capacity requirement.

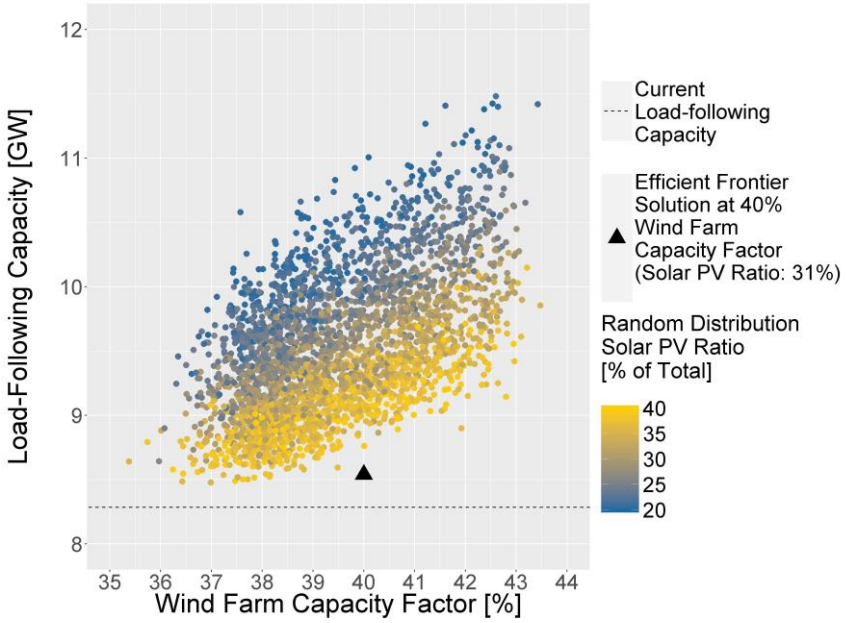

Fig. 9.59 Load-following capacity requirement for the residual load of the random distributions compared to the optimised solution at 40% wind farm capacity factor.

In Fig. 9.60, the base-load capacity requirement that is required to meet the residual load is shown for the random distributions and the optimised solution at 40% wind farm capacity factor. The base-load requirements are considerable less than the base-load requirement for the current load, which is to be expected as the load remained the same while intermittent power sources were added to the system. When considering the random distributions, it is clear that a lower solar photovoltaic ratio results in a lower requirement for base-load capacity. This is partly caused by the higher capacity factors of the wind farm capacity as compared to solar photovoltaic capacity. The efficient frontier solution displays a base-load capacity requirement that is slightly higher than the expected base-load requirement when you compare its solar photovoltaic ratio (approximately 31%) to the random distributions.

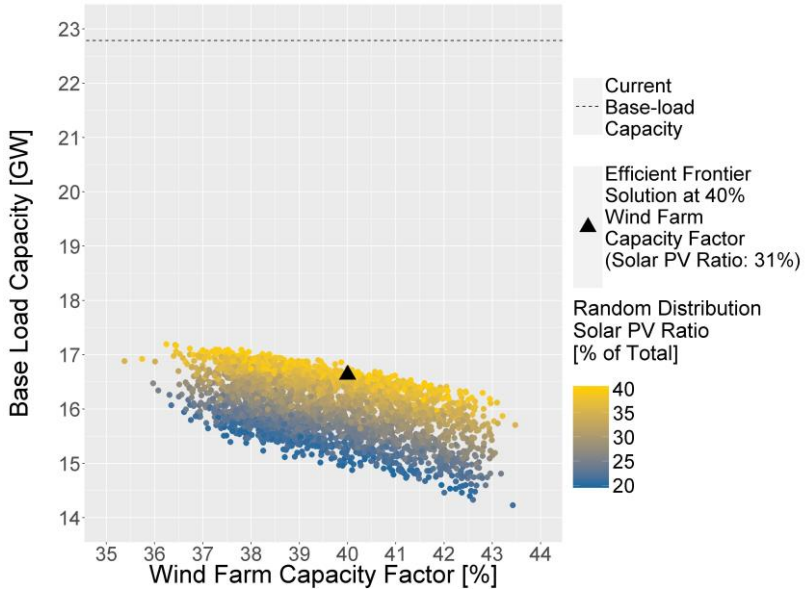

Fig. 9.60 Base-load capacity requirement for the residual load of the random distributions compared to the optimised solution at 40% wind farm capacity factor.

9.9 Results Obtained from Additional Investigations

Several investigations were performed which delivered additional results, but which were not included in this thesis. A brief overview is given here.

Some of the additional findings include:

- An additional distance measure (besides the Euclidian distance measure) was investigated. The distance measure was proposed by Chouakria and Nagabhushan [103] and is based on an automatic adaptive tuning function. The distance measure is intended to take into account both similarity in absolute values and behaviour over time. The similarity measure did not however result in better solutions when combined with the mean-variance optimisation procedure. The efficient frontier solutions using this distance measure was slightly inferior to the case where the Euclidian distance measure was used.
- Two additional clustering methods were examined, namely the density based clustering method and the fuzzy C-means clustering method, but did not deliver any useful results.
- Additional cluster validation measures were inspected to validate the results of the clustering procedure, including the Dunn index [84] and the entropy of the distribution of cluster memberships [104]. The additional cluster validation measures confirmed that using Ward's method of hierarchical clustering is preferred when clustering the simulated wind power and solar photovoltaic time series.
- In terms of the optimal solutions that result from the mean-variance optimisation, an investigation found that the minimised standard deviation of the residual load is not extremely sensitive to the location of the solar photovoltaic power capacity. Only the total size of the solar photovoltaic power capacity really played a role. The only noticeable impacts arose when relocating the large amounts of solar photovoltaic power capacity longitudinally. The optimisation procedure often allocated solar photovoltaic capacity in the western part of the country in order to allow the solar photovoltaic power to try to meet a part of the peak evening load.
- An investigation confirmed that using historical wind and solar data could be used to optimise future distributions of wind power and solar photovoltaic power capacity. In this investigation the simulated power time series data were randomly subset into training and testing subsets, as is common practice in machine learning applications, with the training subset being used as an input to the optimisation procedure in order to obtain efficient frontier solutions, and the efficient frontier solutions being applied to the testing subsets in order to ascertain whether they performed similarly to the training set. The results from the training and testing sets were extremely similar.
- In the clustered mean-variance optimisation the wind and solar photovoltaic power capacity is assigned to clusters instead of individual sites. The centroid time series are used as an input to the optimisation procedure, as well as to calculate the key performance indicators. This effectively means that the capacity assigned to each cluster is spread evenly among the sites in each cluster. An investigation confirmed that distributing the assigned capacity randomly among the sites in each cluster delivered near identical results when compared to the results as measured using the time series centroids of each cluster.

10 Conclusions and Recommendations

10.1 Overview

This section gives the conclusions of the work, as well as recommendations and suggestions for future work. The conclusions will be presented with references to the original project objectives. These are as follows:

- Formulation of a simple model topology for simulation of power output profiles of wind energy and solar photovoltaic energy sources with the view to do long term prediction/forecasting and optimisation.
- Development of an optimisation procedure that incorporates the predicted wind power and solar photovoltaic power generation profiles as well as grid connection capacity constraints in order to produce practicable solutions in terms of the optimal size and geographic distribution of renewable power generation sources from the perspective of the national load profile.
- Analysis of the results of the optimisation procedure in terms of clearly defined key performance indicators, with the view to study the benefits of the optimisation procedure and the impact of stochastic renewable energy sources on utility load-balancing.

10.2 Conclusions

10.2.1 Renewable Energy Simulation

In order to formulate models to simulate wind power and solar photovoltaic power time series, a comprehensive literature review was performed. The insights from the literature are as follows:

- *Wind Power Simulation*: A majority of the large scale wind power studies found in the literature used wind turbine power curves from manufacturers to simulate wind power time series by defining discrete points on the wind turbine power curve and employing a linear interpolation function to convert wind speed to wind power. Some studies employed generic piecewise-defined functions that imitate typical wind turbine power curves. A multi-turbine power curve approach was developed by Norgaard and Holtinen [22] to better approximate the wind power from many wind turbines located in a large area for which only a single wind speed time series dataset is available. Other studies which employed a version of the multi-turbine power curve showed that it displayed good correlation with actual wind power time series [24].
- *Solar Photovoltaic Power Simulation*: Freely available software packages are frequently used to simulate solar photovoltaic power, using temperature data from national weather services and solar irradiance either from ground measurement stations or meteorological satellite data.

After the literature study was concluded, the renewable energy simulation models were formulised. The multi-turbine power curve approach by Norgaard and Holtinen [22] was used to simulate the wind time series, with a small adjustment to account for the overestimation of wind power. A simple solar photovoltaic simulation model was adapted from the PVWatts program [28] that was developed by NREL.

The data that was necessary to simulate the wind power and solar photovoltaic power time series were collected for a South African case study. This included wind speed data from the WASA project [9] in the case of wind power simulations and inclined solar irradiance data from the proprietary SoDa service [43] and temperature data from the South African Weather Service in the case of solar photovoltaic power simulations.

The results of the wind power simulations and solar photovoltaic simulations were satisfactory. In the case of wind power simulations, it was hypothesised that the capacity factor was slightly overestimated, but it is extremely difficult to validate the simulations as actual wind power data in South Africa are proprietary and not available to the public. In the case of solar photovoltaic power simulations, it was hypothesised that the solar photovoltaic power simulations provided a good estimate for actual solar photovoltaic power outputs. The results of the simulation procedures confirmed the excellent potential for renewable power capacity in South Africa.

10.2.2 Development of an Optimisation Procedure

In order to develop an optimisation procedure to optimise the location of wind power and solar photovoltaic power capacity with respect to the national load profile, a comprehensive literature study was performed. The insights from the literature are as follows:

- *Mean-variance optimisation of wind farms*: The majority of studies found in the literature employed a form of mean-variance optimisation to optimise the geographic location of wind farms. The mean-variance optimisation is adapted from finance theory, where it is used to build optimal share portfolios [65]. There are several studies which employ different methods to optimally locate wind farm capacity, but these methods do not provide obvious benefits over the mean-variance optimisation. Some studies have suggested two possible additions to the mean-variance optimisation procedure:

    - Inclusion of solar photovoltaic power: Several studies conclude their wind farm location optimisation procedures by suggesting that solar power be incorporated into the mean-variance optimisation, but only two papers follow through on this, one including solar photovoltaic power simulations [69] and the other concentrated solar power simulations [74], with neither of these studies changing any of the mean-variance constraints to better suit the inclusion of solar power.
    - Inclusion of load profiles: One study suggested the inclusion of the load profile in the mean-variance procedure [17], but concluded that unless the wind power show significant correlation with the load profile, this inclusion will not lead to significantly different results.

- *Time series clustering of renewable power time series*: There are two problems with the mean-variance method that arises as the problem size is scaled up, namely the computational burden of the optimisation procedure and the practicality of the solutions on the efficient frontier. The studies that applied mean-variance optimisation did not address these issues. They often used small case studies or did not elaborate on the practicality of the solutions. Time series clustering was proposed as a method that could be employed in conjunction with mean-variance optimisation in order to address some of these issues [74], but was only employed by a single study that used time series clustering on wind speeds rather than wind power time series [70].

After concluding the literature study, mean-variance optimisation was inspected for its potential to optimally locate wind power and solar photovoltaic capacity with respect to the load profile. A time series clustering pre-processing step was included in order to reduce the computational burden of the optimisation procedure and to ensure the mean-variance optimisation procedure delivered practicable results.

In order to determine the optimal time series clustering procedure, several clustering methods were applied to the simulated wind power and solar photovoltaic time series, with the resulting clusters inspected by several standard cluster validation measures. It was found that Ward's method of hierarchical clustering marginally outperforms the other clustering methods in both the case of wind

power and solar photovoltaic power time series. The average centroid error was consulted to determine the optimal number of wind power clusters, which resulted in 69 clusters being specified. The L-method was applied to the cluster validation measures of the solar photovoltaic power clusters, which resulted in 17 clusters being specified.

The standard constraints of the mean-variance optimisation were adjusted to include solar photovoltaic power time series and the load profile. A complete formulation and description was provided.

10.2.3 Analysis of the Results of the Optimisation Procedure

The literature was consulted to obtain relevant key performance indicators which could be used to access the impact of the optimisation procedure. The literature review included an overview of power system reliability measures, pertaining to both power system security and power system adequacy. The key performance indicators that were selected included the following:

- *Standard deviation of the renewable power output/residual load*: This is the optimisation target of the mean-variance optimisation procedure. It is a measure of the variability of the renewable power output/residual load (that has to be met by conventional generation plants).
- *Mean absolute ramp rate*: This measure is included to provide a measure of the intra-hour differences in load. It is expected that larger penetrations of renewables will increase the variability of the residual load and thereby also increase the intra-hour differences in load that will cause conventional generators to cycle more and increase the need for peaking power plants.
- *Capacity credit*: The capacity credit is the capacity value expressed as a percentage of renewable power capacity. Capacity value is defined as the amount of additional load that can be served due to the addition of the generator, while maintaining the existing levels of reliability [46]. As the conventional generator capacity data is not available, the Garver capacity value approximation method [54] is used, with only the highest 5% of loads considered, similar to the approach employed by Madaeni *et al.* [56].
- *Generator capacity by type metric*: The goal of the generator capacity by type metric is to use a high-level statistical approach to estimate the size and type of generators that will be needed to supply the load/residual load. This approach was first described in the study by Tarroja *et al*. [60].

In order to investigate the results of the mean-variance optimisation procedure, four case studies were performed. The following aspects were studied:

- *Inclusion of solar photovoltaic power and load in the mean-variance optimisation problem*: Case study 1 investigated the inclusion of solar photovoltaic power and load in the mean-variance optimisation problem by considering the wind power and solar photovoltaic power capacities allocated in the IRP 2010 policy document for the year 2030. The results and conclusions were as follows:

    - The mean-variance optimisation considering wind only delivered solutions that indicated that the residual load variability would increase under these wind power and solar photovoltaic power capacity assumptions.
    - Including only load with the wind power optimisation yielded vastly superior results in terms of residual load variability compared to the case where only wind power was considered, which indicates that wind power capacity could to an extent be distributed to match the load profile. The standard deviation of the residual load would either decrease or increase depending on the desired wind farm capacity factor.

  - Including only solar photovoltaic power with the wind power optimisation resulted in a very low solar photovoltaic power capacity allocation, which did result in a slightly lower residual load variability compared to the case where only wind power was considered. However, the standard deviation of the load would still increase marginally under this scenario.
  - Including both solar photovoltaic power and load in the optimisation problem along with wind power resulted in a significantly lower residual load variability, even though the variability of the wind and solar photovoltaic power was higher than when load was excluded. The total size of the allocated solar photovoltaic power capacity was slightly lower than the IRP 2010 assumption, but still a significant proportion of the total allocated capacity. Even though the capacity of wind power and solar photovoltaic power was quite large, the variability of the load could be reduced from current levels if an excessive wind farm capacity factor was avoided.

- *Mean-variance optimisation comparison with the REIPPPP*: In case study 2 the mean-variance optimisation considering wind power, solar photovoltaic power and load was compared to the first three rounds of the REIPPPP by optimally distributing the same capacity and comparing the results with those obtained from REIPPPP simulations. The results and conclusions were as follows:

  - Even though the addition of the REIPPPP wind power and solar photovoltaic power capacity was found to lower the standard deviation of the residual load, the optimised solutions indicated that the standard deviation of the residual could be lowered by another 4% while achieving the same wind farm capacity factor by distributing the exact same wind power and solar photovoltaic power capacity in optimal locations. The scope for an increased energy yield from the wind power capacity was also highlighted.
  - One of the biggest effects of the optimisation procedure was found to be the lower probabilities of extremely high residual load occurrences as compared to the REIPPPP scenario.

- *Combining time series clustering with mean-variance optimisation*: Case study 2 also investigated the use of time series clustering combined with mean-variance optimisation by comparing it to a mean-variance optimisation without the time series clustering procedure. The results and conclusions were as follows:

  - The optimised solutions from the unclustered optimisation yielded slightly better than the clustered solutions in terms of residual load variability, but this was to be expected. However, it could be said that the clustered solutions were near optimal.
  - The spatial distribution of the unclustered optimisation assigned very specific capacities to very specific sites, with some sites being allocated small capacities which would not justify the fixed cost infrastructure of renewable power plants, which makes these solutions all but unfeasible in a real life scenario. This emphasises the main benefit of the time series clustered solutions which allocates capacities to regions rather than individual sites, which makes the solutions practicable.

- *Mean-variance optimised future penetrations of wind power and solar power capacity*: Case study 3 investigated the optimal future penetrations of wind power capacities and solar photovoltaic capacities by applying the mean-variance optimisation to different levels of wind farm penetration, including a load profile which effectively represented the peak load year of 2007, and allowing the optimisation procedure to determine the optimal solar photovoltaic capacity without any constraints. The results and conclusions were as follows:

  - At lower wind farm penetrations the optimisation procedure assigned a relatively large share of solar photovoltaic power capacity due to the correlation of solar photovoltaic power with the

daily load profile. As the wind farm penetration increases, the share of solar photovoltaic power as a percentage of total renewable power reduces drastically, from approximately 82% at 1 GW of wind farm capacity to approximately 22% at 30 GW of wind farm capacity. It is therefore concluded that, in the absence of sufficient large scale grid-level storage, the optimal share of solar photovoltaic power in terms of minimising residual load variability is highly dependent on the level of wind farm penetration.

- Opting for a desired wind farm capacity factor of larger than 40% resulted in significant increases in residual load variability. At 40% wind farm capacity factor, considering the peak load year power profile, approximately 14 GW of wind farm capacity could be installed, with 6.17 GW of complementing solar photovoltaic power capacity, before the standard deviation of the residual load would surpass the level of the current load.
- The capacity credit approximation results indicated that the optimal wind power and solar photovoltaic power capacity would attain a maximum combined capacity credit of around 28% at approximately 14 GW of wind farm capacity, with 6.17 GW of complementing solar photovoltaic power capacity, before slowly decreasing as the wind farm penetration increases.
- The generation capacity by type metric indicated that the peaker plant capacity requirements would not increase significantly as wind power and solar photovoltaic power capacities increased, only showing an initial increased peaker requirement due to the relatively large addition of solar photovoltaic power. The load-following capacity requirement would initially be lower, but would quickly increase beyond the current requirement levels, whereas the need for base load capacity would decrease.

- *Benefits of mean-variance optimisation*: Case study 4 investigated a future optimal distribution of 14 GW of wind farm capacity, with 6.17 GW of complementing solar photovoltaic power capacity, and compared it with random distributions of wind power and solar photovoltaic power capacity. The performance was compared using the key performance indicators. The results and conclusions were as follows:

  - While the optimised solution at 40% wind farm capacity factor displayed approximately the same residual load standard deviation as the current load, the random distributions displayed a residual load standard deviation that was anything from 12% to 30% higher depending on the ratio of solar photovoltaic power, with a higher ratio of solar photovoltaic power resulting in a lower standard deviation ratio.
  - The optimised solution displayed the lowest mean absolute ramp rate, approximately 5% lower than the current absolute ramp rate of the load. The random distributions were more likely to increase the absolute ramp rate, and showed no trend in terms of the solar photovoltaic power ratio.
  - In terms of the capacity credit of the renewable power capacity, the optimised solution compared well with the random distributions, displaying a near maximum capacity credit as compared to random distributions with the same solar photovoltaic power ratio.
  - The generation capacity by type metric indicated that the peaker plant capacity requirement of the optimised solution was similar to that of the random distributions. The main benefit of the optimised solution came in the form of a much lower load-following capacity requirement and a slightly higher base-load capacity requirement.

10.3 Recommendations

10.3.1 Utility in a Real-world Study

It has been shown that mean-variance optimisation can be combined with time series clustering to optimally distribute future wind power and solar photovoltaic power capacity. Including the time series clustering allows the mean-variance optimisation to produce practicable results and comes at minimal cost in terms of performance. The optimisation results in an optimal ratio of wind power capacity to solar photovoltaic power capacity and an optimally distributed wind power capacity (with the location of the solar photovoltaic power capacity not being of critical importance). The performance of the optimisation results includes the following:

- A minimised residual load standard deviation.
- A minimised absolute ramp rate of the residual load.
- A high combined capacity credit for the wind power and solar photovoltaic power capacity.
- A significantly lower requirement for load-following capacity and slightly increased base-load requirement to meet the residual load.

In terms of making a study of this nature applicable to actual renewable energy policy, a GIS study with greater detail is needed, similar to the study done by the CSIR (Council for Scientific and Industrial Research) in their REDZ study (Renewable Energy Development Zones) [105]. In the REDZ study, exact GIS data was used to deem certain areas unavailable for renewable energy development due to the location of cities, national parks and extremely steep terrain. The capacity constraints in the mean-variance optimisation were not manipulated in this thesis, with a single conservative estimate of how much capacity could be built on a single potential wind farm site or solar photovoltaic farm site used instead. The realistic environmental constraints arising from a GIS study could be combined with the latest GCCA assessment (Grid Connection Capacity Constraint) from Eskom [106], in order to determine the realistic capacity constraints for short and medium term penetrations of renewable energy. When studying large future penetrations, the results of the time series clustering and mean-variance optimisation should be combined with an AC-load flow simulation as has been performed by Eser *et al.* [64] to determine the impacts on the conventional fleet in terms of the financial cost of cycling and increased maintenance requirements, as well as the cost of transmission system upgrades. A study of this nature could definitively quantify the financial benefit of the complete optimisation procedure when compared to random distributions of renewable power capacity.

10.3.2 Future Work

Wind speed and solar radiation data with a finer time resolution (15 minutes) and finer spatial resolution (5 km x5 km) from a study by the CSIR is due to become available soon after the publication of this thesis [107]. The CSIR also intends to make available their wind power and solar power simulations. The study covers a 5-year period from 2009 until 2013. It is recommended that the time series clustering and mean-variance optimisation methodology contained in this thesis be applied to this data in order to determine if similar results are achieved.

Another suggestion for future work would be the inclusion of concentrated solar power (CSP) simulations. CSP currently represents the most mature renewable energy technology after wind power and solar photovoltaic power, and has been suggested as a technology that can especially aid in the peak evening demand periods [4]. This would however require the inclusion of a LOCE metric to control for the vastly different price of wind power and solar photovoltaic power compared to CSP.

References

[1] A. Leach, "Race to renewable: five developing countries ditching fossil fuels," *The Guardian*, 2015. [Online]. Available: https://www.theguardian.com/global-development-professionals-network/2015/sep/15/five-developing-countries-ditching-fossil-fuels-china-india-costa-rica-afghanistan-albania. [Accessed: 20-Apr-2016].

[2] S. Mantshantsha, "The reality behind Eskom's load-shedding 'good news,'" *Rand Daily Mail*, 13-May-2016.

[3] "Cost and Performance Characteristics of New Generating Technologies, Annual Energy Outlook 2016," 2016.

[4] A. Eberhard, J. Kolker, and J. Leigland, "South Africa's Renewable Energy IPP Procurement Program: Success Factors and Lessons," 2014.

[5] S. Forder, "Project Database," *Energy Blog*, 2016. [Online]. Available: http://energy.org.za/knowledge-tools/project-database/. [Accessed: 28-Oct-2016].

[6] "Integrated Resource Plan Introduction," *Department of Energy*, 2014. [Online]. Available: http://www.energy.gov.za/files/irp_frame.html.

[7] T. Creamer, "IRP update cuts demand outlook, suggests nuclear decision be delayed," *Engineering News*, 2013. [Online]. Available: http://www.engineeringnews.co.za/article/irp-update-cuts-demand-outlook-suggests-nuclear-decision-be-delayed-2013-12-03. [Accessed: 25-Oct-2015].

[8] F. Ueckerdt, R. Brecha, and G. Luderer, "Analyzing major challenges of wind and solar variability in power systems," *Renew. Energy*, vol. 81, pp. 1–10, 2015.

[9] E. Mabille, "South African Wind Atlas (WASA) Guide," 2014.

[10] Department of Energy, "State of Renewable Energy in South Africa," 2015.

[11] A. Tascikaraoglu and M. Uzunoglu, "A review of combined approaches for prediction of short-term wind speed and power," *Renew. Sustain. Energy Rev.*, vol. 34, pp. 243–254, 2014.

[12] F. Barbieri, S. Rajakaruna, and A. Ghosh, "Very short-term photovoltaic power forecasting with cloud modeling: A review," *Renew. Sustain. Energy Rev.*, no. August 2015, pp. 1–23, 2016.

[13] South African Wind Energy Association, "Reaping reward - South Africa's REIPPP," *Energy Blog*, 2016. [Online]. Available: http://energy.org.za/news/246-reaping-rewards-sa-reippp. [Accessed: 15-Sep-2016].

[14] G. M. Masters, *Renewable and Efficient Electric Power Systems*, 2nd ed. Wiley, 2013.

[15] C. Carrillo, A. F. Obando Montaño, J. Cidrás, and E. Díaz-Dorado, "Review of power curve modelling for wind turbines," *Renew. Sustain. Energy Rev.*, vol. 21, pp. 572–581, 2013.

[16] M. Lydia, S. S. Kumar, A. I. Selvakumar, and G. E. Prem Kumar, "A comprehensive review on wind turbine power curve modeling techniques," *Renew. Sustain. Energy Rev.*, vol. 30,

pp. 452–460, 2014.

[17] Y. Degeilh and C. Singh, “A quantitative approach to wind farm diversification and reliability,” *Int. J. Electr. Power Energy Syst.*, vol. 33, no. 2, pp. 303–314, 2011.

[18] F. J. Santos-Alamillos, D. Pozo-Vázquez, J. A. Ruiz-Arias, V. Lara-Fanego, and J. Tovar-Pescador, “A methodology for evaluating the spatial variability of wind energy resources: Application to assess the potential contribution of wind energy to baseload power,” *Renew. Energy*, vol. 69, pp. 147–156, 2014.

[19] M. K. McWilliam, G. C. van Kooten, and C. Crawford, “A method for optimizing the location of wind farms,” *Renew. Energy*, vol. 48, pp. 287–299, 2012.

[20] C. Lowery and M. O’Malley, “Optimizing wind farm locations to reduce variability and increase generation,” in *2014 International Conference on Probabilistic Methods Applied to Power Systems, PMAPS 2014 - Conference Proceedings*, 2014.

[21] O. Grothe and J. Schnieders, “Spatial dependence in wind and optimal wind power allocation: A copula-based analysis,” *Energy Policy*, vol. 39, no. 9, pp. 4742–4754, 2011.

[22] P. Norgaard and H. Holttinen, “A Multi-Turbine Power Curve Approach,” *Nord. Wind Power Conf.*, no. March, pp. 1–2, 2004.

[23] L. Reichenberg, F. Johnsson, and M. Odenberger, “Dampening variations in wind power generation—the effect of optimizing geographic location of generating sites,” *Wind Energy*, vol. 17, no. April 2013, pp. 657–669, 2014.

[24] G. B. Andresen, A. A. Søndergaard, and M. Greiner, “Validation of Danish wind time series from a new global renewable energy atlas for energy system analysis,” *Energy*, vol. 93, pp. 1074–1088, 2015.

[25] M. J. Woods, C. J. Russell, R. J. Davy, and P. A. Coppin, “Simulation of wind power at several locations using a measured time series of wind speed,” *IEEE Trans. Power Syst.*, vol. 28, no. 1, pp. 219–226, 2013.

[26] Soda, “Plane orientations and radiation components,” 2016. [Online]. Available: http://www.soda-pro.com/help/general/plane-orientations-and-radiation-components. [Accessed: 25-Oct-2016].

[27] O. P. Mahela and A. G. Shaik, “Comprehensive overview of grid interfaced wind energy generation systems,” *Renew. Sustain. Energy Rev.*, vol. 57, no. July 2015, pp. 260–281, 2016.

[28] A. P. Dobos, “PVWatts Version 5 Manual (NREL/TP-6A20-62641),” 2014.

[29] P. Gilman, “SAM Photovoltaic Model Technical Reference SAM Photovoltaic Model Technical Reference,” 2015.

[30] PVSyst Photovoltaic Software, “PVSyst Homepage.” [Online]. Available: http://www.pvsyst.com/en/. [Accessed: 05-Jun-2016].

[31] A. N. Hahmann, J. Badger, C. L. Vincent, M. C. Kelly, P. J. H. Volker, and J. Refslund,

"Wind Atlas for South Africa (WASA): Mesoscale Modeling for the Wind Atlas of South Africa (WASA) Project," 2014.

[32] L. Morales, F. Lang, and C. Mattar, "Mesoscale wind speed simulation using CALMET model and reanalysis information: An application to wind potential," *Renew. Energy*, vol. 48, pp. 57–71, 2012.

[33] I. Troen and E. Lundtang Petersen, *European Wind Atlas*. Roskilde, 1989.

[34] H. G. Beyer and K. Nottebaum, "Synthesis of long-term hourly wind speed time series on the basis of European wind atlas data," *Sol. Energy*, vol. 54, no. 5, pp. 351–355, 1995.

[35] N. G. Mortensen, J. C. Hansen, J. Badger, B. H. Jørgensen, C. B. Hasager, U. S. Paulsen, O. F. Hansen, K. Enevoldsen, L. G. Youssef, U. S. Said, A. A. E.-S. Moussa, M. A. Mahmoud, A. E. S. Yousef, A. M. Awad, M. A.-E. . Ahmed, M. A. M. Sayed, M. H. Korany, and M. A.-E. . Tarad, "Wind atlas for Egypt: Measurements, micro- and mesoscale modelling," 2006.

[36] M. Gastón, E. Pascal, L. Frías, I. Martí, U. Irigoyen, E. Cantero, S. Lozano, and Y. Loureiro, "Wind resources map of Spain at mesoscale. Methodology and validation," *Eur. Wind Energy Conf. Exhib. 2008*, vol. 5, pp. 2715–2724, 2008.

[37] V. Kotroni, K. Lagouvardos, and S. Lykoudis, "High-resolution model-based wind atlas for Greece," *Renew. Sustain. Energy Rev.*, vol. 30, pp. 479–489, 2014.

[38] I. Hall, R. Prairie, H. Anderson, and E. Boes, *Generation of typical meteorological years for 26 SOLMET stations*. Albuquerque, NM: Sandia Laboratories, 1978.

[39] B. Tammelin, T. Vihma1, E. Atlaskin, J. Badger, C. Fortelius, H. Gregow, M. Horttanainen, R. Hyvönen, J. Kilpinen, J. Latikka, K. Ljungberg, N. G. Mortensen, S. Niemelä, K. Ruosteenoja, K. Salonen, I. Suomi, and A. Venäläinen, "Production of the Finnish Wind Atlas," *Wind Energy*, vol. 16, pp. 19–35, 2013.

[40] C. Draxl, A. Clifton, B. M. Hodge, and J. McCaa, "The Wind Integration National Dataset (WIND) Toolkit," *Appl. Energy*, vol. 151, pp. 355–366, 2015.

[41] N. G. Mortensen, J. C. Hansen, M. C. Kelly, E. Prinsloo, E. Mabille, and S. Szewczuk, "Wind Atlas for South Africa (WASA), Western Cape and parts of Northern and Eastern Cape, Station and Site Description Report," 2014.

[42] SolarGis, "SolarGIS Homepage," 2016. [Online]. Available: http://solargis.com/. [Accessed: 02-Aug-2016].

[43] SoDa, "SoDa Homepage," 2016. [Online]. Available: http://www.soda-pro.com/. [Accessed: 20-May-2016].

[44] CRSES, "Publications," 2014. [Online]. Available: http://www.crses.sun.ac.za/research-publications-resources. [Accessed: 12-Jul-2016].

[45] H. Holttinen, M. Milligan, E. Ela, N. Menemenlis, J. Dobschinski, B. Rawn, R. J. Bessa, D. Flynn, E. Gómez-Lázaro, and N. K. Detlefsen, "Methodologies to determine operating reserves due to increased wind power," *IEEE Trans. Sustain. Energy*, vol. 3, no. 4, pp. 713–723, 2012.

[46] A. Keane, M. Milligan, C. J. Dent, B. Hasche, C. D'Annunzio, K. Dragoon, H. Holttinen, N. Samaan, L. Söder, and M. O'Malley, "Capacity value of wind power," *IEEE Trans. Power Syst.*, vol. 26, no. 2, pp. 564–572, 2011.

[47] M. Gholami, G. B. Gharehpetian, and M. Mohammadi, "Online Decision Tree based strategy for power system static security margin improvement using wind farms," *Int. J. Electr. Power Energy Syst.*, vol. 83, pp. 15–20, 2016.

[48] W. Jewell and R. Ramakumar, "The Effects of Moving Clouds on Electric Utilities with Dispersed Photovoltaic Generation," *IEEE Power Eng. Rev.*, vol. PER-7, no. 12, pp. 31–32, Dec. 1987.

[49] I. H. Rowlands, B. P. Kemery, and I. Beausoleil-Morrison, "Managing solar-PV variability with geographical dispersion: An Ontario (Canada) case-study," *Renew. Energy*, vol. 68, pp. 171–180, 2014.

[50] S. Shivashankar, S. Mekhilef, H. Mokhlis, and M. Karimi, "Mitigating methods of power fluctuation of photovoltaic (PV) sources - A review," *Renew. Sustain. Energy Rev.*, vol. 59, pp. 1170–1184, 2016.

[51] R. Billinton and R. N. Allan, *Reliability Evaluation of Power Systems*. Boston, MA: Springer US, 1996.

[52] M. Amelin, "Comparison of capacity credit calculation methods for conventional power plants and wind power," *IEEE Trans. Power Syst.*, vol. 24, no. 2, pp. 685–691, 2009.

[53] R. R. Booth, "Power System Simulation Model Based on Probability Analysis," *IEEE Trans. Power Appar. Syst.*, vol. PAS-91, no. 1, pp. 62–69, 1972.

[54] L. Garver, "Effective Load Carrying Capability of Generating Units," *IEEE Trans. Power Appar. Syst.*, vol. PAS-85, no. 8, pp. 910–919, 1966.

[55] C. J. Dent, A. Keane, and J. W. Bialek, "Simplified methods for renewable generation capacity credit calculation: A critical review," *IEEE PES Gen. Meet. PES 2010*, pp. 1–8, 2010.

[56] S. H. Madaeni, R. Sioshansi, and P. Denholm, "Comparing capacity value estimation techniques for photovoltaic solar power," *IEEE J. Photovoltaics*, vol. 3, no. 1, pp. 407–415, 2013.

[57] C. D'Annunzio and S. Santoso, "Noniterative method to approximate the effective load carrying capability of a wind plant," *IEEE Trans. Energy Convers.*, vol. 23, no. 2, pp. 544–550, 2008.

[58] K. Dragoon and V. Dvortsov, "Z-method for power system resource adequacy applications," *IEEE Trans. Power Syst.*, vol. 21, no. 2, pp. 982–988, 2006.

[59] C. Nguyen, C. Ma, A. Hailu, and M. Chalak, "Factors influencing calculation of capacity value of wind power: A case study of the Australian National Electricity Market (NEM)," *Renew. Energy*, vol. 90, pp. 319–328, 2016.

[60] B. Tarroja, F. Mueller, J. D. Eichman, and S. Samuelsen, "Metrics for evaluating the impacts

of intermittent renewable generation on utility load-balancing," *Energy*, vol. 42, no. 1, pp. 546–562, 2012.

[61] D. P. Schlachtberger, S. Becker, S. Schramm, and M. Greiner, "Backup flexibility classes in emerging large-scale renewable electricity systems," *Energy Convers. Manag.*, pp. 1–11, 2015.

[62] T. Nikolakakis and V. Fthenakis, "The optimum mix of electricity from wind- and solar-sources in conventional power systems: Evaluating the case for New York State," *Energy Policy*, vol. 39, no. 11, pp. 6972–6980, 2011.

[63] S. Becker, B. A. Frew, G. B. Andresen, T. Zeyer, S. Schramm, M. Greiner, and M. Z. Jacobson, "Features of a fully renewable US electricity system: Optimized mixes of wind and solar PV and transmission grid extensions," *Energy*, vol. 72, pp. 443–458, 2014.

[64] P. Eser, A. Singh, N. Chokani, and R. S. Abhari, "Effect of increased renewables generation on operation of thermal power plants," *Appl. Energy*, vol. 164, pp. 723–732, 2016.

[65] H. Markowitz, "Portfolio selection," *J. Finance*, vol. 7, no. 1, pp. 77–91, 1952.

[66] L. M. Hansen, "Can wind be a 'firm' resource? A North Carolina Study," *Duke Environ. Law Policy Forum*, vol. 15, pp. 341–381, 2005.

[67] B. Drake and K. Hubacek, "What to expect from a greater geographic dispersion of wind farms?-A risk portfolio approach," *Energy Policy*, vol. 35, no. 8, pp. 3999–4008, 2007.

[68] L. Hansen and J. Levine, "Intermittent Renewables in the Next Generation Utility," in *PowerGen-RE 2008 Conference*, 2008, pp. 1–16.

[69] J. Traube, L. Hansen, B. Palmintier, and J. Levine, "Spatial and Temporal Interactions of Wind and Solar in the Next," in *WINDPOWER 2008 Conference*, 2008, pp. 1–8.

[70] F. Cassola, M. Burlando, M. Antonelli, and C. F. Ratto, "Optimization of the regional spatial distribution of wind power plants to minimize the variability of wind energy input into power supply systems," *J. Appl. Meteorol. Climatol.*, vol. 47, no. 12, pp. 3099–3116, 2008.

[71] M. Burlando, M. Antonelli, and C. F. Ratto, "Mesoscale wind climate analysis: identification of anemological regions and wind regimes," *Int. J. Climatol.*, vol. 28, no. 5, pp. 629–641, Apr. 2008.

[72] F. Roques, C. Hiroux, and M. Saguan, "Optimal wind power deployment in Europe-A portfolio approach," *Energy Policy*, vol. 38, no. 7, pp. 3245–3256, 2010.

[73] Y. Rombauts, E. Delarue, and W. D'haeseleer, "Optimal portfolio-theory-based allocation of wind power: Taking into account cross-border transmission-capacity constraints," *Renew. Energy*, vol. 36, no. 9, pp. 2374–2387, 2011.

[74] N. S. Thomaidis, F. J. Santos-Alamillos, D. Pozo-Vázquez, and J. Usaola-García, "Optimal management of wind and solar energy resources," *Comput. Oper. Res.*, vol. 66, pp. 284–291, 2015.

[75] Y. Zhang, S. J. Smith, G. P. Kyle, and P. W. Stackhouse, "Modeling the potential for thermal

concentrating solar power technologies," *Energy Policy*, vol. 38, no. 12, pp. 7884–7897, 2010.

[76] F. J. Santos-Alamillos, D. Pozo-Vázquez, J. A. Ruiz-Arias, L. Von Bremen, and J. Tovar-Pescador, "Combining wind farms with concentrating solar plants to provide stable renewable power," *Renew. Energy*, vol. 76, pp. 539–550, 2015.

[77] A. Zagouras, R. H. Inman, and C. F. M. Coimbra, "On the determination of coherent solar microclimates for utility planning and operations," *Sol. Energy*, vol. 102, pp. 173–188, 2014.

[78] S. Liu, J. Jian, Y. Wang, and J. Liang, "A robust optimization approach to wind farm diversification," *Int. J. Electr. Power Energy Syst.*, vol. 53, pp. 409–415, 2013.

[79] J. Schmidt, V. Gass, E. Schmid, F. Strauss, and M. Zeyringer, "A spatially and temporally highly resolved analysis of wind power potentials in Austria," *9th Int. Conf. Eur. Energy Mark. EEM 12*, pp. 1–7, 2012.

[80] V. Gass, J. Schmidt, F. Strauss, and E. Schmid, "Assessing the economic wind power potential in Austria," *Energy Policy*, vol. 53, pp. 323–330, 2012.

[81] T. Leenman and F. Phillipson, "Optimal Placing of Wind Turbines: Modelling the Uncertainty," *J. Clean Energy Technol.*, vol. 3, no. 2, pp. 91–105, 2015.

[82] S. Aghabozorgi, A. Seyed Shirkhorshidi, and T. Ying Wah, "Time series clustering - A decade review," *Inf. Syst.*, vol. 53, pp. 16–38, 2015.

[83] T. Warren Liao, "Clustering of time series data - A survey," *Pattern Recognit.*, vol. 38, no. 11, pp. 1857–1874, 2005.

[84] M. Halkidi, Y. Batistakis, and M. Vazirgiannis, "On Clustering Validation Techniques," *J. Intell. Inf. Syst.*, vol. 17, no. 2/3, pp. 107–145, 2001.

[85] O. Arbelaitz, I. Gurrutxaga, J. Muguerza, J. M. Pérez, and I. Perona, "An extensive comparative study of cluster validity indices," *Pattern Recognit.*, vol. 46, no. 1, pp. 243–256, 2013.

[86] F. Vallée, G. Brunieau, M. Pirlot, O. Deblecker, and J. Lobry, "Optimal wind clustering methodology for adequacy evaluation in system generation studies using nonsequential Monte Carlo simulation," *IEEE Trans. Power Syst.*, vol. 26, no. 4, pp. 2173–2184, 2011.

[87] V. Tola, F. Lillo, M. Gallegati, and R. N. Mantegna, "Cluster analysis for portfolio optimization," *J. Econ. Dyn. Control*, vol. 32, no. 1, pp. 235–258, 2008.

[88] S. R. Nanda, B. Mahanty, and M. K. Tiwari, "Clustering indian stock market data for portfolio management," *Expert Syst. Appl.*, vol. 37, no. 12, pp. 8793–8798, 2010.

[89] K. Harman, "How does the real world performance of wind turbines compare with sales power curves?," Lyon, 2012.

[90] Vestas, "2 MW Platform," 2014.

[91] P. Montero and J. Vilar, "TSclust: An R Package for Time series Clustering," *JSS J. Stat.*

Softw., vol. 62, no. 1, pp. 1–43, 2014.

[92] J. H. Ward, "Hierarchical grouping to optimize an objective function," *Journal of the American Statistical Association*, vol. 58, no. 301. pp. 236–244, 1963.

[93] L. Kaufman and P. J. Rousseeuw, "Clustering by means of Medoids," *Stat. Data Anal. Based L1–Norm Relat. Methods*, pp. 405–416, 1987.

[94] Y. Liu, Z. Li, H. Xiong, X. Gao, and J. Wu, "Understanding of internal clustering validation measures," *IEEE Internatinal Conf. Data Min.*, pp. 911–916, 2010.

[95] S. Salvador and P. Chan, "Determining the number of clusters/segments in hierarchical clustering/segmentation algorithms," *Proc. - Int. Conf. Tools with Artif. Intell. ICTAI*, pp. 576–584, 2004.

[96] B. Pfaff, *Financial Risk Modelling and Portfolio Optimization with R*. New Delhi: Wiley, 2013.

[97] G. C. Runger and D. C. Montgomery, *Applied Statistics and Probability for Engineers*, 5th ed. Wiley, 2011.

[98] J. Nocedal and S. J. Write, *Numerical Optimization*, 2nd ed. Berlin: Springer, 2006.

[99] "Department of Environmental Affairs - Solar Data," 2014. [Online]. Available: http://egis.environment.gov.za/Download.aspx?m=25&amid=66. [Accessed: 15-Jun-2016].

[100] "MATLAB Programming Language." [Online]. Available: http://www.altiusdirectory.com/Computers/matlab-programming-language.php. [Accessed: 03-Nov-2016].

[101] A. Vance, "Data Analysts Captivated by R's Power," 2009. [Online]. Available: http://www.nytimes.com/2009/01/07/technology/business-computing/07program.html?_r=0. [Accessed: 03-Nov-2016].

[102] D. C. U. Conradie, "South Africa's climatic zones: Today, tomorrow," in *International Green Building Conference and Exhibition*, 2012, pp. 1–9.

[103] A. D. Chouakria and P. N. Nagabhushan, "Adaptive dissimilarity index for measuring time series proximity," *Adv. Data Anal. Classif.*, vol. 1, no. 1, pp. 5–21, 2007.

[104] M. Meilă, "Comparing clusterings-an information based distance," *J. Multivar. Anal.*, vol. 98, no. 5, pp. 873–895, 2007.

[105] T. Tsedu, "Strategic search for SA's best wind and sun," *CSIR Media Release*, 2014. [Online]. Available: https://www.csir.co.za/strategic-search-sas-best-wind-and-sun. [Accessed: 10-Mar-2016].

[106] Eskom, "GENERATION CONNECTION CAPACITY ASSESSMENT OF THE 2022 TRANSMISSION NETWORK," 2015.

[107] T. Tsedu, "Wind power potential in South Africa on par with solar - recent CSIR study shows," *CSIR Media Release*, 2016. [Online]. Available: https://www.csir.co.za/wind-power-

potential-south-africa-par-solar-recent-csir-study-shows. [Accessed: 17-Aug-2016].